Quantitative Characterization of Composition and Regulation of Cullin-RING Ubiquitin Ligases

Thesis by

Kurt Michael Reichermeier

In Partial Fulfillment of the Requirements for the

Degree of

Doctor of Philosophy

CALIFORNIA INSTITUTE OF TECHNOLOGY

Pasadena, California

2020

Defended November 22nd, 2019

Kurt Michael Reichermeier
ORCID: 0000-0003-0613-690

ACKNOWLEDGEMENTS

"Great discoveries and improvements invariably involve the cooperation of many minds."

Alexander Graham Bell

The last five years were a rocky journey and led across many valleys and mountains. Balancing various loose ends, many depending on each other, and some not yet tied up while I am writing this thesis, is only possible with the support of real friends and wise mentors with the right mindset:

Ubi voluntas, ibi via.

I thank the Deshaies Lab as a whole for providing a collaborative and stimulating environment to do research at an exceptional level. I thank *Ray Deshaies* for only ever closing his office door for post-lunch catnaps. In all seriousness, I am forever grateful for Ray's support and approachability, from my time as a naïve foreign medical student in 2011 throughout this incredible Ph.D. journey. Many scheduled and unscheduled 'gotta minutes' allowed me to adopt a unique way of tackling the hardest problems in science through deep, analytical thinking combined with the highest level of rigor and creativity. I am thankful to have trained with so many great scientists who taught me biochemistry and molecular biology ever so patiently at their benches – *Ruzbeh Mosadeghi*, for getting me started with *in vitro* biochemistry and for sticking together throughout tough times. *Rati Verma*, for being an invaluable senior mentor and for letting me be part of a beautiful discovery. *Pim den Besten*, for being on my side for all these years, at Caltech and at Genentech, with scientific and non-scientific wisdom. *Justin Reitsma*, for introducing me to mass spectrometry and CRISPR, but much more so for one of few deep friendships, extending far beyond pipetting and 'coffee hours' in the lab, be it on mountain bike trails or in South Dakota sloughs missing nine out of then pheasants. *Rob Oania*, for being our 'Renaissance Man' and friend, who kept the lab alive and running, day and night! *Daphne Shimoda* and *Heenam Park*, for the often invisible but so invaluable support of our daily work.

I also want to thank *Mike Sweredoski* and *Annie Moradian* from the Proteome Exploration Laboratory at Caltech for guiding me through my first steps in a mass spectrometry lab. In particular, I thank 'Magic Mike' for his computational support and friendship, which I hope to keep alive on our yearly fly-fishing adventures.

I thank my thesis committee – *David Chan, Paul Sternberg, and Shu-ou Shan* as well as *Kai Zinn*, who, without hesitation, took on the role of thesis advisor after Ray's departure – for their insightful guidance, and most importantly, for their support to complete my project at Genentech. The move to South San Francisco halfway through my Ph.D. is an excellent example of what Caltech means to me: A truly unique place, where everyone sees solutions rather than problems. I vividly remember sitting in *Doug Rees'* office in March 2017, proposing this crazy idea of moving to a biotechnology company to complete my research project. What followed was a relentless combined effort of the Dean's Office with *Doug Rees and Natalie Gilmore*, my Option Representative *Bruce Hay* and Program Coordinator *Liz Ayala*, the Office of Technology Transfer with *Case Cortese, Maral Gharib,* and later *Steven Chapman*, the Compliance Office with *Grace Fisher-Adams*, as well as the International Student Office with *Laura Flower Kim* and *Daniel Yoder* to make this dream a reality. Within six months, a research agreement was signed and a work authorization issued to enable what turned out to be an unforgettable experience. Thank you, Caltech, for being the incredible place I was privileged to be part of.

I am grateful to *Ingrid Wertz* and *Don Kirkpatrick*, for adopting me at Genentech under such unique circumstances. I could not have asked for a smoother transition and more support from their side. I deeply thank Ingrid, having been a Genentech M.D./Ph.D. student adoptee herself, for mentoring me with her wealth of experience as well as for initially opening the doors and placing me in an environment that turned out to be ideal to finish the CRL4 project. I also thank Don, who in the spirit of Caltech, only saw solutions and very few problems, and who had to sit through numerous calls with attorneys to prevent the construction of a second 'Genentech Hall' in Pasadena or at the various other places I enjoyed to openly and collaboratively interact with. I will forever appreciate Don's patience, trust, and wisdom at every step along the way: be it teaching me the secrets of MS, discussing various science topics, or how to strive in a large corporation.

I also want to thank Andrea Amey and Nicolo Rivolta for legal support, as well as Vishva Dixit and the Genentech Postdoc Program for giving me a new home. A big thank you also goes to all Wertz Lab and Kirkpatrick Lab members as well as the MPL group for fruitful discussions and feedback. Thank you, Genentech, for letting me have a glimpse at drug development and for allowing me to mingle with and learn from your phenomenal scientists.

Finally, I want to thank my friends and family for emotional support at the bottom of valleys and for celebrating the first ascents of various mountains. Most of all, I thank my wife *Ingrid* for guiding me through difficult times, for always keeping a cool head and having my back, for encouraging me every day to be the best I can, and for climbing many snowy peaks together. “Focus, look forward. Step by step. We are almost there…”

New Army Pass, route to Mount Langley, Sierra Nevada, on July 3rd 2017.

ABSTRACT

Induced proteolysis of pathogenic proteins via degrader molecules, such as Proteolysis Targeting Chimeras (PROTACs), is emerging as a promising therapeutic strategy. In particular, induced proximity of Cullin-RING ubiquitin Ligases (CRLs) with various neo-substrates has proven successful in mediating proteasomal degradation of previously undruggable proteins. Hijacking enzymes to carry out biochemical reactions on neo-substrates stands in stark contrast to conventional pharmacological approaches and exposes degrader molecules to unusually complex pharmacodynamics. While the first PROTACs entered the clinic in 2019, much about the organization and regulation of the frequently co-opted CRLs remains elusive. In particular, the COP9 Signalosome (CSN) is essential to regulate CRL activity and assembly through cleaving Nedd8 from cullin scaffolds, yet it remains unknown how CSN becomes activated. We combine structural and kinetic analyses to identify mechanisms that contribute to CSN activation and Nedd8 deconjugation, detailing the kinetic picture of the deneddylation-disassembly cycle that promotes rapid remodeling of the cellular CRL network. Furthermore, we establish Protein Interaction Kinetics and Estimation of Stoichiometries (PIKES) analysis, a systematic proteomic profiling platform that integrates cellular engineering, affinity purification, chemical stabilization and quantitative mass spectrometry to investigate the dynamics of interchangeable multiprotein complexes. Using PIKES, we show that ligase assemblies of Cullin4 with individual substrate receptors differ in abundance by up to 200-fold and that Cand1 acts as an exchange factor to remodel the CRL4 ligase pool. Integrating quantitative data and model simulations of CRL-mediated substrate turnover, we show that high substrate receptor levels can enhance the potency of degraders.

PUBLISHED CONTENT AND CONTRIBUTIONS

1. R Mosadeghi, **KM Reichermeier**, M Winkler, A Schreiber, JM Reitsma, Y Zhang, F Stengel, J Cao, M Kim, MJ Sweredoski, S Hess, A Leitner, R Aebersold, M Peter, RJ Deshaies, RI Enchev; Structural and kinetic analysis of the COP9-Signalosome activation and the cullin-RING ubiquitin ligase deneddylation cycle. eLife (2016); PMID: 27031283; DOI: 10.7554/eLife.12102

   This publication is the basis for Chapter 2 which includes the accepted manuscript draft prior to formatting by *eLife*. This study was conceived by RM and RJD, and KMR designed, performed, and interpreted the binding experiments, developed off-rate assays and performed measurements, designed, performed and interpreted the activity assays, expressed and purified proteins from bacteria, designed cell based assays, performed the cell based assays, and drafted and edited the manuscript; Specifically, KMR contributed to Figure 2.3A, B, C; Figure 2.5A, B; Figure 2.6A,B,C; Figure Supplement 2.2A, B, C, D, F; Figure Supplement 2.3A, E, F, G, H, I, J, K, L, M, P, R; Figure Supplement 2.5A, D, E, F; and Figure Supplement 2.6A.

2. **KM Reichermeier,** R Straube, JM Reitsma, MJ Sweredoski, CM Rose, A Moradian, Willem den Besten, T Hinkle, E Verschueren, G Petzold, N Thomä, IE Wertz, RJ Deshaies, DS Kirkpatrick; *PIKES analysis uncovers response to degraders and key regulatory mechanisms of CRL4 ligase networks* (revised manuscript in press, *Molecular Cell,* DOI: 10.1016/j.molcel.2019.12.013)

   The unrevised manuscript draft, as initially submitted to the journal, is the basis for Chapter 3. This study was initially conceived by KMR and RJD, and later supervised by IEW and DSK. KMR developed the assays and designed, and performed and interpreted all experiments as well as drafted the manuscript.

TABLE OF CONTENTS

LIST OF ILLUSTRATIONS AND/OR TABLES

NOMENCLATURE

26S – 26S Proteasome

A – Adapter for a CRL

Å – Angstrom

A•SR – Adapter•substrate receptor complex for a CRL complex

ACN – Acetonitrile

ADP – Adenosine diphosphate

AMBRA1 – Activating molecule in BECN1-regulated autophagy protein 1

AP-MS – Affinity purification MS

ATP – Adenosine triphosphate

BP(A,B,C) – Beta propeller A,B,C

BRWD – Bromodomain and WD repeat-containing protein

BSA – Bovine serum albumin

CAND1 – Cullin-associated Nedd8-dissociated protein 1

Cks1 – Cyclin-dependent kinases regulatory subunit 1

COP1 – Constitutive photomorphogenesis protein 1 homolog

COPS – Cop9 signalosome subunit

CRBN – Protein cereblon

CRISPR – Clustered regularly interspaced short palindromic repeats

CRLs – Cullin RING Ligases

CSA – Cockayne syndrome WD repeat protein CSA

CSN – Cop9 Signalosome

CTD – C-terminal domain

Cys – Cystein

Da – Dalton

DC50 – Half maximal degradation concentration

DCAF – DDB1-Cullin4-associated factor

DCAF10 – Also termed WDR32

DCAF11 – Also termed WDR23

DCAF12 – WDR40A

DCAF4 – Also termed WDR21

DCAF5 – WDR22

DCAF6 – Also termed ARCP (Androgen receptor complex-associated protein)

DCN – Defective in cullin neddylation protein

DDA1 – DET1- and DDB1-associated protein 1

DDB1 – Damage-specific DNA-binding protein 1

DDB2 - Damage-specific DNA-binding protein 2

DET1 – De-etiolated-1 homolog

DTL – Denticleless protein homolog, also termed CDT2 (CDC10-dependent transcript 2)

DWD – DDB1-binding WD40 domain

EM – Electron microscopy

ERCC8 – DNA excision repair protein ERCC-8, Also termed CSA

ES – Enzyme•Substrate

FBP – Fbox protein

FDA – Food and drug administration

FDR – False discovery rate

FSC – Fourier shell correlation

GLMN – Glomulin

HCD – Higher energy collisional dissociation

HECT – Homologous to the E6AP carboxyl terminus

HEK – Human embryonic kidney cells

IC50 – Half maximal inhibition concentration

IKFZ – Ikaros family zinc finger protein

IMiD – Immunomodulatory drug

INS1 – Insert 1 within CSN5

IP – Immunoprecipitation

IκBα – NF-kappa-B inhibitor alpha

JAMM – JAB1-MPN-MOV34 metalloenzyme motif

KO – Knock-out

LC-MS – Liquid chromatography mass spectrometry

LDS – Lithium dodecyl sulfate

Lys – Lysine

MLN4924 – Nedd8-activating enzyme (NAE) inhibitor

MLN7243 – Ubiquitin-activating enzyme (Ub-E1) inhibitor

Nedd8 – Neuronal precursor cell expressed developmentally down-regulated protein 8

NTD – N-terminal domain

PHIP – PH-interacting protein, also termed WDR11

PI – Proteasome inhibitor

PIKES – Protein Interaction Kinetics and Estimation of Stoichiometries

PRM – Parallel reaction monitoring

PROTAC – Proteolysis Targeting Chimera

PWP1 – Periodic tryptophan protein 1 homologue

QconCAT – Quantification concatemer

RBX1 – RING-box protein 1

RFWD2 – Ring finger and WD repeat domain protein 2, also termed COP1

RING – Really interesting new gene

RR-MM – Relapse-refractory multiple myeloma

RT-qPCR – Reverse transcriptase OR real time quantitative polymerase chain reaction

SAINT – Statistical analysis of interactomes

SCF – Skp1•Cul1•Fbox ligase complex

SDS – Sodium dodecyl sulfate

SEM – Standard error of the mean

SILAC – Stable isotope labeling in cell culture

Skp1 – S-phase kinase-associated protein 1

Skp2 – S-phase kinase-associated protein 2

SR – Substrate Receptor for a CRL

SREF – Substrate receptor exchange factor

TOR1AIP2 – Torsin-1A-interacting protein 2, also termed IFRG15 or LULL1

TRPC4AP – Short transient receptor potential channel 4-associated protein, also termed TRUSS

Ub – Ubiquitin

UBXD7 – UBX domain-containing protein 7

UPS – Ubiquitin Proteasome System

UV – Ultraviolet light

VPRBP – VPR-interacting protein, also termed DCAF1

WCL – Whole cell lysate

WDR – WD repeat-containing protein

WDTC1 – WD and tetratricopeptide repeats protein 1

WHB – winged-helix B

β-TRCP – Fbox/WD repeat-containing protein 1

1 - INTRODUCTION TO CULLIN-RING UBIQUITIN LIGASES

1.1 The Ubiquitin Proteasome System

Facing the challenge of spatially and temporally controlling the abundance and function of billions of protein molecules at a timescale of minutes, eukaryotes evolved hundreds of enzymes, collectively termed the Ubiquitin Proteasome System (UPS) (Hershko and Ciechanover, 2003). In addition to clearing misfolded and dysfunctional proteins, rapid depletion of signaling proteins provides a mechanism to control fundamental processes such as cell cycle (Deshaies, 1995; King et al., 1996). The UPS is highly conserved from yeast to humans, whereby ubiquitin (Ub), a 76-amino-acid polypeptide, can serve as the mark for protein degradation by the 26S proteasome.

Historically, the canonical signal recognized by the proteasome was believed to be a chain of at least four ubiquitin molecules covalently attached to a Lys residue of a protein substrate (Ravid and Hochstrasser, 2008). However, recent research showed that conjugation of substrates with multiple mono-ubiquitins as well as branched chains with various linkages can mediate and even improve recognition by the proteasome (Dimova et al., 2012; Lu et al., 2015b; Meyer and Rape, 2014; Yau and Rape, 2016). The modification of proteins with ubiquitin, referred to as ubiquitination, is achieved through a three-step cascade of biochemical reactions: first, ubiquitin is activated via its C-terminal Gly76 residue in an ATP-dependent process carried out by an E1 ubiquitin-activating enzyme. The intermediate ubiquitin adenylate is bound to a Cys residue of the E1 enzyme via a high-energy thioester linkage. Second, the E1-bound ubiquitin moiety is transferred to a Cys residue on an E2 ubiquitin-conjugating enzyme in a transesterification reaction. In a third step, ubiquitin is transferred to a Lys residue of a substrate protein via an E3 ubiquitin-ligating enzyme (Hershko and Ciechanover, 1998; Varshavsky, 1997). This last step is catalyzed by E3 ubiquitin ligases of two main families that function through distinct mechanisms: HECT (homologous to the E6AP carboxyl terminus) domain ligases first

accept the ubiquitin moiety on a Cys residue before transferring it onto substrates. RING (really interesting new gene) domain ligases use scaffolding proteins to bring substrates into proximity with E2 enzymes which discharge ubiquitin directly onto the substrate to yield a Ub-protein conjugate. In each case, an isopeptide bond forms between the carboxyl group of Ub and the lysine Ɛ-amino group of the substrate. (Deshaies and Joazeiro, 2009a; Zheng and Shabek, 2017). Recently, the discovery of RING-IBR-RING (RBRs) defined a third family of RING-HECT hybrid E3 enzymes (Wenzel et al., 2011; Zheng and Shabek, 2017).

Figure 1.1

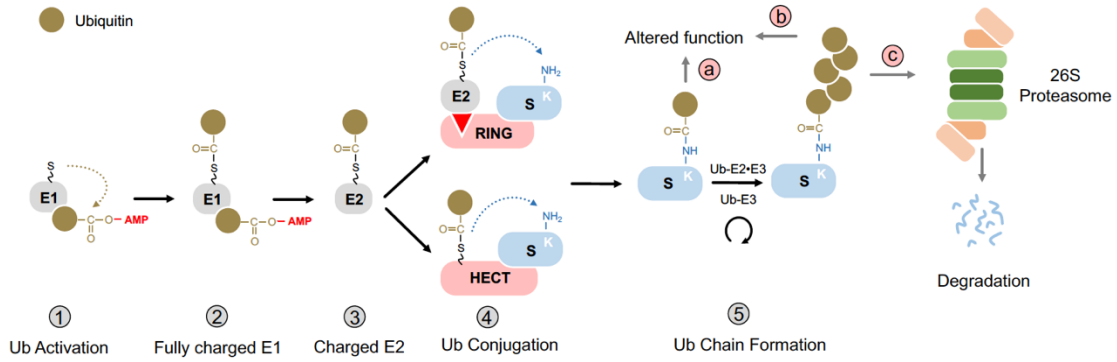

Figure 1.1. The Ubiquitin Proteasome System – UPS. (1) Ubiquitin is activated via binding to a Ub-E1 enzyme and formation of a ubiquitin-adenylate. (2) Activated Ub-AMP is then transferred onto a Cys residue within the E1 enzyme which can then associate with a second Ub molecule to form a fully charged E1 complex. (3) Ubiquitin is then transferred to an E2 enzyme through a transesterification reaction. (4) Several hundred E3 ligases can either serve as a scaffold for E2 and substrate or receive the Ub-moiety from the E2 enzyme on an active site Cys residue to eventually facilitate substrate ubiquitination. (5) Substrate proteins can either be released by E3 ligases as mono-ubiquitin conjugates or enter processive cycles of ubiquitin chain formation to yield poly-ubiquitin conjugates. (6) Mono- and poly-ubiquitination (a,b) of substrate proteins can either alter protein function while poly-ubiquitination via K48 chains is the primary recognition signal or the 26S Proteasome to mediate protein degradation (c). Adopted from (Deshaies and Joazeiro, 2009b; Pickart, 2004)

In humans, selectivity within the UPS is conferred by hundreds of E3 ubiquitin ligases which recognize substrates via degradation signals, referred to as degrons (Zheng and Shabek, 2017). A typical UPS degron comprises a set of characteristics to successfully mediate ubiquitination and proteasomal degradation: i) an interface to recruit the E3 ligase (primary recognition determinant); ii) one or multiple Ub-acceptor Lys moieties; iii) the ability to bind the 26S proteasome; and iv) a location within the substrate, usually in

proximity to an unstructured region, that enables unfolding by the proteasome (Aufderheide et al., 2015; Ravid and Hochstrasser, 2008).

A mono-Ub-protein conjugate can undergo further processive ubiquitination resulting in a poly-Ub-protein conjugate (Pierce et al., 2009). The Lys residue within ubiquitin that serves as the acceptor for the next transfer determines the architecture of emerging chains. The main chain types recognized by the 26S proteasome are linked via Lys48 and Lys11, while Lys29- and Lys63-linked chains mediate proteasomal degradation less frequently. Ubiquitin, attached to proteins in various linkages and branches, serves as a post-transcriptional code which, besides its roles in proteolysis, can regulate the activity, localization, and interactions of many cellular proteins (Komander and Rape, 2012).

Proteins are designed as robust, tightly folded, biological polymers, built from amino acids chemically linked via peptide bonds. The hydrolysis of a peptide bond at physiological pH is estimated to take place at a half-life of ~400 years (Pickart, 2004; Wolfenden and Snider, 2001). The kinetic stability of proteins at physiological conditions underscores the complexity of breaking down thousands of different proteins via one universal molecular machine. Degradation of most cellular proteins is facilitated by a 2.5-MDa, ATP-driven, 32-subunit protease – termed the proteasome – consisting of a 20S core particle capped by one or two 19S particles. While the 20S core harbors proteolytic activity, the 19S cap functions as a substrate recognition, de-ubiquitination, and unfolding module. Ubiquitin receptors within the 19S cap are spatially positioned in a way that a poly-Ub conjugate is recognized with an affinity high enough to initiate substrate de-ubiquitination, unfolding, and subsequently degradation within the 20S proteolytic chamber (Aufderheide et al., 2015; Förster et al., 2013; Matyskiela and Martin, 2013).

1.2 Cullin-RING Ubiquitin Ligases

The human genome encodes more than 600 E3 Ubiquitin ligases, most of which contain a RING domain, and only ~40 E2 and two E1 enzymes (Deshaies and Joazeiro, 2009a; Sarikas et al., 2011). Cells afford such a large number E3 enzymes to ensure specific targeting of individual proteins for ubiquitination. Within the superfamily of RING-E3s,

the Cullin-RING ligases (CRLs) are the largest class and make up as many as 240 distinct enzyme complexes (Skaar et al., 2013; Zheng and Shabek, 2017) which are responsible for ~20% ubiquitin-dependent protein turnover in human cells (Soucy et al., 2009). CRLs are further divided into subfamilies based on the identity of their catalytic cullin scaffolding protein: the founding member Cullin1 or SCF family, and the Cullin2, Cullin3, Cullin4A, and Cullin4B, as well as the Cullin5 and Cullin7 subfamilies. All CRL ligases share a common architecture and bind an Adapter-Substrate Receptor module (A•SR) on the N-terminal end of the scaffold and one of two RING proteins (Rbx1 or Rbx2) on the C-terminal domain. While the A•SR modules mediate substrate recognition and recruitment, the RING serves as a platform to recruit and position an E2 enzyme to compose a fully functional ligase complex. Within each subclass, several dozen individual substrate receptors (SR) utilize the same, subclass-specific adapter (A) protein to assemble with a cullin backbone.

Within prototypical SCF/CRL1 complexes, the Skp1 adapter protein and one of ~69 Fbox proteins form A•SR modules that associate with Cullin1 (Jin et al., 2004). While the SR modules of Cul1-3, Cul5, and Cul7 are structurally related, the Cullin4 subfamily diverges from the norm. Compared to other CRLs, the Cul4 adapter protein DDB1 is considerably larger and more flexible. Cul4 SRs also contain distinct but variable motifs on which ligase assembly is based (Lydeard et al., 2013; Zimmerman et al., 2010). The adapter DDB1 contains three WD40-like beta-propeller domains – BPA, BPB, and BPC (beta-propeller A-C) – of which BPB tethers DDB1 onto the Cul4 scaffold (Zimmerman et al., 2010). Substrate receptors in the cullin4 family are referred to as DCAFs (DDB1-Cul4-associated Factors) or DWDs (DDB1-binding WD40 proteins). The majority of DCAFs contain six or more WD40 motifs which again fold into donut-shaped beta-propeller domains (Angers et al., 2006; He et al., 2006a; Higa et al., 2006; Jin et al., 2006). DCAF proteins associate with DDB1 via a N-terminal alpha-helix motif, termed the H-box, which inserts itself between the BPA and BPC domains of DDB1. The beta-propeller of the DCAF packs against those of DDB1, positioning the ‘top’ surface of the beta-propeller to recruit and present substrates. While the H-box motif can be identified in seven cellular DCAFs, the 13 amino acid motif is poorly conserved, making the prediction and identification of all

human DCAFs a major challenge (Li et al., 2010; Scrima et al., 2008; Zimmerman et al., 2010). Currently, the exact number of true DCAF proteins is not known and estimates

Figure 1.2

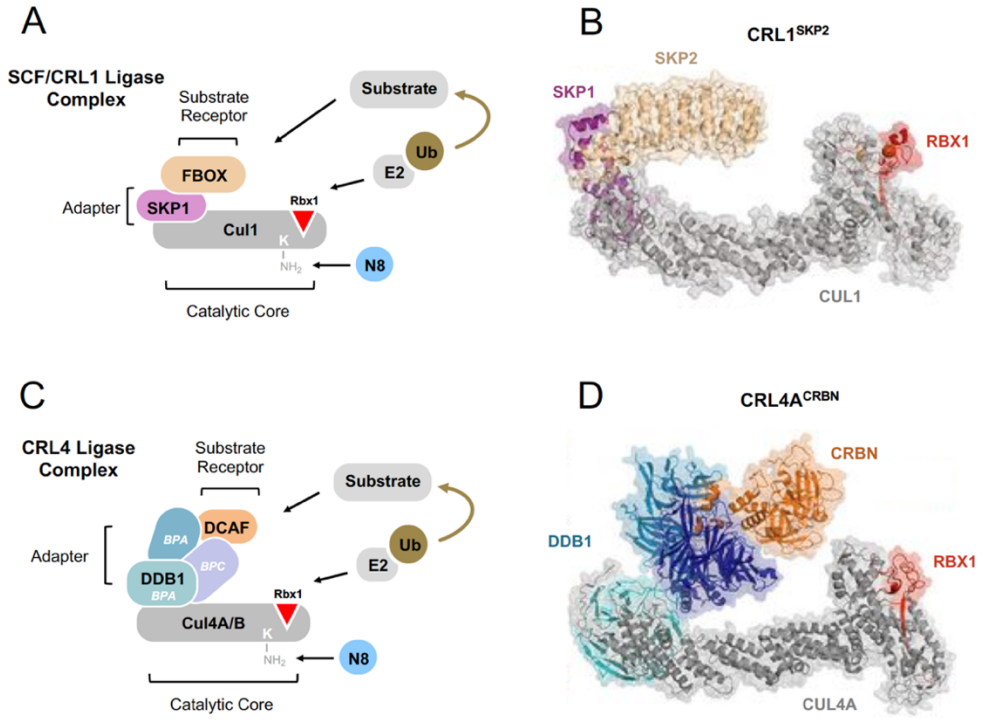

range from 25-115 (Hannah and Zhou, 2015; Lee and Zhou, 2007).

Figure 1.2. Architecture of cullin-RING ubiquitin ligases. (A) The prototypical subfamily CRL ligases is SCF or CRL1, which is composed of a Cul1 scaffold tightly associated with the RING protein Rbx1 on the C-terminal end and assembled with one of 69 individual A•SR modules. Skp1 serves as the CRL1 adapter protein while various Fbox proteins serve as specific substrate recognition subunits. (B) Structural model of a $CRL1^{SKP2}$ ligase complex (PDB xxx). (C) The architecture of CRL4 complexes resembles SCF except for a few important distinctions. CRL4 uses DDB1 as the adapter protein and DCAFs or DWDs as substrate receptors. Structurally, CRL4s are distinct due to their large and mobile adapter protein and a A•SR binding mode that differs from other CRL families. (D) Structural model of a CRL^{CRBN} ligase complex (PDB xxx). The structural models in (B) and (D) are adopted from (Cavadini et al., 2016).

The combinatorial nature of CRLs reminds of a drill that uses an adapter with multiple different bits to work on various types of screws. The engineering of drills as well as the modular evolution of CRLs comes with three advantages: first, it appears economical to evolve an efficient catalytic core once and then expand its applicability through additional specificity modules. Second, the use of an adapter allows for virtually unlimited expansion

of the repertoire of substrate receptors, providing CRLs with functionality and plasticity. Third, separating specificity modules from catalytic cores and only assembling full ligases when they are needed, might prevent promiscuous ubiquitination of unintended substrates, which could potentially be caused by the enormous speed of CRL-mediated ubiquitination occuring in milliseconds (Pierce et al., 2009). Considering all of the above, regulating proper CRL ligase assembly and function on a time scale that allows for rapid responses to cellular signals within minutes poses a major challenge to all eukaryotic cells.

1.3 Regulation of CRL Ligases via Nedd8, Cand1, and CSN

Following the discovery of SCF/CRL1 as the first CRL ubiquitin ligase complex ~20 years ago (Feldman et al., 1997; Patton et al., 1998; Skowyra et al., 1997), most research on CRL regulation has been conducted on the prototypical SCF complexes. Definitive experimental evidence about regulation of CRL complexes other than SCF is sparse, although structural similarities and shared regulatory proteins suggest uniform mechanisms (Lydeard et al., 2013). In brief, all CRL ligases are thought to undergo cycles of activation and inactivation via Nedd8 and the Cop9 Signalosome (CSN), as well as cycles of substrate receptor exchange driven by Cand1. These mechanisms are posited to ensure timed activation and stable CRL assembly when substrates are present.

Early studies in Arabidopsis thaliana and budding yeast revealed that cullin scaffolds are modified with the protein Rub1 (Liakopoulos et al., 1998; Linghu et al., 2002; Del Pozo and Estelle, 1999). In humans, the Rub1 homologue and ubiquitin-like protein Nedd8 is conjugated onto conserved Lys residues of cullin scaffolds in a three-step cascade similar to that of ubiquitination. This process is termed neddylation. The Nedd8-E2 (Ubc12 or UBE2F) enzyme binds cullins via the RING domain of Rbx1/2, and with the help of DCN proteins (Nedd8 E3s) positions its active site close to a Lys moiety on the C-terminal globular domain of the cullin to discharge Nedd8 (Enchev et al., 2015). The modification of a cullin complex with Nedd8 has two major regulatory roles: first, cullin neddylation leads to activation of ubiquitin transfer activity by inducing structural rearrangements of the C-terminal domain and the RING. This conformational change allows the Ub-E2 to be positioned nearby its substrate, closing a gap that is estimated to be as wide as 50Å in the

non-neddylated state (Boh et al., 2011; Duda et al., 2008; Saha and Deshaies, 2008; Yamoah et al., 2008). Second, modification with Nedd8 blocks Cand1 from accessing the cullin scaffold to prevent A•SR exchange (Liu et al., 2002; Zheng et al., 2002a).

Initially, Cand1 was thought to be an inhibitor of CRL function since structural studies revealed that it tightly wrapped around the cullin core, occupying both, the N-terminal A•SR binding site as well as the C-terminal neddylation site. The Cullin•Cand1 complex was deemed incompatible with Ubiquitin or Nedd8 transfer activity (Goldenberg et al., 2004). For many years, this observation stood in contrast with genetic studies performed in plants and worms which suggested a positive role of Cand1 in CRL regulation (Bosu et al., 2010; Chuang et al., 2004; Feng et al., 2004; Lo and Hannink, 2006; Zhang et al., 2008). This longstanding paradox was resolved when Cand1 was shown to act as an A•SR module exchange factor (Pierce et al., 2013; Wu et al., 2013; Zemla et al., 2013). The necessity of an A•SR exchange factor within the SCF system became apparent when *in vitro* studies revealed that Skp1•Fbox modules dissociate from Cul1 with a half-life of more than one week (Pierce et al., 2013). These extreme stabilities (K_d values in the picomolar range) restrict the re-arrangement and plasticity of SCF complexes dramatically, particularly when considering that cullin scaffolds are present at limiting amounts and A•SR modules in multiple fold excess (Bennett et al., 2010). Practically, this would have meant that a free A•SR would have to wait several days to assemble with a cullin scaffold following substrate engagement in order to take is turn to form an active ligase. This conundrum resolved when it was shown that Cand1 can act as a catalyst for A•SR exchange by increasing the off-rate of Skp1•Fbox modules from Cul1 by one million-fold. This exchange activity shortens SCF complex dissociation to less than one second (Pierce et al., 2013). Cand1 can only exhibit its exchange function on inactive, de-neddylated CRL complexes. To ensure that Cullin cores are held in prompt equilibrium with their A•SR pools, Nedd8 must be deconjugated from CRLs once substrate demand decreases to make them accessible to Cand1's exchange function.

The Cop9 Signalosome (CSN) is an eight-subunit protein complex harboring a JAMM motif (JAB1-MPN-MOV34 metalloenzyme motif) within a metalloprotease active site.

CSN serves as the main cullin deneddylase (Cope et al., 2002; Lyapina et al., 2001). The holoenzyme as well as its CSN5 active site subunit in isolation display no activity towards non-cullin Nedd8-conjugates. This lack of activity suggests an autoinhibitory mechanism preventing promiscuous deneddylation activity (Birol et al., 2014; Lingaraju et al., 2014). Structural and biochemical studies, including the work described in this thesis, revealed that the C-terminal cullin domain is wedged in between CSN subunits CSN2 and CSN4, leading to the optimal positioning of the CSN5/6 active site dimer and the release of autoinhibition allowing CRL-specific deneddylation (Cavadini et al., 2016; Mosadeghi et al., 2016). Additionally, the CSN-CRL binding mechanisms evolved so that CSN senses whether the CRL is occupied by a substrate. CSN competes with substrate proteins for the space around the A•SR module on the N-terminal domain of the cullin. Through this competition, substrates inhibit CSN's deneddylation activity when bound to CRLs (Cavadini et al., 2016; Emberley et al., 2012; Enchev et al., 2012; Fischer et al., 2011a). Interestingly, CSN can stably associate with its product and thereby inhibit non-neddylated CRLs. This phenomenon cannot be explained by current kinetic models but it has been proposed that substrates compete with CSN for CRL access to trigger their own ubiquitination (Bennett et al., 2010; Emberley et al., 2012; Enchev et al., 2015).

The regulatory factors Nedd8, Cand1 and CSN join forces to ensure proper CRL ligase function through timed cycles of inhibition and activation (Figure 1.3) (Liu et al., 2018; Sievers et al., 2018). In human cells, only ~10% of all Skp1•Fbox modules assemble into ~250 nM SCF ligases at steady state (Figure 1.3-1). Cul1 scaffolds are limiting with a Skp1•Fbox pool in four-fold excess over total Cul1 (Reitsma et al., 2017). This quantitative picture of SCF ligase organization makes obvious that efficient recycling of cullin scaffolds is paramount to enable new ligase assembly through integration of A•SR modules from a large free repertoire (~90%). This is ensured via the exchange activity of Cand1, which keeps Cul1 in a rapid and dynamic equilibrium with the A•SR pool. CRLs can escape rapid cycles of exchange and neddylation/deneddylation via substrate association (Figure 1.3-2), creating a disequilibrium that favors the assembly of A•SR modules for which substrates are available. Once the N-terminal end of a cullin is occupied by a substrate, deneddylation via CSN is inhibited and the exchange cycle put on hold. The CRL complex becomes

trapped in its fully activated state, polyubiquitinating the substrate until it is released and degraded. Once substrate dissociates, CSN is able to bind the CRL to facilitate rapid de-neddylation which allows the complex to re-enter the Cand1 exchange cycle (Figure 1.3-3). In this complex regulatory network, the role of Nedd8 and CSN is similar to a chuck key which is used to tighten or loosen the adapter of a drill. Nedd8, just like the tightening chuck key, ensures stability and function at high speeds, while CSN, like the loosing chuck key, reverses this activating signal and enables exchange to a different adapter•bit combination.

Figure 1.3

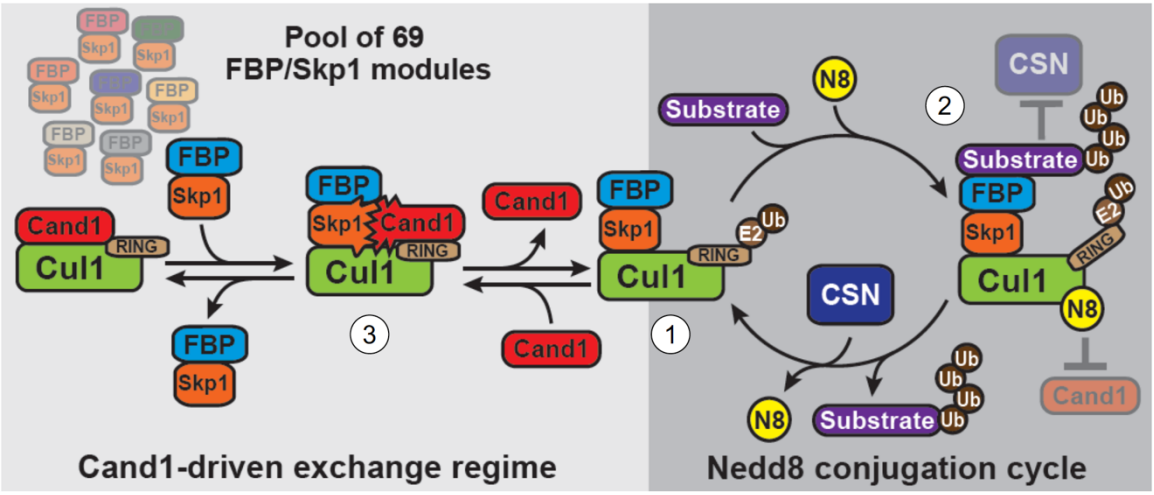

Figure 1.3. The Cand1-Nedd8-CSN Regulation Cycle on the example of SCF/CRL1. (1) Once a fully assembled SCF complex is born, it can either become neddylated and bind substrate (2), or, if substrate is not available become de-neddylated rapidly to enter the Cand1-driven exchange regime (3). Cand1-mediated exchange ensures that limited amounts of Cul1 scaffold is kept in equilibrium with large pools of A•SR modules (FBP/SKP1 for Fbox protein and SKP1 complexes). An adaptive disequilibrium is created towards CRL complexes with available substrates due to the substrate's ability to inhibite CSN-mediated de-neddylation and therefore Cand1-mediated A•SR exchange. This illustration is adopted from (Reitsma et al., 2017).

1.4 Pharmacological Targeting of the UPS and CRLs

The UPS is essential to cellular function and involved in every major signaling pathway. Besides proteostasis and cell cycle, the UPS also regulates immune signaling, mitochondrial fission, fusion and degradation, and different forms of cell death including apoptosis, neuronal function and tumorigenesis (Thibaudeau and Smith, 2019). Upon realization that cancer cells frequently rely on a functional UPS, initial discoveries of 26S proteasome inhibitors (PIs) in the 1990's (Rock et al., 1994) were followed by the development of bortezomib (Velcade®) as a first-generation PI approved for relapse-refractory multiple myeloma (RR-MM). Since its approval in 2003, bortezomib continues to be an important cornerstone in MM therapy (Goldberg, 2007). Bortezomib is based on an early lead compound termed MG-132, a peptide aldehyde which continues to be used in research due to its low cost, decent potency and reversibility (Thibaudeau and Smith, 2019). Several years later, carfilzomib (Kyprolis®) was developed from the naturally derived compound epoxomicin and shown to act through a different mechanism of action. Carfilzomib was approved by the FDA as a second-generation PI for RR-MM in 2012. In 2015 ixazomib was approved as the first orally bioavailable PI, showing promising results for indications beyond MM in ongoing trials (Thibaudeau and Smith, 2019).

The profound role of neddylation in CRL biology and its involvement in various cancers spurred the development of potent inhibitors of the Nedd8-E1 (NAE) enzyme and CSN (Brownell et al., 2010; Schlierf et al., 2016; Soucy et al., 2009). Prevonedistat, a NAE enzyme inhibitor (MLN4924), is currently being evaluated in 34 clinical trials, 20 of which are actively recruiting (www.clinicaltrials.gov). MLN4924 and CSN5i-3 (CSN inhibitor) also serve as valuable tools to study cullin-RING ligase function and regulation in research. Millennium Therapeutics (now Takeda), the same company which developed the Nedd8-E1 inhibitor MLN4924, subsequently developed a highly potent Ubiquitin-E1 inhibitor (Hyer et al., 2018). While clinical trials so far have failed, MLN7243, just like CSN5-3 and MLN4924, provides a valuable research tool.

While substrate recognition through E3 enzymes is highly specific, the chemistry of conjugating ubiquitin molecules to a Lys residue within a protein substrate is fairly

promiscuous. This realization led to the hypothesis that it should be possible for any substrate protein to be ubiquitinated and subsequently degraded through the UPS if brought in proximity with a Ub-E3 enzyme. The concept of artificial and targeted protein degradation via proteolysis targeting chimeras (PROTACs) was experimentally demonstrated for the first time in the early 2000's by the Crews and Deshaies laboratories (Sakamoto et al., 2001, 2003). These seminal studies made it obvious that targeting of the UPS was not limited to conventional pharmacology of inhibiting enzyme activity but could be extended to co-opting the proteolytic machinery for therapeutic benefit. While initial development of PROTAC molecules was limited to a few ligase-ligands and targets, mechanistic discoveries involving lenalidomide and other IMiDs sparked new enthusiasm. IMiDs were initially banned for then teratogenic effects, but later repurposed to treat multiple myeloma and leprosy. IMiDs were subsequently shown to recruit zinc finger transcription factors to the $CRL4^{CRBN}$ ubiquitin ligase which mediates the IMiD-dependent ubiquitination and proteasomal degradation of IKZF1 and IKZF3 (Gandhi et al., 2014; Krönke et al., 2014; Lu et al., 2014). This discovery not only provided in-vivo proof that chemically inducible protein degradation can work in humans, but also revealed a new ligase-ligand which could be conjugated to other substrate-recruiting moieties to target a variety of neo-substrates for inducible degradation (Nabet et al., 2018; Winter et al., 2015). Within the last five years, more than thirty PROTAC-like molecules have been reported. The field of targeted protein degradation currently holds the promise against many previously undruggable proteins and represents a new class of medicines (An and Fu, 2018; Deshaies, 2015; Paiva and Crews, 2019; Scudellari, 2019). The emergence of these new pharmaceuticals moved cullin-RING ligases into the spotlight of drug development. The complex mechanism involved with redirecting CRL ligases towards novel target proteins exposes degrader drugs to unusually complicated pharmacodynamics (Bulatov and Ciulli, 2015). Therefore, it is of great general interest to investigate the composition, dynamics, and regulation of CRL ligases in detail. These studies aim to guide rational design for

degraders and facilitate a better understanding of how these medicines will work in patients.

2 - STRUCTURAL AND KINETIC ANALYSIS OF CSN ACTIVATION AND THE CULLIN-RING UBIQUITIN LIGASE DENEDDYLATION CYCLE

This chapter is based on the accepted manuscript draft prior to formatting by eLife which was published as:

R Mosadeghi, **KM Reichermeier**, M Winkler, A Schreiber, JM Reitsma, Y Zhang, F Stengel, J Cao, M Kim, MJ Sweredoski, S Hess, A Leitner, R Aebersold, M Peter, RJ Deshaies, RI Enchev; Structural and kinetic analysis of the COP9-Signalosome activation and the cullin-RING ubiquitin ligase deneddylation cycle. eLife (2016); PMID: 27031283; DOI: 10.7554/eLife.12102

2.1 Summary

The COP9-Signalosome (CSN) regulates cullin–RING ubiquitin ligase (CRL) activity and assembly by cleaving Nedd8 from cullins. Free CSN is autoinhibited, and it remains unclear how it becomes activated. We combine structural and kinetic analyses to identify mechanisms that contribute to CSN activation and Nedd8 deconjugation. Both CSN and neddylated substrate undergo large conformational changes upon binding, with important roles played by the N-terminal domains of Csn2 and Csn4 and the RING domain of Rbx1 in enabling formation of a high affinity, fully active complex. The RING domain is crucial for deneddylation, and works in part through conformational changes involving insert-2 of Csn6. Nedd8 deconjugation and re-engagement of the active site zinc by the autoinhibitory Csn5 glutamate-104 diminish affinity for Cul1/Rbx1 by ~100-fold, resulting in its rapid ejection from the active site. Together, these mechanisms enable a dynamic deneddylation-disassembly cycle that promotes rapid remodeling of the cellular CRL network.

2.2 Introduction

Cullin–RING ubiquitin ligases comprise one of the largest families of regulatory enzymes in eukaryotic cells (Deshaies and Joazeiro, 2009a). With as many as 240 different enzyme complexes, these E3s control a broad array of biological processes (Skaar et al., 2013). CRLs comprise seven distinct cullin–RING cores, each of which interacts with its own dedicated set of adaptor–substrate receptor complexes. Although ubiquitination by CRL enzymes is often regulated by covalent modifications of the substrate that stimulate binding to the substrate receptor, the CRL enzymes themselves are also subject to regulation.

A key mechanism that controls the activity of all known CRLs is the conjugation of the ubiquitin-like protein Nedd8 to a conserved lysine residue in the cullin subunit (e.g. K720 in human Cul1) (Enchev et al., 2015). The available structural and biochemical data indicate that Nedd8 conjugation (neddylation) stabilizes a profound conformational change in the C-terminal domain of the cullin. It loosens the interaction of the WHB domain with the RING subunit, allowing both of them to sample a greater conformational space (Duda et al., 2008), thereby enhancing the ability of the RING domain to promote ubiquitin transfer to substrate (Duda et al., 2008; Saha and Deshaies, 2008; Yamoah et al., 2008).

In addition to direct effects on ubiquitin ligase activity, Nedd8 also protects Skp1/Cul1/F-box (SCF) complexes from the substrate receptor exchange factor (SREF) Cand1 (Pierce et al., 2013; Schmidt et al., 2009; Wu et al., 2013; Zemla et al., 2013). Cand1 binds unmodified SCF complexes and promotes rapid dissociation of the F-box protein (FBP)/Skp1 substrate receptor–adaptor module from the Cul1/Rbx1 core. Cand1 can subsequently be dissociated from Cul1 by a different FBP/Skp1 complex, and as a result Cand1 functions as an SREF that accelerates the rate at which Cul1/Rbx1 comes to equilibrium with different FBP/Skp1 substrate receptor–adaptor complexes (Pierce et al., 2013). Importantly, the SREF activity of Cand1 is tightly restricted by Nedd8. Cand1 is not able to bind stably to Cul1 and promote dissociation of FBP/Skp1 when Cul1 is conjugated to Nedd8 (Liu et al., 2002; Pierce et al., 2013). These observations underscore

the importance of neddylation not only for controlling the enzymatic activity of CRLs, but also potentially for controlling the repertoire of assembled CRLs.

The key role of Nedd8 in CRL biology highlights the importance of the enzymatic pathways that attach and remove Nedd8 (Enchev et al., 2015). Of particular significance is the rate of Nedd8 deconjugation, because it serves as the gateway for the exchange cycle; once Nedd8 is removed, a CRL complex is susceptible to the potent SREF activity of Cand1, and its substrate receptor can be exchanged (Pierce et al., 2013). Deconjugation of Nedd8 is mediated by the COP9-signalosome (CSN), which is an eight-subunit Nedd8 isopeptidase (Lyapina et al., 2001). The enzymatic activity of CSN resides in its Csn5 subunit, which contains a metalloprotease active site referred to as the 'JAMM' domain (Cope et al., 2002). The JAMM domain has the general structure E_{76}-Xn-H_{138}-X-H_{140}-X10-D_{151} (the subscripts refer to the sequence position of these residues in human Csn5), wherein the H and D residues coordinate a zinc ion. The fourth zinc-coordination site is occupied by a water molecule that that also forms a hydrogen bond to E76 (Ambroggio et al., 2004; Sato et al., 2008; Tran et al., 2003). Deneddylation of CRLs by CSN is rapid but can be regulated by CRL substrates (Emberley et al., 2012; Enchev et al., 2012; Fischer et al., 2011b). Structural analysis suggests that a CRL ubiquitination substrate bound to a substrate receptor sterically prevents concurrent binding of CSN (Enchev et al., 2012; Fischer et al., 2011b). This suggests a model wherein a CRL complex has a higher probability of being conjugated to Nedd8 (and therefore of being shielded from Cand1) as long as it is bound to substrate. Upon dissociation of substrate, a race ensues between binding of either a new substrate or CSN. If CSN wins, Nedd8 is removed, paving the way for Cand1 to initiate substrate receptor exchange.

Recently, a crystal structure of free CSN was determined (Lingaraju et al., 2014). A major insight to emerge from the structure was the unexpected finding that Csn5 was present in an autoinhibited state, wherein a glutamate (Csn5-E104) within the 'insert-1' (INS1) sequence common to JAMM family members (Sato et al., 2008) forms a fourth ligand to the zinc, displacing the catalytic Csn5-E76-bound water molecule and shifting Csn5-E76. Csn5-E104 is found in all Csn5 orthologs, but not in other JAMM proteins, suggesting that

this mode of regulation is conserved but unique to CSN. Comparison of the structure of free CSN to the structure of a catalytically-dead mutant CSN bound to Nedd8-conjugated SCF^{Skp2} determined by negative stain electron microscopy (Enchev et al., 2012) implied that binding of substrate to CSN may induce several conformational changes in the latter, including movement of the N-terminal domains (NTD) of Csn2 and Csn4 towards the cullin. The latter movement, in turn, might be further propagated to the Csn5/6 module (Lingaraju et al., 2014). Moreover, it is reasonable to expect that during catalysis INS1 moves out of the active site and Csn5-E76 adopts a position similar to that observed in a crystallographic structure of Csn5 in isolation (Echalier et al., 2013). Interestingly, if Csn5-E104 is mutated to an alanine, CSN more rapidly cleaves the simple model substrate ubiquitin-rhodamine (Lingaraju et al., 2014). This was interpreted to mean that the primary reason for the autoinhibited state is to keep CSN off until it binds a physiologic substrate, which would prevent spurious cleavage of non-cullin Nedd8 conjugates and possibly even ubiquitin conjugates. However, the full extent of the conformational changes required to form an activated complex between CSN and its neddylated substrate, as well as the detailed molecular basis for these changes, remains to be established. Therefore, at present, the mechanism of how CSN is switched on and off and the significance of this switching behavior remains unknown.

2.3 Results

Structural insights from cryo EM and single particle analysis of a CSN-SCF-Nedd8Skp2/Cks1 complex

To gain detailed insights into the molecular determinants underlying activation of CSN, we performed cryo electron microscopy (cryo EM) and single particle analysis of CSN^{5H138A} (we use the nomenclature $CSN^{\#x}$ where # refers to subunit number and x to the specific mutation) in complex with neddylated $SCF^{Skp2/Cks1}$ (the sample is described in Enchev et al., 2012) (Figure 2.1A – figure supplements 2.1A–D). The Csn5-H138A mutant lacks one of the JAMM ligands that coordinate the catalytic zinc. This mutant forms a normal CSN complex that has been extensively characterized (Enchev et al., 2012). We

used ~75000 single molecular images for the final three-dimensional reconstruction and the structure was refined to a nominal resolution of 7.2 Å, according to the 'gold standard' criterion of a Fourier shell correlation (FSC) of 0.143 (Rosenthal and Henderson, 2003; Scheres and Chen, 2012) (Figure 2.1–figure supplements 2.1C–D). However, some regions in the density map were better defined than others (see below). To avoid over-interpretation, for the subsequent analysis we low-pass filtered the map to 8.5 Å, according to the more stringent criterion of an FSC of 0.5.

The cryo EM structure reported here, alongside the available crystal structure of CSN (Lingaraju et al., 2014), enabled us to visualize a broad array of conformational changes that take place upon complex formation in both CSN and neddylated Cul1/Rbx1, well beyond what was possible with the prior lower resolution model based on negative stain EM (Figure 2.1). Specifically, this allowed us to describe movements of the N-terminal domains of Csn2 and Csn4, the MPN domains of Csn5 and Csn6. Moreover, in contrast to our previous work, we could locate the RING domain of Rbx1, as well as Nedd8 and the winged-helix B (WHB) domain of Cul1 relative to Csn5. Nevertheless, the present resolution precludes the determination of the exact orientations of the latter domains, but notably the relative positions of the RING, WHB, and Nedd8 reported here have not been reported in any structural model of a cullin, and strongly suggest that both the enzyme and substrate undergo significant conformational rearrangements to enable catalysis.

To obtain the model shown in Figure 2.1, we initially docked the crystal structure of CSN (Lingaraju et al., 2014) and a model of Cul1-Nedd8/Rbx1/Skp1/Skp2/Cks1 (Enchev et al., 2012) as rigid bodies into the electron density map (Figure 2.1–figure supplements 2.1E–H). We observed very good matches between the respective map segments and the atomic coordinates for the scaffold subunits Csn1, Csn3, Csn7, and Csn8, the winged-helix domains of Csn2 and Csn4 (Figure 2.1–figure supplement 2.1E), and the helical bundle formed by the C-termini of all eight CSN subunits (Figure 2.1–figure supplement 2.1F) as well as the expected recovery of secondary structure at this resolution. Similarly, there was a very good overlap between the coordinates of Cul1 (with the exception of helix29 and the WHB domain, see below) and Skp1 and the corresponding electron density segments

(Figure 2.1–figure supplement 2.1G). However, the local resolution was lower without recovery of secondary structure in the N-terminal domain of Cul1. Moreover, the density of the substrate receptor Skp2/Cks1 was poorly defined (Figure 2.1–figure supplement 2.1G), indicating a potential flexibility in this region. Since the presence of Skp1/Skp2 had modest effects on the affinity and deneddylation activity (see below), we did not interpret this observation further.

In contrast to the large segments of CSN that were unaltered upon binding substrate, there was nearly no overlap between the EM density map and the N-terminal portions of Csn2 and Csn4, as well as the MPN-domains of Csn5 and Csn6, the RING domain of Rbx1, the WHB domain of Cul1, and Nedd8 (Figure 2.1–figure supplement 2.1H). We thus docked these domains individually (Figure 2.1B). A Csn2 N-terminal fragment encompassing the portion between its crystallographically resolved N-terminus (amino acid 30) through to a flexible loop at amino acid 180 was docked as a rigid body (Figure 2.1–figure supplement 2.1I), positioning it close to the four-helical bundle and helix 24 of Cul1 (Zheng et al., 2002b). An N-terminal fragment of Csn4, spanning amino acids 1 to 295, which ends in a previously reported hinge loop (Lingaraju et al., 2014), was also docked independently as a rigid body (Figure 2.1–figure supplement 2.1J). The resulting conformation of Csn4 resembles a crystal form of Csn4 observed in isolation (Lingaraju et al., 2014). The two N-terminal helical repeat motifs of Csn4 make contacts with the winged-helix A domain of Cul1 (Figure 2.1B and Figure 2.1–figure supplement 2.1J, right hand panel, red arrow and green circle). Moreover, these positions of Csn2 and Csn4 delineated a density in the map, which could accommodate the RING domain of Rbx1 (Figure 2.1B and Figure 2.1–figure supplement 2.1J, right hand panel, black ellipse), with the RING proximal to two conserved helices between amino acids 160 and 197 of Csn4 (Figures 2.1B and Figure 2.1–figure supplement 2.1K, black arrow) and a loop in Csn2 located between residues 289 and 306. The exact orientation of the RING domain awaits a structure at higher resolution.

To improve the fit of Csn5 and Csn6, we moved their MPN domains as rigid bodies into the neighboring map segment of similar shape and dimensions (Figure 2.1–figure supplement 2.1L). The local resolution in this region was lower, presumably due to higher

flexibility around the catalytic site. Importantly, after docking Csn5, we observed two empty neighboring densities (Figure 2.1–figure supplement 2.1L, right hand panel, circles), which accommodated the two yet undocked protein components – Nedd8 and the WHB domain of Cul1 (Figure 2.1–figure supplement 2.1M). The docking of the latter was enabled by allowing helix 29 and the WHB, amino acids 690 to the C-terminus of Cul1, to move as a rigid body towards Csn5. However, we did not observe an electron density around helix 29 of Cul1, consistent with a structural flexibility in this region. This model places the neddylated WHB domain in close binding proximity to the RING domain, as well as both INS1 and INS2 of Csn5. The hydrophobic patch of Nedd8 is facing INS1, and not the WHB domain, as has been reported for the isolated neddylated C-terminal domain of Cul5 (Duda et al., 2008). Similar to the RING domain, we cannot be fully certain about the exact orientations of Nedd8 and the WHB domain at the present resolution. Nevertheless, to further substantiate this docking, we mutagenized conserved charged residues in the INS2 domain of Csn5 as well as the WHB domain, and as expected all of these constructs showed reduced catalytic activity in deneddylation assays (Figure 2.1–figure supplement 2.1N, O).

We sought orthogonal experimental validation for the molecular docking of the individual subunits and domains in the electron density map by performing cross-linking coupled to mass spectrometric analysis of the cross-linked peptides (Leitner et al., 2014) following the procedure described in (Birol et al., 2014)(Supplemental tables 2.1-2.5). For the cross-linker used in this study (disuccinimidylsuberate H_{12}/D_{12}), the maximum predicted distance between two cross-linked lysine residues is generally accepted to be below ~ 30 Å (Politis et al., 2014). As shown in supplementary files 1, out of the 39 high-confidence inter-subunit cross-links detected within the CSN^{5H138A}–N8-$SCF^{Skp2/Cks1}$ complex at a false discovery rate (FDR) of 5 percent, the great majority was within regions of modeled atomic structure and only six links exhibited a distance larger than 30 Å when mapped onto our model. However, all of these larger-distance links are connected to the flexibly positioned Skp2 density. Moreover, we further performed similar cross-linking experiments on a number of different CSN-CRL complexes, varying the substrate receptor, the cullin, and the neddylation state (Supplemental tables 2.1-2.5). All results were consistent with the

architecture proposed here for CSN^{5H138A}-N8-$SCF^{Skp2/Cks1}$. Intriguingly, when taking into account cross-links with an FDR of up to 0.25 (Supplemental tables 2.2 and 2.3), we found two cross-links that support proximity of K290 in Csn4 and K89 in the RING domain (Supplemental table 2.2), as well as K32 in Csn4-NTD and K587 in Cul1, which is in the immediate vicinity of the WHA domain of Cul1 (Supplemental table 2.3), as suggested by our EM reconstruction.

Development and validation of an assay to measure binding of CSN to substrate and product.

To understand how the structure of CSN and the CSN–SCF complex relates to substrate binding and the mechanism of deneddylation, we sought to develop quantitative binding assays to measure interaction of CSN with its substrates and products. To this end, the environmentally-sensitive dye dansyl was conjugated to the C-terminus of Cul1 using 'sortagging' (Theile et al., 2013) to generate dansylated Cul1/Rbx1 ($Cul1^{d}$/Rbx1)(Figure 2.2–figure supplement 2.2A). $Cul1^{d}$/Rbx1 exhibited normal E3 activity (Figure 2.2–figure supplement 2.2B) and bound CSN with an affinity similar to Cul1/Rbx1 based on their IC_{50} values for competitive inhibition of a deneddylation reaction (Figure 2.2–figure supplement 2.2C; Emberley et al., 2012). When $Cul1^{d}$/Rbx1 was incubated with CSN (all CSN preparations used in this work are shown in Figure 2.2–figure supplement 2.2D), we observed an increase in dansyl fluorescence (Figure 2.2A). This signal was due to specific binding because it was chased upon addition of excess unlabeled Cul1/Rbx1 (Figure 2.2A, titration shown in Figure 2.2–figure supplement 2.2E) or Cand1 (Figure 2.2–figure supplement 2.2F), which competes for substrate deneddylation by CSN (Emberley et al., 2012; Enchev et al., 2012). Thus, we concluded that the increase in dansyl fluorescence accurately reported on the interaction of CSN with $Cul1^{d}$/Rbx1. Using this assay we determined that CSN bound $Cul1^{d}$/Rbx1 with a K_d of 310 nM (Figure 2.2B). $Cul1^{d}$/Rbx1 binding to CSN was only modestly affected by the addition of free Nedd8 (Figure 2.2–figure supplement 2.2G) or assembly with Skp2/Skp1 (Figure 2.2–figure supplement 2.2H) or Fbxw7/Skp1 (Figure 2.2–figure supplement 2.2I).

We next sought to measure binding of neddylated Cul1^{d}/Rbx1 (Cul1^{d}-N8/Rbx1) to CSN but it was not possible because the substrate was rapidly deneddylated. To circumvent this problem, we performed binding assays with the extensively characterized inactive mutant CSN^{5H138A} (assay confirming loss of activity is shown in Figure 2.2–figure supplement 2.2A). Remarkably, CSN^{5H138A} bound Cul1^{d}-N8/Rbx1 ~200-fold more tightly than CSN bound Cul1^{d}/Rbx1 (K_d 1.6 nM vs. 310 nM; Figures 2.3A–B). Note that the estimated K_d falls well below the fixed concentration of Cul1^{d}-N8/Rbx1 used in the assay. This introduces greater uncertainty into our estimate but nevertheless we can conclude with confidence that the binding of substrate to CSN^{5H138A} is very tight (≤5 nM; see Materials and Methods for further discussion of this matter). As reported above for CSN binding to product, addition of Skp2/Skp1 or Fbxw7/Skp1 had comparatively minor effects on affinity (Figure 2.3–figure supplements 2.3B–C). Thus, for the sake of simplicity, we used Cul1^{d}/Rbx1 heterodimer for the remaining binding experiments.

The strikingly high affinity we observed for binding of CSN^{5H138A} to Cul1^{d}-N8/Rbx1 led us to question whether it was mainly due to Nedd8 or whether the H138A mutation might also enhance affinity. To this end, we measured binding of CSN^{5H138A} to Cul1^{d}/Rbx1 and observed an unexpectedly low K_d of ~10 nM (Figure 2.3B, Figure 2.3–figure supplement 3D), which was confirmed with an independent preparation of CSN^{5H138A} (Figure 2.3–figure supplement 2.3E). Thus, neddylation improved affinity of Cul1^{d}/Rbx1 for CSN^{5H138A} by ~6-fold, whereas the Csn5-H138A mutation improved affinity for Cul1^{d}/Rbx1 by ~30-fold. The high affinity binding of CSN^{5H138A} to substrate was supported by an orthogonal competition experiment in which 100 nM CSN^{5H138A} completely blocked deneddylation of 75 nM Cul1-N8/Rbx1 (Figure 2.3–figure supplement 2.3A). We considered the possibility that the Csn5-H138A mutation might enable formation of an aberrant, super-tight enzyme:substrate ([ES]) complex that does not normally form between the wild type proteins. However, as will be described later on, this hypothesis was rejected based on kinetic arguments.

We next sought to determine whether the large differences we observed in K_d values were due to differences in k_{on} or k_{off}. Remarkably, despite a 200-fold difference in K_d for

CSN^{5H138A} binding to substrate compared to CSN binding to product, the k_{on} values for formation of these complexes were nearly identical (2.0×10^7 M^{-1} sec^{-1} for CSN–product and 2.2×10^7 M^{-1} sec^{-1} for CSN^{5H138A}–substrate; Figure 2.3C). This suggested that the difference in affinity was driven by a large difference in k_{off}. To test this hypothesis, we directly measured k_{off} values for select [ES] and enzyme-product complexes by pre-forming the complex and then adding excess unlabeled Cul1/Rbx1 chase and monitoring the reduction in dansyl fluorescence over time (Figure 2.3C and Figure 2.3–figure supplement 3F-I; for this and a subsequent experiment in Figure 2.4B, we used $CSN^{5E76A/\ 5H138A}$ in one of the assays instead of CSN^{5H138A}; the double mutant behaved like CSN^{5H138A} in that it bound $Cul1^{d}$/Rbx1 with the same affinity as shown in Figure 2.3–figure supplement 2.3J.). Consistent with the predictions from the K_d and k_{on} values, substrate dissociated very slowly from $CSN^{5E76A,5H138A}$, whereas product dissociated ~65-fold faster from CSN. This suggests that as substrate is deneddylated to product, its affinity for CSN is strongly reduced and its k_{off} speeds up.

The N-terminal domains of Csn2 and Csn4 and the RING of Rbx1 promote enzyme–substrate interaction.

Armed with assays to measure binding and deneddylation of substrate, we next sought to test the implications that emerged from our structural analysis of the CSN^{5H138A}–N8-$SCF^{Skp2/Cks1}$ complex. First, we investigated the roles of the NTDs of Csn2 and Csn4, both of which, upon binding substrate, underwent conformational changes and made contact with Cul1 and the RING domain of Rbx1 (Figures 2.1B–C, Figure 2.1–figure supplements 2.1I–K) (Lingaraju et al., 2014). To measure the effect of these mutations on binding to $Cul1^{d}$-N8/Rbx1, we combined them with Csn5-H138A to prevent deneddylation. Deletion of the first 269 amino acids of Csn2, observed to interact with Cul1 but not the RING domain of Rbx1, caused a massive loss in binding to substrate (K_d > 1300 nM; Figure 2.3B, Figure 2.3–figure supplement 2.3K). Thus, the contact we observed between Csn2-NTD and N8-$SCF^{Skp2/Cks1}$ was critical to formation of the [ES] complex. By contrast, deletion of the first 297 amino acids NTD of Csn4 (4ΔN), a portion which was observed to form interfaces with both Cul1 and the RING domain of Rbx1, had a relatively modest effect;

$CSN^{4\Delta N,5H138A}$ bound $Cul1^{d}$/Rbx1 and $Cul1^{d}$-N8/Rbx1 with K_d values of > 750 nM and 20 nM, respectively (Figure 2.3B, Figure 2.3–figure supplement 2.3L-M).

In addition to the motions of the Csn2 and Csn4 NTDs, our structural analysis revealed formation of substantial interfaces between CSN and the RING domain of Rbx1. To test the role of the RING domain in complex formation, we generated both Cul1/Rbx1 and $Cul1^{d}$/Rbx1 in which the RING domain can be deleted by introducing a TEV protease cleavage site (Dougherty et al., 1989) after residue 37 of Rbx1 to generate Cul1 (or $Cul1^{d}$)/$Rbx1^{TEV}$ (Figure 2.4A). This was essential, because it would not be possible to conjugate Nedd8 to Cul1/Rbx1 expressed as a mutant lacking the RING domain. After conjugating Nedd8 to the purified complex, we treated it with TEV protease to remove the RING domain, yielding Cul1 (or $Cul1^{d}$)-N8/$Rbx1^{\Delta RING}$ (Figure 2.4A). The truncated Cul1/$Rbx1^{\Delta RING}$ was inactive in an ubiquitylation assay (Figure 2.4–figure supplement 2.4A) but behaved as a monodisperse sample with the expected hydrodynamic radius upon size exclusion chromatography (Figure 2.4–figure supplement 2.4B). Notably, $Cul1^{d}$-N8/$Rbx1^{\Delta RING}$ bound $CSN^{5E76A,5H138A}$ and CSN^{5E76A} with affinities (12 nM and 13 nM respectively; Figure 2.3B, Figure 2.3–figure supplement 2.3N) similar to that observed for binding of wild type $Cul1^{d}$-N8/Rbx1 to $CSN^{4\Delta N,5H138A}$. Given the similar effects of the Csn4-ΔNTD and Rbx1-ΔRING mutations on complex formation, we next tested whether their effects arose from loss of the interface that forms between these domains (Figure 2.1–figure supplement 2.1K). However, double mutant analysis suggested that the Csn4-ΔN and Rbx1-ΔRING mutations had largely independent effects on binding (Figure 2.4B). The overall picture that emerged from these studies in light of the structural data is that the interaction of Csn2-NTD with neddylated substrate makes a large contribution to binding energy, with modest enhancements independently provided by the Csn4-NTD and Rbx1-RING domains.

The 'E-vict' enables efficient clearance of product from the CSN active site

The striking difference in the K_d for CSN^{5H138A} binding to substrate compared to CSN binding to product suggested that a conformational rearrangement of the [ES] complex

occurs upon cleavage of the isopeptide bond, resulting in a large increase in the product k_{off}, and thereby preventing the enzyme from becoming product-inhibited. However, we were puzzled by the relatively minor impact of Nedd8 on the affinity of Cul1^{d}/Rbx1 for CSN^{5H138A}; whereas substrate bound with K_d of 1.6 nM, product binding was only ~6-fold weaker (Figure 2.3B). Why, then, did CSN bind so much less tightly to product? We reasoned that a key difference between CSN^{5H138A} and CSN is the absence of the active site zinc from CSN^{5H138A}, which prevents formation of a stable apo-CSN complex in which E104 of the INS1 domain of Csn5 is bound to the active site zinc. If this conjecture is correct, it makes the prediction that CSN^{5E104A}, which should also be unable to form stable apo-CSN, should likewise exhibit high affinity for product. This was confirmed: CSN^{5E104} bound Cul1^{d}/Rbx1 with a K_d of 26 nM (Figure 2.3B, Figure 2.3–figure supplement 2.3O). Furthermore, measurement of k_{off} values revealed that product dissociated from CSN^{5H138A} and CSN^{5E104A} about 8-fold more slowly than it dissociated from CSN (Figure 2.3C). Based on these observations, we propose the 'E-vict' hypothesis, which is described in more detail in the Discussion. The essence of this hypothesis is that, following cleavage of the isopeptide bond and dissociation of Nedd8, INS1 of Csn5 engages the active site zinc. This accelerates the rate of dissociation of deneddylated Cul1/Rbx1, thereby preventing CSN from becoming clogged with product. We note that Csn5-E76 also contributes to the operation of this mechanism, because CSN^{5E76A} bound tightly to product (Figure 2.3–figure supplement 2.3P). We speculate that engagement of the active site zinc by Csn5-E104 forces Csn5-E76 into a configuration that promotes egress of product. Further insights into the exact sequence of events that accelerates product dissociation await high-resolution structures of CSN bound to Cul1/Rbx1 in various states.

Kinetic effects of binding-defective mutations on substrate deneddylation

We next sought to address the effects of the enzyme and substrate mutations described in the preceding sections on the deneddylation reaction. We previously showed that CSN$^{2\Delta N}$ has severely reduced catalytic activity (Enchev et al., 2012), which is consistent with the binding data reported here. CSN$^{4\Delta N}$ exhibited a 20-fold defect in substrate cleavage (Figure 2.5A, Figure 2.5–figure supplement 2.5A). Meanwhile, the k_{cat} for cleavage of Cul1-

N8/Rbx1$^{\Delta RING}$ by CSN was reduced by a staggering ~18,000-fold relative to wild type substrate (Figures 2.5A–B). Given that the neddylated ΔRING substrate bound to CSN with only modestly reduced affinity, we surmised that the principal defect of this mutant might be its failure either to induce the activating conformational change in CSN, and/or to position accurately the isopeptide bond in the active site. Although we do not have the tools to address the latter point, we queried the former by examining the Csn6-ΔINS2 mutation, which partially mimics the effect of substrate binding in that it destabilizes the autoinhibited state (Lingaraju et al., 2014). The Csn6-ΔINS2 mutation slightly weakened binding to wild type product (Figure 2.3B, Figure 2.3–figure supplement 2.3Q) but completely suppressed the modest binding defect of the neddylated ΔRING substrate (Figure 2.3B, Figure 2.3–figure supplement 2.3R) and promoted an ~8-fold increase in its deneddylation rate (Figure 2.5–figure supplement 2.5B). This partial suppression effected by Csn6-ΔINS2 suggests that the RING domain contributes to the constellation of conformational changes in CSN that occur upon substrate binding. Note that the CSN$^{6\Delta INS2}$ enzyme nevertheless exhibited a > 1,000-fold defect towards the Cul1-N8/Rbx1$^{\Delta RING}$ substrate, strongly indicating further functions of the RING domain, which may include a potential role in substrate positioning as well.

A noteworthy feature of the deneddylation reactions carried out with CSN$^{4\Delta N}$ enzyme or ΔRING substrate is that although k_{cat} was reduced in both cases, K_M was also reduced (Figure 2.5A). Whereas these results imply that deletion of the Csn4-NTD or Rbx1-RING improved affinity of the [ES] complex, our direct binding measurements indicated this was not the case. To understand this apparent paradox, it is essential to consider the kinetic behavior of CSN-mediated deneddylation. The formal definition of K_M for a deneddylation

Equation 1: Cul1-N8/Rbx1 deneddylation by CSN. The vertical red bar indicates the cleaved bond.

$$[\text{CSN}] + [\text{Cul1-N8/Rbx1}] \underset{k_{off}}{\overset{k_{on}}{\rightleftharpoons}} [\text{CSN–Cul1-N8/Rbx1}] \xrightarrow{k_{cat}} [\text{CSN–Cul1} \mid \text{N8/Rbx1}]$$

reaction (Equation 1), as stipulated by Briggs and Haldane (Briggs and Haldane, 1925), is: $K_M = (k_{off} + k_{cat})/k_{on.}$. In the special case of Michaelis-Menten kinetics, which is based on the assumption that k_{off} is much larger than k_{cat}, the expression simplifies to k_{off}/k_{on}, or K_d.

However, k_{cat} for CSN (~1.1 sec^{-1}) is actually much faster than k_{off} measured for dissociation of substrate from the $CSN^{5E76A, 5H138A}$ mutant (0.017 sec^{-1}). The implication of this is that almost every binding event between CSN and substrate results in catalysis, and K_M (200 nM; Figure 2.5A and (Emberley et al., 2012) is much larger than K_d (1.6 nM, Figure 2.3B). But, if k_{cat} is reduced by mutation, the Briggs-Haldane equation predicts that K_M should approach K_d. Indeed, this is exactly what we see for reactions that exhibit reduced k_{cat}, including reactions with mutant $CSN^{4\Delta N}$ enzyme or mutant ΔRING substrate (Figure 2.5A). In the slowest reaction (cleavage of $Cul1/Rbx1^{\Delta RING}$ by CSN) the K_M (5 nM) is in the same range as the K_d with which this substrate bound to $CSN^{5E76A, H138A}$ (12 nM; Figure 2.3B), and approaches the K_d measured for binding of substrate to CSN^{5H138A} (1.6 nM). This provides strong support for our proposal that the CSN^{5H138A}–$Cul1^{d}$/Rbx1 complex is representative of the affinity that develops during normal catalysis.

Functional significance of Csn5 INS1 *in vitro* and in cells

To understand the significance of the E-vict mechansim to CSN function *in vitro* and in cells, we measured the k_{cat} for CSN^{5E104A} and observed that it is 2.5-fold slower than for CSN (Figure 2.5A, Figure 2.5–figure supplements 2.5C–E). This was unexpected, because it was reported that the Csn5-E104A mutation enhances the catalytic activity of CSN towards an unnatural substrate (Lingaraju et al., 2014). Interestingly, a similar reduced rate was observed in both single- and multi-turnover reactions, indicating that under our specific reactions conditions, the activating conformational changes/chemical step are affected at least as much as product dissociation. This may not be the case in cells, where substrate receptors and other factors may further stabilize product binding.

To test if Csn5-E104 contributes to CSN function *in vivo*, we generated a partial knockout of Csn5 in HEK293T cells using CRISPR/Cas9 (Shalem et al., 2014). This cell line expressed severely reduced levels of Csn5 and consequently displayed hyper-accumulation of Nedd8-conjugated endogenous Cul1 (Figure 2.6A), but retained sufficient protein to survive. We introduced either an empty retrovirus or retroviruses coding for Flag-tagged wild type or mutant Csn5 proteins into these cells, and then monitored the Cul1 neddylation

status by immunoblotting. In contrast to wild type ^{Flag}Csn5, cells expressing ^{Flag}Csn5-E104A, H138A, or E76A did not regain a normal pattern of Cul1 neddylation (Figure 2.6A). The same was observed for Cul2, Cul3, Cul4A, and Cul5 (Figure 2.6–figure supplement 2.6A). Consistent with reduced CSN activity, as revealed by increased cullin neddylation, Skp2 levels were reduced in cells expressing mutant Csn5 proteins (Figure 2.6A) (Cope and Deshaies, 2006; Wee et al., 2005). To test whether mutations in the catalytic site of Csn5 resulted in increased affinity for Cul1, we immunoprecipitated wild type and mutant ^{Flag}Csn5 proteins and probed for co-precipitation of endogenous Cul1. In addition to the mutants described above, we surveyed a much broader panel of catalytic site substitutions to determine whether the results observed in our *in vitro* experiments were specific to the mutations employed or were a general consequence of disrupting the active site. As shown in Figure 2.6B, the results were concordant with what was observed *in vitro*. On the one hand, ^{Flag}Csn5–H138A retrieved high levels of Cul1-N8. The same was true for ^{Flag}Csn5 carrying mutations in other core residues of the JAMM domain (e.g. H140 and D151) (Cope et al., 2002). On the other hand, ^{Flag}Csn5-E104A retrieved high levels of unmodified Cul1. We propose that this arises from its ability to bind and deneddylate substrate (albeit at a reduced rate), but then remain tightly bound to the product due to loss of the E-vict mechanism.

The unexpected reduction in activity observed for Csn5-E104A both *in vitro* and in cells (Figures 2.5A, 2.6A) suggested that the adjacent residue, T103, may also be important for deneddylation. A T103I mutation in *Drosophila melanogaster* impedes proper interaction of photoreceptor neurons with lamina glial cells in the developing brain. If this mutant also causes a loss of CSN deneddylase activity, it would explain the recessive nature of this mutation in flies (Suh et al., 2002). Indeed, like Csn5-E104A, Csn5-T103I did not restore a normal Cul1 neddylation pattern when expressed in Csn5-depleted cells (Figure 2.6C) and exhibited low deneddylase activity *in vitro* (Figures 2.5A, Figure 2.5–figure supplement 2.5F). In contrast to CSN^{5E104A}, however, CSN^{5T103I} bound Cul1^{d}/Rbx1 product with low affinity, both *in vitro* (Figure 2.3B, Figure 2.3–figure supplement 2.3S) and in cells (Figure 2.6B). Therefore, although CSN^{5E104A} and CSN^{5T103I} both have diminished catalytic activity, their defects appear to have distinct molecular bases. To further explore

the divergent effects of Csn5-E104A and Csn5-T103I mutations on Cul1 binding, HEK293T stably expressing wild type or mutant versions of ^{Flag}Csn5 were grown in 'heavy' SILAC medium (wild type), or 'light' SILAC medium (mutants). Each mutant lysate was individually mixed with wild type lysate, and then subjected to immunoprecipitation and SILAC mass spectrometry. Whereas all CSN subunits exhibited light:heavy ratios of ~1 (Figure 2.6–figure supplement 2.6B), the ^{Flag}Csn5-E104A pull-down showed elevated levels of all cullins compared to wild type, whereas ^{Flag}Csn5-T103I pulled down cullins at levels equal to or less than wild type ^{Flag}Csn5 (Figure 2.6D).

2.4 Discussion

'Induced fit' underlies interaction of substrate with CSN and triggers enzyme activation

Figure 2.7 displays a model that incorporates published data and data presented in this manuscript. Panels A-C show a schematic view of the structural transitions that occur upon substrate binding, and collectively contribute to efficient catalysis, whereas panel D provides the rate constants for the deneddylation cycle. We tentatively propose the following sequence of events. Free CSN exists in an inactive state in which E104 of Csn5-INS1 forms a fourth ligand to zinc (Figure 2.7A) (Lingaraju et al., 2014). In this state the NTDs of both Csn2 and Csn4 are in "open" conformations relative to the cullin substrate, and the MPN domains of Csn5/Csn6 are in a distal position relative to it. Substrate binds this state rapidly (Figure 2.7B), likely driven by electrostatic interactions between Cul1 and Csn2-NTD. This would account for the similar, extremely fast k_{on} values that we measured for different combinations of Cul1^{d}/Rbx1 and CSN. Binding of CSN to neddylated substrate results in a series of conformational changes in both complexes (Figure 2.7B). These include (i) the translocation of the N-terminal helical repeats of Csn2 towards the CTD of Cul1, (ii) the movement of the NTD of Csn4 towards the RING domain of Rbx1 and the WHA domain of Cul1, (iii) the translocation of the MPN domains of Csn5–Csn6 towards the neddylated WHB domain of Cul1, (iv) movement of the WHB domain towards Csn5, (v) the opening of the interface between Nedd8 and the WHB domain, and

(vi) the formation of a new interface between Csn5 and Nedd8 probably involving the hydrophobic patch of Nedd8 and neighboring residues, as well as a tenuous interface between the WHB and the Rbx1 RING domain. Furthermore, although not structurally resolved in the present study, movements of Csn5-E76 and E104 towards and away from the zinc atom (vii), respectively, probably similar to the conformation reported in (Echalier et al., 2013), must occur to enable catalysis. Finally, a series of other unresolved movements are likely to be germane including (viii) positioning of the extended C-terminus of Nedd8, and the corresponding portion of the WHB domain for catalysis as well as contacts between the INS1 and INS2 domains of Csn5 and the WHB domain of Cul1.

To probe the significance of the conformational changes summarized above, we generated and analyzed mutant enzymes. Deletion of Csn2-NTD virtually eliminated substrate binding (Figure 2.3–figure supplement 2.3K), suggesting that movement of this domain (motion i) enables a high affinity interaction between CSN and neddylated CRLs. Meanwhile a mutant lacking Csn4-NTD, $CSN^{4\Delta N,5H138A}$, bound Cul1-N8/Rbx1 ~10-fold less tightly than CSN^{5H138A}, albeit still with a relatively high affinity (20 nM, Figure 2.3B). A similar effect on binding affinity was seen with a substrate lacking the RING domain of Rbx1 (Figure 2.3B). Even though the RING and Csn4-NTD domains are adjacent in the enzyme-substrate [ES] complex (Figure 2.1), double mutant analysis suggests that they make substantially independent contributions to binding energy (Figure 2.4B). Interestingly, enzyme assays revealed a much greater effect of deleting the RING than deleting the Csn4-NTD, suggesting that the RING domain makes a profound contribution to catalysis in a manner that does not depend on its proximity to Csn4-NTD. We do not know the extent to which the reduced catalytic rates for these mutants arise from defects in enzyme activation versus substrate positioning, but we note that cleavage of ΔRING substrate was accelerated by ~8-fold upon deletion of Csn6-INS2, suggesting that at least a small part of the problem with this substrate is that it failed to properly trigger activating conformational changes in CSN.

In addition to the movements of individual domains, formation of the [ES] complex is accompanied by wholesale translocation of the Csn5 and Csn6 subunits. We suggest that

this motion contributes primarily a k_{cat} effect, because deletion of Csn6-INS2, which is proposed to facilitate this motion, enhanced k_{cat} but had no noteworthy impact on binding to substrate (Figure 2.3B), and removal of Csn5 from the complex did not substantially affect CSN assembly with substrate (Enchev et al., 2012). We cannot conclude much about the other motions enumerated above, but we note that mutations that are predicted to reside near the interface of the Csn5-INS2 and Cul1-WHB domains cause significant reductions in substrate deneddylation (Figure 2.1–figure supplements 2.1N–O). In addition, reorientation of Nedd8 away from Cul1-WHB and towards Csn5 as predicted here is consistent with the prior observation that the hydrophobic patch of Nedd8 recruits UBXD7 to neddylated CRLs (Besten et al., 2012). Presumably, the conformational changes that occur during the activation process are connected in some manner. Interestingly, CSN^{5E104A} and $CSN^{6\Delta INS2}$ both cleave ubiquitin-rhodamine at 0.04 sec^{-1} (which is ~6-fold faster than wild type CSN), but $CSN^{5E104A,6\Delta INS2}$ is yet 5-fold faster (0.2 sec^{-1}) than either single mutant (Lingaraju et al., 2014). The activities of the single and double mutants imply that the Csn6-ΔINS2 mutation must destabilize binding of Csn5-E104 to the catalytic zinc, but only in a small fraction (≤20%) of complexes. Meanwhile, movements at the Csn4/6 interface must do more to the active site than simply disrupt the interaction of Csn5-E104 with the catalytic zinc, implying the existence of at least two inputs to CSN activation. Resolving how binding of substrate is connected to enzyme activation awaits high-resolution structural analyses of the enzyme and substrate in various states.

A kinetic model for the CSN enzyme cycle reveals an essential role for the E-vict mechanism in sustaining rapid catalysis

Upon formation of an [ES] complex, the conformational changes that occur in both CSN and substrate culminate in cleavage of the isopeptide bond that links Nedd8 to cullin. Although we don't know the microscopic rate constants for the various conformational changes and bond cleavage, all evidence points to the former being slower than the latter, which can occur with $k \geq 6.3$ sec^{-1}, based on the k_{cat} for cleavage of N8-$CRL4A^{DDB2}$ by $CSN^{6\Delta INS2}$ (Lingaraju et al., 2014). The actual cleavage may be even faster because this measurement was made under multi-turnover conditions, in which case product

dissociation may have been rate limiting. Regardless, the sum total rate of the activating conformational motions plus isopeptide bond cleavage reported here (~1 sec^{-1}) is considerably faster than substrate dissociation from CSN^{5H138A} (~0.017 sec^{-1}), indicating that CSN conforms to Briggs-Haldane kinetics and essentially every [ES] complex that forms proceeds to cleavage, the physiological implications of which are considered in the next section.

Cleavage of the isopeptide bond initiates a series of events leading to product release. Removal of Nedd8 increases dissociation of Cul1/Rbx1 by ~7-10 fold. We propose that dissociation of the cleaved Nedd8 also removes an impediment to Csn5-INS1, which can now bind the catalytic site zinc via E104 to return CSN to its apo state. This engagement, which we refer to as the 'E-vict' mechanism, is a critical step in what is likely to be a series of conformational rearrangements that include repositioning of Csn5-E76. Collectively, these movements reduce the affinity of CSN for product and accelerate its rate of dissociation by an additional order of magnitude. The removal of Nedd8 and E-vict together bring about an ~100-fold loss in affinity of Cul1/Rbx1 for CSN. The slow dissociation of product from CSN mutants that were unable to undergo E-vict (0.12-0.16 sec^{-1}; Figure 2.3C) suggests that this mechanism is important for maintaining physiological rates of CRL deneddylation. This is further supported by the observation that Csn5-E104A, but not wild type Csn5, co-precipitates substantial amounts of deneddylated Cul1 from cells (Fig. 2.6B). Slow clearance of product could explain, in part, the failure of this mutant to complement a Csn5 deficiency (Fig. 2.6A). The E-vict mechanism presents an elegant solution to a fundamental challenge facing enzymes: how to achieve high specificity without compromising rapid turnover.

We note that the product k_{off} for $Cul1^{d}$/Rbx1 (1.1 sec^{-1}) is similar to the k_{cat} we measured for both single- and multi-turnover reactions. This suggests that depending on the exact structure of the neddylated CRL substrate, the rate-limiting step may vary from one deneddylation reaction to another. Regardless, our biochemical and cell-based data suggest that if the E-vict mechanism did not exist, product dissociation would become the Achilles heel of deneddylation reactions.

CSN in its cellular milieu

The kinetic parameters reported here coupled with quantitative measurements of protein concentrations by selected reaction monitoring mass spectrometry ((Bennett et al., 2010) and J.R. and R.J.D., unpublished data) allow a preliminary estimate of the steady-state distribution of CSN in cells. The total cullin concentration in the 293T cell line used in this work is ~2200 nM. Meanwhile, the CSN concentration is ~450 nM. Although the total amount of Nedd8-conjugated cullins was not measured, immunoblot data suggest that ~1000 nM is a reasonable estimate. The K_d reported here for the [ES] complex (~2 nM), thus predicts potentially near-complete saturation of the cellular CSN pool with neddylated cullins. This implies that formation of new [ES] complexes is limited by the slowest step in the catalytic cycle, i.e. either the conformational rearrangements or product dissociation. *In vitro*, CSN follows Briggs-Haldane kinetics and cleaves Nedd8 off nearly every neddylated CRL that it binds. Because CSN is not in equilibrium with its substrates in our simplified *in vitro* system, it cannot rely on differences in substrate K_d to achieve specificity. Thus, differences in k_{off} on the order of ≤10-fold, which might occur with different cullins or substrate adaptors, would be predicted to have minimal effects on catalytic efficiency provided that k_{on} remains roughly the same, as was observed for different configurations of substrate and product in this study. Importantly, this parameter can potentially be profoundly altered by ubiquitylation substrates, E2 enzyme, or other *in vivo* binding partners of Nedd8-conjugated CRLs, which compete with CSN (Emberley et al., 2012; Enchev et al., 2012; Fischer et al., 2011b) and thus should reduce its apparent k_{on}. It is also conceivable that binding partners might alter the partitioning of the CSN–N8-CRL complex either by increasing k_{off} and/or reducing k_{cat}, such that N8-CRL bound to an ubiquitylation substrate dissociates prior to completion of the conformational rearrangements that culminate in its deneddylation.

Based on measurements reported here, it is likely that CSN complexes in cells are constantly undergoing catalysis, dissociating rapidly from product, and rebinding other CRLs on the time-scale of a few seconds or less. Consistent with this picture, addition of a Nedd8 conjugation inhibitor to cells leads to nearly complete disappearance of neddylated

cullins within 5 minutes, and this does not account for the time it takes the drug to equilibrate across the membrane and deplete the cellular pool of Nedd8~Ubc12 thioesters (Soucy et al., 2009). The dynamic properties of CSN measured here reveal a CRL network of extreme plasticity that can be reconfigured in minutes to respond to changing regulatory inputs. Although quantitative studies of CRL network dynamics remain in their infancy, it is evident that the tools are at hand to begin to understand how these remarkable enzymes function and are regulated within cells.

2.5 Materials and Methods

Cloning. All eight wild type CSN subunits were cloned into a single pFBDM baculovirus transfer MultiBac vector (Berger et al., 2004). His_6-Csn5 was inserted into the first multiple cloning site (MCS1) of a pFBDM vector using NheI/XmaI and Csn1 was put into MCS2 of the same vector with BssHII/NotI. Similarly, Csn2 was inserted into a second pFBDM vector using BssHII/NotI and $StrepII^{2x}$-Csn3, containing an N-terminal PreScission-cleavable $StrepII^{2x}$-tag, using NheI/XmaI. From this plasmid the Csn2/$StrepII^{2x}$-Csn3 gene cassette was excised out with AvrII/PmeI and inserted into $pFBDM^{Csn1/His6Csn5}$, whose multiplication module had been linearized with BstZ17I and SpeI, yielding $pFBDM^{Csn1/His6-Csn5/Csn2/StrepII2x-Csn3}$. A $pFBDM^{Csn4/Csn7b}$ vector was generated using BssHII/NotI to insert Csn4 and NheI/XmaI for Csn7b, and the resultant gene cassette was inserted into linearized $pFBDM^{Csn1/His6-Csn5/Csn2/StrepII2x-Csn3}$, resulting in $pFBDM^{Csn1/His6-Csn5/Csn2/StrepII2x-Csn3/Csn4/Csn7b}$. Finally, a $pFBDM^{Csn6/Csn8}$ vector was generated using BssHII/NotI for Csn6 and NheI/XmaI for Csn8 insertion. Once again the resultant gene cassette was inserted into linearized $pFBDM^{Csn1/His6-Csn5/Csn2/StrepII2x-Csn3/Csn4/Csn7b}$, yielding the full wild type CSN vector $pFBDM^{Csn1/His6-Csn5/Csn2/StrepII2x-Csn3/Csn4/Csn7b/Csn6/Csn8}$. A similar cloning strategy was applied for the generation of CSN^{5E76A}, $CSN^{5E76A, H138A}$, $CSN^{5E212R, D213R}$, and $CSN^{4\Delta N1-297}$, except that site-directed mutageneses were performed on $pFBDM^{Csn1/His6Csn5}$ and $pFBDM^{Csn4/Csn7b}$ respectively. CSN^{5E104A} and CSN^{5T103I} were generated with the same general approach, except that that site-directed mutagenesis and sequence validation were performed on a pCRIITOPO plasmid (Invitrogen) containing $StrepII^{2x}$-Csn5. Those mutants were then ligated into a MCS1 linearized $pFBDM^{Csn1}$ plasmid. For the production

of $CSN^{6\Delta Ins2}$ we used co-expression from two separate viruses. To this end we applied site-directed mutagenesis on the $pFBDM^{Csn6/Csn8}$ vector to delete amino acids 174-179 in Csn6, generating $pFBDM^{Csn6\Delta Ins2/Csn8}$. The gene cassette of the latter was excised out using AvrII/PmeI and inserted into BstZ17I/SpeI linearized $pFBDM^{Csn4/Csn7b}$, yielding $pFBDM^{Csn4/Csn7b/Csn6\Delta Ins2/Csn8}$. The resultant bacmid was used together with a bacmid generated from $pFBDM^{Csn1/His6\text{-}Csn5/Csn2/StrepII2x\text{-}Csn3}$ in order to generate two baculoviruses, which were used for co-infection to generate $CSN^{6\Delta Ins2}$. An analogous strategy was applied to generate $CSN^{4\Delta N/6\Delta Ins2}$, $CSN^{5H138A/6\Delta Ins2}$, and $CSN^{5H138A/4\Delta N}$.

The TEV site in Rbx1 as well as mutations in the WHB domain of Cul1 were obtained by site-directed mutagenesis on the pFBDM-Cul1/Rbx1 vector described in (Enchev et al., 2010), which further contained a C-terminal sortase tag described in the next section. Cloning of Cul3/Rbx1 used in the crosslinking/mass spectrometry experiments, Nedd8-pro-peptide-$StrepII^{2x}$ and $StrepII^{2x}$-Den1 are described in (Orthwein et al., 2015). Recombinant bacmid and virus generation as well as protein expression proceeded as described in (Enchev et al., 2012). All genes were validated by sequencing as wild type or mutant.

Protein Purification and modifications. CSN and its mutant forms were purified as described in (Enchev et al., 2012). Nedd8-activating and conjugating enzymes were purified as described in (Emberley et al., 2012; Enchev et al., 2012). Fluorescently-labeled Cul1 substrates were conjugated with untagged Nedd8. Cul1-sortase was designed with GGGGSLPETGGHHHHHH inserted after the final amino acid of Cul1 into the pGEX vector described in (Emberley et al., 2012). All sortase reactions were done at 30 °C overnight with 30 µM Cul1/Rbx1, 50 µM Sortase and 250 µM GGGGK-dansyl in 50 mM Tris pH 7.6, 150 mM NaCl and 10 mM $CaCl_2$ and purified by size exclusion chromatography to yield $Cul1^{d}$/Rbx1. $Cul1^{d}$/Rbx1 was neddylated and purified as in (Emberley et al., 2012) to yield $Cul1^{d}$-N8/Rbx1. Cand1 and Sortase were purified as described in (Pierce et al., 2013). Production of Cul1/Rbx1 and Cul3/Rbx1 baculovirus constructs used for electron microscopy and crosslinking mass spectrometry, bacterial split-and-co-express $Cul1/Rbx1^{\Delta RING}$, Nedd8 with native N- and C-termini, used for

electron microscopy and crosslinking mass spectrometry and for the experiments involving Cul1/Rbx1^{TEV}, Den1 as well as the respective preparative neddylation were performed as described in (Enchev et al., 2012; Orthwein et al., 2015). Den1 was used in 1:50 ratio for 10 min at 25 °C to remove poly-neddylation. Cul1/Rbx1 complexes with mutations in the WHB domain of Cul1 (Figure 2.1–figure supplement 2.1N, O) and Cul1/Rbx1$^{TEV\Delta RING}$ were purified from High Five insect cells as described in (Enchev et al., 2010). Dansylation of Cul1/Rbx1 variants expressed in insect cells was performed for 8 to 12 h at 30 °C while spinning at 5000 *g*, and purified by passing the dansylation reaction through a 5 ml HisTrap FF column (GE Healthcare) in 50 mM Tris-HCl, pH 7.6, 400 mM NaCl, 20 mM imidazole. The Cul1^{d}/Rbx1-containing flow through was concentrated, neddylated (if required), and further purified over a Superdex 200 size exclusion column (GE Healthcare) equilibrated with 15 mM HEPES, pH 7.6, 150 mM NaCl, 2 mM DTT, 2 % (v/v) glycerol. Neddylation of Cul1/Rbx1$^{TEV\Delta RING}$ was performed at 25 °C for 12-14 h in 50 mM Tris-HCl, pH 7.6, 100 mM NaCl, 2.5 mM $MgCl_2$, 150 μM ATP, spinning at 2000 *g,* and was followed by 30 min incubation with 1:50 (w/w) Den1 to remove poly-neddylation. The reaction was purified over a Strep-Tactin Superflow Cartridge (QIAGEN), and eluted in 15 mM HEPES, pH 7.6, 250 mM NaCl, 2 mM DTT, 2 % (v/v) glycerol, 2.5 mM *d*-desthiobiotin. RING cleavage was performed for 12-14 hours at 25 °C, spinning at 2000 *g,* in the presence of 100 mM EDTA, pH 8 and 1:1 (w/w) TEV. Dansylation proceeded as described above.

Deneddylation Assays. All deneddylation assays were performed in a buffer containing 25 mM Tris-HCl, pH 7.5, 100 mM NaCl, 25 mM trehalose, 1 mM DTT, 1 % (v/v) glycerol, 0.01 % (v/v) Triton X-100 and 0.1 mg/ml ovalbumin or BSA. Radioactive deneddylation reactions with bacterially expressed substrates were done as described (Emberley et al., 2012). Radioactive deneddylation reactions with substrates expressed in insect cells were performed at 24 °C with 0.5 nM CSN (Figure 2.2–figure supplement 2.2C) or 2 nM CSN (Figure 3.5B). All remaining radioactive deneddylation reactions were performed with bacterially expressed Cul1-N8/Rbx1 substrates (50 nM) and 2 nM CSN unless otherwise noted. Single-turnover reactions were done with 25 nM Cul1 substrates and 1 μM CSN on a Kintek RQF-3 Rapid Quench Flow at 24 °C. Single-turnover data were fit to one phase decay function: Y=(Y0 - EP)*exp(-k_{cat}*X) + EP (where EP corresponds to reaction end

point value), to determine the $k_{cat.}$ Deneddylation assays in Figure 3.1–figure supplement 3.1N, O were performed with 800 nM substrate and 20 nM enzyme and visualized by Coomassie stain. Depending on the exact protein preparations used and the laboratory, we observed rates for the wild type reaction ranging from 1.1-2.6 sec^{-1}.

Fluorescence Assays. All assays were performed in a buffer containing 30 mM Tris pH 7.6, 100 mM NaCl, 0.25 mg/ml ovalbumin or BSA and 0.5 mM DTT with 30 nM dansyl-labeled Cul1/Rbx1 and titrated concentrations of CSN. The mixtures were allowed to reach equilibrium by incubation at room temperature for ~ 10 minutes prior to measurements. Equilibrium binding assays using Cul1/Rbx1 variants expressed in insect cells (Figure 2.2, Figure 2.2–figure supplement 2.2E, Figure 2.3–figure supplement 2.3N, 2.3R, Figure 2.4B) were read at 530 nm on a CLARIOstar plate reader (BMG Labtech) in 384-well plates (Corning, low flange, black, flat bottom), 90 ul per well, while binding assays using bacterially expressed Cul1/Rbx1 variants were performed on a Fluorolog-3 (Jobin Yvon) (all other binding data figures). Binding assay with $Cul1^{d}$-N8/Rbx1 (substrate) and CSN^{5E76A} were allowed to equilibrate for only 45 seconds, because although this mutant exhibited an ~300-fold decrease in activity (data not shown) the residual activity was high enough to cause substantial deneddylation in a 10 minute incubation. It should be noted that several of the K_d values reported for CSN binding to $Cul1^{d}$-N8/Rbx1 or $Cul1^{d}$/Rbx1 are below the concentration of the dansylated ligand (30 nM). While this is generally not the preferred approach, we found that 30 nM was the lowest concentration that consistently yielded highly reproducible results. The estimated K_d is very sensitive to the density of data points at the inflection point of the curve, and thus these estimates can be more prone to error. Nevertheless, different investigators in Zurich and Pasadena have consistently obtained an estimate of 1.6-5 nM for binding of CSN^{5H138A} to $Cul1^{d}$-N8/Rbx1 and of 9-13 nM for binding to CSN^{5H138A} to $Cul1^{d}$/Rbx1, using different protein preparations. To estimate K_d, all data points were fitted to a quadratic equation, Y = Y0+(Ymax-Y0)*(K_d+A+X-sqrt((K_d+A+X)^2-4A*X))/2*A where A equals concentration of labeled protein, using Prism (Graph Pad). On-rate and off-rate measurements were performed on a Kintek Stopped-flow SF-2004 by exciting at 340 nM and collecting emissions through a 520 +/- 20 nm filter. For off-rate measurements, the concentrations of proteins used in each

reaction are provided in the legend of Figure 3–figure supplements 3F–I. Off rate data were fit to one phase decay function: Y=(Y0 - EP)*exp(-k_{off}*X) + EP (where EP corresponds to reaction end point value).Whereas K_d, on-rate, and off-rate measurements with different configurations of Cul1 or different CSN mutants are directly comparable, off-rate measurements are not directly comparable to k_{cat} measurements and may differ from expectation by a few fold because different buffers were used, the Cul1/Rbx1 preparations were from different sources (bacterial for k_{cat}, baculoviral for k_{off}), and the Cul1/Rbx1 preparations carried different labels (dansylated Cul1 for k_{off}, [^{32}P]-Nedd8 for k_{cat}.

Cell Culture and SILAC Mass Spectrometry. Cells were grown in Lonza DMEM containing 10% FBS (Invitrogen). Transient transfections were done with FugeneHD per the manufacturers instructions (Roche). Flag-tagged *CSN5* coding sequences were cloned into a modified MSCV-IRES-GFP vector (containing a pBabe multiple cloning site) via BamHI and EcoRI. Lenti-CRISPR constructs were made as described (Shalem et al., 2014) using the targeting sequences 5'- CACCGCTCGGCGATGGCGGCGTCC - 3' and 3' - AAACGGACGCCGCCATCGCCGAGC - 5'. Lenti- and retroviruses were produced in 293T cells and the supernatant subsequently used for transduction to establish stable cell lines. For Western Blot analysis cells were directly lysed in 2X SDS sample buffer. Lysates were sonicated for 15 seconds at 10 % of maximum amplitude using a Branson Digital Sonifier and boiled for 10 minutes at 100 ºC. SILAC labeling was in Invitrogen DMEM containing 10% FBS and $^{13}C_6{}^{15}N_2$-lysine and $^{13}C_6$-arginine from Cambridge Isotope Laboratory. For immunoprecipitations, cells were lysed in Pierce Lysis Buffer containing cOmplete Protease Inhibitor Cocktail (Roche) and lysates were sonicated for 10 seconds at 10 % of maximum amplitude using a Branson Digital Sonifier. After a 5 minute clearing at 18000 x g at 4°C, proteins were immunoprecipitated with M2 Flag agarose beads (Sigma) for 30 minutes and prepared for mass spectrometry as described in (Pierce et al., 2013) Samples were analyzed using an EASY-nLC 1000 coupled to an Orbitrap Fusion and analyzed by MaxQuant (v 1.5.0.30).

Digested peptides (250 ng) were loaded onto a 26-cm analytical HPLC column (75 µm ID) packed in-house with ReproSil-Pur C_{18}AQ 1.9 µm resin (120 Å pore size, Dr. Maisch,

Ammerbuch, Germany). After loading, the peptides were separated with a 120 min gradient at a flow rate of 350 nL/min at 50°C (column heater) using the following gradient: 2-6% solvent B (7.5 min), 6–25% B (82.5 min), 25-40% B (30min), 40-100% B (1min), and 100% B (9 min) where solvent A was 97.8% H_2O, 2% ACN, and 0.2% formic acid) and solvent B was 19.8% H_2O, 80% ACN, and 0.2% formic acid. The Orbitrap Fusion was operated in data-dependent acquisition (DDA) mode to automatically switch between a full scan (m/z=350–1500) in the Orbitrap at 120,000 resolving power and a tandem mass spectrometry scan of Higher energy Collisional Dissociation (HCD) fragmentation detected in ion trap (using TopSpeed). AGC target of the Orbitrap and ion trap was 400,000 and 10,000 respectively.

SILAC MS data analysis. Thermo RAW files were searched with MaxQuant (v 1.5.3.8) (Cox and Mann, 2008; Cox et al., 2011). Spectra were searched against human UniProt entries (91 647 sequences) and a contaminant database (245 sequences). In addition, spectra were searched against a decoy database (generated by reversing the target sequences) to estimate false discovery rates. Trypsin was specified as the digestion enzyme with up to two missed cleavages allowed. Variable modifications included oxidation of methionine and protein N-terminal acetylation. Carboxyamidomethylation of cysteine was specified as a fixed modification. SILAC was specified as the quantitation method with Arg6 and Lys8 specified as the heavy labeled amino acids. Precursor mass tolerance was less than 4.5 ppm after recalibration and fragment mass tolerance was 0.5 Da. False discovery rates at the peptide and protein levels were less than 1% as estimated by the decoy database search. Ratios were calculated for proteins quantified in at least two of the four biological replicates. 95% confidence intervals and adjusted p-values were calculated using the R package limma (Ritchie et al., 2015).

Cross-linking coupled to mass spectrometry (XL-MS). Chemical cross-linking of purified complexes was performed using DSS H_{12}/D_{12} (Creative Molecules) as cross-linking agent and as previously described(Birol et al., 2014). Subsequent MS analysis and cross-link assignment and detection were carried out essentially as described (Leitner et al., 2014) on an Orbitrap Elite (Thermo Scientific) using the *xQuest/xProphet* software pipeline.

Western Blot Analysis. Proteins were separated by SDS-PAGE gel electrophoresis and transferred to a nitrocellulose membrane by wet blot. Primary antibodies used for detection were: anti-CSN5 mouse monoclonal Santa Cruz Biotechnology sc-393725, anti-Cul1 mouse monoclonal Santa Cruz Biotechnology sc-17775, anti-Cul2 rabbit polyclonal Thermo Scientific #51-1800, anti-Cul3 rabbit polyclonal Cell Signaling #2769, anti-Cul4A rabbit polyclonal Cell Signaling #2699, anti-Cul5 rabbit polyclonal Bethyl Laboratories A302-173A, anti-β-actin mouse monoclonal Sigma A5316, and anti-GFP mouse monoclonal Clontech #632381.

Sample preparation for electron microscopy and data collection. CSN^{5H138A}-SCF-$Nedd8^{Skp2/Cks1}$samples for cryo-electron microscopy were generated by pre-incubating the purified components as described in (Enchev et al., 2012) and ran over a Superose 6 increase 3.2/300 column (GE Healthcare) at 4 °C, eluting 50 µl fractions in 15 mM HEPES, pH 7.6, 100 mM NaCl, 0.5 mM DTT. The sample was kept on ice and its homogeneity and mono-dispersity from the peak elution was immediately confirmed by visualization in negative stain. For cryo EM preparation, the sample was diluted to 0.1 mg/ml and 2 µl were applied to Quantifoil grids (R1.2/1.3 Cu 400 mesh), freshly coated with an extra layer of thin carbon and glow-discharged for 2 min at 50 mA and 0.2 mbar vacuum. The grids were manually blotted to produce a thin sample film and plunge-frozen into liquid ethane. Data were collected automatically using EPU software in low dose mode on a Titan Krios transmission electron microscope, equipped with a Falcon II direct electron detector (FEI), and operated at 300 kV, an applied nominal defocus from -2.5 to - 5.0 µm in steps of 0.25 µm, and 80,460-fold magnification, resulting in a pixel size of 1.74 Å on the sample scale. Images were collected as seven separate frames with a total dose of 25 $e^-/Å^2$.

Electron microscopy data analysis. CTF-estimation and subsequent correction were performed using RELION (Scheres, 2012) and CTFFIND3 (Mindell and Grigorieff, 2003). All micrographs were initially visually inspected and only those with appropriate ice thickness as well as Thon rings in their power spectra showing regularity and extending to 6 Å or beyond were used for subsequent analysis. In order to generate 2D references for automated particle selection, ~ 4,000 single particles were manually picked and subjected

to 2D classification in RELION. Six well-defined 2D class averages were selected, low-pass filtered to 35 Å to prevent reference bias, and used as references. Approximately 150,000 single particles were automatically selected and subjected to reference-free 2D and 3D classification, in order to de-select the particles, which resulted in poorly defined or noisy averages. Approximately half of these single particles resulted in a well-defined 3D class average, which resembled the previously published negative stain EM map of the same complex (Enchev et al., 2012). This dataset was subject to 3D auto-refinement in RELION, using a version low-pass filtered to 50 Å as an initial reference. The converged map was further post-processed in RELION, using MTF-correction, FSC-weighting, and a soft spherical mask with a 5-pixel fall-off.

Modeling, docking, and visualization. Csn7b was modeled using Csn7a as a template on the Phyre2 server (Kelley et al., 2015) and the modeled coordinates were aligned to Csn7a in PDB ID 4D10 (Lingaraju et al., 2014), effectively generating a CSN atomic model for the Csn7b-containing complex. Model visualization, molecular docking, distance measurements, and morph movie generation were performed with UCSF Chimera (Pettersen et al., 2004).

Accession codes. The cryo electron microscopy density map of $CSN^{Csn5H138A}$-SCF-$Nedd8^{Skp2/Cks1}$ will be deposited prior to publication in the Electron Microscopy Data Bank under accession code EMD###.

Author contributions

RM developed the binding assay, designed, performed and interpreted the binding experiments, developed off-rate assays and performed measurements, developed and performed the single turn- over deneddylation assays, designed, performed, and interpreted the activity assays, expressed and purified proteins from bacteria, designed cell based assays, drafted and edited the manuscript; KMR designed, performed, and interpreted the binding experiments, developed off-rate assays and performed measurements, designed, performed, and interpreted the activity assays, expressed and purified proteins from bacteria, and designed cell based assays, performed the cell based assays, and drafted and

edited the manuscript; MW designed, performed, and interpreted the binding experiments, designed, performed, and interpreted the activity assays, expressed in insect cells and produced CSN, Cul1/Rbx1, and Cul3/Rbx1 samples, generated the Cul1-N8/Rbx1 reagents, and expressed and purified proteins from bacteria; AS expressed in insect cells and produced CSN, Cul1/Rbx1 and Cul3/Rbx1 samples, conceived the design and production of Cul1-N8/Rbx1, and gave critical input into drafting and editing the manuscript; JMR performed SILAC mass spectrometry of $_{Flag}$Csn5, and gave critical input into drafting and editing the manuscript; YZ, expressed and purified proteins from bacteria, interpreted the binding, off-rate and activity assays; FS and RA performed cross-linking mass spectrometry and analysed the data, and gave critical input into drafting and editing the manuscript; JC aided cell based assays; MK assisted in development of the binding assay; MJS and SH performed SILAC mass spectrometry of $_{Flag}$Csn5; AL performed cross-linking mass spectrometry and analysed the data; MP and RJD, managed the project and participated in the design and interpretation of the experiments, drafted and edited the manuscript; RIE performed electron microscopy sample preparation, data collection, single particle analysis, docking and interpretation of the structural data, developed the binding assay, designed, performed, and interpreted the binding experiments, developed off-rate assays, designed, performed and interpreted the activity assays, designed all CSN constructs, and all Cul1/Rbx1 and Cul3/Rbx1 samples from insect cells, expressed in insect cells and produced CSN, Cul1/Rbx1 and Cul3/Rbx1 samples, expressed and purified proteins from bacteria, conceived the design and production of Cul1-N8/Rbx1, expressed and purified proteins from bacteria, analyzed the data, and drafted and edited the manuscript.

2.6 Figures and Supplemental Figures

Figure 2.1

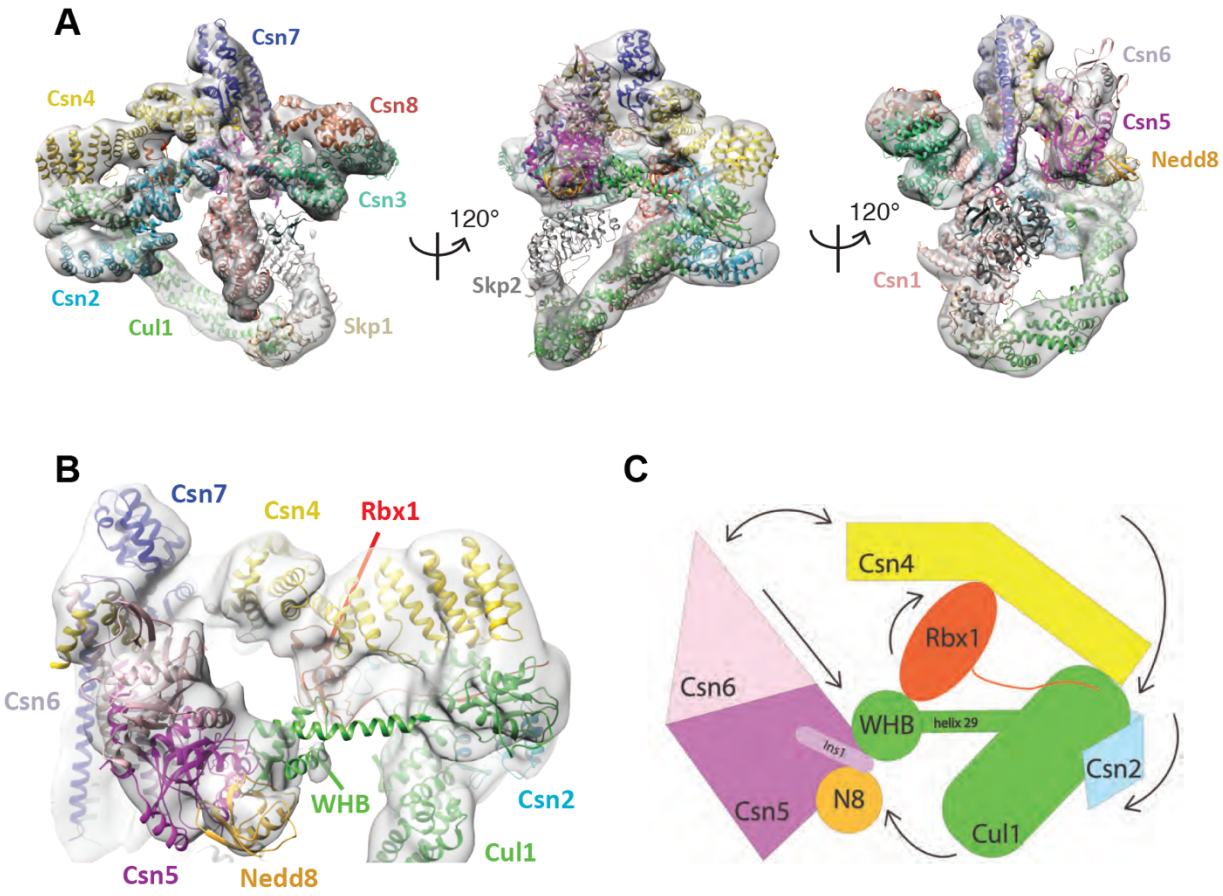

Figure 2.1. Cryo-electron microscopy of a CSN-SCF complex. (A) Molecular model of CSN^{5H138A}-SCF-$N8^{Skp2/Cks1}$ docked into the cryo-electron density map (gray mesh). (B) Close-up view of the model, showing the observed conformations of Csn2, Csn4, Rbx1, Csn5/6, and WHB-Nedd8 and (C) a cartoon representation of the differences between the apo CSN and substrate-bound state.

Figure 2.2

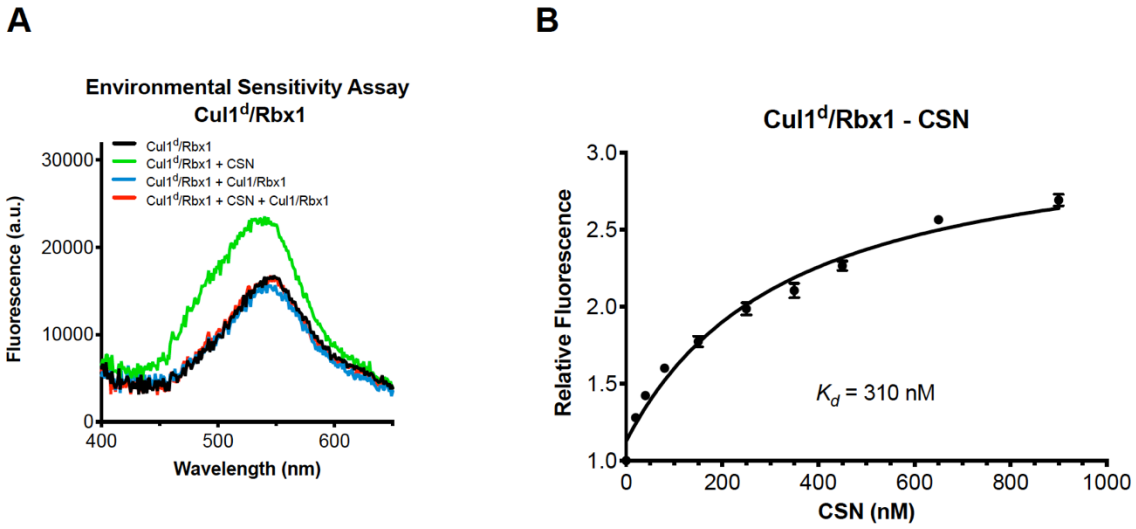

Figure 2.2. Development and validation of a binding assay for CSN–Cul1/Rbx1 interaction. (A) Equilibrium binding of CSN to Cul1d/Rbx1 and competition by unlabeled Cul1/Rbx1. The indicated proteins were mixed and allowed to equilibrate prior to determination of dansyl fluorescence in a fluorometer. Note that Cul1/Rbx1 blocks the fluorescence enhancement caused by CSN. CSN, Cul1d/Rbx1, and Cul1/Rbx1 were used at 350, 30, and 4000 nM, respectively. (B) Equilibrium binding of CSN to Cul1d/Rbx1. Cul1d/Rbx1 (30 nM) was mixed with increasing concentrations of CSN and the proteins were allowed to equilibrate prior to determining the change in dansyl fluorescence in triplicate samples. Error bars represent standard deviation.

Figure 2.3

A

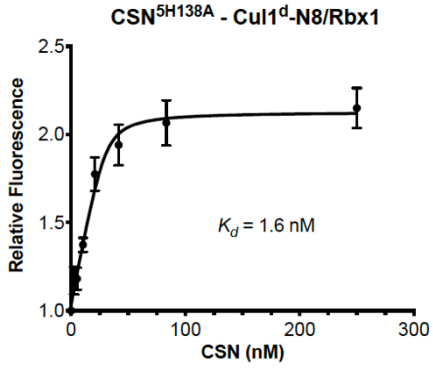

B

Ligand K_d (nM)

CSN \ Ligand	*Cul1^d/Rbx1*	*Cul1^d-N8/Rbx1*	*Cul1^d-N8/Rbx1$^{\Delta RING}$*
wt	*310*		
5^{H138A}	*10*	*1.6*	*N.D.*
5^{E76A,H138A}	*13*	*N.D.*	*12*
5^{E104A}	*26*		
2$^{\Delta N}$,5^{H138A}	*> 1300*	*N.D.*	*N.D.*
4$^{\Delta N}$,5^{H138A}	*> 750*	*20*	*292*
5^{H138A},6$^{\Delta INS2}$	*23*	*N.D.*	*0.4**
5^{T103I}	*390*		

C

CSN \ Ligand	k_{on} (10^7 M^{-1} sec^{-1})		calculated k_{off} (sec^{-1})		measured k_{off} (sec^{-1})	
	Cul1^d/Rbx1	*Cul1^d-N8/Rbx1*	*Cul1^d/Rbx1*	*Cul1^d-N8/Rbx1*	*Cul1^d/Rbx1*	*Cul1^d-N8/Rbx1*
wt	*2.0*		*6.2*		*1.1*	
5^{E104A}	*N.D.*		*0.48**		*0.13*	
5^{H138A}	*1.3*	*2.2.*	*0.13*	*0.035*	*0.16*	*N.D.*
5^{E76A,H138A}	*N.D.*	*N.D.*	*0.26**		*0.12*	*0.017*

Figure 2.3. Quantitative determination of enzyme–substrate binding affinities for wild type and mutant proteins. (A) Tight binding of CSN5H138A to substrate. Cul1d-N8/Rbx1 and CSN5H138A were mixed and allowed to equilibrate prior to determining the change in dansyl fluorescence. (B) Summary of Kd measurements for the indicated CSN complexes tested against unmodified Cul1d/Rbx1, Nedd8-conjugated Cul1d-N8/Rbx1 or Cul1d-N8/Rbx1ΔRING ligand. Boxes shaded in gray indicate combinations that could not be analyzed due to deneddylation during the binding reaction. For some complexes that bound weakly it was not feasible to titrate to saturation and so a lower boundary for Kd is indicated. N.D., not determined. *, due to the configuration of our assay, extremely low Kd values cannot be reliably determined. (C) Summary of kon and koff measurements for the indicated CSN complexes tested against Cul1d/Rbx1 or Cul1d-N8/Rbx1. Each reported koff is the mean of at least 8 replicates. For comparison, koff values calculated from kon and Kd measurements are also shown. For cases where kon was not measured (marked with asterisks) we assumed a value that was the average (1.83 x 107 M-1 sec-1) of the three measured kon values. Boxes shaded in gray indicate combinations that could not be analyzed due to deneddylation upon complex formation. N.D., not determined.

Figure 2.4

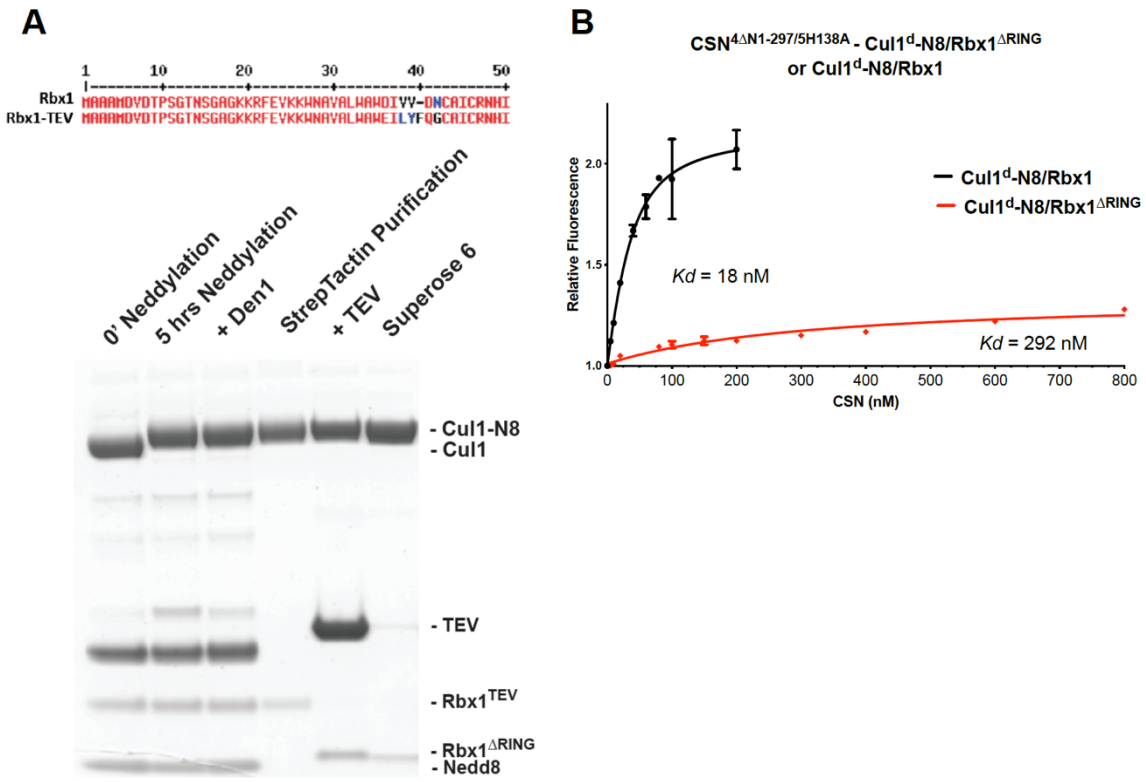

Figure 2.4. The N-terminal domains of Csn2 and Csn4 and the RING domain of Rbx1 play key roles in substrate binding and deneddylation. (A) Generation of Cul1-N8/Rbx1$^{\Delta RING}$. Top: a TEV protease site was engineered between the N-terminal β-strand and the RING domain of Rbx1 as indicated. Only the first 50 amino acids of Rbx1 are shown. Bottom: Purified protein was subjected to the indicated treatments (see Materials and Methods for details) and reactions were fractionated by SDS-PAGE and stained with Coomassie Blue. (B) Deletion of the Csn4-NTD and Rbx1-RING domains independently reduce affinity of CSN for substrate. The indicated proteins were mixed and allowed to equilibrate prior to determining the change in dansyl fluorescence in triplicate samples. Error bars represent standard deviation. K_d values measured in this experiment are also reported in Figure 3B.

Figure 2.5

A

CSN	k_{cat} (sec^{-1})	K_M (nM)	k_{cat} (sec^{-1})	k_{cat} (sec^{-1})
wt	*1.1*	*200*	*1.1*	*0.00006*
$4^{\Delta N}$	*0.05*	*40*	*N.D.*	*N.D.*
$6^{\Delta INS2}$	*N.D.*	*N.D.*	*1.7*	*0.00048**
5^{E104A}	*0.4*	*N.D.*	*0.4*	*N.D.*
5^{T103I}	*≤ 0.09*	*90*	*N.D.*	*N.D.*
turnover	*multi*		*single*	*multi*
substrate	*Cul1-N8/Rbx1*			*Cul-N8/Rbx1$^{\Delta RING}$*

B

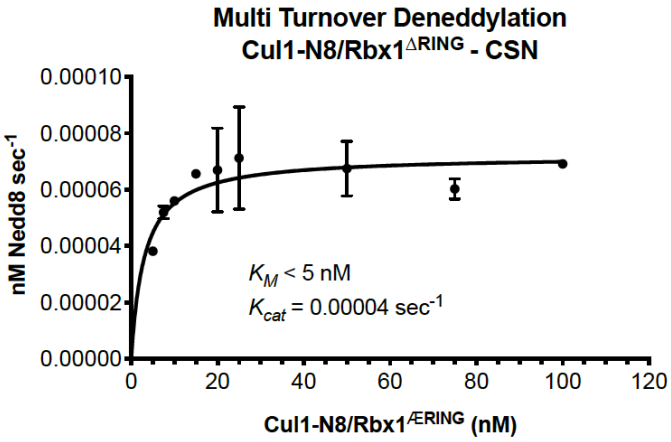

Figure 2.5. The N-terminal domains of Csn2 and Csn4 and the RING domain of Rbx1 are important for CSN-mediated deneddylation. (A) Summary of kinetic parameters for the indicated CSN mutants in multi- or single-turnover deneddylation reactions with Cul1-N8/Rbx1 or Cul1-N8/Rbx1$^{\Delta RING}$ substrate. Note that there may be modest discrepancies between these k_{cat} values and k_{off} values due to differences in assay configurations as described in Materials and Methods. The ΔRING substrate used here and in panel B contains the sortase sequence at the C-terminus of Cul1 that was used for generation of dansylated Cul1. Control experiments revealed that this tag, with or without dansylation, reduced k_{cat} by ~4-fold. In addition the wild type control for the ΔRING reaction exhibited k_{cat} of 2.6 sec^{-1}. The rates shown have been correspondingly adjusted to normalize them to other rates reported here. *, This rate is estimated from Figure 5–figure supplement 5B. (B) Kinetic analysis of deneddylation of Cul1-N8/Rbx1$^{\Delta RING}$ by CSN.

Figure 2.6

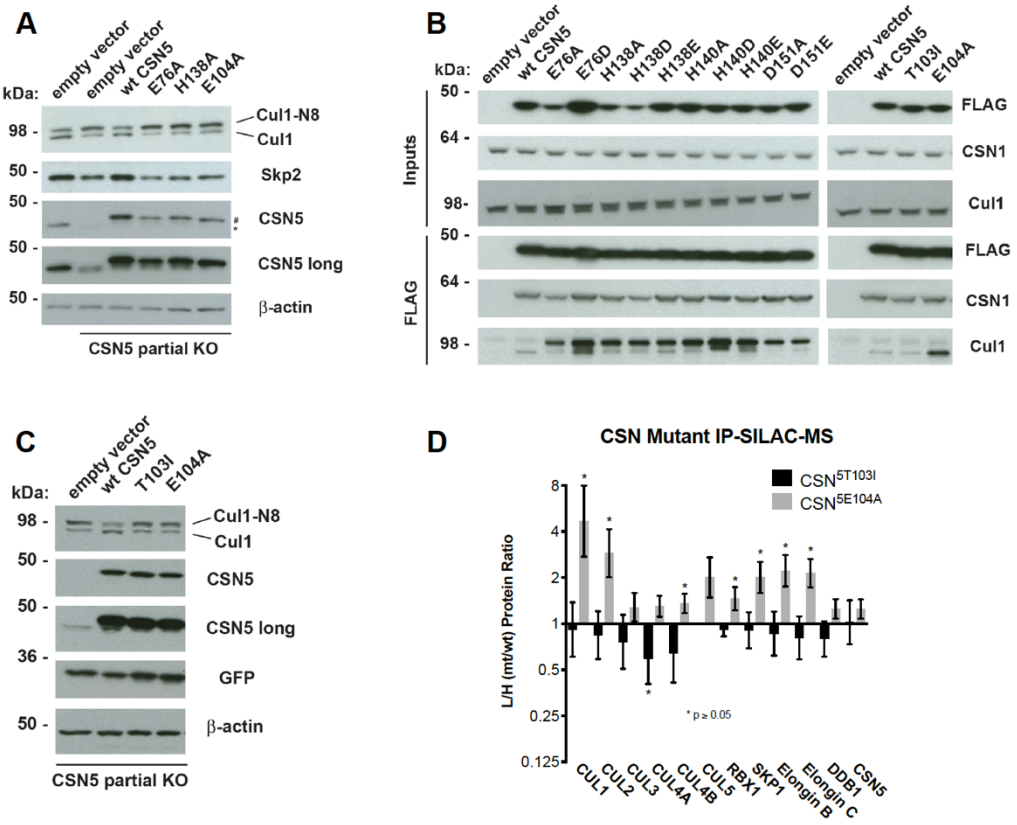

Figure 2.6. Functional analysis of Csn5 active site and INS1 mutants in biochemical and cellular assays. (A) Csn5-E104 is important for CSN function in cells. *CSN5* alleles in HEK293T cells were partially knocked out (KO) by CRISPR/Cas9 to yield a major decrease in Csn5 that was nonetheless compatible with viability. Wild type and the indicated Flag-tagged *CSN5* mutants were reintroduced by transduction of recombinant retroviruses that co-expressed GFP. Lysates of transduced cells were separated by SDS-PAGE and blotted with antibodies to the indicated proteins. CSN5 long refers to a long exposure of the Csn5 blot, captured to reveal residual Csn5 in the knock-out cells. # refers to transduced ^{Flag}Csn5 and * refers to endogenous Csn5. (B) Any mutation of a core JAMM domain residue in Csn5 results in enhanced binding to Cul1. Same as (A), except additional Csn5 mutants were tested and the cell lysates were immunoprecipitated with anti-Flag and the immunoprecipitates were blotted for the indicated proteins. (C) Csn5-T103 is important for CSN function in cells. Same as (A) except that the Csn5-T103I mutant was analyzed in parallel with Csn5-E104A and wild type. (D) SILAC mass spectrometry of endogenous proteins bound to ^{Flag}Csn5-E104A or ^{Flag}Csn5-T103I, relative to wild type ^{Flag}Csn5. Cells expressing mutant and wild type ^{Flag}Csn5 proteins were grown in light and heavy medium, respectively. L:H ratios >1 indicate higher recovery of the listed protein from cells expressing mutant ^{Flag}Csn5, whereas ratios <1 indicate higher recovery from cells expressing wild type ^{Flag}Csn5. Gray bars: ^{Flag}Csn5-E104A; black bars: ^{Flag}Csn5-T103I. Error bars represent the 95% confidence interval as calculated by limma (Smyth). Each protein was quantified in at least two of the four biological replicates and error bars represent standard deviations. Ratios indicated by * differed significantly from 1.0 ($p<0.05$). For CSN, only Csn5 is shown; the remainder is shown in Figure 6–figure supplement 6B.

Figure 2.7

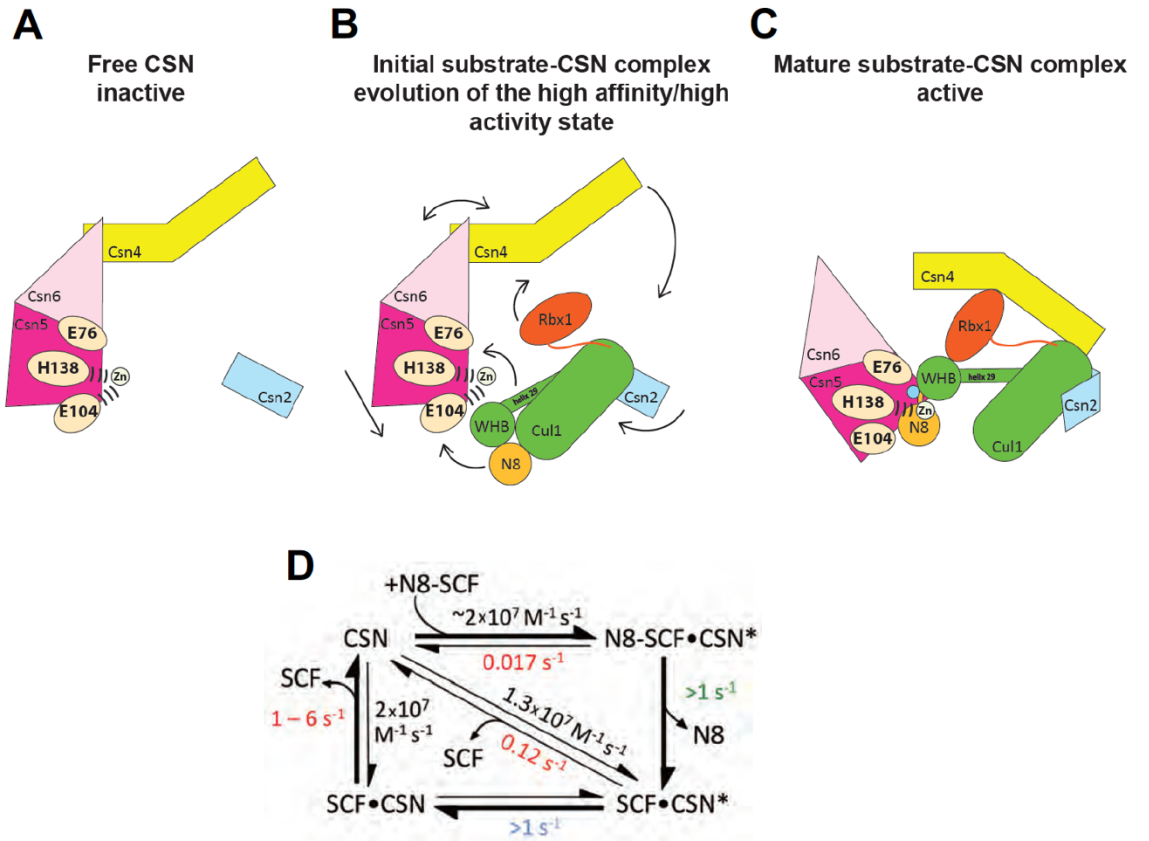

Figure 2.7. Structural and kinetic models for CSN activation and the CSN enzyme cycle. (A-C) Proposed conformational changes that precede substrate cleavage. (D) Kinetic model for the deneddylation cycle. Substrate cleavage is indicated by the slash between N8 and SCF. The asterisk denotes the activated form of CSN. Numbers in red, black, green, and blue represent k_{off} (sec^{-1}), k_{on} (M^{-1} sec^{-1}), k_{cat} (sec^{-1}), and conformational change (sec^{-1}) rates, respectively. For rates >1, the actual rate has not been measured but it is inferred to be >1 sec^{-1} because the overall rate for multiturnover catalysis is at least 1.1 sec^{-1} and thus all sub-steps must be at least this fast. The k_{off} of SCF from CSN varied depending upon whether the rate was measured directly or inferred from K_d and k_{on} (see Fig. 3C). The arrow connecting CSN and N8-SCF•CSN* combines two separate steps: binding of N8-SCF to CSN, and activation of CSN to CSN*.

Figure Supplement 2.1 A-C

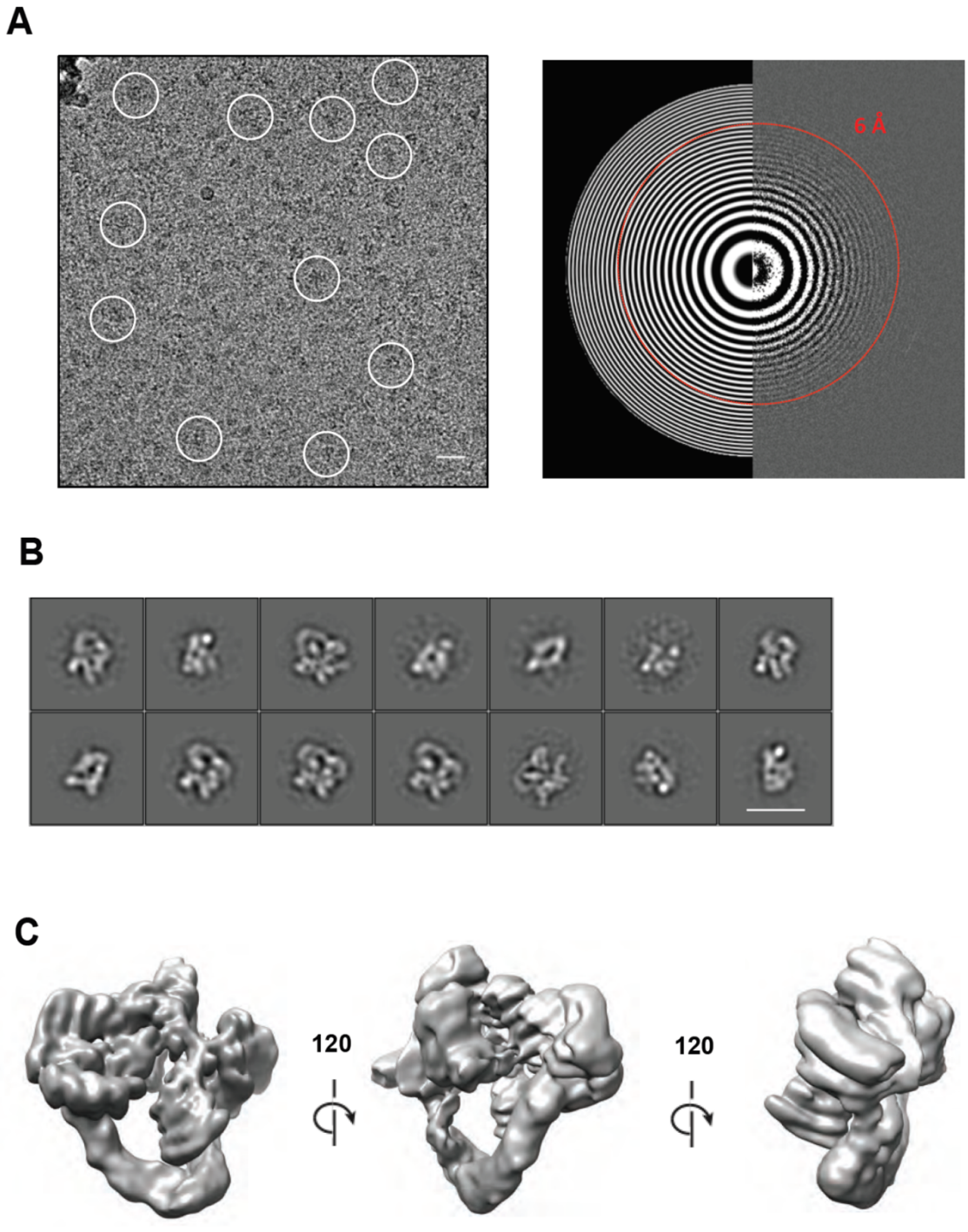

Figure Supplement 2.1 D-I

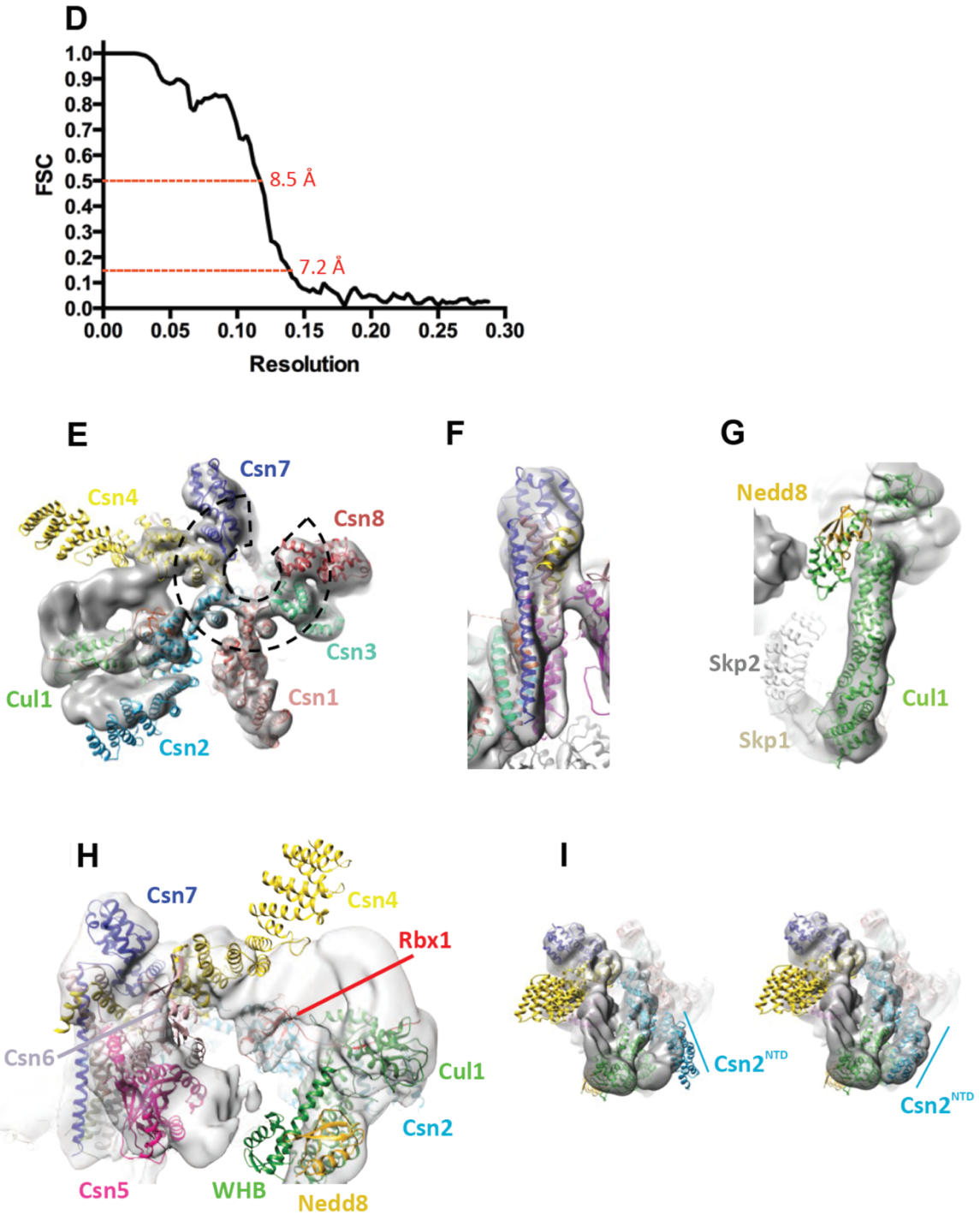

Figure Supplement 2.1 J-O

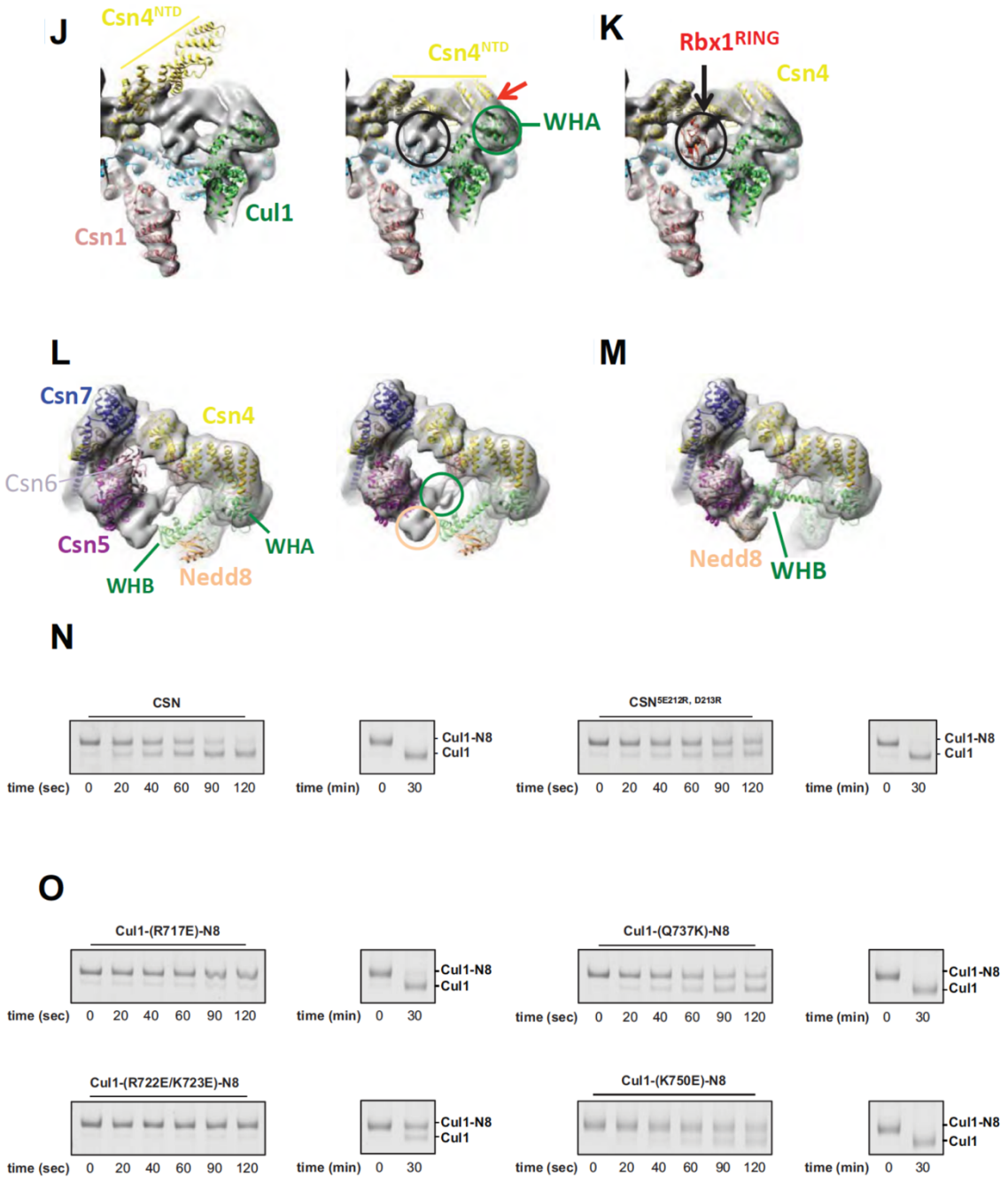

Figure supplement 2.1. Cryo-electron microscopy and single particle analysis of a CSN5H138A-N8-SCFSkp2/Cks1 complex. (A) A representative cryo-electron micrograph of a CSN5H138A-N8-SCFSkp2/Cks1 complex with some single molecular views indicated by white circles (left) and a power spectrum indicating Thon rings reaching 6 Å (right). Scale bar is 200 Å. (B) Representative two-dimensional class averages from the curated dataset, used for the subsequent analysis. Scale bar is as in (A). (C) Surface

views of the final, post-processed cryo-electron map. (D). Resolution estimate according to the FSC criteria of 0.143 and 0.5. (E) Fit of the PCI-domain containing CSN subunits in the cryo-electron density map. Csn1,3,7, and 8 match the density very well but the N-terminal domains of Csn2 and Csn4 do not, but their winged-helix domains fit well. The horseshoe arrangement of the six winged-helix domains is indicated with a dotted black line. (F) All the C-terminal helices of the CSN subunits match well the electron density map. (G) Fit of SCF in the electron density map. (H) Same view as in Fig 1B but prior to flexible docking of the N-terminal domains of Csn2 and Csn4, the MPN domains of Csn5&6, the WHB domain of Cul1, and Nedd8. (I) Movement of the N-terminus of Csn2 from its crystallographically-determined position (left) into the EM density map (right). (J) Movement of the N-terminus of Csn4 from its crystallographically-determined position (left) into the EM density map (right). The two N-terminal helical repeats of Csn4, red arrow, are in close proximity to the WHA domain of Cul1 (green circle). (K) Localization of the RING domain of Rbx1. The unfilled density that is indicated by a black ellipse in the right-hand panel of S1J accommodates Rbx1 (shown in red). The helices of Csn4 in close proximity to the RING domain of Rbx1 are indicated by a black arrow. (L) Re-localization of Csn5/6. Comparing the left and right panels, Csn5/6 move leftward to occupy unfilled density. The tan and green circles below Csn5/6 indicate densities that are occupied by Nedd8 and the WHB domain, as depicted in (M). (N, O) Deneddylation assays with (N) wild type Cul1-N8/Rbx1 and indicated CSN variants and (O) wild type CSN and mutant Cul1 variants. Note that all Cul1 constructs have an uncleaved C-terminal sortase tag, which is the reason for slower deneddylation of wild type Cul1-N8/Rbx1 by wild type CSN relative to the kinetics reported elsewhere in this work.

Figure Supplement 2.2 A-D

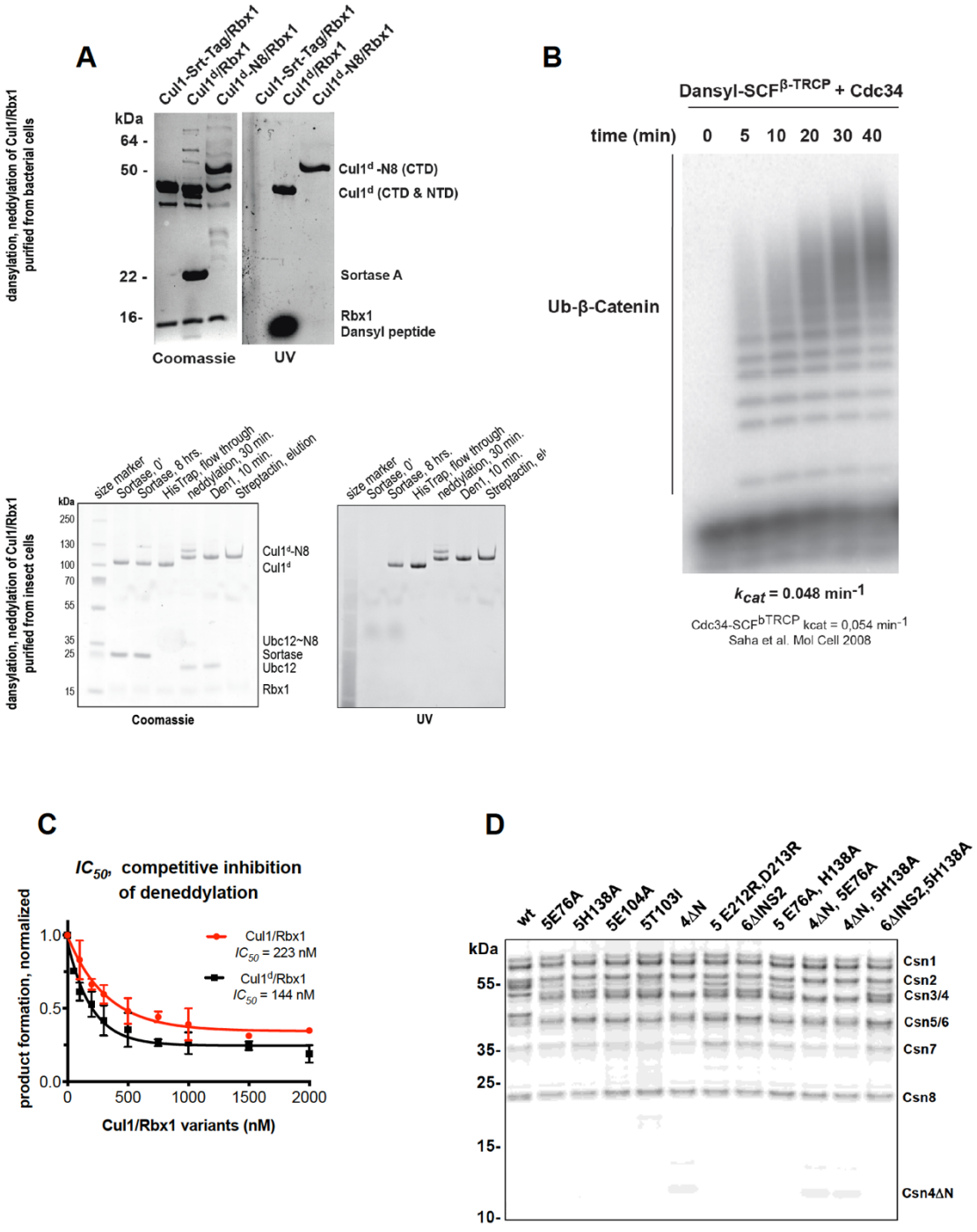

Figure Supplement 2.2 E-I

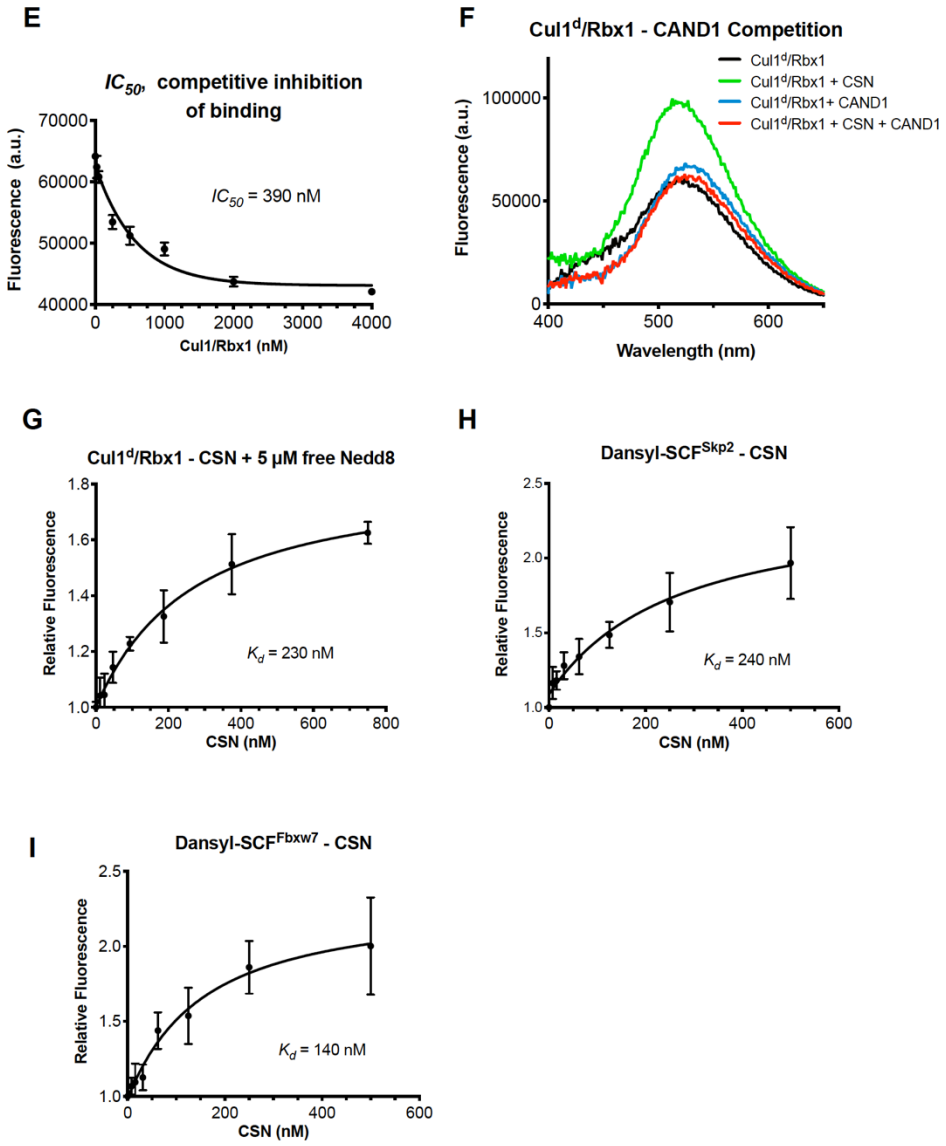

Figure supplement 2.2. Supporting data for development and validation of CSN–Cul1d/Rbx1 binding assay. (A) Dansylation of Cul1/Rbx1 constructs. Upper panel: dansylation of bacterially expressed and purified Cul1/Rbx1. Lower panel: dansylation of Cul1/Rbx1 expressed and purified from insect cells. For details, see Materials and Methods. (B) Ubiquitination of 32P-labeled beta-catenin substrate peptide by dansylated SCF-TrCP was monitored as described (Saha and Deshaies, 2008). The kcat measured here (0.048 min-1) compares favorably with that previously determined for wild type unmodified SCF (0.054 min-1)(Saha and Deshaies, 2008). (C) IC50 study of the inhibitory effects of unlabeled (red) or dansylated (black) product. Cul1/Rbx1 and Cul1d/Rbx1 were separately titrated into a deneddylation reactions containing 50 nM Cul1-[32P]N8/Rbx1 substrate and 0.5 nM CSN, and the resulting reaction rate was measured. (D) CSN preparations used in this study. 600 ng of each sample were fractionated by SDS-PAGE and stained with SYPRO Ruby. (E) IC50 for competitive inhibition of CSN-Cul1d/Rbx1 complex formation by unlabeled Cul1/Rbx1 (~ 390 nM) agrees with the Kd measured for binding of Cul1d/Rbx1 to CSN (310 nM). (F)

Equilibrium binding of 100 nM CSN to 50 nM Cul1d/Rbx1 and competition by 500 nM Cand1. The indicated proteins were mixed and allowed to equilibrate prior to determination of dansyl fluorescence. (G-I) Free Nedd8 and F-box box proteins do not appreciably change affinity of Cul1d/Rbx1 for CSN. Same as Figure 2C, except that either 5 μM free Nedd8 (G), 100 nM Skp2/Skp1 (H) or 100 nM Fbxw7/Skp1 (I) was included in the binding reaction. All binding and activity measurements reported in this legend were carried out in triplicate and error bars represent standard deviation.

Figure Supplement 2.3 A-K

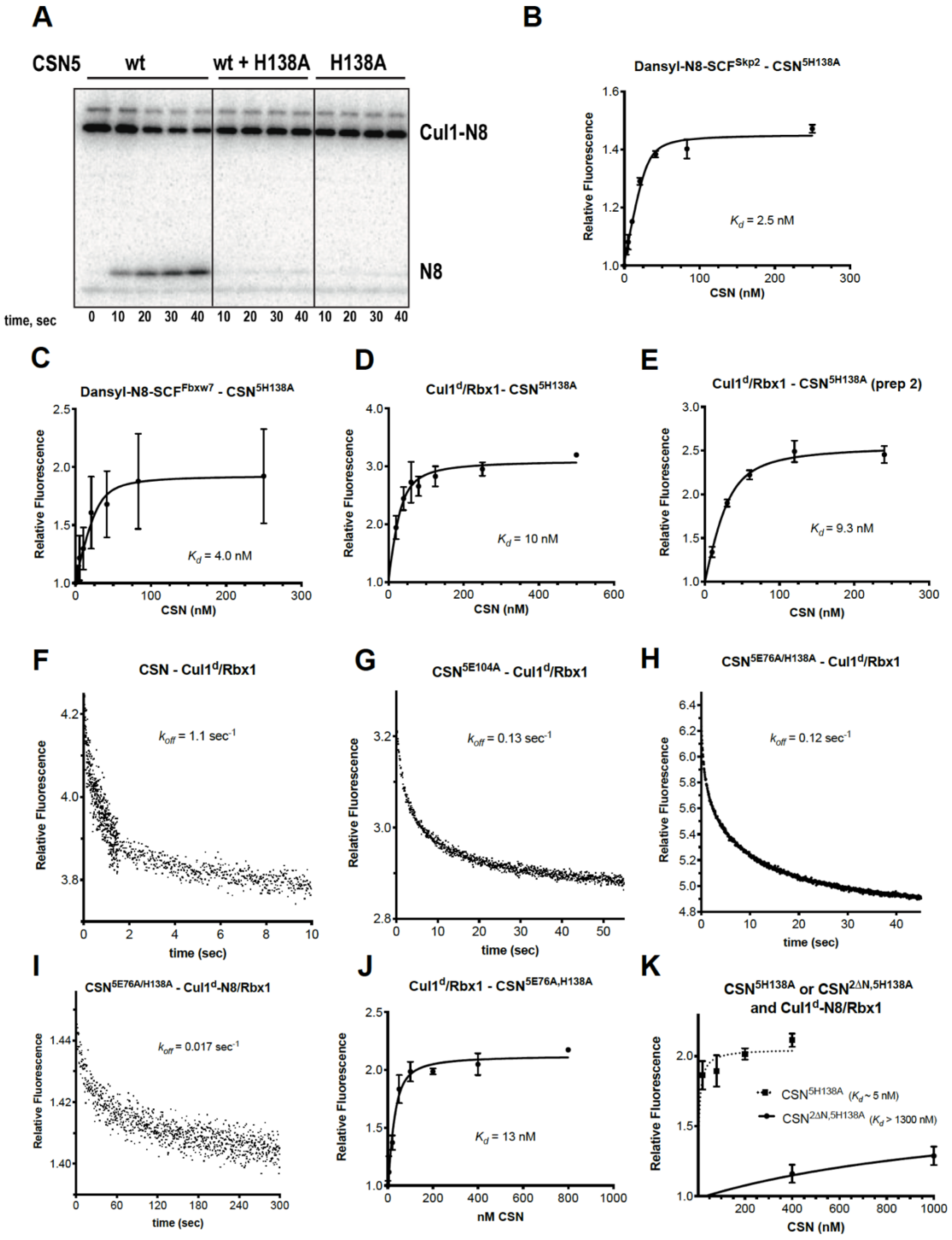

Figure Supplement 2.3 L-R

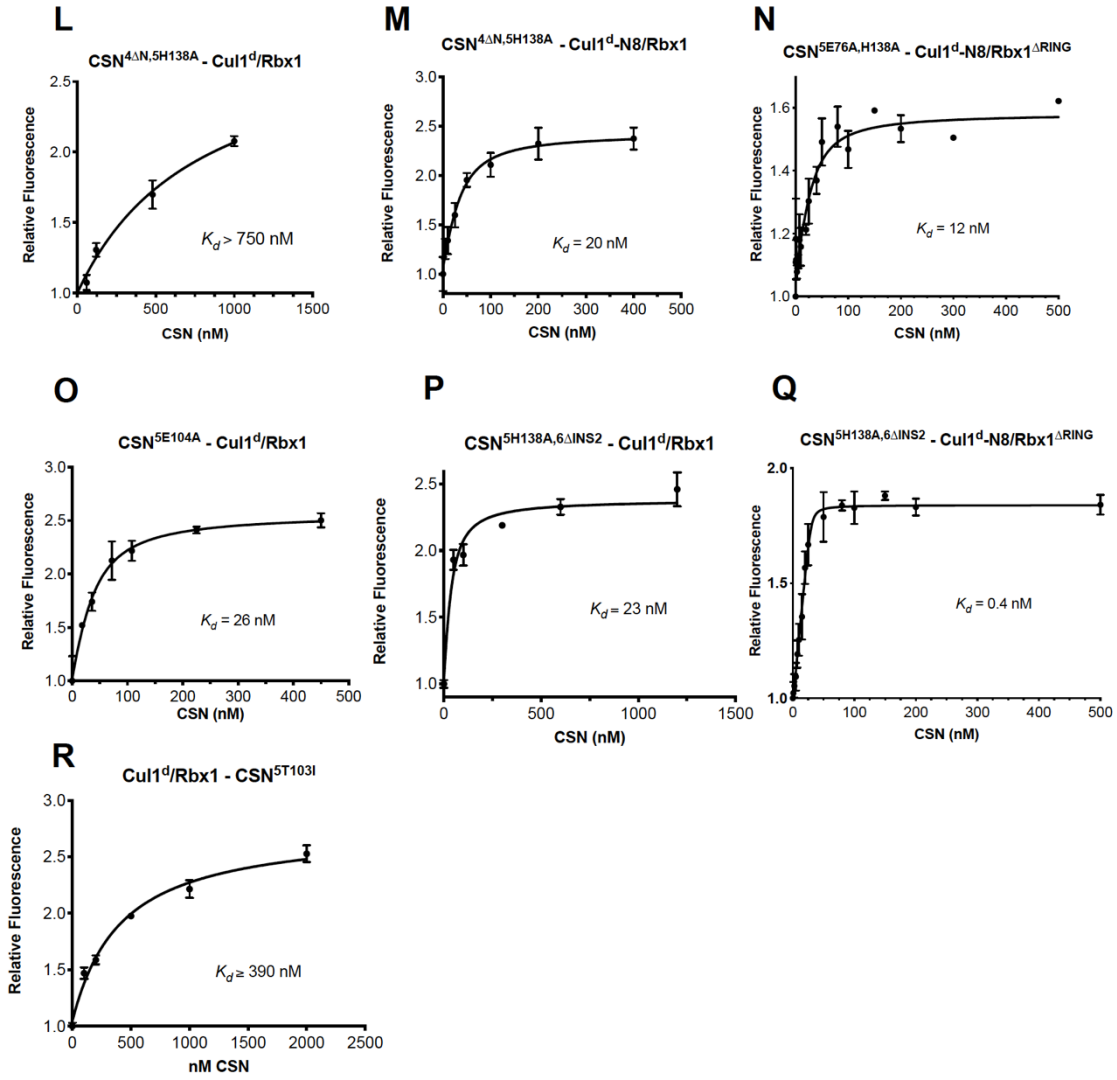

Figure supplement 2.3. Supporting experiments and titration curves for binding data in Figures 3B–C. (A) CSN5H138A is inactive and is a dominant-negative inhibitor of deneddylation. CSN, CSN5H138A , and substrate were used at 2 nM, 100 nM, and 75 nM, respectively. For reactions containing with CSN and CSN5H138A, mutant enzyme was preincubated with substrate for 30 sec prior to initiating time-course by adding CSN. (B-E): The indicated proteins were mixed and allowed to equilibrate prior to determining the change in dansyl fluorescence. (B) CSN5H138A and dansylated, Nedd8-conjugated SCFSkp2. (C) CSN5H138A and dansylated, Nedd8-conjugated SCFFbxw7. Note that addition of Fbxw7–Skp1 greatly increased the variability in the measurement for unknown reasons. (D) CSN5H138A (first prep) and Cul1d/Rbx1, (E) CSN5H138A (second prep) and Cul1d/Rbx1, (F-I): The indicated CSN complexes were preincubated with Cul1d/Rbx1 for 10 min, followed by addition of unlabeled Cul1/Rbx1 chase and measurement of the decay in dansyl fluorescence over time. Final protein concentrations are listed for each experiment. (F) CSN (2000 nM), Cul1d/Rbx1 (200 nM), and Cul1/Rbx1 (3000 nM), (G) CSN5E104A (600 nM), Cul1d/Rbx1 (200 nM), and Cul1/Rbx1 (3000 nM), (H) CSN5E76A,5H138A (400 nM), Cul1d/Rbx1 (200 nM), and Cul1/Rbx1 (3000 nM), (I) CSN5E76A,5H138A (200 nM), Cul1d-N8/Rbx1 (100 nM), and Cul1/Rbx1 (1500 nM), (J-S): The indicated proteins were mixed and allowed to equilibrate prior to

determining the change in dansyl fluorescence. (J) CSN5E76A, 5H138A and Cul1d/Rbx1, (K) CSN5H138A or CSN2ΔN,5H138A and Cul1d-N8/Rbx1, (L) CSN4ΔN,5H138A and Cul1d/Rbx1, (M) CSN4ΔN,5H138A and Cul1d-N8/Rbx1, (N) CSN5E76A or CSN5E76A,5H138A and Cul1d-N8/Rbx1ΔRING, (O) CSN5E104A and Cul1d/Rbx1, (P) CSN5E76A and Cul1d/Rbx1, (Q) CSN5H138A,6ΔINS2 and Cul1d/Rbx1, (R) CSN5H138A,6ΔINS2 and Cul1d-N8/Rbx1ΔRING, (S) CSN5T103I and Cul1d/Rbx1. All measurements in panels B-E and J-S were carried out in triplicate and error bars represent standard deviation. The measurement in panel P was performed in duplicates but the experiment was repeated on three independent occasions, obtaining similar results. Several of these results were independently confirmed in Zurich and Pasadena including panels J, M, O, P, and Q.

Figure Supplement 2.4

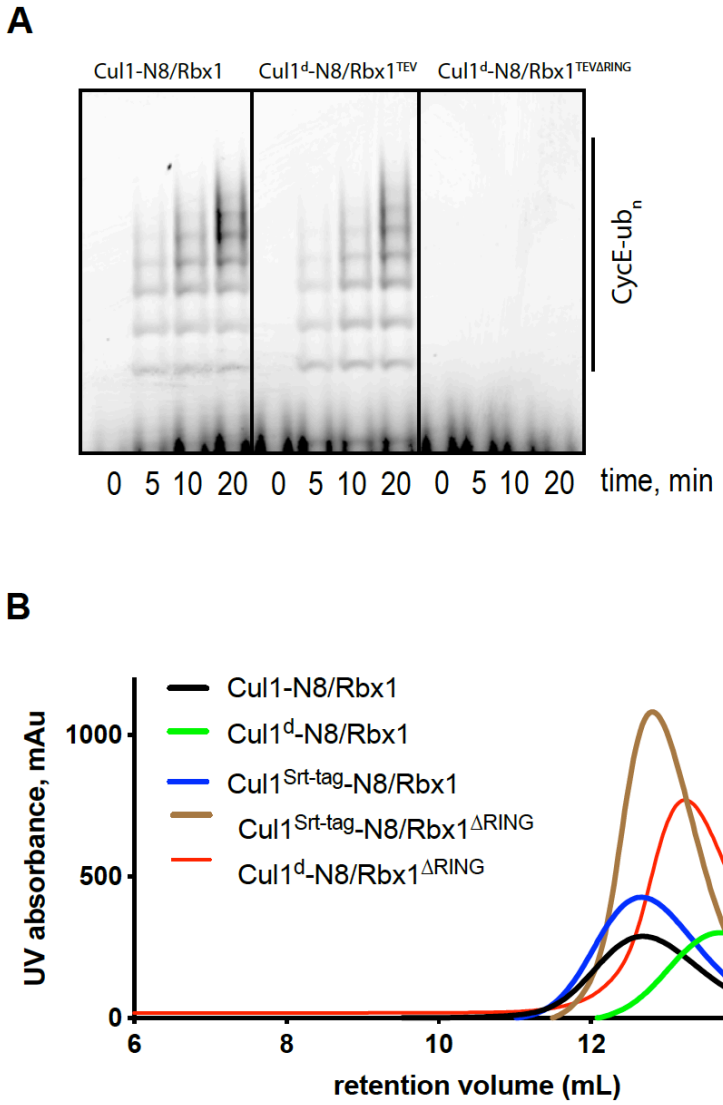

Figure supplement 2.4. Biochemical characterization of Cul1/Rbx1TEVΔRING proteins. (A) Ubiquitination assay using the indicated Cul1-N8/Rbx1 variants (500 nM each) as an E3. Each reaction contained, in addition, 100 nM Ube1, 1000 nM Cdc34b, 750 nM Skp1/Fbxw7 and 4000 nM CyclinE phosphopeptide, labeled with FAM. The samples were incubated at 25°C for the indicated time points, analyzed by SDS PAGE and visualized by excitation at 473 nm. (B) Overlay of Superdex 200 size exclusion profiles of purified Cul1/Rbx1 variants isolated from insect cells.

Figure Supplement 2.5

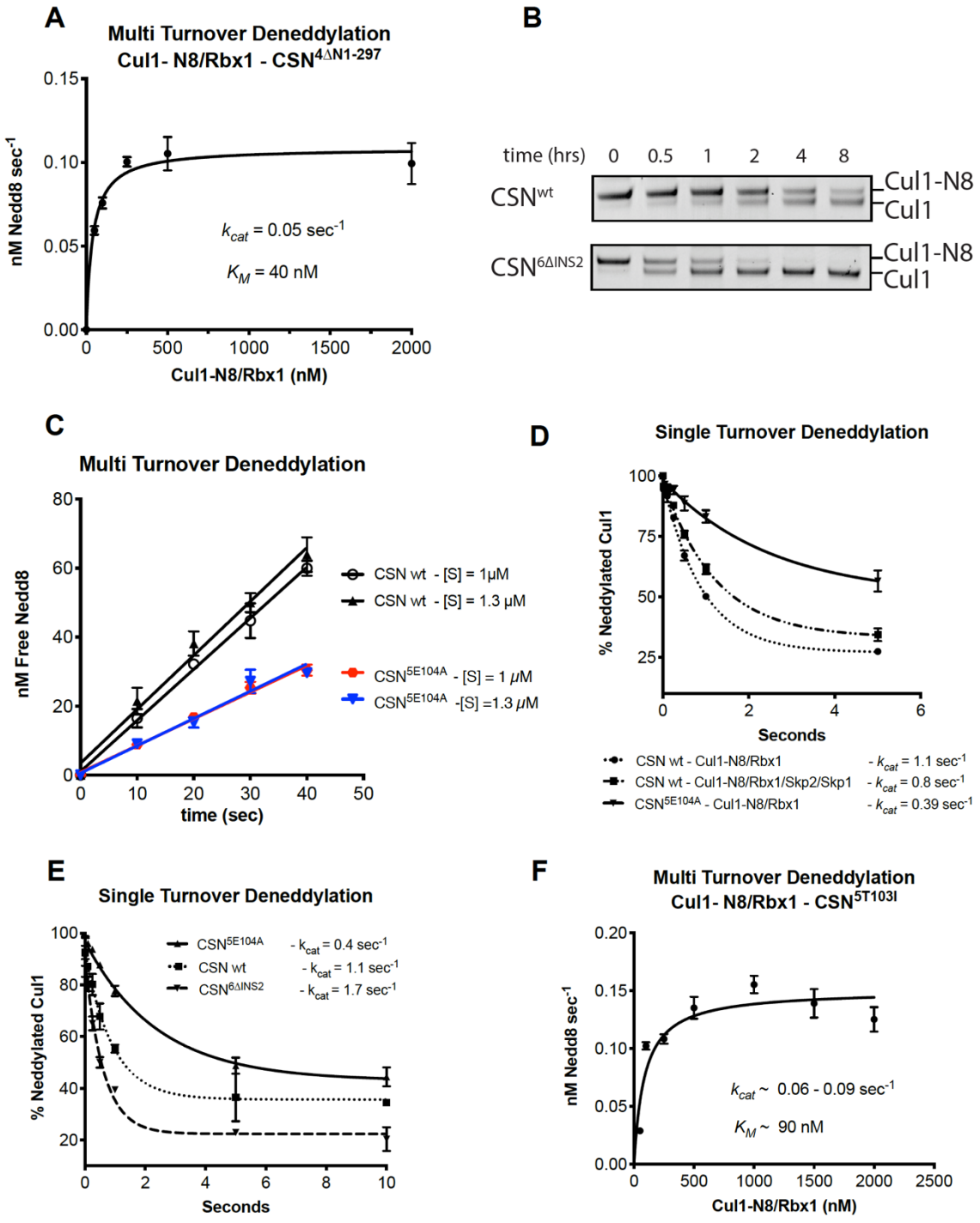

Figure supplement 2.5. Kinetic analysis of deneddylation. (A) Deneddylation reactions were carried out in triplicate with CSN4ΔN at varying concentrations of Cul1-[32P]N8/Rbx1 substrate and quantified to generate the curve shown. Estimates of kcat and KM are indicated. (B) Deneddylation assays of Cul1-

N8/Rbx1ΔRING (100 nM), incubated with CSN (200 nM, upper panel) or CSN6ΔINS2 (200 nM, lower panel). Samples were taken at the indicated time points, and visualized by SDS PAGE and Sypro Ruby staining. Note that the ΔRING substrate contained an unreacted Sortase tag at the C-terminus of Cul1 that reduced kcat by ~4-fold. (C) Multi-turnover deneddylation reactions were carried out with CSN or CSN5E104A and Cul1-[32P]N8/Rbx1. Substrate was assayed at 1 and 1.3 μM to confirm that saturation was achieved. (D) Single-turnover deneddylation reactions were carried out with CSN on Cul1-[32P]N8/Rbx1 +/- Skp1/Skp2, and with CSN5E104A on Cul1-[32P]N8/Rbx1. (E) Same as panel D except that CSN6ΔINS2 was also evaluated. (F) Multi-turnover deneddylation reactions were carried out in triplicate with CSN5T103I at varying concentrations of Cul1-[32P]N8/Rbx1 substrate and quantified to generate the curve shown. Estimates of kcat and KM are indicated.

Figure Supplement 2.6

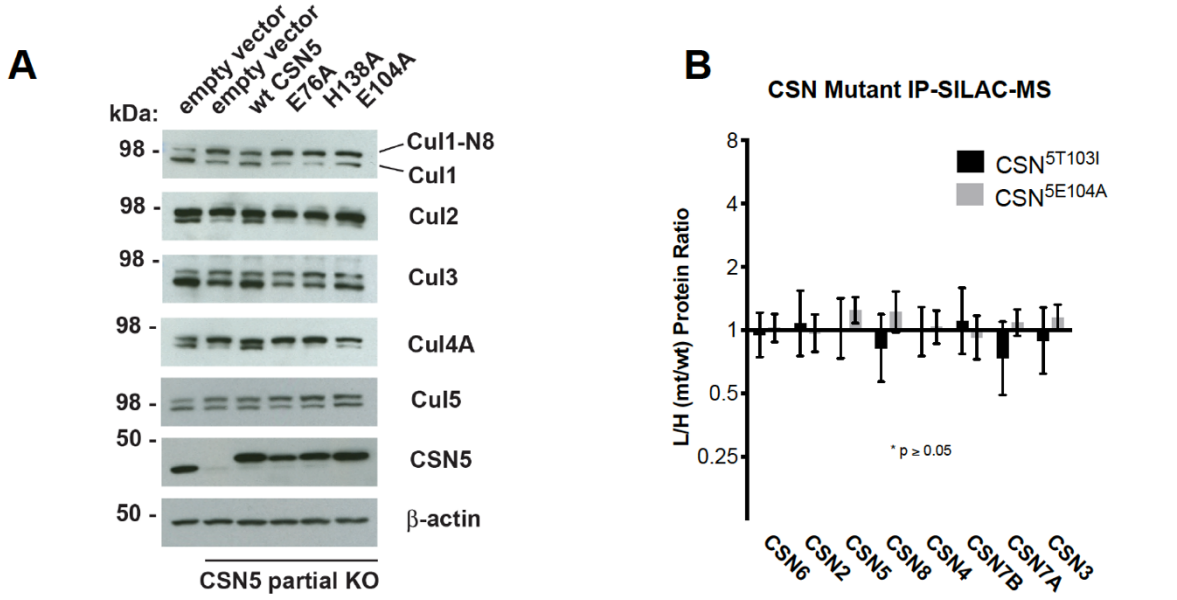

Figure supplement 2.6. Time course and titration data for Figure 6A and supplementary immunoblot for Figure 6B. (A) Same as Figure 6B except that samples were immunoblotted for different cullins. (B) SILAC data for CSN subunits from pull-down analysis shown in Figure 6D.

Supplemental Table 2.1

Table S1: Cross-links within CSN5H138A-SCF-N8Skp2/Cks1.								
Id	Protein1	Protein2	Residue1	Residue2	deltaS	Id-Score	FDR	distance (in Angstrom)
TFNIKNDFTEEEEAQVR-RPKLNR-a5-b3	Skp1	Skp2	142	86	0.36	55.77	0	residues not modeled
SQEGRPVQVIGALIGKQEGR-MLATLFKDER-a16-b7	Csn6	Csn4	75	251	0.73	49.35	0	21
GSDKDFVIVR-GKTPEEIR-a4-b2	Skp2	Skp1	77	130	0.4	42.38	0	residues not modeled
YTALDKWTNQLNSLNQAVVSK-STTFEKSLLMGK-a6-b6	Csn2	Csn1	426	418	0.16	41.71	0	13
KTFNIKNDFTEEEEAQVR-RPKLNR-a6-b3	Skp1	Skp2	142	86	0.64	41.56	0	residues not modeled
YTALDKWTNQLNSLNQAVVSK-STTFEKSLLMGKEFQR-a6-b6	Csn2	Csn1	426	418	0.88	41.31	0	13
KTFNIKNDFTEEEEAQVR-RPKLNR-a1-b3	Skp1	Skp2	137	86	0.33	40.39	0	residues not modeled
IPPAIKSANSELGGIWSVGQR-KQPLR-a6-b1	Csn8	Csn3	65	152	0.44	39.52	0.042	15
MFQDIGVSKDLNEQFKK-LGKLYLER-a9-b3	Cul1	Csn2	552	157	0.38	39.19	0.042	16
GKTPEEIRK-RPKLNR-a2-b3	Skp1	Skp2	130	86	0.48	38.17	0.042	residues not modeled
TWELANNMQEAQSIDEIYKYDKK-VKTLTGK-a19-b2	Csn5	Nedd8	30	6	0.41	38.15	0.042	27
INFKLTNFPEMMNR-DLNEQFKK-a4-b7	Csn2	Cul1	81	559	0.84	37.89	0.042	12
SQNPHGLKQIGLDQIWDDLR-RPKLNR-a8-b3	Cul1	Skp2	50	86	0.51	37.24	0.042	residues not modeled
TWELANNMQEAQSIDEIYKYDKK-VKTLTGK-a22-b2	Csn5	Nedd8	33	6	0.52	37.1	0.042	9
GKTPEEIR-RPKLNR-a2-b3	Skp1	Skp2	130	86	0	36.98	0.042	residues not modeled
TQQQVEAEVTNIKK-KSEDKLAK-a13-b1	Csn7	Csn5	217	295	0.54	36.05	0.042	residues not modeled
RAKAMMLR-KNLQK-a3-b1	Csn1	Skp2	431	295	0.77	35.49	0.042	34
LTKTFLTLSLQDMASR-STTFEKSLLMGK-a3-b6	Csn3	Csn1	349	418	0.34	35.44	0.042	14
MFQDIGVSKDLNEQFKK-LGKLYLEREEYGK-a9-b3	Cul1	Csn2	552	157	0.76	35.41	0.042	16
LSDPIVNTLAKNSNLVR-KQPLR-a11-b1	Skp2	Csn3	228	152	0.38	35.08	0.042	89
SMGSQEDDSGNKPSSYS-TQQQVEAEVTNIKK-a12-b13	Csn3	Csn7	455	217	0	34.53	0.042	residues not modeled
DGMVSFHDNPEKYNNPAMLHNIDQEMLK-STTFEKSLLMGKEFQR-a12-b6	Csn3	Csn1	403	424	0.34	34	0.042	21
TISAGKVNLGAFR-ANQYKENHNR-a6-b5	Csn5	Csn7	180	199	0.27	33.99	0.042	residues not modeled
AMDQEITVNPQFVQKSMGSQEDDSGNKPSSYS-KNLQK-a15-b1	Csn3	Skp2	443	295	0.36	32.82	0.042	22
NLVNKHSETFTR-KNLQK-a5-b1	Csn3	Skp2	318	295	0.31	32.53	0.051	55
IDQVNQLLELDHQKR-STTFEKSLLMGK-a14-b6	Csn2	Csn1	415	418	0.63	32.43	0.051	21
NLVNKHSETFTR-RPKLNR-a5-b3	Csn3	Skp2	318	86	0.31	32.43	0.051	residues not modeled
FIKPLSNAYHELAQVYSTNNPSELR-KNLQK-a3-b1	Csn3	Skp2	291	295	0.32	32.11	0.051	39
SMGSQEDDSGNKPSSYS-KSEDKLAK-a12-b5	Csn3	Csn5	455	299	0.27	31.89	0.051	residues not modeled
AMDQEITVNPQFVQKSMGSQEDDSGNKPSSYS-NQIHVKSPPR-a15-b6	Csn3	Csn1	443	447	0.32	31.83	0.051	residues not modeled
FINNNAVTKMAQSSSK-VKTLTGK-a9-b2	Cul1	Nedd8	447	6	0.5	31.57	0.051	62
NQIHVKSPPREGSQGELTPANSQSR-LSDPIVNTLAKNSNLVR-a6-b11	Csn1	Skp2	447	228	0.79	31.53	0.051	residues not modeled
DGMVSFHDNPEKYNNPAMLHNIDQEMLK-KPVAGALDVSFNK-a12-b1	Csn3	Csn8	403	166	0.3	31.47	0.051	residues not modeled
LKAMDQEITVNPQFVQK-ANQYKENHNR-a2-b5	Csn3	Csn7	428	199	0.93	31.15	0.051	10
DGMVSFHDNPEKYNNPAMLHNIDQEMLK-STTFEKSLLMGK-a12-b6	Csn3	Csn1	403	418	0.28	30.6	0.051	17
LKAMDQEITVNPQFVQK-KSEDKLAK-a2-b1	Csn3	Csn5	428	295	0.43	30.54	0.051	residues not modeled
LSDPIVNTLAKNSNLVR-NLVNKHSETFTR-a11-b5	Skp2	Csn3	228	318	0.46	30.49	0.051	69
LKAMDQEITVNPQFVQK-KSEDKLAK-a2-b5	Csn3	Csn5	428	299	0.45	30.4	0.051	residues not modeled
IDQVNQLLELDHQKR-TISAGKVNLGAFR-a14-b6	Csn2	Csn5	415	180	0.49	30.28	0.051	28

Supplemental Table 2.1-2.5. Cross-links within CSN^{5H138A}-SCF-N8$^{Skp2/Cks1}$. "Id" gives the amino acid sequence of the cross-linked peptides and the exact position of the two cross-linked lysine residues is indicated by the numbers of the letters *a* and *b* respectively for the first and second peptide. "**Protein1"** and "**Protein2**" denote the cross-linked protein names and "**Residue 1"** and "**Residue 2"** respectively defines the position of the cross-linked lysine within the sequence of the protein. "**deltaS"** is the delta score of the respective cross-link, which serves as a measure for how close the best assigned hit was scored in regard to the second best. "**Id_Score**" is a weighted sum of four subscores: xcorrc, xcorrx, match-odds, and TIC that is used to assess the quality of the composite MS2 spectrum as calculated by *xQuest*. "**FDR**" denotes the false-discovery rate as calculated by *xProphet*. The measured distance in Å is given for all cross-links, which fall within modeled residues.

Supplemental Table 2.2

Table S2: Cross-links within CSN5H138A-SCFSkp2/Cks1.							
Id	**Protein1**	**Protein2**	**Residue1**	**Residue2**	**deltaS**	**Id-Score**	**FDR**
TFNIKNDFTEEEEAQVR-RPKLNR-a5-b3	Skp1	Skp2	142	86	0.35	52.26	0
SQEGRPVQVIGALIGKQEGR-MLATLFKDER-a16-b7	Csn6	Csn4	75	251	0.78	44.69	0
IPPAIKSANSELGGIWSVGQR-KQPLR-a6-b1	Csn8	Csn3	65	152	0.38	44.31	0
GKTPEEIRK-RPKLNR-a2-b3	Skp1	Skp2	130	86	0.42	40.01	0
GKTPEEIR-RPKLNR-a2-b3	Skp1	Skp2	130	86	0.47	38.28	0
KTFNIKNDFTEEEEAQVR-RPKLNR-a6-b3	Skp1	Skp2	142	86	0.34	38.13	0
KTFNIKNDFTEEEEAQVR-RPKLNR-a1-b3	Skp1	Skp2	137	86	0.45	37.71	0
LTKTFLTLSLQDMASR-STTFEKSLLMGK-a3-b6	Csn3	Csn1	349	418	0.24	37.37	0
AMDQEITVNPQFVQKSMGSQEDDSGNKPSSYS-NQIHVKSPPR-a15-b6	Csn3	Csn1	443	447	0.27	37.29	0
TISAGKVNLGAFR-ANQYKENHNR-a6-b5	Csn5	Csn7	180	199	0.66	36.95	0
NLVNKHSETFTR-NQIHVKSPPR-a5-b6	Csn3	Csn1	318	447	0.61	36.94	0
YTALDKWTNQLNSLNQAVVSK-STTFEKSLLMGK-a6-b6	Csn2	Csn1	426	418	0.28	36.42	0
MFQDIGVSKDLNEQFK-LGKLYLER-a9-b3	Cul1	Csn2	552	157	0.29	36.17	0
NLVNKHSETFTR-VDSHSKILYAR-a5-b6	Csn3	Csn1	318	402	0.72	35.43	0
NLVNKHSETFTR-RPKLNR-a5-b3	Csn3	Skp2	318	86	0.51	35.22	0
NLVNKHSETFTR-KLSEATR-a5-b1	Csn3	Csn1	318	81	0.57	34.91	0.043
LKAMDQEITVNPQFVQK-ANQYKENHNR-a2-b5	Csn3	Csn7	428	199	0.43	34.55	0.043
LSDPIVNTLAKNSNLVR-KQPLR-a11-b1	Skp2	Csn3	228	152	0.38	34.49	0.043
DGMVSFHDNPEKYNNPAMLHNIDQEMLK-SLLMGKEFQR-a12-b6	Csn3	Csn1	403	424	0.21	34.4	0.043
TQQQVEAEVTNIKK-KSEDKLAK-a13-b5	Csn7	Csn5	217	299	0.56	34.07	0.043
TQQQVEAEVTNIKK-KSEDKLAK-a13-b1	Csn7	Csn5	217	295	0.56	34.06	0.043
IDQVNQLLELDHQKR-WLKTR-a14-b3	Csn2	Rbx1	415	145	0.72	33.99	0.043
IDQVNQLLELDHQKR-TISAGKVNLGAFR-a14-b6	Csn2	Csn5	415	180	0.73	33.95	0.043
NQIHVKSPPREGSQGELTPANSQSR-SMGSQEDDSGNKPSSYS-a6-b12	Csn1	Csn3	447	455	0.29	33.43	0.083
SQNPHGLKQIGLDQIWDDLR-RPKLNR-a8-b3	Cul1	Skp2	50	86	0.57	32.68	0.12
SMGSQEDDSGNKPSSYS-NQIHVKSPPR-a12-b6	Csn3	Csn1	455	447	0.2	31.16	0.154
IDQVNQLLELDHQKR-STTFEKSLLMGK-a14-b6	Csn2	Csn1	415	418	0.64	30.33	0.185
EGIPPQQQRLIYSGKQMNDEK-QILEKAIQLSGAEQLEALK-a15-b5	Nedd8	Csn4	48	32	0.54	28.94	0.243
IDQVNQLLELDHQKR-NQIHVKSPPR-a14-b6	Csn2	Csn1	415	447	0.67	28.68	0.243
TQVLIKLIKPYTR-MRKVLK-a6-b3	Csn2	Cul1,Rbx1	361	760, 3	0.74	28.38	0.243
LSDPIVNTLAKNSNLVR-NLVNKHSETFTR-a11-b5	Skp2	Csn3	228	318	0.42	27.13	0.243
GNQLQEFAAMLMPHQKATTADGSSILDR-WLKTR-a16-b3	Csn4	Rbx1	290	145	0.43	26.73	0.243
TISAGKVNLGAFR-MLATLFKDER-a6-b7	Csn5	Csn4	180	251	0.67	25.99	0.243
AMDQEITVNPQFVQKSMGSQEDDSGNKPSSYS-KNLQK-a15-b1	Csn3	Skp2	443	295	0.26	25.57	0.243
KTLKATASSSAQEMEQQLAER-MAQSSSKSPELLAR-a4-b7	Csn7	Cul1	221	454	0.57	25.06	0.263

Supplemental Table 2.3

Table S3: Cross-links within CSN-Cul1/Rbx1.							
Id	**Protein1**	**Protein2**	**Residue1**	**Residue2**	**deltaS**	**Id-Score**	**FDR**
SQEGRPVQVIGALIGKQEGR-MLATLFKDER-a16-b7	Csn6	Csn4	75	251	0.76	42.99	0
IPPAIKSANSELGGIWSVGQR-KQPLR-a6-b1	Csn8	Csn3	65	152	0.37	42.99	0
YTALDKWTNQLNSLNQAVVSK-STTFEKSLLMGK-a6-b6	Csn2	Csn1	426	418	0.1	42.93	0
TISAGKVNLGAFR-ANQYKENHNR-a6-b5	Csn5	Csn7	180	199	0.68	38.81	0
NLVNKHSETFTR-KLSEATR-a5-b1	Csn3	Csn1	318	81	0.34	38.52	0
YTALDKWTNQLNSLNQAVVSK-STTFEKSLLMGKEFQR-a6-b6	Csn2	Csn1	426	418	0.91	38.29	0
TISAGKVNLGAFR-MLATLFKDER-a6-b7	Csn5	Csn4	180	251	0.63	36.72	0
LTKTFLTLSLQDMASR-STTFEKSLLMGK-a3-b6	Csn3	Csn1	349	418	0.21	36.67	0
LKAMDQEITVNPQFVQK-ANQYKENHNR-a2-b5	Csn3	Csn7	428	199	0.91	36.53	0
NLVNKHSETFTR-NQIHVKSPPR-a5-b6	Csn3	Csn1	318	447	0.52	35.96	0
TQQQVEAEVTNIKK-KSEDKLAK-a13-b5	Csn7	Csn5	217	299	0.64	35.88	0
IDQVNQLLELDHQKR-TISAGKVNLGAFR-a14-b6	Csn2	Csn5	415	180	0.6	35.55	0
AMDQEITVNPQFVQKSMGSQEDDSGNKPSSYS-DKLFNQINIS-a15-b2	Csn3	Csn5	443	326	0.9	34.64	0
TQQQVEAEVTNIKK-KSEDKLAK-a13-b1	Csn7	Csn5	217	295	0.56	34.53	0
VDSHSKILYAR-ANQYKENHNR-a6-b5	Csn1	Csn7	402	199	0.53	33.64	0
NQIHVKSPPREGSQGELTPANSQSR-SMGSQEDDSGNKPSSYS-a6-b12	Csn1	Csn3	447	455	0.55	33.34	0.048
SMGSQEDDSGNKPSSYS-NQIHVKSPPR-a12-b6	Csn3	Csn1	455	447	0.22	33.07	0.048
IDQVNQLLELDHQKR-NQIHVKSPPR-a14-b6	Csn2	Csn1	415	447	0.59	33.04	0.048
IDQVNQLLELDHQKR-WLKTR-a14-b3	Csn2	Rbx1	415	145	0.71	31.99	0.048
IDQVNQLLELDHQKR-STTFEKSLLMGK-a14-b6	Csn2	Csn1	415	418	0.6	31.51	0.048
SMGSQEDDSGNKPSSYS-TQQQVEAEVTNIKK-a12-b13	Csn3	Csn7	455	217	0	31.24	0.048
LTWLYQLSKGELVTNCFKNR-QILEKAIQLSGAEQLEALK-a18-b5	Cul1	Csn4	633	32	0.32	30.34	0.087
DGMVSFHDNPEKYNNPAMLHNIDQEMLK-SLLMGKEFQR-a12-b6	Csn3	Csn1	403	424	0.34	30.19	0.087
KTLKATASSSAQEMEQQLAER-MAQSSSKSPELLAR-a4-b7	Csn7	Cul1	221	454	0.54	26.27	0.216
NLVNKHSETFTR-ANQYKENHNR-a5-b5	Csn3	Csn7	318	199	0.37	26.17	0.216
DGMVSFHDNPEKYNNPAMLHNIDQEMLK-IDQVNQLLELDHQKR-a12-b14	Csn3	Csn2	403	415	0.42	26.09	0.216
SMGSQEDDSGNKPSSYS-KSEDKLAK-a12-b5	Csn3	Csn5	455	299	0	26.05	0.216
AMDQEITVNPQFVQKSMGSQEDDSGNKPSSYS-NQIHVKSPPREGSQGELTPAN	Csn3	Csn1	443	447	0.27	25.01	0.216

Supplemental Table 2.4

Table S4: Cross-links within CSN5H138A-SCF-N8Fbw7FL.							
Id	**Protein1**	**Protein2**	**Residue1**	**Residue2**	**deltaS**	**Id-Score**	**FDR**
YTALDKWTNQLNSLNQAVVSK-STTFEKSLLMGK-a6-b6	Csn2	Csn1	426	418	0.2	39.12	0
IPPAIKSANSELGGIWSVGQR-KQPLR-a6-b1	Csn8	Csn3	65	152	0.43	36.68	0
NLVNKHSETFTR-KLDHGSEVR-a5-b1	Csn3	Fbw7fl	318	208	0.67	33.36	0
TISAGKVNLGAFR-ANQYKENHNR-a6-b5	Csn5	Csn7	180	199	0.47	30.42	0
FINNNAVTKMAQSSSK-VKTLTGK-a9-b2	Cul1	Nedd8	447	6	0.54	30.4	0
TQQQVEAEVTNIKK-KSEDKLAK-a13-b1	Csn7	Csn5	217	295	0.6	29.4	0
MAGEQKPSSNLLEQFILLAK-SFSLGKKPCK-a6-b7	Csn7	Fbw7fl	6	223	0.51	29.22	0
YTALDKWTNQLNSLNQAVVSK-KAEARLLEEQR-a6-b1	Csn2	Cul1	426	300	0.27	29.15	0
VEEKEGIPPQQQR-EEYGKLQKILR-a4-b5	Nedd8	Csn2	33	167	0.94	28.92	0
LTKTFLTLSLQDMASR-STTFEKSLLMGK-a3-b6	Csn3	Csn1	349	418	0.46	28.62	0

Supplemental Table 2.5

Table S5: Cross-links within CSN5H138A-SCF-N8Fbw7trunc							
Id	**Protein1**	**Protein2**	**Residue1**	**Residue2**	**deltaS**	**Id-Score**	**FDR**
SQEGRPVQVIGALIGKQEGR-MLATLFKDER-a16-b7	Csn6	Csn4	75	251	0.72	44	0
IPPAIKSANSELGGIWSVGQR-KQPLR-a6-b1	Csn8	Csn3	65	152	0.52	40.55	0
YTALDKWTNQLNSLNQAVVSK-STTFEKSLLMGK-a6-b6	Csn2	Csn1	426	418	0.18	38.91	0
MFQDIGVSKDLNEQFK-LGKLYLER-a9-b3	Cul1	Csn2	552	157	0.27	38.66	0
IDQVNQLLELDHQKR-STTFEKSLLMGK-a14-b6	Csn2	Csn1	415	418	0.56	36.03	0

3 – CELLULAR ORGANIZATION, KINETICS, AND REGULATION OF CULLIN4-RING UBIQUITIN LIGASES

This chapter is based on the manuscript draft as submitted to the journal prior to revision and formatting by Molecular Cell:

KM Reichermeier, R Straube, JM Reitsma, MJ Sweredoski, CM Rose, A Moradian, Willem den Besten, T Hinkle, E Verschueren, G Petzold, N Thomä, IE Wertz, RJ Deshaies, DS Kirkpatrick; *PIKES analysis uncovers response to degraders and key regulatory mechanisms of CRL4 ligase networks* (revised manuscript in press, *Molecular Cell,* DOI: 10.1016/j.molcel.2019.12.013)

3.1 Summary

Immunomodulatory Drugs (IMiDs) used for the treatment of multiple myeloma function by co-opting a Cullin4 RING ubiquitin Ligase (CRL4) to inducibly degrade oncogenic drivers. Despite intense efforts to rationally design degrader molecules that co-opt CRL4s, much about the organization and regulation of these ligases remains elusive. Here, we establish Protein Interaction Kinetics and Estimation of Stoichiometries (PIKES) analysis, a systematic proteomic profiling platform that integrates cellular engineering, affinity purification, chemical stabilization, and quantitative mass spectrometry to investigate the dynamics of interchangeable multiprotein complexes. Using PIKES, we show that ligase assemblies of Cullin4 with individual substrate receptors differ in abundance by up to 200-fold and that Cand1 acts as an exchange factor to remodel the CRL4 ligase pool. Integrating quantitative data and model simulations of CRL-mediated substrate turnover, we show that high substrate receptor levels can enhance the potency of degraders. Beyond the CRL4 network, we show how PIKES can reveal systems level biochemistry for cellular protein networks important to drug development.

3.2 Introduction

Cullin-RING Ligases (CRLs) represent a collection of ~250 enzyme complexes that ubiquitinate protein substrates to alter their function or mark them for proteasomal degradation (Deshaies and Joazeiro, 2009a). Among these, the Cul4 family of CRLs regulate cell cycle, DNA damage repair, and are co-opted by therapeutic compounds to promote degradation of oncogenic protein (Hannah and Zhou, 2015; Jackson and Xiong, 2009; Kortüm et al., 2015). CRL4s are composed of either a Cullin4A•Rbx1 or Cullin4B•Rbx1 catalytic core (hereafter Cul4A or Cul4B, or if referred to both Cul4) and an interchangeable adapter-substrate receptor module (A•SR). Like a drill that uses an adapter and various bits to accommodate a diverse range of screws, Cul4A/B scaffolds use the DDB1 adapter to engage an array of DDB1-Cul4 Associated Factors (DCAFs; substrate receptors) and ubiquitinate a range of substrates (Figure 3.1).

The idea of chemically induced degradation was conceived nearly 20 years ago with the first Proteolysis Targeting Chimeras (PROTACs) (Sakamoto et al., 2001) and surged when $CRL4^{CRBN}$ emerged as the long elusive target of thalidomide and its paralogs – also known as IMiDs (Gandhi et al., 2014; Ito et al., 2010; Krönke et al., 2014; Lu et al., 2014). IMiDs act as molecular glues to induce neo-substrate recruitment through the substrate receptor CRBN, catalyzing their ubiquitination and subsequent degradation. These initial discoveries were followed by a wave of studies demonstrating that IMiD-based PROTACs, as well as molecules co-opting other E3 ligases, can potently induce degradation of neo-substrates (Bondeson et al., 2015; Han et al., 2017; Neklesa et al., 2017; Ottis et al., 2017; Paiva and Crews, 2019; Uehara et al., 2017; Winter et al., 2015; Zengerle et al., 2015; Zhang et al., 2018). Since 2015, more than thirty PROTAC-like molecules have been reported, giving rise to a promising new class of medicines (An and Fu, 2018; Deshaies, 2015; Paiva and Crews, 2019).

CRLs are dynamic protein assemblies with sophisticated regulatory mechanisms, exposing new degrader drugs to unusually complex pharmacodynamics (Bulatov and Ciulli, 2015). The cellular organization of endogenous CRL4 assemblies and their modes of regulation

have been hypothesized based on a recent model of Skp1-Cul1-Fbox (SCF/CRL1) complexes, for which Cand1/2 act as exchange factors for pools of non-substrate-bound A•SRs (Skp1•Fbox) residing in a dynamic equilibrium. Limiting amounts of Cul1 mandate that the system displays plasticity to cope with changes in SR expression (Liu et al., 2018; Pierce et al., 2013; Reitsma et al., 2017; Straube et al., 2017; Wu et al., 2013; Zemla et al., 2013). Though rapid, the exchange cycle can temporarily be put on hold through substrate binding. This creates an adaptive disequilibrium favoring the stable assembly of ligase complexes for which substrates are present. Substrate driven assembly persists because fully assembled and substrate-bound SCF ligases become trapped in the Nedd8-modified state ($_{\text{Nedd8}}$-Cul1$^{\text{A•SR•Substrate}}$) and are protected from Cand1-mediated exchange. In this model, substrate sterically hinders the Cop9 Signalosome (CSN) Nedd8 deconjugase from accessing the neddylated SCF complex (Cavadini et al., 2016; Emberley et al., 2012; Enchev et al., 2012; Fischer et al., 2011b; Mosadeghi et al., 2016). Once substrate is released, CSN can bind SCF and quickly remove Nedd8, allowing Cand1/2-mediated recycling of catalytic cores.

Given its clinical importance for the efficacy of IMiDs, sulfonamides (Han et al., 2017; Uehara et al., 2017) and emerging PROTAC molecules, understanding how the CRL4 network is regulated is paramount. Key outstanding questions include: How many DDB1•DCAF modules exist per cell? What are the concentrations of the Cul4-bound and unbound DDB1•DCAF pools? Does Cand1 act as a CRL4 exchange factor and is it required for degradation of CRL4 substrates? How do substrate recruitment and DCAF expression affect CRL4 assembly and function? Importantly for degrader drug development, what factors determine the efficacy of molecules targeting CRL4s and what effect do these molecules have on the CRL4 network and its dynamics?

Previously published studies have begun to elucidate the composition of cellular CRL4 complexes (Angers et al., 2006; Bennett et al., 2010; He et al., 2006b; Higa et al., 2006; Jin et al., 2006). One challenge in interpreting past work is that over-expression and post-lysis exchange can be confounding factors for CRLs (Reitsma et al., 2017). To shed light on CRL4 assembly and regulation, we developed a proteomic profiling platform to study

the dynamics, stoichiometry and regulatory mechanisms of endogenous CRL4 ligases in human cells. Protein Interaction Kinetics and Estimation of Stoichiometries (PIKES) analysis revealed new CRL4 biology and key considerations for degrader drug development. Looking beyond CRL4 ubiquitin ligases, PIKES provides a framework for systematic proteomic profiling of dynamic and interchangeable protein complexes.

3.3 Results

A toolbox to monitor endogenous CRL4 complexes

The human genome encodes ~100 DCAF proteins that are predicted based on sequence to associate with DDB1 (Angers et al., 2006; He et al., 2006b; Higa et al., 2006; Lee and Zhou, 2007). It is currently unknown how many DCAFs truly assemble into CRL4s. Human embryonic kidney cells (293T/17) were genetically engineered using CRISPR to express either a 3xFLAG tag fused to the N-terminus of Cul4A, a 3xHA tag fused to the NTD of Cul4B, or both tags in the same cell (Figure 3.1). Selected single cell clones were tested for homozygous insertion of the epitope tags via western blot and genomic PCR. Morphology, cell doubling time and Cul4A and Cul4B mRNA expression closely resembled those of the parent population (Supplemental Item 3.1A-L). Using these engineered cell lines, endogenous CRL4A and CRL4B complexes were immunoprecipitated via their respective epitope tags and the eluates analyzed via LC-MS. Significance Analysis of Interactomes (SAINT) (Choi et al., 2011) identified 26 DCAFs to be associated with Cul4A and Cul4B, of which 24 were confirmed as DDB1-dependent in SILAC AP-MS experiments (Figure Supplement 3.1A-G). Besides DCAF proteins, all subunits of the Cop9 Signalosome (CSN), Cand1 (but not Cand2), cullin inhibitor glomulin (Duda et al., 2012; Tron et al., 2012), neddylation enzyme DCN1 (Cope and Deshaies, 2003; Kurz et al., 2005; Wei and Deng, 2003), and p97 adapter protein Ubxd7 (Alexandru et al., 2008; Besten et al., 2012) were identified. The only proteins that weren't predicted to assemble with Cul4 were three subunits of phosphatidylinositol 5-phosphate 4-kinase Type II (PIP4K2A, B and C) which were found to associate with Cul4B. Based on these initial experiments, we developed a targeted proteomics assay to quantitatively monitor 37

Cul4 interacting proteins. For this purpose, we used Parallel Reaction Monitoring (PRM) (Peterson et al., 2012) which allows targeted analysis of a selected subset of peptides to achieve more sensitivity compared to regular shotgun MS methods as well as accurate relative or absolute quantification when used with internal standards (Figure Supplement 3.1H, I).

Cand1/2 are CRL4 exchange factors and required for efficient substrate degradation

After defining the endogenous repertoire of Cul4•DDB1•DCAF complexes, we sought to determine the stability of these interchangeable complexes during immunoprecipitation. Based on SCF ligases (Liu et al., 2018; Reitsma et al., 2017) and the robust association of Cand1 with endogenous Cul4, we hypothesized that CRL4s might exchange A•SR modules, with post-lysis exchange complicating interpretation of experimental results. A SILAC-based CRL4 exchange assay (Figure 3.2A) confirmed the time dependent exchange of nearly all CRL4 interactors (Figure 3.2B). Western blot analysis revealed that the majority of Cul4 molecules were rapidly de-neddylated upon cell lysis (Figure 3.2C), supporting the hypothesis that most CRL4 complexes are susceptible to Cand1/2-mediated exchange. To directly test whether Cand1/2 are driving A•SR exchange from cellular CRL4s, experiments were performed under three different conditions (Figure 3.2D): In lysates from cells (1) lacking Cand1/2, (2) pre-treated with small molecule inhibitor CSN5i-3 (Schlierf et al., 2016) to preserve endogenous Cul4 neddylation which prevents Cand1/2 binding (Figure 3.2E,F,), or (3) spiked with excess recombinant Cul4A•Rbx1 to act as a molecular sponge for unassembled A•SR modules and Cand1/2 (Figure 3.2F). Under all three conditions, CRL4 complexes remained stable over the course of 60 minutes (Figure 3.2D, Figure Supplement 3.2B). DCAFs that differed from the norm included AMBRA1, PHIP, and PWP1. These proteins were significantly enriched in the bead background and displayed relatively low signal to noise ratios under our experimental conditions, as noted in later experiments (Figure Supplement 3.4E, Figure Supplement 3.5E). To determine the functional impact of Cand1/2 on CRL4-mediated substrate degradation we chose to monitor the degradation of RBM39 upon treatment with

indisulam, a recently reported molecular glue that recruits RBM39 to $CRL4^{DCAF15}$ (Han et al., 2017; Uehara et al., 2017). As anticipated, cells lacking Cand1/2 degraded RBM39 significantly slower than a wild type population at the same dose of indisulam (Figure Supplement 3.2C, D). Taken together, these results confirm that Cand1/2 function as efficient A•SR exchange factors for most CRL4s, supporting a model of adaptive exchange (Figure 3.2F). Standing in contrast to the model, a subset of DCAFs including VPRBP (DCAF1) and BRWD3 were highly stable, dissociating less than 10% in 3 hours (Figure 3.2B, Figure Supplement 3.2A). These unusually stable CRL4 complexes were not further destabilized by pre-treatment with Nedd8-E1 inhibitor MLN4924 (Brownell et al., 2010; Soucy et al., 2009), a condition that increased exchange of all A•SRs in the SCF system (Reitsma et al., 2017) (Figure Supplement 3.2E). One explanation for this is that Cand1-mediated exchange might not be as efficient for some CRL4 complexes as for SCF. To test this, CRL4B complexes lacking Cand1 were purified from Cand1/2 KO cell lysates under conditions allowing for de-neddylation. Purified CRL4B complexes were then incubated for 1 hr with or without excess recombinant Cand1, followed by PRM LC-MS. While most (~70%) DDB1•DCAF modules were dislodged by exogenous Cand1, a few DCAFs showed much less dissociation (Figure Supplement 3.2F). VPRBP, DDB2, BRWD1/3, and DCAF11 displayed good signal-to-noise ratios and were dislodged much slower than other DCAFs, suggesting that these complexes either resist deneddylation or are refractory to Cand1/2 exchange.

CRL4 complexes are stabilized by N8 Block and Molecular Sponge

Having identified conditions to suppress post-lysis exchange, we were curious about the effects of such treatments on the immunoprecipitated CRL4 complexes. To assess the effect of N8 Block and molecular sponge on Cul4B complexes, we performed Cul4B IPs and PRM MS analysis from cells pulsed for 5 min with 1μM MLN4924+CSN5i-3, pulsed with either molecule alone, or from cells lysed in the presence of either 2.5 μM molecular sponge $Cul4A•Rbx1^{GST}$ or GST control. As anticipated, both N8 Block and molecular sponge substantially increased DDB1•DCAF complexes co-precipitated with endogenous Cul4B, indicating successful conservation of CRL4B assemblies during the IP process

(Figure 3.2G). Consistent with the finding that de-neddylation is fast in lysates (Figure 3.2C), brief MLN4924 treatment did not display any additional destabilizing effect. Treatment with CSN5i-3 alone or in combination with MLN4924 had a very similar effect on CRL4B complexes which we attribute to the fact that most CRL4s are highly neddylated to begin. N8 Block and molecular sponge showed the same trends. Yet, discrepancies in preservation of individual DCAFs do occur, the consequences of which are likely minor as discussed below. Taken together, these observations provide evidence that the assembly and stability of most CRL4 complexes is regulated by the neddylation cycle and the Cand1/2 exchange factors.

Individual CRL4 ligases show Cullin-scaffold preferences and differ up to 200-fold in absolute abundance

Experimentally suppressing post-lysis exchange permitted us the unique opportunity to capture CRL4 assemblies in their native states. Next, we aimed to comprehensively define stoichiometries for the cellular CRL4 ligase network by measuring the cellular concentration of network components, the stoichiometry of assembled CRL4 complexes and the composition of the free DDB1•DCAF reserve. While synthetic peptide standards facilitate inter-sample relative quantification, direct comparisons of inter-protein stoichiometries and cellular concentrations remain challenging due to the cumulative variability of many independent concentration measurements. To circumvent this issue, we designed a synthetic CRL4 QconCAT polypeptide consisting of 67 concatenated equimolar reference peptides for 31 proteins (Pratt et al., 2006; Scott et al., 2016) (Figure 3.3A, Figure Supplement 3.3A, B). Whole cell lysates from 293T/17$^{\text{Flag-Cul4A/HA-Cul4B}}$ cells were mixed with the QconCAT standard and analyzed via PRM LC-MS (Figure 3.3B, Figure Supplement 3.3C). This data revealed three interesting findings: 1) Cul4B was ~2-fold more abundant than Cul4A, consistent with data from the proteome abundance atlas of 29 healthy tissues (Wang et al., 2019), where Cul4B is on average found ~1.8-fold (range 0.8 – 4.8-fold) more abundant than Cul4A (Figure Supplement 3.3D). 2) DDB1 was present in ~7-fold excess over total Cul4. DDB1 protein levels detected in the 29 human tissues (Wang et al., 2019) are similarly ~3-fold in excess over Cul4 (range 1.5-4.9-fold) (Figure

Supplement 3.3E). 3) The concentration of all DCAFs combined to roughly equal the concentration of DDB1, exceeding DDB1 only by ~15%. This last observation supports the hypothesis that most DCAFs exist and function as stable heterodimers with DDB1. Next, we performed a combined immunoprecipitation of FLAG-Cul4A and HA-Cul4B from cells pulsed with N8 Block. Enriched samples were spiked with CRL4 QconCAT and analyzed with PRM LC-MS, allowing the determination of stoichiometric relationships for purified CRL4 complexes from aggregate peptide measurements (Figure 3.3D-E, Figure Supplement 3.3F). Importantly, these measurements meet several control criteria which are explicated in detail in the STAR methods. Overall, the 22 $Cul4^{DCAF}$ ligase complexes displayed dramatic differences in abundance. $Cul4^{CRBN}$, the target of IMiD-based degraders, accounted for ~20% of all CRL4 ligases in our cell system, whereas $Cul4^{DET1}$ only totaled ~0.1% (Figure 3.3D). The data reveal that ~89% of Cul4 associated with DDB1 and only ~27% with Cand1. These measurements suggest a non-negligible population of Cul4 exists as a ternary complex with DDB1 and Cand1 (Figure 3.3E). Integrating the cellular amount of Cul4 and its relative occupancy with DDB1 allows estimation of CRL4 levels at ~200nM, or ~230,000 ligase complexes per cell. This estimate agrees well with the sum of calculated abundances of individual CRL4s (~180nM) which range from as little as 0.2nM ($Cul4^{DET1}$) to 42nM ($Cul4^{CRBN}$) (Figure 3F). Furthermore, ~55% of Cul4 was neddylated and associated with a CSN complex, showing that the N8 Block successfully conserved Cul4-neddylation and led to co-precipitation of large amounts of inhibited CSN (Figure 3.3E, Figure Supplement 3.3G). This is consistent with observations made for catalytically-dead CSN, which traps substrate in a high affinity conformation to prevent CRL4 release (Cavadini et al., 2016; Mosadeghi et al., 2016). In contrast, without blocking de-neddylation in lysates, the Cul4 occupancy shifted to 66% DDB1 and 54% Cand1, reflecting a net loss of ~25% CRL4 complexes due to post-lysis de-neddylation and dislocation of DDB1 by Cand1 (Figure Supplement 3.3G, H).

DCAFs of highly abundant ligases show high relative assembly

Interestingly, most DCAFs were expressed at similar levels (Figure 3.3G). This observation implies that the 200-fold differences in abundances of assembled CRL4

complexes wasn't driven by protein expression. Consistent with this, no correlation could be found between protein expression and fractional contribution of each DCAF to all assembled CRL4 complexes (Figure Supplement 3.3I). Ultimately, this implies that the fraction of each DCAF that is Cul4-assembled versus in the free pool might correlate with ligase abundance. We call this parameter Relative Assembly (% assembly) which can be computed using the quantitative information of cellular concentrations and complex stoichiometries. Similar to overall abundance, calculated % assembly varied across two orders of magnitude and indeed correlated well with ligase abundance (% of individual $Cul4^{DCAF}$ amongst all CRL4s) (Figure 3.3H, Figure Supplement 3.3J). This supports the hypothesis that abundant CRL4s are formed by allowing high relative assembly of individual DCAFs over others. To test the accuracy of our calculations, we performed sequential Cul4A and Cul4B IPs in the presence of molecular sponge to capture the free pool of assembly-competent DDB1•DCAFs and the individual assemblages of CRL4A and CRL4B (Figure Supplement 3.3K). For DDB1, one of the most robust measurements in both assays, we calculated ~12% Cul4-bound and measured ~7% (Figure 3.3E, Figure Supplement 3.3L). Of 21 DCAFs that were accurately assessed in both assays, 15 (70%) showed values within +/- 2.5-fold (Figure Supplement 3.3M). DCAFs showing the largest discrepancies were previously noted proteins with low signal to noise ratios like PHIP and PWP1 (Figure Supplement 3.3N) or proteins with the lowest abundances like DET1 and RFWD2.

DCAFs show selective binding to Cul4A or Cul4B

In addition to providing measurements for relative assembly, the sequential IP approach revealed that certain DCAFs displayed preferences for either Cul4A or Cul4B. While all DDB1•DCAF modules detected associated with both Cul4 scaffolds, a subset showed up to 4-fold preference for one over the other. We further validated this finding via an orthogonal approach using the N8 Block and single IPs of Cul4A and Cul4B (Figure 3.3I). Interestingly, the two scaffolds show different localization patterns, with Cul4A localized in both the nuclear and cytoplasmic compartments and Cul4B primarily in the nucleus (Figure Supplement 3.3O). This agrees with previous studies (Zou et al., 2009) and begs

the question of whether subcellular compartmentalization is a key determinant of ligase assembly. The Cul4 family is unique amongst CRLs with two similar scaffolds serving as the catalytic cores (Hannah and Zhou, 2015). The lack of proper methods to analyze and quantify the CRL4 network has until now prevented functional and compositional differentiation between CRL4A and CRL4B complexes. If used in combination with more advanced model systems, we anticipate our PIKES assays could help illuminate long-standing mysteries of why all vertebrates conserved two independent Cul4 genes which display different phenotypes when mutated in human diseases (Chen et al., 2012; Jiang et al., 2013; Liu et al., 2009; Vulto-van Silfhout et al., 2015; Wang et al., 2014; Zou et al., 2007).

CRL4s reshape their assemblies and form Cul4A•Cul4B dimers upon UV-induced DNA damage

One fundamental question in CRL biology involves regulation of ligase assembly. For both CRL4 and SCF, protein levels of most SRs lie between 25-100 nM while the relative assembly of A•SR modules varies more than 200-fold (Figure 3B, Reitsma et. al. 2017). These dramatic differences in assembly must arise either from affinity differences of individual A•SR modules towards cullins or another more complex mechanism. SCF complexes are regulated by a just-in-time assembly system wherein substrate stabilizes ligase complexes by creating a disequilibrium favoring certain A•SRs over others (Liu et al., 2018; Reitsma et al., 2017). Based on many parallels observed in our experiments, we hypothesized that physiological stimuli which change substrate abundance might reshape CRL4 assemblies. To the test this idea, we used a UV-induced DNA damage model in which cells accumulate 4-6 photoproducts and pyrimidine-dimers which are recognized by the DCAF DDB2 (Chu and Chang, 1988). This is thought to create a ubiquitination zone around the lesions that initiates nucleotide excision repair (Fischer et al., 2011b; Scrima et al., 2008). In the process of initiating repair, DDB2 is itself auto-ubiquitinated, extracted from chromatin and quickly degraded (Figure 3.4A). To monitor changes in CRL4 assemblies induced by DNA damage, we pulsed cells with UV light, incubated for varying times post-damage and analyzed Cul4B complexes via PRM-MS. While most proteins

associated with Cul4B did not change in abundance, we observed significant changes for four proteins (Figure 3.4B, Figure Supplement 3.4A). As expected, DDB2 rapidly dissociated from Cul4 after initiation of repair and was degraded by the proteasome (Figure 3.4C). Additionally, association of VPRBP and DDA1 with Cul4B increased following DNA damage (Figure 3.4D, E). $Cul4^{VPRBP}$ functions as the E3 ligase that targets MCM10 stalled on UV-induced DNA lesions for degradation (Kaur et al., 2012). DDA1 is thought to be a co-factor for CRL4 complexes (Han et al., 2017) that associates with multiple DDB1•DCAF modules (Olma et al., 2009; Shabek et al., 2018). Surprisingly, Cul4A also increased in Cul4B complexes isolated from UV-treated cells (Figure 3.4F). As for DDB2, VPRBP and DDA1, Cul4A signal was well above bead background, confirming the presence of Cul4A•Cul4B heterodimers in a physiological context (Figure Supplement 3.4B-F). Dimerization of Cul4•DDB1•VPRBP has been proposed to enhance substrate ubiquitination *in vitro* (Ahn et al., 2011). While future studies are needed to determine the functional consequences, these results demonstrate the power of PIKES to monitor dynamic and inducible interactions within conserved protein families.

Abundance of pre-formed ligase complex does not predict turnover efficiency of individual CRL4s

The approach of co-opting E3 ubiquitin ligases to target neo-substrates for proteasomal degradation raised interest in CRL4s as promising drug targets (Deshaies, 2015). IMiD-based compounds have been shown to successfully induce degradation of a variety of neo-substrates in human cell lines and mice via $Cul4^{CRBN}$ (Lu et al., 2015a; Nabet et al., 2018; Sun et al., 2019; Winter et al., 2015). Recently, $CRL4^{DCAF15}$ was shown to inducibly specify degradation of RBM39 in the presence of aryl sulfonamides (Han et al., 2017; Uehara et al., 2017). Interestingly, $CRL4^{CRBN}$ and $CRL4^{DCAF15}$ differ by ~70-fold in abundance in our cell system (Figure 3.5A, B). To test the efficiency of these two ligases in degrading neo-substrates we chose to evaluate four different degraders: the sulfonamide indisulam to target RBM39 via DCAF15, as well as lenalidomide (CK1α and ZFP91), dBET1 (BRD4) and dTAG-13 (exogenous $FKBP12^{F36V}$-GFP) which each utilize CRBN. Surprisingly, despite substantially lower amounts of pre-formed $CRL4^{DCAF15}$, RBM39 was

degraded faster than all endogenous CRBN neo-substrates (Figure 3.5C, D, Figure Supplement 3.5A-D). To derive substrate turnover in molecules per minute, substrate copy numbers were estimated from the proteome atlas (Wang et al., 2019) (Figure 3.5E-F). While substrate half-lives differed up to ~5-fold, the quantities of molecules per minute turned over by $CRL4^{DCAF15}$ compared to $CRL4^{CRBN}$ differed by up to ~60-fold (Figure 3.5G). This suggests that the degree of Cul4-occupancy at steady state is not indicative of how well a DCAF might serve as a co-opted ligase. Instead, factors like ternary complex stability (Roy et al., 2019), substrate lysine accessibility, differences in re-synthesis rates, counteracting de-ubiquitination or pre-proteasomal processing by factors like p97 (Nguyen et al., 2017), each have the potential to modulate degradation rates downstream of a substrate-ligase pair. Furthermore, high levels of endogenous and neo-substrates have the potential to competitively inhibit turnover, particularly in the case of IMiDs which target multiple zinc finger proteins for degradation (Sievers et al., 2018; Sperling et al., 2019).

Degrader molecules minimally reshape ligase assemblies without disturbing the overall CRL4 network

We were next interested in the broad effects of degrader molecules on the Cul4 network. Based on observations that Cand1 and Nedd8 establish adaptive disequilibria in favor of substrate engaged DCAFs, we hypothesized that ligase assembly might be elicited by degrader molecules. To test this, cells were treated with the four degrader compounds followed by Cul4 immuno-enrichment and PRM MS analysis. Surprisingly, lenalidomide caused a small decrease in assembled $Cul4^{CRBN}$ complexes, while dTAG-13 and dBET1 showed little if any change in CRBN assembly (Figure 3.5H,I, Figure Supplement 3.5E). $CRL4^{CRBN}$ represents the highest assembled Cul4 ligase in the basal state, suggesting the presence of endogenous, likely transient stabilizing factors such as substrates. In this case, lenalidomide and IMiD-based PROTACs would need to compete for CRBN against endogenous substrates with the assembly disequilibrium depending on the relative abundance of neo-substrates versus endogenous substrates. DCAF15 on the other hand is one of the lowest assembled CRL4 ligases and we reasoned it might be a better candidate to observe this phenomenon of adaptive ligase assembly. Indeed, when cells were exposed

to indisulam, we detected a ~2-fold increase in DCAF15 assembly as early as 30 min following treatment (Figure 3.5J, K, Figure Supplement 3.5F). We hypothesized that if this increase in assembled DCAF15 ligase was stabilized via Nedd8, pretreatment of cells with MLN4924 should blunt this effect. MLN4924 indeed blocked indisulam-induced assembly of Cul4B complexes (Figure Supplement 3.5 G-I) and inhibited the degradation of RBM39 (Figure Supplement 3.5J). Furthermore, brief pre-treatment with CSN inhibitor CSN5i-3 also blocked degradation of RBM39, albeit not as dramatically as inhibition of Ub-E1, Nedd8-E1 or the proteasome (Figure Supplement 3.5J, K). While similar quantities of $Cul4^{DCAF15}$ are assembled upon inhibition of CSN (Figure Supplement 3.5H, I), scaffold exchange is dramatically suppressed (Figure 3.2D). Together with the extension of RBM39 half-life in Cand1/2 KO cells (Figure Supplement 3.2C, D), these results suggest that Cand1-driven recycling of Cul4 scaffolds enables sampling of the DDB1•DCAF pool for proper substrate degradation. Moreover, the quantities of pre-formed ligase play a minor role. These data provide a cell-based demonstration of substrate driven CRL assembly and the factors modulating this process. Furthermore, these results underscore the remarkable adaptability of CRL4s in response to physiological stimuli and degrader drugs that occurs without compromising other ligase assemblies within the Cul4 network.

Higher DCAF expression can result in faster substrate degradation and increased degrader potency

One fundamental question regarding multi-protein networks like CRLs is how quantities of individual components influence function. While our measurements showed that most DDB1•DCAF modules exist at cellular concentrations ≤100nM in 293T/17 cells (Figure 3.3D), recent proteomic analyses reveal that levels of individual DCAFs can range across two orders of magnitude between different human tissues (Wang et al., 2019) (Figure 3.6A). If DCAF expression positively affected ligase assembly and rate of substrate degradation, variations in DCAF levels could provide opportunities to fine tune the specificity of degrader molecules. However, a recently developed mathematical model of SCF regulation predicts that higher expression levels of Cul1 substrate receptor β-TRCP do not increase degradation of IκBα (Liu et al., 2018). Mechanistically, a significant

difference between endogenous IκBα and chemically induced neo-substrates is requisite IκBα phosphorylation, a potential limiting factor. To test this hypothesis in silico, we lowered the $t_{1/2}$ of IκBα phosphorylation from 15min to 1min in the SCF model to simulate the rate of IκBα degradation at wild type or increased β-TRCP levels. Indeed, under conditions of rapid phosphorylation, higher levels of β-TRCP would shorten the predicted $t_{1/2}$ of IκBα by 2.6-fold (Figure 3.6B). Translating this hypothesis to CRL4s, we engineered 293T/17$^{Flag\text{-}Cul4A/HA\text{-}Cul4B}$ cells to stably over-express DCAF15 and tested whether higher DCAF expression can enhance chemically induced substrate turnover. Using the QconCAT PRM MS approach, the cellular concentration of DCAF15 measured 795nM versus 60nM in wild type cells (Figure 3.6C). This ~13-fold difference resulted in ~3.6-fold faster $t_{1/2}$ (Figure 3.6D). Mechanistically, this effect is explained by increases in pre-assembled CRL4^{DCAF15} as well as increased ternary complex formation (Figure 3.6E, F). Furthermore, the faster RBM39 degradation rate in cells overexpressing DCAF15 translates into a 17.5-fold lower DC_{50} (Figure 3.6G). These observations provide functional evidence that DCAF protein expression could serve as an important pharmacodynamic biomarker for agents invoking molecular glue mechanisms (Han et al., 2017). Moreover, since DCAF expression varies between tissues (Pontén et al., 2008; Wang et al., 2019), this provides an opportunity to achieve specific substrate degradation in cancer cells by engaging an CRL substrate receptor with elevated expression levels.

3.4 Discussion

A systematic proteomic profiling toolbox to study CRLs

In this study, we developed PIKES (Protein Interaction Kinetics and Estimation of Stoichiometries), a proteomics platform to systematically decipher the composition, biochemical dynamics and regulatory mechanisms of endogenous Cul4-RING ligases. A set of mapping experiments defined the endogenous repertoire of assembled CRL4 ligases and served as the basis to develop targeted proteomics assays. A key breakthrough here was the CRL4 QconCAT reference standard (Pratt et al., 2006; Scott et al., 2016) that enabled the facile determination of stoichiometric relationships between ~30 proteins in

cell lysates and immunoprecipitated samples. Extending from the previously reported Molecular Sponge technique (Reitsma et al., 2017), another factor that propelled this work was the ability to freeze CRL4 pathway components chemically for isolation and quantitative analysis, allowing efficient determination of the stoichiometric relationships. Suppressing post-lysis exchange with a cocktail of MLN4924 (Brownell et al., 2010; Soucy et al., 2009) and CSN5i-3 (Schlierf et al., 2016) at the time of harvest dramatically enhanced experimental throughput and is extensible to other pathways where rich chemical biology toolboxes also exist.

It still is underappreciated that many protein networks and scaffolding proteins form highly dynamic, rather than stable assemblies. Signaling networks like mitogen-activated protein kinase modules, or Cadherin-based cell adhesion complexes, long considered to form stable complexes have been shown to be very dynamic (Garbett and Bretscher, 2014). Another group of highly conserved proteins forming holoenzyme complexes from a shared catalytic subunit and various regulatory modules are Ser/Thr phosphatases (Shi, 2009) which have been successfully targeted with specific small molecule inhibitors (Das et al., 2015; Krzyzosiak et al., 2018), yet much about their cellular abundances, stoichiometries, and dynamics remains elusive. Beyond Cullin RING ligases, we believe that PIKES analysis provides a powerful tool to elucidate dynamic protein assemblies to uncover novel biology.

CRL4 assembly, exchange and function is regulated by Nedd8, CSN and Cand1/2

The discovery of CRL4s as targets of molecular glues and their successful utilization as chemically inducible ligases raises interest in their key regulatory mechanisms. As our study was in progress, genetic screens were published identifying CSN and CAND1 as regulatory factors required for efficacy of IMiDs and IMiD-based PROTACs, but leave open the biochemical mechanisms underlying these effects (Liu et al., 2019a; Mayor-Ruiz et al., 2019; Patil et al., 2019; Sievers et al., 2018). Our mechanistic studies clearly show that neddylation and de-neddylation processes toggle the stability of assembled complexes, with Cand1/2 acting as a neddylation sensitive exchange factors for A•SR (DDB1•DCAF)

modules. Experiments in Cand1/2 deficient cells or those subjected to N8 Block with MLN4924 and CSN5i-3 revealed that dynamic re-cycling of Cul4 scaffolds is essential for efficient sampling of the free DDB1•DCAF pool and substrate degradation. The existence of a CRL4-Nedd8-Cand1 exchange regime predicts that substrate engagement drives the non-equilibrium assembly states of CRL4 ligases. In support of this, we show that physiological stimuli and degrader molecules induce disequilibrium states that favor binding of A•SRs based on substrate availability. The fact that our method detects specific rearrangements of endogenous CRL4 ligases opens up the possibility to use this technique to screen for new molecular glues or physiological states of substrate engagement early in the drug development process.

Systematic quantitative assessment of CRLs promises deeper understanding of degrader MOAs and therapeutic windows

Our analysis of cellular protein concentrations as well as complex stoichiometries of the CRL4 network revealed several insights into the organization of Cul4-RING ligases: (1) The DDB1•DCAF pool is in (~7x) excess over limiting amounts of Cul4 scaffold with only ~10% of DDB1•DCAF modules being assembled into functional ligases at steady-state. This posits that substrate interactions primarily occur prior to engagement of a catalytic scaffold, which in turn requires efficient re-cycling to enable substrate ubiquitination. (2) Interestingly, the quantities of pre-assembled ligase do not correlate with the efficiency of substrate degradation. This is best demonstrated by $CRL4^{CRBN}$ which represents the most assembled CRL4 but turns over less neo-substrates per minute than the much lesser assembled $CRL4^{DCAF15}$. In addition to more or less favorable ternary complex structures and stabilities, this divergence of activities implies the existence of counteracting mechanisms such as neo-substrate competition or de-ubiquitination which negatively impact the efficacy of degrader drugs. (3) The concentrations of most DCAFs in our cellular system lie between 20-100nM. However, analyses of a variety of human tissues show that protein levels of individual DCAFs span two orders of magnitude (Wang et al., 2019). Our proof-of-concept study was restricted to one cell type and we do not generally conclude that concentrations and stoichiometries can be translated to other cell types or

tissues. However, we suggest that stoichiometric relationships between scaffold, exchange factors, adapter protein and regulatory proteins are likely conserved to support the complex regulatory mechanisms. This is illustrated by the tight regulation of CRL4 core subunit protein levels in all tissues while substrate receptor levels vary widely (Figure 3.6A). Individual substrate receptor expression and CRL4 complex formation is likely tissue specific and might even differ between single cells and clonal populations (Lin et al., 2014; Liu et al., 2019b). As a resource for future research, our CRL4 SpikeMix peptide library includes reference standards for each of these proteins and enables application of PIKES to other cell lines or model systems (Table Supplement 3.1).

Using $CRL4^{DCAF15}$ and indisulam-induced neo-substrate RBM39 as a case study, we demonstrate how PIKES analysis can be used to efficiently dissect complex mechanisms like chemically induced protein degradation. Through mimicking the potential physiological or pathophysiological scenario of different substrate receptor levels in two tissues we show that increased DCAF15 protein expression leads to higher pre-formed amounts $CRL4^{DCAF15}$ and substrate engaged ternary complex. Functionally, this enhances substrate degradation leading to a significantly lower DC50 with the potential to translate into a wider therapeutic window in vivo. While future studies are needed to understand whether the relationship of CRL substrate receptor expression and potency of degrader molecules extends to other DCAF family members, similarities in regulation across CRL4s and SCFs suggest that this will be a key consideration for degrader drug development efforts (Liu et al., 2018; Reitsma et al., 2017).

3.5 Materials and Methods

Transient transfections. Plasmid DNA was transiently transfected into 293T/17 or 293 Flp-In T-Rex cells using Lipofectamine3000 and the P3000 reagent following the manufacturer protocol.

Generation of CRISPR/Cas9 reagents and knock-in cell lines. Cul4 specific pX330 constructs were cloned as described in Cong et al. (2013) using the guide sequence 5'-CACCGCGGCGGTTCCGGCCCAGCCA-3' (Rev.: 5'-AAACTGGCTGGGCCGGAACCGCCGC-3') specifically targeting the region around the start codon for Cul4A as well as 5'-CACCGTTGGAAACATGAAAATAGCG–3' (Rev.: 5'-AAACCGCTATTTTCATGTTTCCAAC-3') specifically targeting the start of Cul4B. To insert epitope tags at the N-termini of both Cul4 proteins, we engineered donor DNA plasmids to serve as templates for homologous repair after CRISPR/Cas9-induced double strand breaks. The general design included 300-500bp 5' homology arm, a Kozak sequence, an antibiotic resistance cassette (puromycin or hygromycin) followed by a P2A site, the epitope tag sequence (3xFLAG/3xHA), and the 3' homology arm of 300-500bp starting with the original start codon (Figure 3.1). These donor sequences were either synthesized as double stranded DNA gBlocks (Integrated DNA Technologies) or step-wise cloned via PCR techniques followed by blunt-end insertion into pCR II Blunt-Topo vectors (Invitrogen). 293T/17 or 293 Flp-in T-REx cells were transiently transfected with Cul4A or Cul4B px330/donor pairs at a molar ratio of 3:1 at ~90% confluency in a 6-well dish on day 1 followed by splitting into 10cm plates on day 2. On day 3, cells were exposed to either 1 μg/ml puromycin or 100μg/ml hygromycin to select for successful insertion of donor sequences. Heterogeneous cell populations carrying resistance were recovered, collected and single cells were seeded into 96-well plates via FACS or dilution. Once single cell clones reached confluency, they were screened for homozygous insertion of the donor sequences via genomic PCR (Figure S1D-F) and tested for protein expression of endogenous ^{3xFLAG}Cul4A and ^{3xHA}Cul4B via western blot (Figure S1G, H). The cell clones used for experiments in this study are 293T/17$^{3xFLAG\text{-}Cul4A}$ clone A22, 293T/17^{3xHACul4B} clone B15 and 293T/17$^{3xFLAG\text{-}Cul4A\ \&\ 3xHA\text{-}Cul4B}$ clone A22_B21.

Genomic DNA extraction and PCR genotyping. 100.000 cells or 25% of cells grown in a 24-well plate were resuspended in 250µl QuickExtract solution followed by 15min incubation at 65C and 10min at 98C in a ThermoMixer to extract and solubilize genomic DNA. Subsequently, 1 µl per sample was used as a template for PCR which was carried out in 25µl total volume with 12.5 µl 2x Q5 High Fidelity Polymerase Master Mix (NEB) and 0.5µM of each primer. Primers used to amplify Cul4B locus: FWD 5'-CACTCCCTGAGGTTGACACC-3' and REV 5'- GCCGAATCCCTGGGTTGTAA-3', T_a = 68C. Primers used to amplify Cul4A locus: FWD 5'-GAGGGGGTGTCCGAATCTCT-3' and REV 5'-TCACCTGGTAGAGCTCCTCG-3', T_a = 64C. PCR cycle: 4min initial denaturation at 98C, 35 cycles of 1min denaturation at 98C, 30sec annealing at T_a and 1min extension at 72C, followed by 4min final extension. DNA was resolved using agarose gels with ethidium bromide and imaged on an iBright FL1000 (Thermo Fisher Scientific).

Quantitative reverse transcription PCR. RNA was extracted using the Qiagen RNeasy Kit following manufacturer instructions, RNA content measured via NanoDrop and concentrations adjusted to 0.5µg/µl for each sample. The reverse transcriptase reaction was performed using the Qiagen QuantiTect RT PCR Kit following manufacturer instructions. Quantitative PCR was carried out using Qiagen QuantiTect SYBR Green PCR Master Mix following manufacturer instructions at a T_a of 62°C on a Thermo Scientific StepOnePlus RT qPCR instrument using StepOne software v2.3. Primer efficiency E was determined for each primer pair by performing a dilution series, determination of the slope and calculation of $E = -1+10^{(-1/slope)}$. Data was analyzed and relative expression ratios calculated using the Pfaffl Method (Pfaffl, 2001). Primers used to quantify mRNA levels: GAPDH: Fwd: 5′-ACCCACTCCTCCACCTTTGAC-3′, Rev_5′-CTGTTGCTGTAGCCAAATTCGT-3′; Cul4B: Fwd1_5'-GAAAGAAGCA-GTGGAAGCTATTC-3′, Rev1_5′-TGCCAGCATCTATCAATCTTCT-3′; Cul4A: Fwd2_5'-CTCTACAAGCAACTGCGTCA-3′, Rev2_5′-GGCAGCGTGGAGTTCTG-3′; PCID2: FWD2_5'-CAAGTGCCAGACCGTGATAG-3′, REV2_5′-CCGGAAACAGCTCATCAGT-AA-3′.

Denaturing cell lysis in 2xLDS buffer and western blotting. Cells grown in a 6-well dish (~2x10^6 cells/well) were lysed in 600µl 2x LDS (Lithium dodecyl sulfate) sample buffer , sonicated for 10sec with 1sec ON and 1sec OFF at 20% amplitude on a Qsonica Q500 (Converter Model CL-334, Probe ½" #4220, microtip 1/8" #418-A) or for 10sec with 1sec ON and 1sec OFF at 55% amplitude on a Qsonica Q125 (Converter Model CL-18, microtip 1/8" #422-A). Samples were then boiled at 70°C for 10-15min and either stored at -80°C or processed via SDS PAGE using Novex Bolt Bis-Tris 4-12% precast gels and Bolt MOPS SDS running buffer. Subsequently, proteins were transferred to PVDF membranes using a wet blot system and Tris-Glycine transfer buffer (Novex LC3675 + 20% Methanol) containing 20% methanol at 4°C. Membranes were blocked with 5% non-fat dry milk for at least 5min before incubation with primary antibodies. Primary and secondary antibody incubations were carried out for 60min, each followed by three brief washes with TBS-Tween (Tris-buffered saline; 50mM Tris-Cl, 150mM NaCl, pH 7.5, 0.1% Tween) and one wash on an orbital shaker for 20min.

To quantify proteins via western blotting, cells were lysed in 2xLDS and processed as described above. PVDF membranes were then blocked using LI-COR Odyssey blocking Buffer TBS (LI-COR Part No. 927-50000) for 30min followed by simultaneous incubation of primary and fluorescent secondary antibodies in 1% non-fat dry milk in TBS-Tween over-night. Membranes were then washed with three in-hand washes using TBS-Tween, one wash in TBS-Tween on an orbital shaker for 20min followed by one more wash in PBS for 10min.

Native cell lysis and CRL-exchange blocking techniques. Cells were trypsinized and harvested in growth medium, followed by cell counting. If cells were exposed to treatments, cells were harvested in the pre-conditioned or treatment-containing growth medium. Cells were then collected via centrifugation at 1200xg for 2min, and (1) either lysed without blocking CRL-exchange or (2) lysed in the presence of 2.5 µM Molecular Sponge (^{His6}-Cul4A•Rbx1^{GST}) or (3) resuspended in 4ml growth medium containing 1µM MLN4924 and CSN5i-3 (N8 Block) followed by 3min incubation and another 2min centrifugation at 1200xg and resuspension in lysis buffer. The concentration of 1µM

MLN4924 was chosen as the maximum concentration that allows NAE1 specificity without inhibition of Ubiquitin E1 (Soucy et al., 2009). The treatment time was chosen as the shortest practically possible time in which full inhibtion of NAE1 as well as CSN could be achieved consistently as shown by samples treated with either inhibitor itself, resulting in either full de-neddylation or neddylation within 5min (Figure 3.2G). Cells from two 15cm plates (~$80x10^6$) were lysed using sonication in 3.6ml and cells from one 15cm plate (~$40x10^6$) in 2.1ml of Pierce IP Buffer (25mM Tris-HCl pH 7.4, 150mM NaCl, 1% NP-40, 1mM EDTA, 5% glycerol) containing a protease inhibitor cocktail (Roche). Sonication was either carried out on a Qsonica Q500 (Converter Model CL-334, Probe ½" #4220, microtip 1/8" #418-A) for 10sec with 1sec ON and 1sec OFF at 20% amplitude or on a Qsonica Q125 (Converter Model CL-18, microtip 1/8" #422-A) for 10sec with 1sec ON and 1sec OFF at 55% amplitude. Lysates where cleared by centrifugation at 18.000xg for 2min at 4°C and supernatants used for affinity purification.

Whole cell lysis and sample preparation for LC-MS analysis. To estimate cellular protein concentrations via the CRL4 QconCAT PRM LC-MS assay, $4x10^6$ cells were resuspended in 500µl of 8M urea in 100mM ammonium bicarbonate solution containing 5mM TCEP reducing agent and sonicated on a Qsonica Q125 (Converter Model CL-18, microtip 1/8" #422-A) for 20sec with 1sec ON and 1sec OFF at 55% amplitude. Lysates where cleared by centrifugation at 18.000xg for 2min at 4°C whereby no insoluble pellet was visible. Protein content of whole cell lysates was measured using NanoDrop A280. Subsequently, 200µg of lysate was diluted to a final volume of 50µl containing 50fmol or 100fmol CRL4 QconCAT standard. Samples were then incubated at 23°C for 30min in a ThermoMixer, before addition of 0.78µl of 700 mM iodoacetamide for alkylation of cysteine residues (final conc. 10.75 mM) for 15min. Subsequently, samples were diluted to 6M urea by adding 16µl of 50mM ammonium bicarbonate and the protein digest was started by adding 7µg LysC for 1-4 hours at 23ºC. After that, samples were diluted using 50mM ammonium bicarbonate to a concentration of 2M urea before adding 1mM $CaCl_2$ and 10µg trypsin for over-night incubation.

Affinity-Purification, elution and sample preparation for LC-MS analysis. All experiments and digests were performed in 5ml or 1.5ml LoBind Eppendorf tubes. Lysates at volumes of 3.6ml and 2.1ml were exposed to 150µl or 75µl of anti-FLAG or anti-HA resin (~75µl and ~37.5µl packed beads) for 45 min unless otherwise stated. Subsequently, the resin was collected via centrifugation at 2000xg for 2min and the flow through was removed with a 26G subcutaneous needle under vacuum until the resin was almost dry. The beads were then washed once in 3ml and once in 1ml Pierce IP buffer, twice in 1ml reconstituted IP Buffer without NP-40 and twice in 1ml of 100mM Tris-HCl pH 7.5, followed by removal of as much liquid as possible with a 26G needle under vacuum. Immunoprecipitated complexes were eluted twice in 150µl 10% NH_4OH at 37°C for 5min at 950rpm in a ThermoMixer. Eluates were then collected by filtering the bead suspension through 5µm spin filters at 8000xg followed by flash freezing on dry ice and lyophilization. Eluted proteins were then resuspended in 50µl 8M urea in 100mM ammonium bicarbonate solution containing 5mM TCEP reducing agent for 30min at 23ºC, followed by the addition of 0.78µl of 700 mM iodoacetamide for alkylation of cysteine residues (final conc. 10.75 mM) for 15min at 23°C at 750rpm in a ThermoMixer protected from light. Subsequently, samples were diluted to 6M urea by adding 16µl of 50mM ammonium bicarbonate and the protein digest was started adding 1.78µg LysC for 1-4 hours at 23ºC. After that, samples were diluted using 50mM ammonium bicarbonate to a concentration of 2M urea before adding 1mM $CaCl_2$ and 2.5µg trypsin for over-night incubation.

C18 desalting of digested samples. Digested WCL or IP protein samples were acidified through addition of 25µl 50% formic acid and diluted by adding 250µl buffer A (98% H_2O, 2% acetonitrile, 0.2% formic acid) before a desalting step using 10mg SOLA HRP SPE cartridge (Thermo Scientific Prod. No. 11879163). SPE cartridges were equilibrated in methanol and washing steps were performed in H_2O containing 0.2% formic acid. Elution of peptides was carried out in 300µl elution buffer (50% H_2O, 50% acetonitrile, 0.2% formic acid) and samples were flash frozen on dry ice followed by lyophilization. Lyophilized samples were resuspended in 11-21 µl Buffer A for subsequent LC-MS analysis.

Mapping of endogenous CRL4 complexes using label-free AP-MS and SAINT. 293T/17 wild type cells as well as 293T/17$^{3xFLAG\text{-}Cul4A}$ (clone A22) and 293T/17$^{3xHA\text{-}Cul4B}$ (clone B15) were grown to 90% confluency in 15cm plates, lysed and lysates immunoprecipitated with either anti-FLAG or anti-HA resin. Elution and sample preparation for LC-MS were carried out as described above. MS data was acquired on an Orbitrap Fusion Lumos mass spectrometer (Thermo Fisher Scientific, San Jose, CA) and peptide searches performed using COMET and analyzed using SAINT as described below.

Mapping of DDB1-Cul4 associated factors (DCAFs) via SILAC AP-MS. On day 1, 293T/17 cells were transiently transfected (~8x10^6 cells in a 10cm plate) with either wild type 3xHA-Cul4 (transcript variant 1) or 3xHA-Cul4B (transcript variant 2) and grown in heavy SILAC medium (K8R6) or with 3xHA-Cul4A$^{\Delta DBD(K41\text{-}L93)}$ and 3xHA-Cul4B$^{\Delta DBD(K177\text{-}L229)}$ lacking the DDB1 binding domain and grown in light SILAC medium and split into a 15cm plate on day 2. Cells were then lysed on day 3 (w/o Nedd8-Block), and lysates immunoprecipitated with anti-HA resin and eluted as described above. IP-eluates of WT and mutant IPs were mixed 1:1 and subsequently processed for LC-MS analysis (described above, Figure S1A).

CRL4 SILAC Exchange Assay. Wild type cells were grown in light SILAC medium and engineered cells carrying a 3xHA epitope tag on Cul4B were grown in heavy SILAC (K8R10) for at least ten doublings. Some individual experiments were carried out with swapped labels, whereby wild type cells were labeled heavy and epitope-tagged cells were labeled light, and no differences in results were observed. Cells were harvested via trypsin and mixed 1:1 (80x10^6 cells total, 1x15cm plate each) before lysis and immunoprecipitation as described above. IPs were carried out for 20min, 60min or 180min counting from moment of cell lysis by sonication. LC-MS data was acquired an Orbitrap Fusion Lumos mass spectrometer (Thermo Fisher Scientific, San Jose, CA) and peptide search as well as data analysis was performed as described below.

CRL4 SpikeMix PRM LC-MS Assay. For development of a targeted proteomics assay to quantitatively monitor the CRL4 protein network, three, in some cases two, target peptides for each of 142 previously reported or predicted CRL4 network proteins were selected

following established guidelines (Picotti and Aebersold, 2012; Picotti et al., 2010) yielding a peptide library of 418 peptides. Priority was given to peptides observed in our initial AP-MS experiments or to peptides that have previously been observed on our instruments, an approach that covered ~80% of all proteins of interest. Peptides for the other ~20% of proteins were chosen using SRMAtlas (Kusebauch et al., 2016). This comprehensive peptide library of 418 peptides was synthesized as a SpikeMix by JPT Peptide Technologies isotopically heavy labeled with (K8R10 = $^{13}C_6$ $^{15}N_2$-lysine and $^{13}C_6$ $^{15}N_4$-arginine). Lyophilized peptide standards (0.3-0.5 nmol per peptide) were first resuspended in 80µl of 20% acetonitrile and 0.2% formic acid to yield a CRL4 SpikeMix master stock solution of ~3-5pmol/peptide/µl. The master stock was further diluted 1:50 in Buffer A (2% acetonitrile, 0.2% formic acid) to yield aliquots at ~60-100fmol/peptide/µl which were used for experiments or stored long term at -80C. PRM LC-MS analysis of standard peptides alone confirmed no significant signal in the light channel. A standard Cul4-IP eluate from $40x10^6$ cells was resuspended in 21µl of Buffer A containing 1.5-2.5fmol/peptide/µl, yielding a peptide mixture of ~0.25µg/µl of which 2-4 µl were injected for LC-MS analysis. After determining the specific Cul4-interactome in our cell system, we excluded proteins that did not interact with Cul4 and settled for a method targeting 58 individual peptides to monitor 37 Cul4 interacting proteins (see Table Supplement 3.2 for PRM mass table). LC-MS data was acquired on an Orbitrap Fusion Lumos mass spectrometer (Thermo Fisher Scientific, San Jose, CA) and data analysis was performed as described below.

QconCAT PRM LC-MS Assay. For development of targeted proteomics assay capable of measuring concentrations of CRL4 components within individual WCL or IP samples, we designed a CRL4 QconCAT protein standard consisting of 67 concatenated reference peptides (Table Supplement 3.3) for 31 proteins yielding one polypeptide chain with equimolar amounts of each standard (Pratt et al., 2006; Scott et al., 2016). The QconCAT was synthesized and purified by PolyQuant GmbH, Bad Abbach, Germany, with stable isotope labeled arginine (R10; $^{13}C_6{}^{15}N_4$) and and lysine (K8; ($^{13}C_6{}^{15}N_2$) (labeling efficiency ~98%) yielding a homogenous protein reagent (Figure Supplement 3.3A, B). The amounts of QconCAT standard added to WCL or IP samples was chosen so that all PRM ratios

measured were well beyond the ~2% background signal (Figure Supplement 3.3C, F). After initial tests, 61 peptides were targeted to monitor 31 proteins (see Table Supplement 3.4 for PRM mass table). LC-MS data was acquired on an Orbitrap Fusion Lumos mass spectrometer (Thermo Fisher Scientific, San Jose, CA). Data analysis was performed as described below.

LC-MS data acquisition for label-free and SILAC analyses. For all experiments, except the ones displayed in Figure Supplement 3.1D-F, peptides were separated using either a prepacked 25cm column from New Objective (PicoFrit Acquity® BEH130Å C18 column, 1.7 µM, 100 µM x 250 mm) or IonOpticks (Aurora Series) via a Dionex UltiMate 3000 RSLCnano Proflow system (Thermo Fisher Scientific, Sunnyvale, CA) or a nanoAcquity UPLC (Waters) with a gradient of 2% buffer A (98% H20, 2% ACN with 0.1% formic acid) to 35% buffer B (98% ACN, 2% H20, 0.1% formic acid) with a flow rate of 450 nL/min over 90 minutes. Eluting peptides were sprayed into a Fusion Lumos mass spectrometer (Thermo Fisher Scientific) at a voltage of 1.9kV (NewObjective column) or 1.5kV (IonOpticks column). Full MS scans were collected in the orbitrap at 240,000 resolution, across a range from 350 to 1350 m/z, with an automatic gain control (AGC) target of 1×10^6, and a maximum injection time of 50ms. MS2 ions were selected in 0.7 Da isolation width using a top speed data dependent mode and fragmented with HCD energy of 30%, over a scan range of 200-1200 m/z and AGC target of 2×10^4 at a maximum injection time of 11ms. All mass spectrometry raw files have been deposited into the MassIVE database (http://massive.ucsd.edu/).

For experiments displayed in Figure Supplement 3.1D-F, peptides were resuspended in 0.2% formic acid and directly loaded onto a PicoFrit column (New Objective, Woburn, MA) packed in house with ReproSil-Pur C18AQ 1.9 um resin (120A° pore size, Dr. Maisch, Ammerbuch, Germany). The 25cm x 50µm ID column was heated to 60° C. The peptides were separated with a 120 min gradient at a flow rate of 220 nL/min using a nanoflow LC system, EASY-nLC 1000 or 1200 (Thermo Fisher Scientific). The gradient was as follows: 2–6% Solvent B (7.5 min), 6-25% B (82.5 min), and 25-40% B (30 min), to 100% B (1min) and 100% B (9min). Solvent A consisted of 97.8% H2O, 2% ACN, and

0.2% formic acid and solvent B consisted of 19.8% H2O, 80% ACN, and 0.2% formic acid. The separated peptides were ionized by a Nanospray Flex ion source and subjected to MS/MS analysis using either a QExactive HF Orbitrap or Fusion Orbitrap mass spectrometer (Thermo Fisher Scientific, San Jose).

The QExactive HF Orbitrap was operated in data dependent mode. Spray voltage was set to 2.5 kV, S-lens RF level at 50, and heated capillary at 275 °C. Full scan resolution was set to 60,000 at m/z 200. Full scan target was 3×10^6 with a maximum injection time of 15 ms (profile mode). Mass range was set to 300−1650 m/z. For data dependent MS2 scans the loop count was 12, target value was set at 1×10^5, and intensity threshold was kept at 1×10^5. Isolation width was set at 1.2 m/z and a fixed first mass of 100 was used. Normalized collision energy was set at 28. Peptide match was set to off, and isotope exclusion was on. Ms2 data was collected in centroid mode.

The Fusion Orbitrap was operated in data dependent mode using a top-speed approach (cycle time of 3 s). Spray voltage was set to 2.5 kV, S-lens RF level at 60, and heated capillary at 275 °C. Full scan resolution was set to 120,000 at m/z 200. Full scan target was 4×10^5 with a maximum injection time of 50 ms (profile mode). Mass range was set to 350−1500 m/z. The MS2 was performed in HCD cell with detection in Orbitrap. For MS2 scans Orbitrap resolution was set to 30,000 at m/z 200 and target value was set at 1×10^5 with a maximum injection time of 50 ms (centroid mode). Isolation width was set at 1.6 m/z and a fixed first mass of 120 was used. Normalized collision energy was set at 35.

LC-MS data acquisition for PRM analyses. For all PRM experiments, peptides were separated using either a prepacked 25cm column from New Objective (PicoFrit Acquity® BEH130Å C18 column, 1.7 µM, 100 µM x 250 mm) or IonOpticks (Aurora Series) via a Dionex UltiMate 3000 RSLCnano Proflow system (Thermo Fisher Scientific, Sunnyvale, CA) or a nanoAcquity UPLC (Waters) with a gradient of 2% buffer A (98% H20, 2% ACN with 0.1% formic acid) to 35% buffer B (98% ACN, 2% H20, 0.1% formic acid) with a flow rate of 450 nL/min over 75 minutes. Eluting peptides were sprayed into a Fusion Lumos mass spectrometer (Thermo Fisher Scientific) at a voltage of 1.9kV (NewObjective column) or 1.5kV (IonOpticks column). MS1 scans were collected in the Orbitrap at 60,000

resolution, across a range from 300 to 1200 m/z, with an automatic gain control (AGC) target of 1 x 10^6 and a maximum injection time of 50ms. Trigger peptides were placed on an inclusion list with their corresponding m/z, z and retention time window of 5min (for inclusion lists see Table Supplement 3.2 and 3.4). Trigger peptides were selected for MS2 across an isolation window of 1.2 m/z, fragmented by CID (Collision Energy 30%), and the resulting fragments analyzed in the Orbitrap (resolution 60,000, range 288-2000 m/z, AGC target $2e^5$). Hereby, the maximum injection time was 118ms for all peptides except DCAF15 (R0K0 DSPPASEAPASEPGYVNYTK, m/z 1040.47862) which was allowed a max. injection time of 500ms. All mass spectrometry raw files have been deposited into the MassIVE database (http://massive.ucsd.edu/).

Expression and purification of recombinant proteins. ^{His6}Cul4A/Rbx1^{GST}, Cul1/Rbx1^{GST}, and Cand1 were expressed and purified from B21 E.coli cultures as described in Pierce et al. 2013, Liu et al. 2018.

Quantitative western blotting. Images were acquired using a LI-COR Odyssey XR and quantified via the ImageStudio software using the median background subtraction method (Segment All). The signal of the protein of interest was normalized towards the signal of a loading control. Data from triplicate experiments (n=3) was plotted and further analyzed using GraphPad PRISM. Statistical parameters are reported in the figure legends.

LC-MS Data analysis. SILAC AP-MS Data (QE-HF): Thermo raw files were processed and searched using MaxQuant (v. 1.5.5.1) (Cox and Mann, 2008; Cox et al., 2011). Spectra were searched against human UniProt entries and a common contaminant database. Trypsin was specified as the digestion enzyme and up to two missed cleavages were allowed. False discovery rates were estimated using a target-decoy approach, where the decoy database was generated by reversing the target database sequences. Protein, peptide, and PSM scores were thresholded to achieve a 1% FDR at each level. Carbamidomethylation of cysteine was specified as a fixed modification. Protein N-terminal acetylation and methionine oxidation were specified as variable modifications. Precursor mass tolerance was 4.5 ppm after mass recalibration and fragment ion tolerance was 20 ppm. Search type was specified as “Standard”, with multiplicity of 2 and K8 ($^{13}C_6$

$^{15}N_2$-lysine) and R6 ($^{13}C_6$-arginine) were specified as heavy labels. Both re-quantify and match-between-runs were enabled. In some cases, multiple technical replicates were included and these were pooled together under the same experiment name.

Protein ratios were calculated as the geometric mean of the biological replicates. Statistical significance of the protein ratio was calculated using the moderated t-test in the R package limma (Smyth et al., 2011).

SILAC Exchange Data (Fusion Lumos): MS/MS spectra were searched using Mascot (v.2.4.1) (Pappin et al., 1999) against a human UniProt DB (2017_08) database with a taxonomy filter of '9606' containing common contaminating proteins and concatenated by all decoy sequences. Search parameters included trypsin cleavage with allowance of up to 2 missed cleavage events, a precursor ion tolerance of 50 ppm, and a fragment ion tolerance of 0.8 Da. Searches permitted variable modifications of methionine oxidation (+15.9949 Da), K8 (+8.0142 Da), R10 (+10.00827 Da), and static modifications of cysteine (+57.0215 Da) for carbamidomethylation. Peptide spectra matches (PSMs) were filtered with a false discovery rate (FDR) of 5% on the peptide level and subsequently at 5% on the protein level using linear discrimination. SILAC log2 ratios of identified peptides were quantified with an in-house software package known as VistaQuant (Bakalarski et al., 2008). SILAC log2 ratios of each sample were transformed to H/L ratios and normalized to the overall median H/L ratio to account for variations in cell mixing. If epitope-tagged cells were grown in light and wild type cells were grown in heavy, percent exchange was determined based on the median normalized H/L ratio, a ratio of 1 indicating 100% exchange of the individual Cul4 interacting protein.

Label-free data: All MS/MS spectra were searched using the Comet (v2017.01) (Eng et al., 2013) search algorithm against a concatenated target-decoy database composed of the UniProt (2017_08) human protein sequences, known contaminants and the reversed versions of each sequence. A 50ppm precursor ion mass tolerance and 0.8 Da fragment ion tolerant were selected and tryptic specificity was defined with up to 2 missed cleavages. Variable modifications were permitted for methionine oxidation (+15.9949 Da) and the iodoacetamide adduct for cysteine residues (+57.0215 Da). Peptide assignments were first

filtered to a 1% false discovery rate (FDR) at the peptide level and subsequently to a 1% FDR at the protein level. Peptide Spectral Matches (PSMs) per protein were summed per sample and used as input for the Statistical Analysis of INTeractome (SAINT) algorithm (SAINTExpress-spc 3.6.1) (Choi et al., 2011). SAINT was run with default settings comparing the sum of PSMs for all identified proteins enriched in bait IPs versus the respective control IPs, across all replicates. Interactions with a positive SAINT logOddsScore and Bayesian False Discovery Rate (BFDR) < 0.05 were marked as significant.

PRM data: PRM raw files were loaded into Skyline version 4.1 (MacLean et al., 2010) pre-populated with target peptides and proteins using a transition filter allowing for precursor charges 2 and 3, ion charges 1 and 2 and y-ion types, followed by manual peak analysis. To be considered for quantitative analysis, peptides needed to yield at least two product ions with intensities > 1000 counts/second present in all samples of the experiment. Peptides that were not detected and inferring product ions were removed. Peptide ratio data were exported using the Export>Report>Peptide Ratio Results function. Peptide Ratio Result files were further processed using RStudio version 1.1.442 (R version 3.4.4) to transform individual peptide data into protein ratios or concentrations. Statistical analysis was performed using GraphPad Prism and statistical parameters are indicated in individual figure legends.

In general, experiments analyzed with CRL4 SpikeMix peptides and relative quantification included a control sample that was left untreated to which every other condition was compared to. In experiments analyzed with CRL4 QconCAT standard and "absolute" quantification samples were directly compared to each other.

Calculation of cellular abundances. Data was manually analyzed via Skyline as described above and the peptide ratio results output file was loaded into R Studio to perform calculations of cellular abundances using the following script:

```
#Read Skyline output file
df <- fread(PeptideRatioResults ")

# Select columns for calculations
df <- select(df,Peptide_Sequence, Protein_Name, Replicate_Name, Ratio_To_Standard)

# Group and Summarize by protein name - CAVE: ONLY for QconCAT possible to group al peptide ratios

df <- df %>%
  group_by(Protein_Name, Replicate_Name) %>%
  summarise(avg_Ratio = mean(Ratio_To_Standard, na.rm = T),
            peptides = paste(unique(Peptide_Sequence), collapse = ", "))

# Spread for horizontal display of samples
df <- spread(df, Replicate_Name, avg_Ratio)

# Parameters for Calculation - units µl, excep Vc is L, and nM:
# VL=Vol Lysate, VS = Volume Sample, Vst = Vol Standard, VD = Vol digest, Cst = Conc standard, Nc = Number of cells, Dc = Diameter of Cells,
effNc = Number of cells used,effective number Vc = Vol of Cell
# measure and adjust for individual experiments

VL=500
VS=36.5
Vst1=4
VD=50
Cst=25
Nc=4.39*10^6
Dc1=15.09
pi=3.14159265359
effNc = Nc*(VS/VL)
Vc1=((4/3*pi*(((Dc1/10^6)/2)^3))*1000)
Na=6.022140857*10^23


# Calculation of nM cellular concentration
# Formula: (((((avg_Ratio *((Cst*Vst)/VD))*(VD*10^-6))/effNc)/10^9)/Vc)*10^9

df <- df %>%
  mutate(S1_nM = (((((S1 *((Cst*Vst1)/VD))*(VD*10^-6))/effNc)/10^9)/Vc1)*10^9)

# Calculation of molecules per cell
#Formula ((((avg_Ratio *((Cst*Vst)/VD))*(VD*10^-6))/effNc)/10^9)*Na


df <- df %>%
  mutate(S1_molecules = (((((S1 *((Cst*Vst1)/VD))*(VD*10^-6))/effNc)/10^9)*Na))


write_csv(df, 'WCL_cellular_nM_Molecules.csv')
```

Stoichiometric analysis of CRL4 complexes. As displayed in Figure Supplement 3.3F, all DCAFs except RFWD2, PHIP, and PWP1 displayed a signal to noise ratio of > 5. If the measurements displayed in Figure 3C were accurate, several control criteria should be met: First, our assay detected peptides that were either shared (representing all Cul4 = Cul4A+Cul4B) by or unique to Cul4A and Cul4B. Therefore, the values measured for the shared peptides need to approximately match the sum of values obtained for the unique peptides. Second, since cullin proteins are only stable when in complex with Rbx1, the amount of total Cul4 should match Rbx1. Third, based on excess Cand1 and DDB1•DCAF over total Cul4 within cells and relatively high binding affinities, we would expect the scaffold to be occupied by either Cand1 or DDB1•DCAFs at all times. If so, the sum of DDB1 and Cand1 should approximately match total Cul4 or exceed Cul4 by a bit if ternary

complexes are detected. Fourth, every DCAF bound to Cul4 requires one adapter molecule DDB1. Hence, if DDB1 doesn't occupy Cul4 by itself, the sum of all 22 DCAFs assessed in our assay should roughly equal the total amount of DDB1. All four control criteria are met with relatively small discrepancies: (1) Cul4A + Cul4B = Cul4 +/- 12%; (2) Cul4 = Rbx1 +/- 5-18%; (3) Cand1 + DDB1 = Cul4 +/- 10-23%, (4) 22 DCAFs Total = DDB1 +/- 15%.

3.6 Figures and Supplemental Figures

Figure 3.1

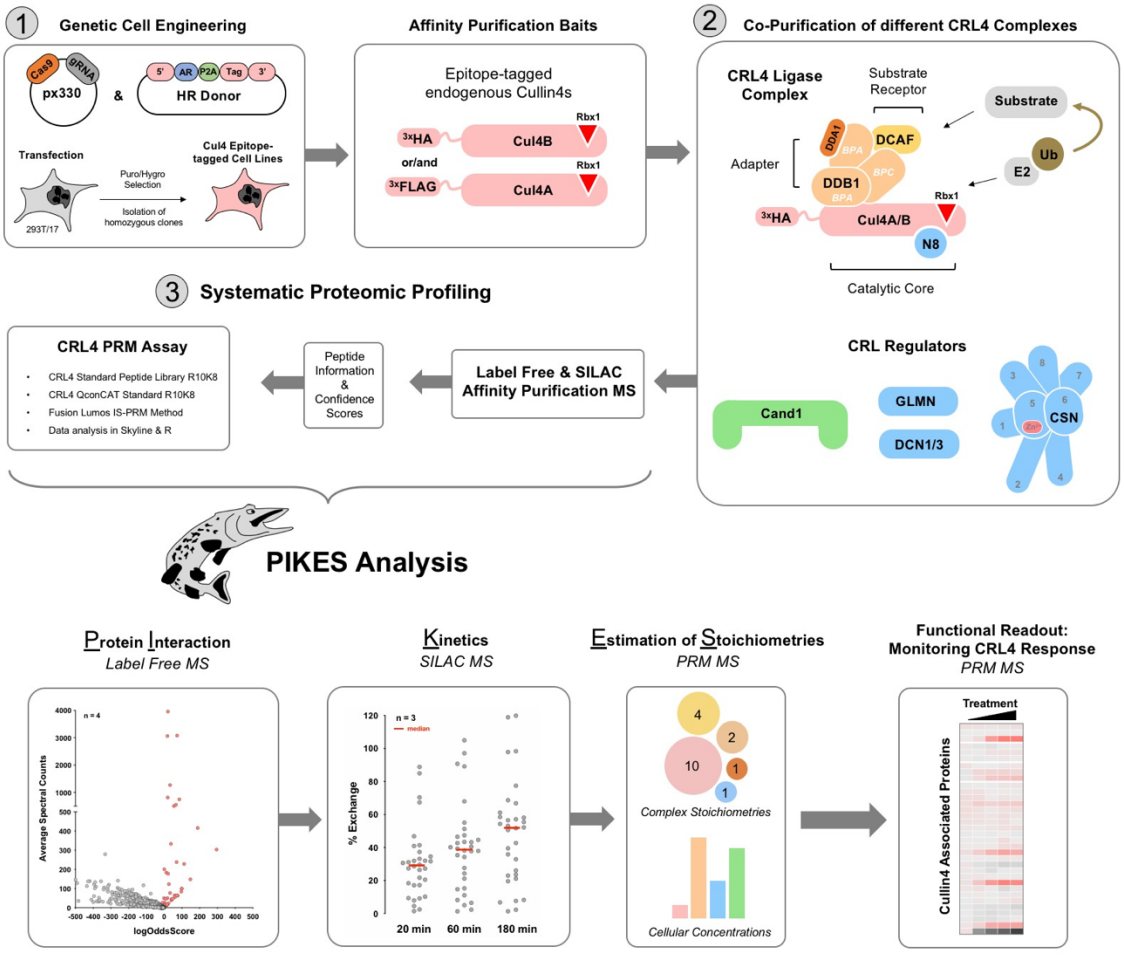

Figure 3.1. A toolbox to monitor endogenous CRL4 complexes. Schematic representation of the PIKES approach: (1) 293T/17 cells were genetically engineered to carry a 3xFLAG or 3xHA on Cul4A or Cul4B or both to enable rapid and efficient (2) immunoprecipitation of endogenous CRL4 assemblages. (3) Endogenous CRL4 ligase complexes were then evaluated systematically using global and targeted proteomic approaches. First, the protein interaction network of interest was analyzed at endogenous protein levels followed by a kinetic characterization of these interactions, which prompted the development of chemical and biochemical methods to control and preserve the composition of protein complexes. Subsequently, the cellular concentrations and complex stoichiometries were analyzed using QconCAT standards, and induced changes in complex composition were monitored quantitatively.

Figure 3.2

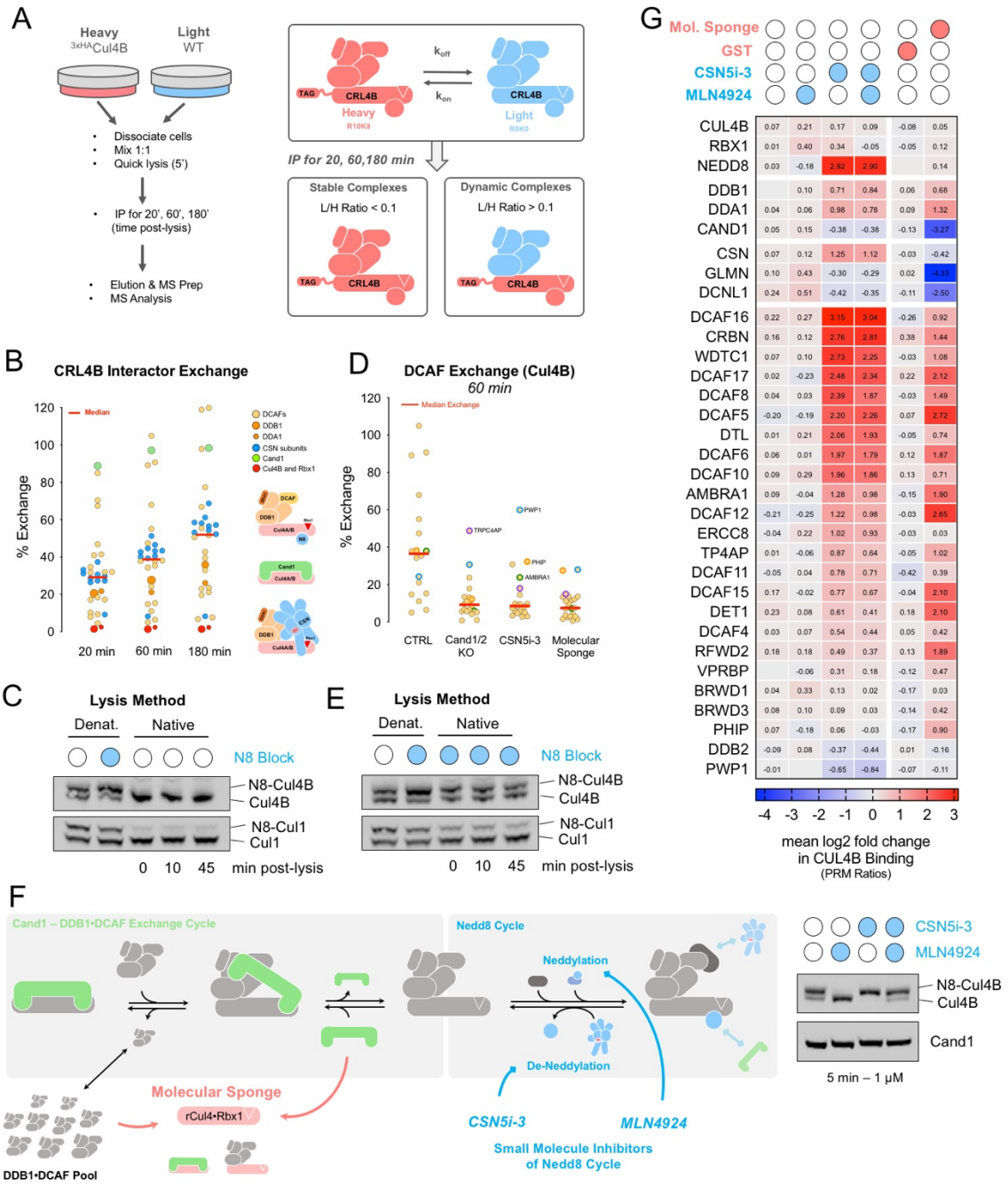

Figure 3.2. CRL4 complexes exchange DDB1•DCAFs via Cand1 and are stabilized by CSN5i-3 and Molecular Sponge. (A) Schematic display of CRL4 SILAC exchange assay. (B) and (D) CRL4B interactor exchange is suppressed in Cand1/2 KO, upon CSN de-neddylase inhibition with CSN5i-3 (maintaining Nedd8-Cul4), and in the presence of molecular sponge. (C) and (E) Conservation of CRL neddylation via N8-block, a brief pre-treatment with 1µM MLN4924 and CSN5i-3 for 5min before cell lysis. F) Schematic representation of CRL4 Nedd8-Cand1-cycle and methods to suppress it post-lysis. The N8 Block is based on

rapid and simultaneous chemical inhibition of both arms of the Nedd8 cycle using MLN4924 to inhibit NAE1 and CSN5i-3 to inhibit CSN. The molecular sponge technique was pioneered by Reitsma et al. 2017 on the SCF system and is based on biochemical inhibition of Cand1/2-mediated CRL exchange. The recombinant cullin scaffold added in excess "sponges up" any free A•SR complexes as well as exchange factors Cand1/2, thereby preventing artifacts caused by post-lysis exchange while conserving protein assemblies that were formed pre-lysis. (G) Effect of CRL4 stabilizing treatments N8-Block and molecular sponge on endogenous Cul4B complexes as measured by PRM LC-MS.

Figure 3.3

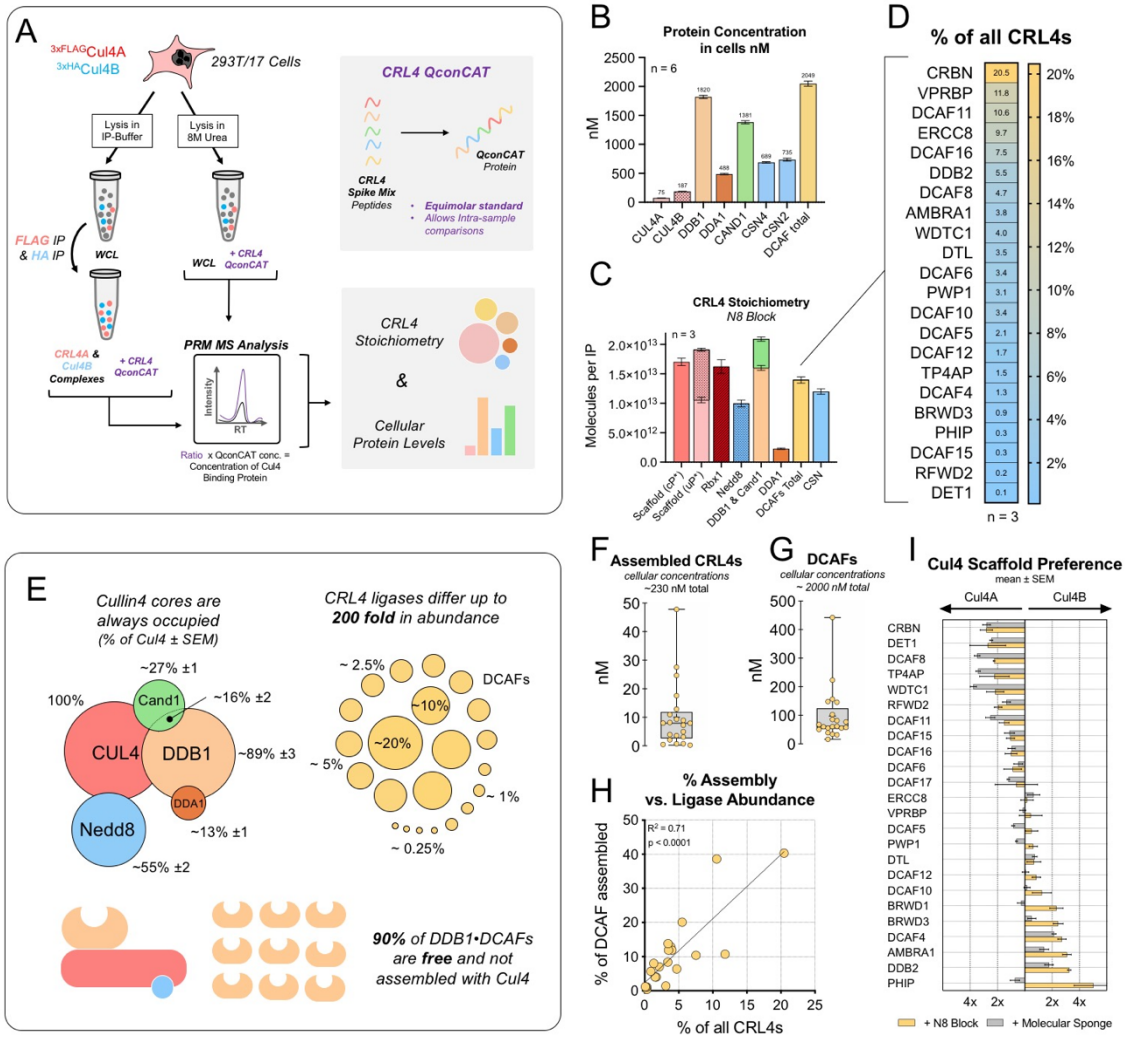

Figure 3.3. Individual CRL4 ligases show Cullin-scaffold preferences and differ up to 100-fold in absolute abundance. (A) Schematic of CRL4 QconCAT experiments to determine cellular concentrations and complex stoichiometries. (B-D) Absolute quantification of CRL4 components in whole cell lysates as well as immunoprecipitated Cul4 complexes. *Cul4 scaffolds were measured by targeting peptides common (cP) or unique (uP) to Cul4A and Cul4B (E) Summary of cellular organization of CRL4 complexes. (F) and (G) Cellular concentrations of assembled CRL4s as well as DCAFs. (H) Correlation plot of % assembled and % all CRL ligases (i.e. fraction of overall CRL4 pool) of individual DCAFs. (I) Cul4 Scaffold preference of individual DCAFs as measured via two independent assays and six independent experiments. In all figures, error bars represent the mean ± SEM. The box and whisker plots represent the median, lower, and upper quartile as well as the highest and lowest observation.

Figure 3.4

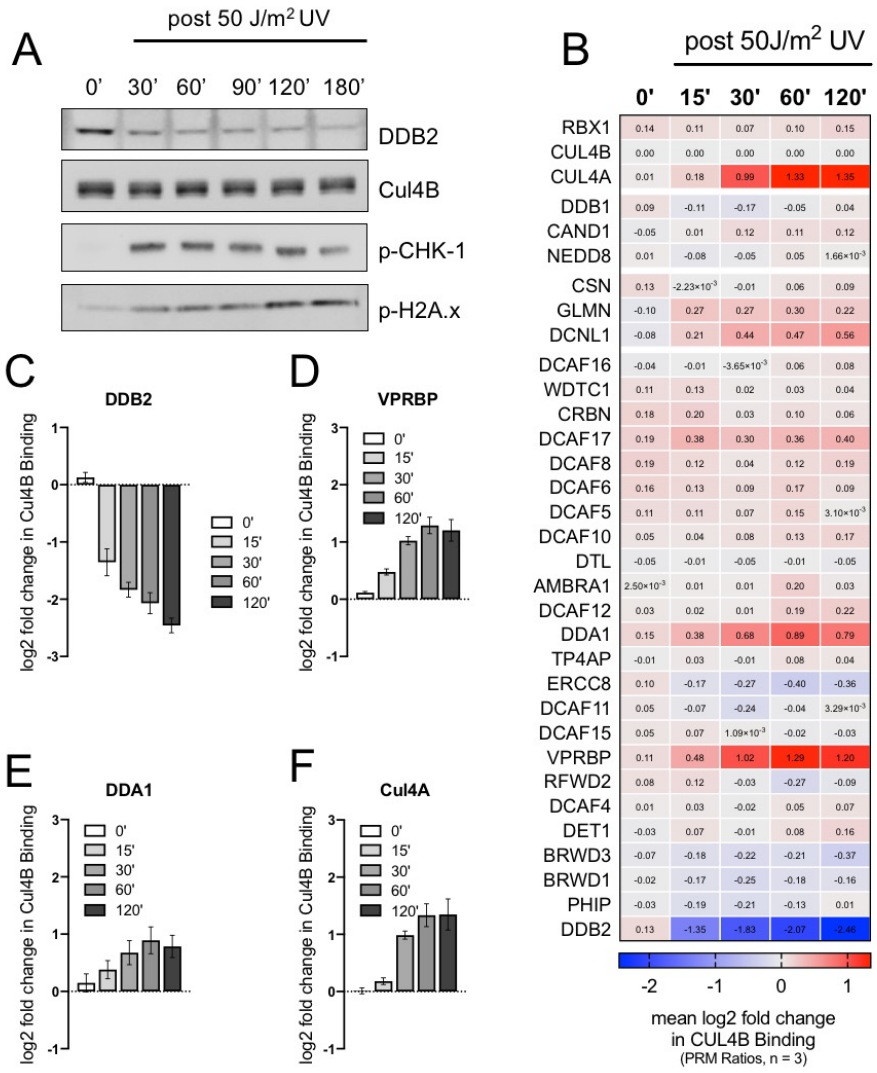

Figure 3.4. CRL4s reshape their assemblies and form Cul4A•Cul4B dimers upon UV-induced DNA damage. (A) 293T/173xHA-Cul4B cells were exposed to UV light at a dose of 50 J/m2 and lysed in SDS sample buffer at indicated time points followed by SDS PAGE and western blot. (B) Heatmap of CRL4B response to UV light at a dose of 50 J/m2, as measured via PRM LC-MS analysis of immunoprecipitated CRL4B complexes. Mean changes in proteins associated with Cul4B were transformed to log2 values and graphed as heatmap. (C-F) Individual bar graphs of protein responses displayed in (B). Error bars represent the mean ± SEM. The specificity of the signals measured was tested against bead-background as displayed in Figure S5.

Figure 3.5

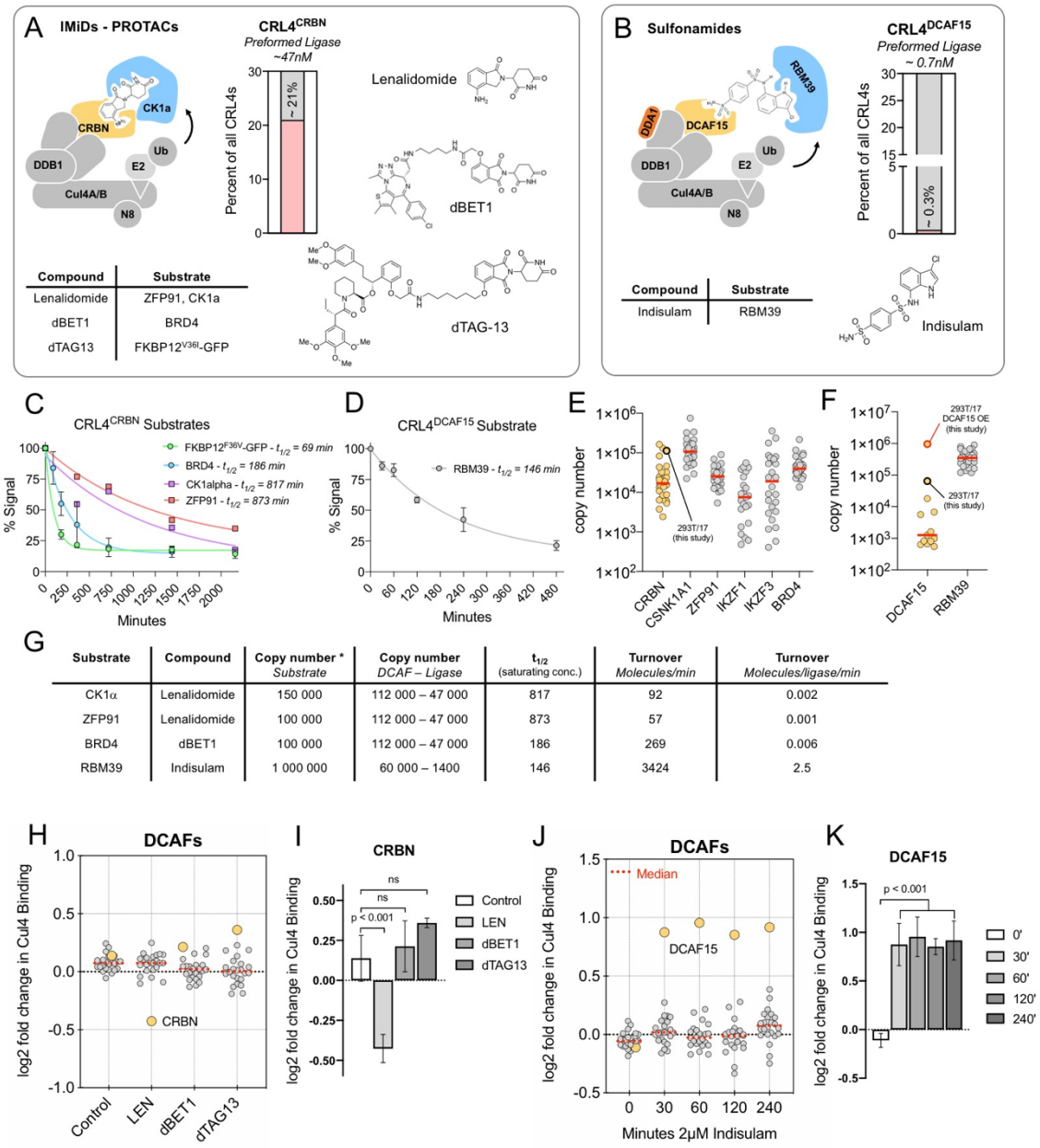

Figure 3.5. Degrader molecules minimally reshape ligase assemblies without disturbing the overall CRL4 network. (A) and (B) Schematic representation of degrader drugs, ligases and substrates used in this study. Bar graphs show % of all CRL4s for CRBN and DCAF as obtained in experiments displayed in Figure 3. (C) and (D) Turnover of CRL4 neo-substrates CK1□, ZFP91, BRD4 and RBM35 as assessed via quantitative western blot. Data of Figure S5C was fitted to a single exponential decay function to obtain t1/2. (E) and (F) Copy number estimates for DCAF-neo-substrate pairs extracted from data published by Wang et al. 2019. Each dot represents the copy number in one tissue and the red line represents the median. (G) Calculations of molecule turnover rates for studied CRL4-neosubstrates. (H-K) Changes in DCAF binding to Cul4 upon treatment with different degrader molecules. For (H, I), cells were treated for 1 hour with 30µM lenalidomide, 100nM dBET1 or 500nM dTAG-13. Each dot represents a DCAF, yellow dots represent CRBN. For (J, K), cells were treated with 2µM indisulam for different times. Immunoprecipated Cul4

complexes were analysed via PRM LC-MS, for details see Material & Methods. Each dot represents a DCAF, and yellow dots represent DCAF15. Error bars represent the mean ± SEM.

Figure 3.6

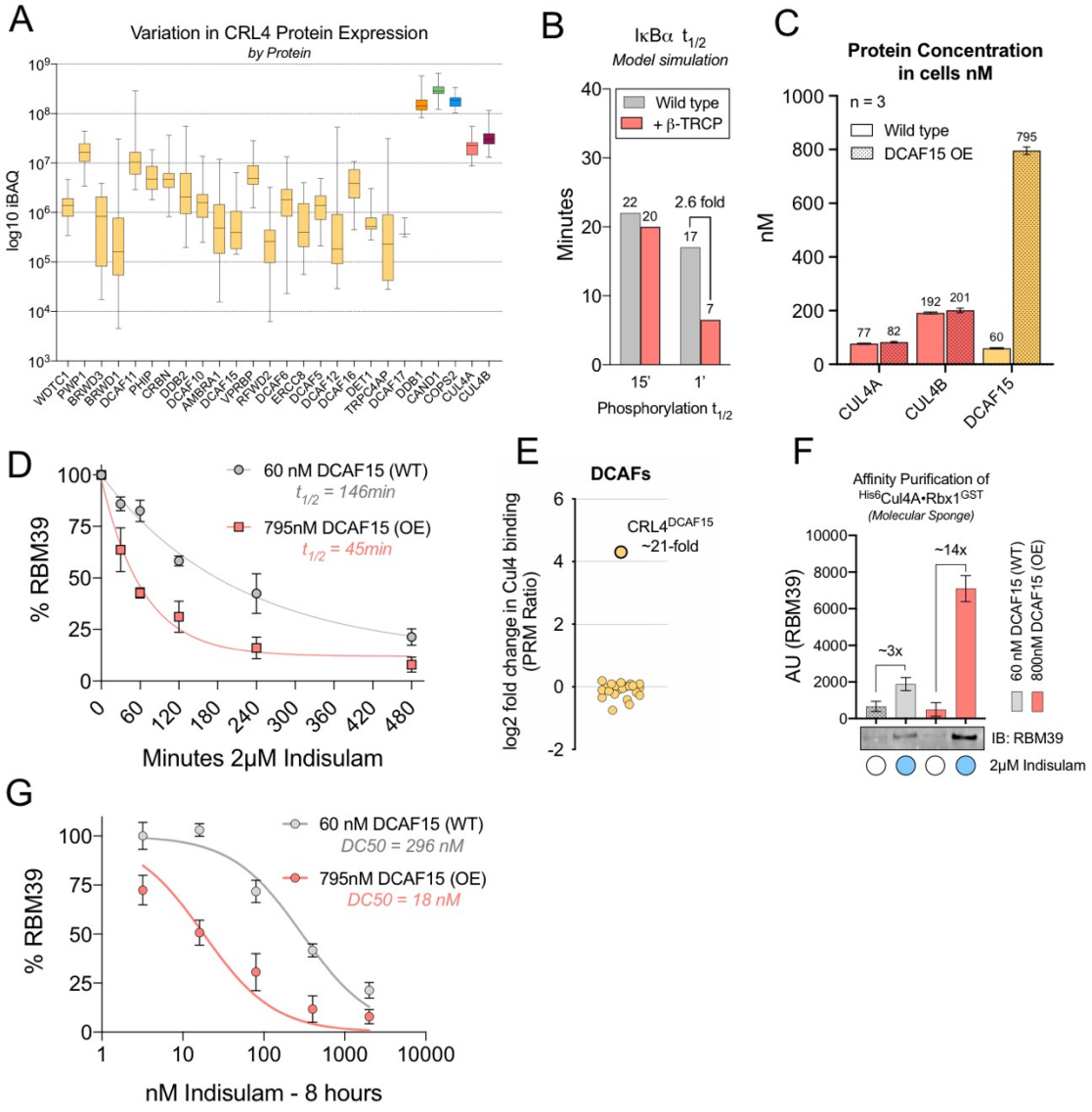

Figure 3.6. Higher DCAF expression can result in faster substrate degradation and increased degrader potency. (A) Variation of CRL4 component protein expression across 29 healthy human tissues. Data extracted from Wang et al. 2019. The box and whisker plots represent the median, lower and upper quartile as well as the highest and lowest observation of iBAQ values for each protein in up to 29 tissues. (B) Simulation of IκBα degradation using the Liu et al. 2018 model of SCF regulation under different conditions. (C) Protein levels of Cul4 and DCAF15 as measured via CRL4 QconCAT PRM LC-MS in wild type and DCAF15 over-expressing 293T/17$^{3xFLAG\text{-}Cul4A\ \&\ 3xHA\text{-}Cul4B}$ cells. (D) Turnover of RBM39 assessed via quantitative western blot in wild type and DCAF15 over-expressing cells. Data of Figure S6D was fitted to a single exponential decay function to obtain $t_{1/2}$. (E) Change in composition of CRL4 complexes when DCAF15 is overexpressed as assessed via CRL4 SpikeMix PRM LC-MS. Data was corrected for unspecific binding to beads of over-expressed DCAF15 as shown and described in Figure S6B, C. (F) Ternary complex formation of DCAF15•indisulam•RBM39 as assessed via capturing free DCAFs using molecular sponge and

quantitative western blot, for details see Material & Methods. (G) Dose response curve of indisulam assessed in 293T/17$^{3xFLAG\text{-}Cul4A\ \&\ 3xHA\text{-}Cul4B}$ wild type or DCAF15 over-expressing cells. The figure was generated on the basis of data from Figure S6A and dose response model ([drug] vs. normalized response) fit was applied to obtain a DC50. Error bars represent mean ± SEM, except for box-whisker plots in (A).

Figure Supplement 3.1

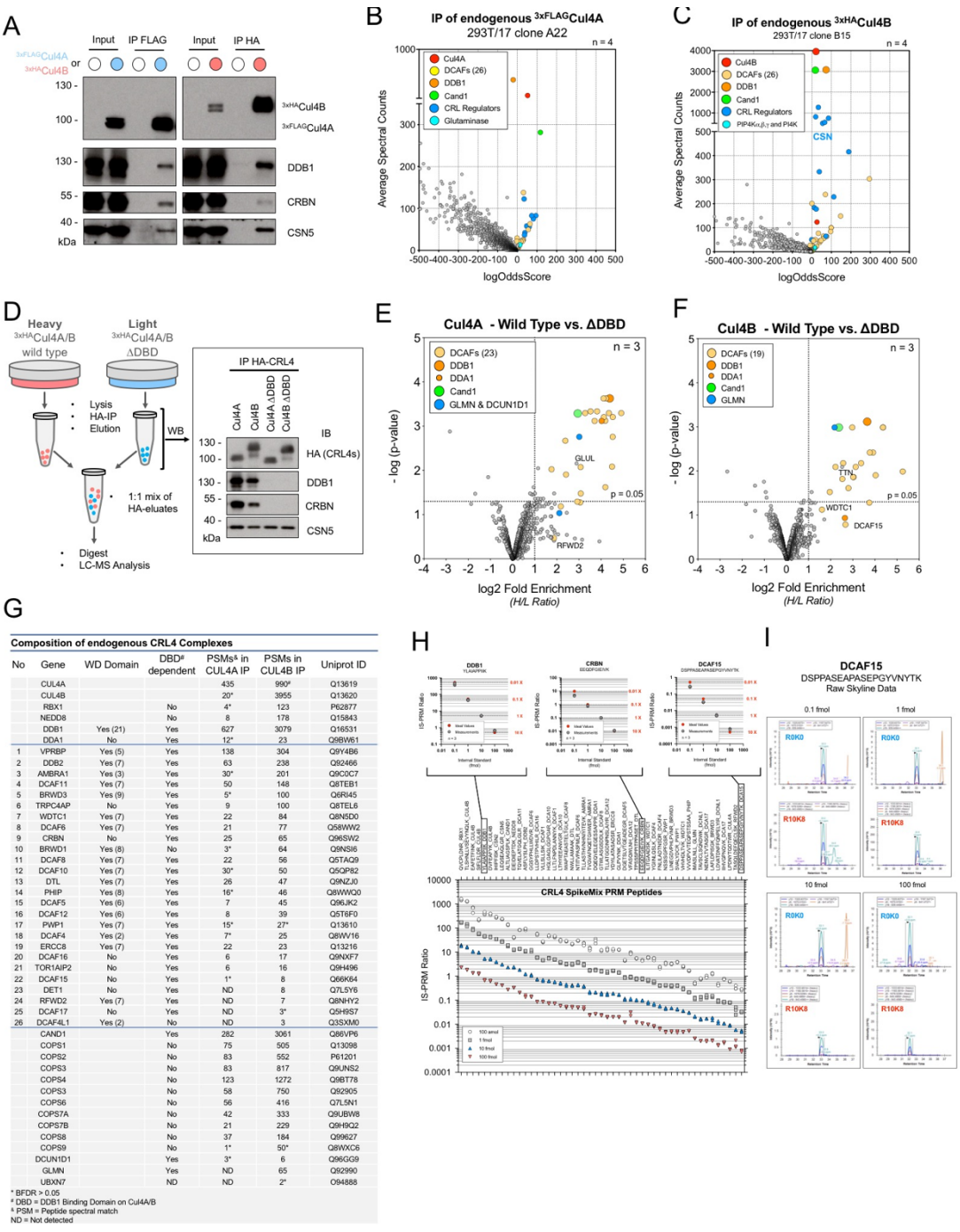

Composition of endogenous CRL4 Complexes

No	Gene	WD Domain	DBD# dependent	PSMs$ in CUL4A IP	PSMs in CUL4B IP	Uniprot ID
	CUL4A			435	990*	Q13619
	CUL4B			20*	3955	Q13620
	RBX1		No	4*	123	P62877
	NEDD8		No	8	178	Q15843
	DDB1	Yes (21)	Yes	627	3079	Q16531
	DDA1	No	Yes	12*	23	Q9BW61
1	VPRBP	Yes (5)	Yes	138	304	Q9Y4B6
2	DDB2	Yes (7)	Yes	63	238	Q92466
3	AMBRA1	Yes (3)	Yes	30*	201	Q9C0C7
4	DCAF11	Yes (7)	Yes	50	148	Q8TEB1
5	BRWD3	Yes (9)	Yes	5*	100	Q6RI45
6	TRPC4AP	No	Yes	9	100	Q8TEL6
7	WDTC1	Yes (7)	Yes	22	84	Q8N5D0
8	DCAF6	Yes (7)	Yes	21	77	Q58WW2
9	CRBN	No	Yes	25	65	Q96SW2
10	BRWD1	Yes (8)	No	3*	64	Q9NSI6
11	DCAF8	Yes (7)	Yes	22	56	Q5TAQ9
12	DCAF10	Yes (7)	Yes	30*	50	Q5QP82
13	DTL	Yes (7)	Yes	26	47	Q9NZJ0
14	PHIP	Yes (8)	Yes	16*	46	Q8WWQ0
15	DCAF5	Yes (6)	Yes	7	45	Q96JK2
16	DCAF12	Yes (6)	Yes	8	39	Q5T6F0
17	PWP1	Yes (7)	Yes	15*	27*	Q13610
18	DCAF4	Yes (2)	Yes	7*	25	Q8WV16
19	ERCC8	Yes (7)	Yes	22	23	Q13216
20	DCAF16	No	Yes	6	17	Q9NXF7
21	TOR1AIP2	No	Yes	6	16	Q9H496
22	DCAF15	No	Yes	1*	8	Q66K64
23	DET1	No	Yes	ND	8	Q7L5Y6
24	RFWD2	Yes (7)	Yes	ND	7	Q8NHY2
25	DCAF17	No	Yes	ND	3*	Q5H9S7
26	DCAF4L1	Yes (2)	No	ND	3	Q3SXM0
	CAND1		Yes	282	3061	Q86VP6
	COPS1		No	75	505	Q13098
	COPS2		No	83	552	P61201
	COPS3		No	83	817	Q9UNS2
	COPS4		No	123	1272	Q9BT78
	COPS3		No	58	750	Q92905
	COPS6		No	56	416	Q7L5N1
	COPS7A		No	42	333	Q9UBW8
	COPS7B		No	21	229	Q9H9Q2
	COPS8		No	37	184	Q99627
	COPS9		No	1*	50*	Q8WXC6
	DCUN1D1		Yes	3*	6	Q96GG9
	GLMN		Yes	ND	65	Q92990
	UBXN7		ND	ND	2*	O94888

* BFDR > 0.05
# DBD = DDB1 Binding Domain on Cul4A/B
$ PSM = Peptide spectral match
ND = Not detected

Figure Supplement 3.1. A toolbox to study endogenous CRL4 complexes. (A-C) 293T/17$^{3xFLAG\text{-}Cul4A}$ (clone A22) and 293T/17$^{3xHA\text{-}Cul4B}$ (clone B15) were lysed and immunoprecipitated via anti-FLAG and anti-HA resin followed by elution of CRL4 complexes and LC-MS analysis. SDS-PAGE and western blot analysis (A) confirms successful capture of intact CRL4 complexes and specifically enriched proteins are pictured in two volcano-plot like graphs featuring average spectral counts and logOddsScores. (D-F) 293T/17 cells were

either grown in heavy (R6K8) SILAC medium or light medium and transiently transfected with wild type 3xHA-Cul4A or Cul4B (heavy labeled cells) or a 3xHA-Cul4A/B deletion mutant missing the DDB1-binding domain (ΔDBD) (light labeled cells). Cells were lysed and immunoprecipitated via anti-HA resin followed by elution and 1:1 mixing of Cul4A/B wild type and Cul4A/BΔDBD complexes followed by LC-MS analysis (D). Volcano plots showing DDB1-dependent Cul4 interacting proteins significantly enriched in the analyzed immunoprecipitates (E, F). (G) Table summarizing the composition of endogenous CRL4 complexes based on experiments displayed in (A-F). (H-F) Assessment of CRL4 SpikeMix PRM MS assay. Immunoprecipitated Cul4B complexes were eluted and digested followed by addition of CRL4 SpikeMix standards at four different concentrations and PRM analysis. Displayed are the PRM ratios of all successfully targeted and detected peptides on a log scale as well as the ratio to concentration relationship for three peptides with a high (DDB1), medium (CRBN) and low PRM-Ratio (DCAF15) (H). (I) Raw Skyline chromatograms of the lowest abundant peptide in the assay.

Figure Supplement 3.2

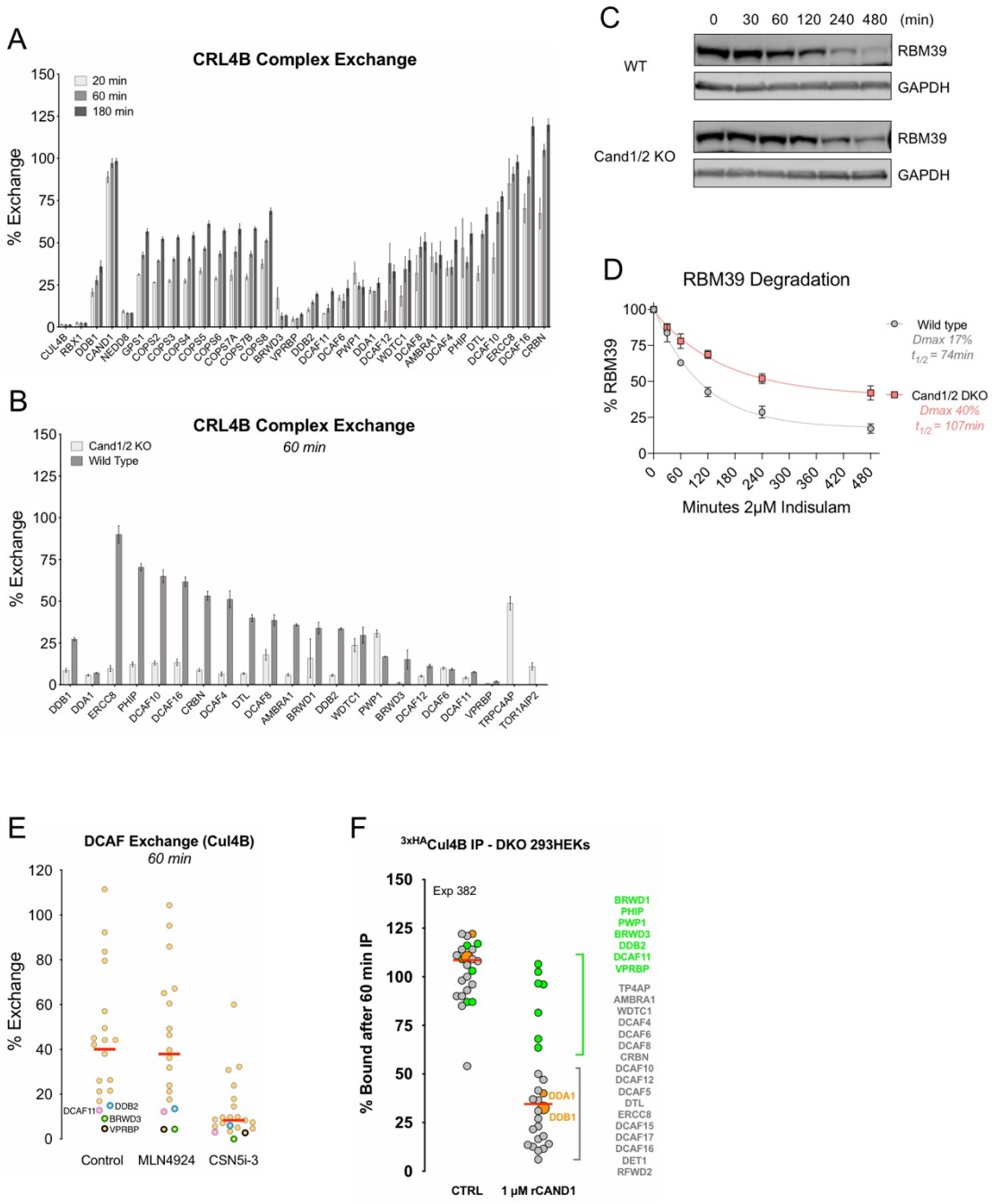

Figure Supplement 3.2. CRL4 complexes exchange DDB1•DCAFs via Cand1 and are stabilized by CSN5i-3 and Molecular Sponge. (A) 293T/173xHA-Cul4B cells were grown in heavy medium and 293T/17 WT cells in light medium, harvested and mixed at a ratio of 1:1, followed by lysis and anti-HA immunoprecipitation for different periods of time as well as LC-MS analysis. SILAC ratios of Cul4-binding proteins of ~1 translate to 100% exchange. This data is displayed as a dot-plot in Figure 3.2B. (B) Flp-In T-REx HEK2933xHA-Cul4B Cand1/2 double knock out (DKO) cells were grown in light medium and Flp-In

T-REx HEK293 DKO cells in heavy medium and processed as for (A). This data is displayed as a dot-plot in Figure 3.2C. (C, D) Flp-In T-REx HEK2933xHA-Cul4B Cand1/2 double knock out (DKO) and wild type cells were treated with 2μM indisulam for indicated times, lysed in 2x LDS buffer and processes for quantitative western blotting. Data was plotted and fitted to a single exponential to yield t1/2. (E) 293T/173xHA-Cul4B cells were grown in heavy medium and 293T/17 WT cells in light medium, either pre-treated with 1μM MLN4924 or 1μM CSN5i-3 for 4h and processes as for (A). (F) Flp-In T-REx HEK2933xHA-Cul4B Cand1/2 double knock out (DKO) cells were grown in light medium, lysed and immunoprecipated via anti-HA resin and either exposed to lysis buffer or lysis buffer with 1μM Cand1 and incubated for 60min under rotation at 4C. Bead-bound complexes were then washed and processed for PRM LC-MS analysis. Error bars represent the main ± SEM.

Figure Supplement 3.3

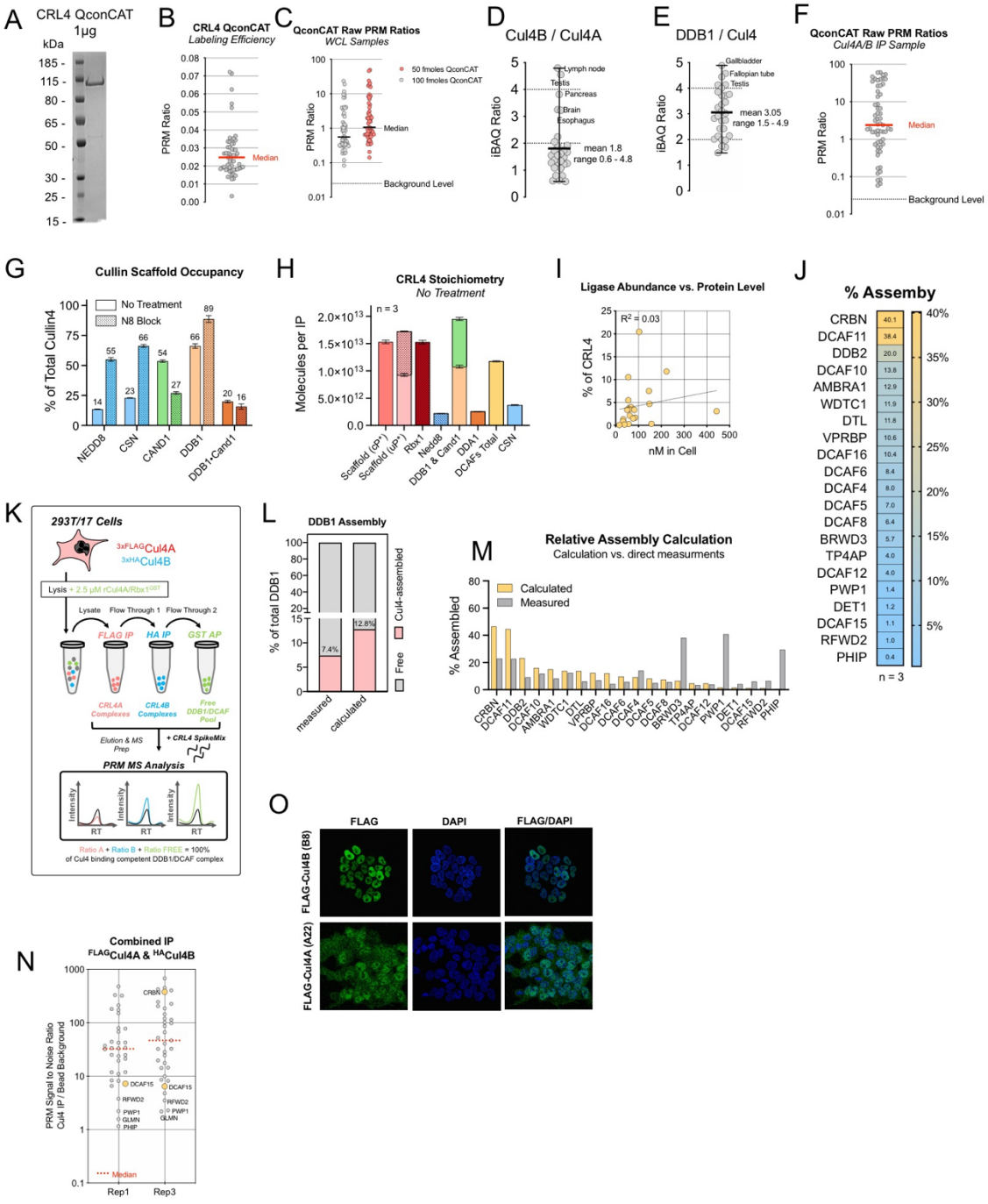

Figure Supplement 3.3. Individual CRL4 ligases show Cullin-scaffold preferences and differ up to 200-fold in absolute abundance. (A) Coomassie stained SDS-PAGE gel of 1µg CRL4 QconCAT standard. (B) CRL4 QconCAT protein was digested with trypsin and analysis via PRM MS to determine the labeling efficiency. (C) 293T/173xFLAG-Cul4A & 3xHA-Cul4B cells were lysed in 8M Urea, spiked with CRL4 QconCAT protein standard followed by tryptic digest and PRM LC-MS analysis. Heavy to Light ratios were

converted to nM cellular concentrations as described in the methods section. Shown in (C) are the PRM ratios measured for the experiment displayed in Figure 3B. The spiked concentration of the QconCAT standard was chosen so that all PRM ratios measured were well beyond the ~2% background signal. (D, E) iBAQ values for the indicated proteins were extracted from Wang et al. 2019 and Cul4B/Cul4A ratios as well as DDB1/Cul4 Ratios calculated and plotted. (F) CRL4 complexes were immunopurified from 293T/173xFLAG-Cul4A & 3xHA-Cul4B cells pulsed N8 Block (5min 1μM CSN5i-3 & 1μM MLN4924) via combined anti-HA and anti-FLAG IP, eluates spiked with CRL4 QconCAT protein standard and analyzed via PRM LC-MS. Shown are the PRM ratios measured for the experiment displayed in Figure 3C. (G) Occupancies of the Cul4 scaffold by various proteins as calculated from experiments displayed in Figure 3B, C. (H) CRL4 stoichiometries as measured for a Cul4 IP sample from cells where post-lysis exchange was not inhibited. (I) Correlation plot of cellular concentrations of DCAFs and their overall % representation within all captured CRL4 complexes. (J) Percent Assembly (Percent of DCAF bound to Cul4 versus free) of each DCAF as calculated from stoichiometry data. (K) 293T/173xFLAG-Cul4A & 3xHA-Cul4B cells were pulsed with N8 Block and lysed in the presence of 2.5 μM rCul4A•Rbx1GST molecular sponge followed by sequential immunoprecipation via anti-FLAG, anti-HA and GSH resin to capture assembled CRL4 complexes or free DDB1•DCAF modules. IP-eluates were digested, spiked with CRL4 SpikeMix peptide standard and analyzed via PRM LC-MS. (L) Percent Assembly of DDB1 as measured via (K) or calculated from stoichiometries and cellular concentrations. (M) comparing Percent Assembly for all assessed DCAF proteins as measured in (K) or calculated from stoichiometries and concentrations. (N) Lysates from 293T/173xFLAG-Cul4A & 3xHA-Cul4B or 293T/17 wild type cells were immunoprecipitated with either anti-FLAG or anti-HA resin and eluates spiked with CRL4 SpikeMix followed by PRM analysis. PRM ratios obtained from CRL4 IPs were then related to PRM ratios obtained from bead background samples to derive the displayed signal to noise ratios. (O) 293T/173xFLAG-Cul4A and 293T/173xFLAG-Cul4B cells were fixed on a cover slip and stained with anti-FLAG antibodies followed by microscopic analysis. In all figures, error bars represent the mean ± SEM.

Figure Supplement 3.4

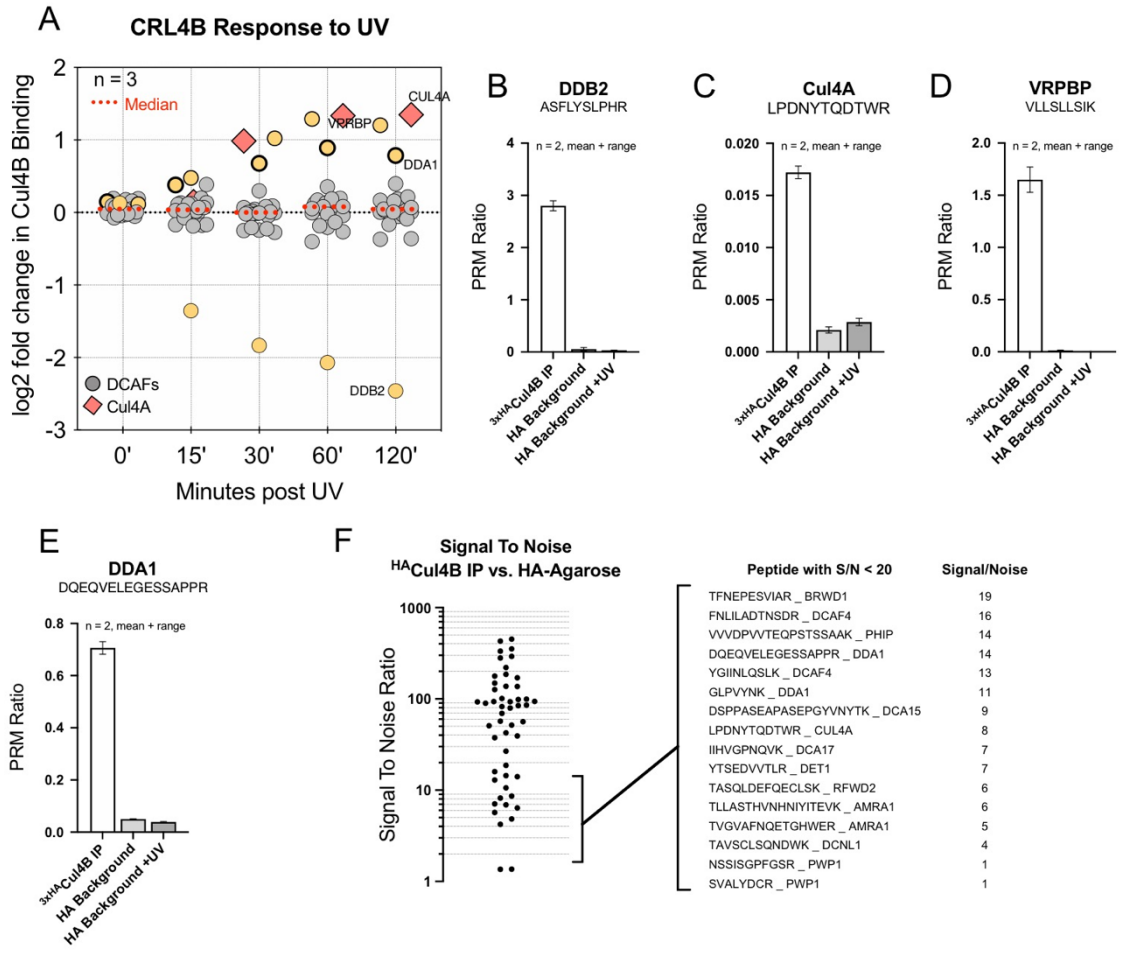

Figure Supplement 3.4. CRL4s reshape their assemblies and form Cul4A•Cul4B dimers upon UV-induced DNA damage. (A) 293T/17$^{3xHA\text{-}Cul4B}$ cells were exposed to UV light at a dose of 50 J/m^2 and lysed indicated time points followed by anti-HA immunoprecipitation and PRM MS analysis. Displayed is data from Figure 3.4B as a dot plot. (B-E) Background signal assessment for individual proteins in experiment (A). Untagged wild type 293T/17 cells were either treated or not with 50 J/m^2 UV light followed by lysis and incubation with anti-HA resin followed by PRM MS analysis. (F) Dot plot of signal to noise ratios as computed from measured PRM ratios in a HA-Cul4B IP sample divided by measured PRM ratios in a HA background sample. In all figures, error bars represent the mean ± SEM.

Figure Supplement 3.5

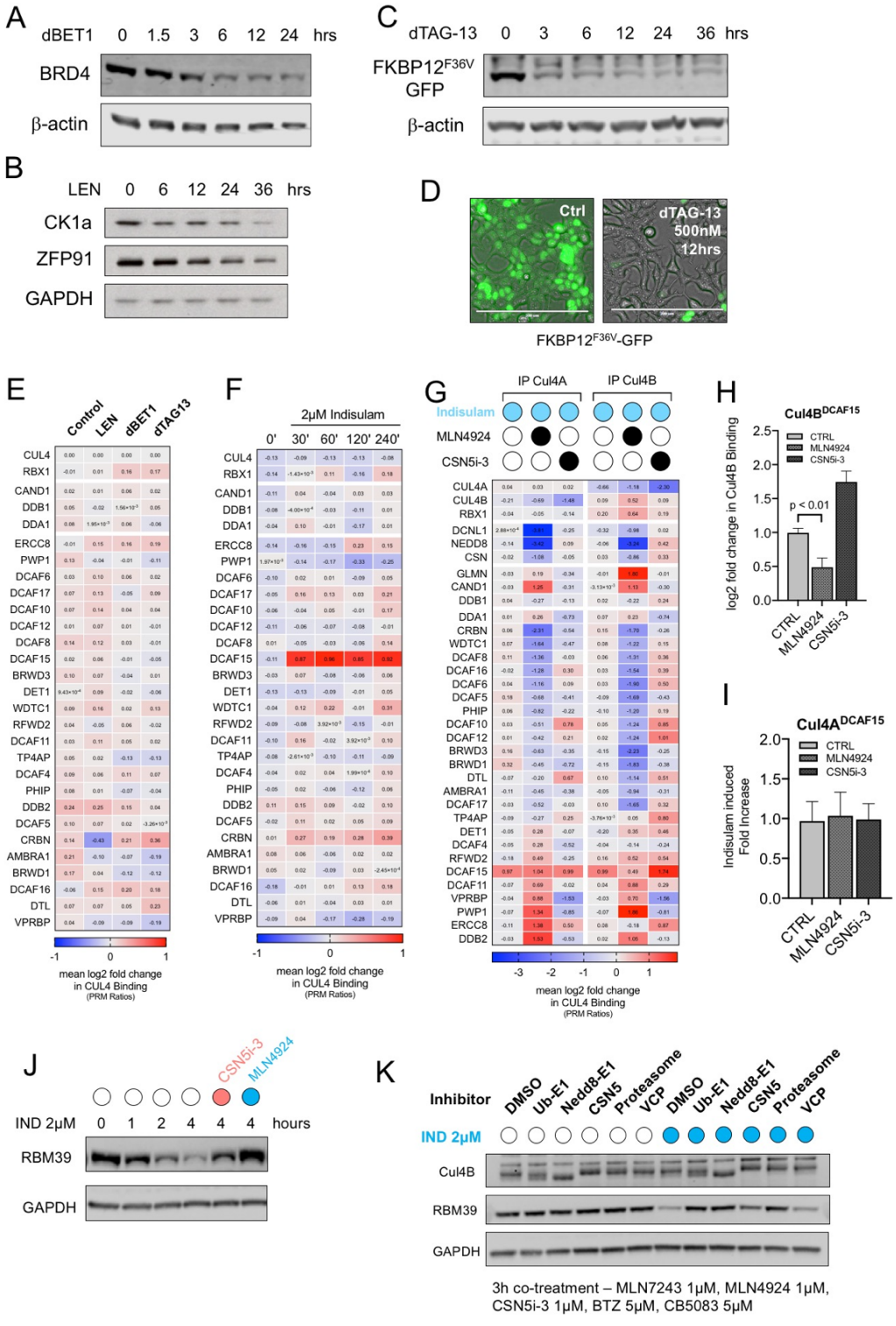

Figure Supplement 3.5. Degrader molecules minimally reshape ligase assemblies without disturbing

the overall CRL4 network. (A) 293T/17 cells were treated with 100nM dBET1 (A) or 30μM Lenalidomide (B) for indicated times, lysed in SDS sample buffer followed by SDS Page and quantitative western blot. (C, D) 293T/173xFLAG-Cul4A & 3xHA-Cul4B cells stably over-expressing FKBP12F36V-GFP were treated with 500nM dTAG-13 for indicated times, lysed in SDS sample buffer followed by SDS-PAGE and quantitative wester blotting (C) or treated for 12 hours and imaging of GFP-fluorescence signal per light microscope (D). (E) 293T/173xFLAG-Cul4A & 3xHA-Cul4B cells were treated for 1 hour with 30μM Lenalidomide, 100nM dBET1 or 500nM dTAG-13, pulsed with N8 Block before harvest. Lysates were immunoprecipitated with anti-HA and anti-FLAG resin to capture CRL4 complexes followed by PRM LC-MS analysis. Heatmap for data displayed in Figure 3.5H and 5I. (F) 293T/173xFLAG-Cul4A & 3xHA-Cul4B cells were treated with 2μM Indisulam for the indicated times, pulsed with N8 Block and lysates immunoprecipitated for via anti-HA and anti-FLAG to capture CRL4 complexes followed by PRM LC-MS. Heatmap for data displayed in Figure 3.5J and 5K. (G) 293T/173xFLAG-Cul4A & 3xHA-Cul4B cells were pre-treated or not with 1μM MLN4924 or 1μM CSN5i-3 for 30 min followed by treatment with 2μM Indisulam for 60 min, pulsed with N8 Block and lysates immunoprecipitated for either via anti-FLAG or anti-HA to capture CRL4A and CRL4B complexes individually, followed by PRM LC-MS. (H, I) Bar graphs of log2 fold changes of DCAF15 bound to Cul4B and Cul4A for data displaye din heatmap (G). (J) 293T/173xFLAG-Cul4A & 3xHA-Cul4B cells were treated with 2μM indisulam for indicated times with or without co-treatment of MLN4924 or CSN5i-3 followed by lysis in 2x SDS sample buffer and SDS-PAGE as well as western blotting. (K) 293T/173xFLAG-Cul4A & 3xHA-Cul4B cells were treated with 2μM indisulam for 3 hours with or without co-treatment of 1μM ubiquitin E1 inhibitor MLN7243, 1μM Nedd8 E1 inhibitor MLN4924, 1μM CSN inhibitor CSN5i-3, 5μM proteasome inhibitor Bortezomib or 5μM p97/VCP inhibitor CB5083, followed by lysis in 2x SDS sample buffer and SDS-PAGE as well as western blotting. In all figures, error bars represent the mean ± SEM.

Figure Supplement 3.6

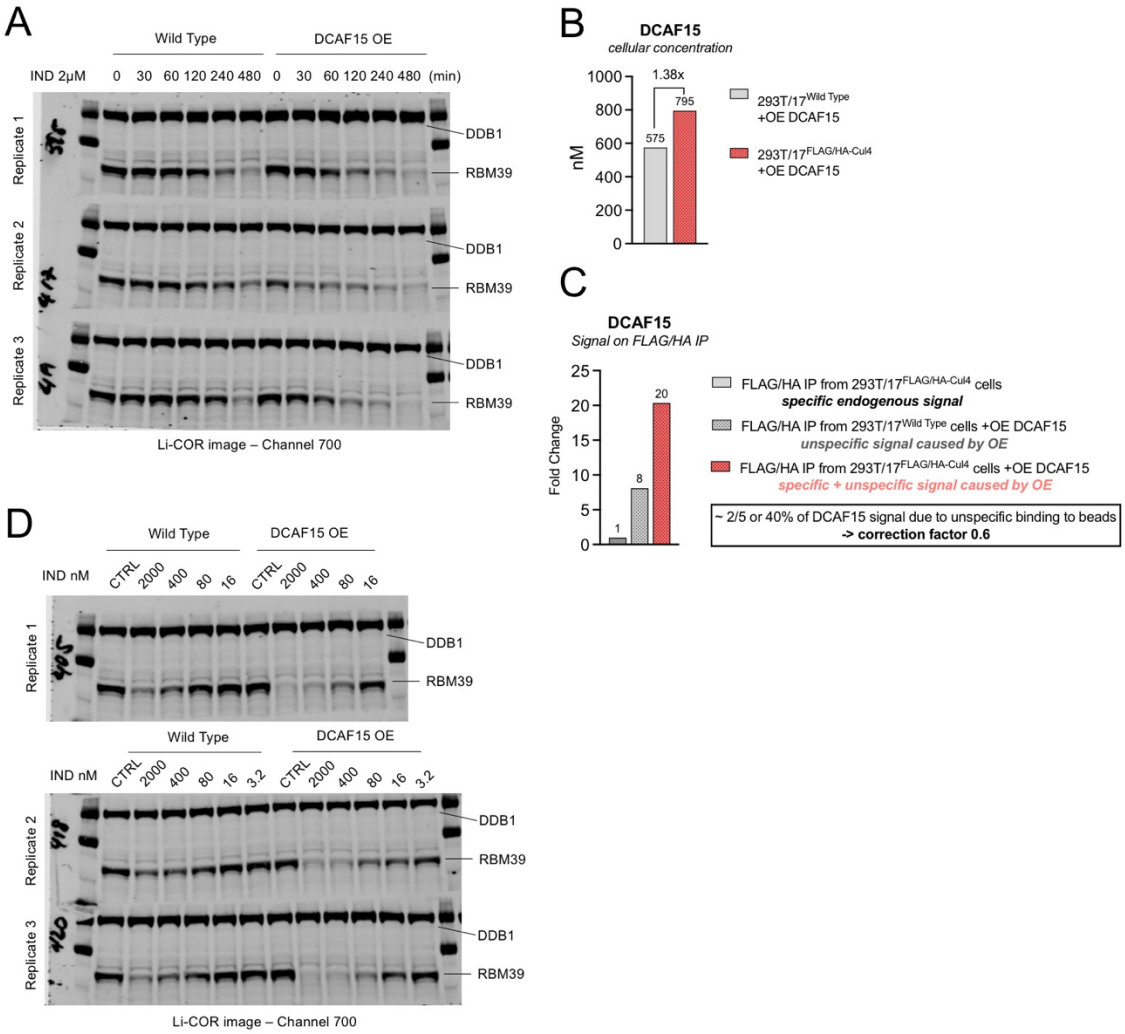

Figure Supplement 3.6. Higher DCAF expression can result in faster substrate degradation via increased substrate occupancy. (A) 293T/17$^{3xFLAG\text{-}Cul4A\ \&\ 3xHA\text{-}Cul4B}$ wild type or DCAF15 over-expressing cells were treated with 2µM indisulam for indicated times, lysed in 2xSDS sample buffer and processed via SDS-PAGE for quantitative western blotting. (B) 293T/17 and 293T/17$^{3xFLAG\text{-}Cul4A\ \&\ 3xHA\text{-}Cul4B}$ cells over-expressing DCAF15 were lysed in 8M urea and processed for CRL4 QconCAT PRM analysis to measure cellular concentrations. (C) Anti-HA resin was exposed to lysates from 293T/17$^{3xFLAG\text{-}Cul4A\ \&\ 3xHA\text{-}Cul4B}$ cells, 293T/17 cells over-expressing DCAF15 or 293T/17$^{3xFLAG\text{-}Cul4A\ \&\ 3xHA\text{-}Cul4B}$ cells over-expressing DCAF15 to evaluate the unspecific background binding of over-produced DCAF15 to Anti-HA resin. The measured PRM ratios were normalized to over-expressed DCAF15 levels. To correct for ~40% unspecific background signal, DCAF15 PRM ratios displayed in Figure 3.6E were corrected by a factor of 0.6.

Supplemental Item 3.1

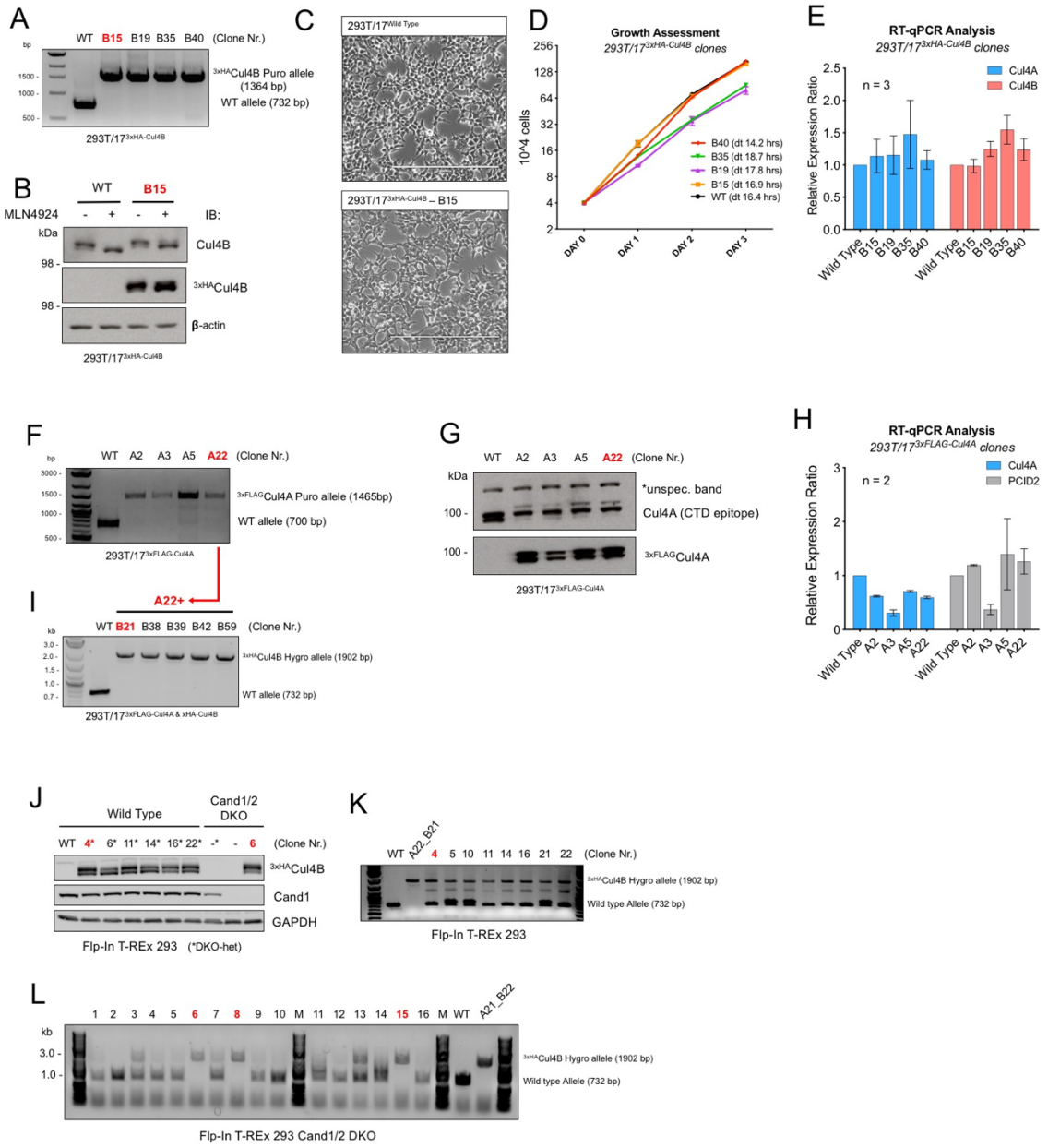

Supplemental Item 3.1. Genetic engineering of epitope tagged cell lines. (A-E) Assessment of CRISPR/Cas9-engineered 293T/17$^{3xHA\text{-}Cul4B}$ single cell clones using genomic PCR to evaluate genomic insertion (A), SDS-PAGE and western blotting to evaluate protein levels (B), light microscopy to evaluate morphology (C), growth assessment (D) as well as quantitative RT-PCR to evaluate mRNA levels. (F-H) Assessment of CRISPR/Cas9-engineered 293T/17$^{3xFLAG\text{-}Cul4A}$ single cell clones using genomic PCR (F), SDS-PAGE and western blotting (G) and RT-qPCR (H). Western blotting for the FLAG-tag revealed successful integration and unaffected neddylation status. Therefore, the anti-Cu4A antibody against a C-terminal epitope likely does not associate well with the C-terminally neddyalted Cul4A. RT-qPCR of the essential gene PCID2 that is located upstream of Cul4A on chromosome 13 revealed normal levels for 3 out

of 4 genes while Cul4A levels were slightly lower after in clones carrying the insert. (I) Assessment of CRISPR/Cas9-engineered 293T/17$^{3xFLAG\text{-}Cul4A\ \&\ 3xHA\text{-}Cul4B}$ via genomic PCR. (J-L) Assessment of CRISPR/Cas9-engineered Flp-In T-REx HEK293$^{3xHA\text{-}Cul4B}$ wild type and Cand1/2 double knock out (DKO) single cell clones via SDS-PAGE and western blotting (J) and genomic PCR (K-L). The clones marked in red in each figure were used for experiments in this study.

Supplemental Table 3.1

CRL4 SpikeMix Library – 418 peptides, 142 proteins			
Index	Sequences Customer	C-terminus	Peptide ID
1	TLLASTHVNHNIYITEVK	K	AMBRA1
2	TVGVAFNQETGHWER	R	AMBRA1
3	WLPEPGLGLAYGTNK	K	AMBRA1
4	EQNYSDDVLANMISEPR	R	APP
5	MQQNGYENPTYK	K	APP
6	THPHFVIPYR	R	APP
7	LIDPQTQVSR	R	APPL2
8	LNQTALQAVTPITSFGK	K	APPL2
9	TGLVTTTWER	R	APPL2
10	DISQDSLQDIK	K	ARIH1
11	LFAECHVINPSK	K	ARIH1
12	VLLQHVHEGYEK	K	ARIH1
13	GCLTFVSK	K	ARPC1A
14	LAWVSHDSTVSVADASK	K	ARPC1A
15	TLESSIQGLR	R	ARPC1A
16	ASSEGGTAAGAGLDSLHK	K	ARPC1B
17	TLESSIQGLR	R	ARPC1B
18	VAWVSHDSTVCLADADK	K	ARPC1B
19	HQEELTELHK	K	ATG16L1
20	ITALDLNPER	R	ATG16L1
21	TTEENQELVTR	R	ATG16L1
22	HVAPDHLLQICQR	R	BRWD1
23	IIPELVGSPTQSTSSR	R	BRWD1
24	TFNEPESVIAR	R	BRWD1
25	IWQYQQQEWK	K	BRWD3
26	LAFLDPISGK	K	BRWD3
27	LINEGDVPHLPVNR	R	BRWD3
28	GLDHIAENILSYLDAK	K	BTRC
29	GVYCLQYDDQK	K	BTRC
30	DFITALPAR	R	BTRC
31	ALTLIAGSPLK	K	CAND1
32	ITSEALLVTQQLVK	K	CAND1
33	LTLIDPETLLPR	R	CAND1
34	FLISDQPHPIDPLLK	K	CAND2
35	LGDDLEPTLLLLLDR	R	CAND2
36	SNPELAALFESIQK	K	CAND2
37	EPGLLASCSDDGEVAFWK	K	CIAO1
38	SVAWAPSGNLLATCSR	R	CIAO1
39	SVLSEGHQR	R	CIAO1
40	ASNLENSTYDLYTIPK	K	COPA
41	GITGVDLFGTTDAVVK	K	COPA
42	LLHDQVGVIQFGPYK	K	COPA
43	LQFIADHCPTLR	R	COPS1
44	GHDDLGDHYLDCGDLSNALK	K	COPS1
45	AHTDFFEAFK	K	COPS2
46	IHIPFISK	K	COPS2
47	SINSILDYISTSK	K	COPS2
48	YATDTFAGLCHQLTNALVER	R	COPS3
49	VQLSGPQEAEK	K	COPS3
50	YTSQIVGR	R	COPS3
51	NAAQVLVGIPLETGQK	K	COPS4
52	AIQLSGAEQLEALK	K	COPS4
53	LYLEDDDPVQAEAYINR	R	COPS4
54	LEQSEAQLGR	R	COPS5

55	LLELLWNK	K	COPS5
56	QYYALEVSYFK	K	COPS5
57	ASEAGEVPFNHEILR	R	COPS6
58	FNVLYDR	R	COPS6
59	IGVDHVAR	R	COPS6
60	ELAESDFASTFR	R	COPS7A
61	NLPPLTEAQK	K	COPS7A
62	HLTIVSLASR	R	COPS7B
63	NQLLEVDFCIGR	R	COPS7B
64	FIPLSEPAPVPPIPNEQQLAR	R	COPS8
65	SANSELGGIWSVGQR	R	COPS8
66	KPVAGALDVSFNK	K	COPS8
67	EAQFGTTAEIYAYR	R	CRBN
68	EEQDFGIEIVK	K	CRBN
69	SALLPTIPDTEDEISPDK	K	CRBN
70	GGQQALLQHWSEYIK	K	CUL4A
71	LPDNYTQDTWR	R	CUL4A
72	TLGHNLLVSELYNQLK	K	CUL4A
73	SIFLFLDR	R	CUL4A_B
74	DVFEAFYK	K	CUL4A_B
75	QYQIDAAIVR	R	CUL4A_B
76	EAFETFINK	K	CUL4B
77	LPENYTDETWQK	K	CUL4B
78	TLSHNLLVSEVYNQLK	K	CUL4B
79	FSPTHCQIASGCLSGR	R	DCAF10
80	HGLGAGLGGPGAR	R	DCAF10
81	LTHYIEEANVGR	R	DCAF10
82	FAVFSIAVSSDGR	R	DCAF11
83	FSPIHSTGQQFIYSGCSTGK	K	DCAF11
84	TQVELATGQLGLR	R	DCAF11
85	DGSMGLWEVTDDVLTK	K	DCAF12
86	TLLATGGDNPNSLAIYR	R	DCAF12
87	VFASQWLNHR	R	DCAF12
88	ASSSLDSMPGPAGR	R	DCAF12L2
89	GPAGLQGFEGELR	R	DCAF12L2
90	VFASQWLNAR	R	DCAF12L2
91	MDGPGYGDEEEPLHTILGK	K	DCAF13
92	NYDPALHPFEVPR	R	DCAF13
93	SIYSQIQEQR	R	DCAF13
94	AHSEPLALCGETAPR	R	DCAF15
95	DSPPASEAPASEPGYVNYTK	K	DCAF15
96	ISGQLSPR	R	DCAF15
97	DHATLNGALQFATK	K	DCAF16
98	LLDPSTPVHILR	R	DCAF16
99	TEPINTTYSYTDFQK	K	DCAF16
100	IIHVGPNQVK	K	DCAF17
101	NENVLTVTASGR	R	DCAF17
102	YLSWDTPQEVIAVK	K	DCAF17
103	FNLILADTNSDR	R	DCAF4
104	LLPGHNNCNPLTK	K	DCAF4
105	YGIINLQSLK	K	DCAF4
106	GAAPGLLMAVR	R	DCAF4L1
107	SLDPSSLASDR	R	DCAF4L1
108	SQLGFLNVTSYSR	R	DCAF4L1
109	GAPGLLMAVR	R	DCAF4L2
110	VQIHSWDPSSLASDR	R	DCAF4L2
111	DGETSLVTGEADEGR	R	DCAF5
112	GLHGDPLLTQDFQR	R	DCAF5

113	SLETICANHNNGR	R	DCAF5
114	FIPSHLNNK	K	DCAF6
115	GGSYPHLLWDVR	R	DCAF6
116	NTITVPASFMLR	R	DCAF6
117	GVYPDLLATSGDYLR	R	DCAF7
118	LALGSFVEEYNNK	K	DCAF7
119	NTFDHPYPTTK	K	DCAF7
120	GTWLASGSDDLK	K	DCAF8
121	IWAPTAEASTELTGLK	K	DCAF8
122	LQHGLEGHTGCVNTLHFNQR	R	DCAF8
123	FLDLWNK	K	DCUN1D1
124	LDVATDNFFQNPELYIR	R	DCUN1D1
125	TAVSCLSQNDWK	K	DCUN1D1
126	DFYQFTFTFAK	K	DCUN1D2
127	EFLDGMTELGCDSMEK	K	DCUN1D2
128	LDEATDSFFQNPDSLHR	R	DCUN1D2
129	EEQVPPCGKPGGDILVNGTK	K	DCUN1D3
130	FCNDLCVDPTEFR	R	DCUN1D3
131	FTFQFGLDSEEGQR	R	DCUN1D3
132	DQWCNVLEFSR	R	DCUN1D4
133	LDAQNMGYFTLQEWLK	K	DCUN1D4
134	SFLNDSTNFK	K	DCUN1D4
135	LISGEEHFSSK	K	DCUN1D5
136	SMLALLLGR	R	DCUN1D5
137	SQLNDISSFK	K	DCUN1D5
138	DQEQVELEGESSAPPR	R	DDA1
139	FHADSVCK	K	DDA1
140	GLPVYNK	K	DDA1
141	ICYQEVSQCFGVLSSR	R	DDB1
142	LPSFELLHK	K	DDB1
143	SVLLLAYKPMEGNFEEIAR	R	DDB1
144	YLAIAPPIIK	K	DDB1
145	ASFLYSLPHR	R	DDB2
146	ATSLAWHPTHPSTVAVGSK	K	DDB2
147	VYSASQWDCPLGLIPHPHR	R	DDB2
148	AGTHWHQVR	R	DET1
149	NATLHSEVQFPCSASSNNFAR	R	DET1
150	YTSEDVVTLR	R	DET1
151	DEEQTDEELAVDLEALVSK	K	DNAI2
152	DPVYGTIWLQSK	K	DNAI2
153	GSLVAELSTIESSHR	R	DNAI2
154	NWLLAMAAK	K	DTL
155	LSTVGWASQK	K	DTL
156	TPSSSPPITPPASETK	K	DTL
157	EGDPLVFATVGSNR	R	EED
158	HYVGHGNAINELK	K	EED
159	VTLYECHSQGEIR	R	EED
160	ALTPQTAETDAIR	R	EIPR1
161	NVLLHQAGEIWHISASPADR	R	EIPR1
162	YNHSHDQLVLTGSSDSR	R	EIPR1
163	ASPSPQPSSQPLQIHR	R	EML4
164	LAISEDHVASVK	K	EML4
165	LSLPQNETVADTTLTK	K	EML4
166	IHGGGINTLDIEPVEGR	R	ERCC8
167	VNGLCFTSDGLHLLTVGTDNR	R	ERCC8
168	YDYILATASADSR	R	ERCC8
169	EGFITEDWDQPVADWK	K	FBXO44
170	EVSHTFSNYPPGVR	R	FBXO44

171	IFDLGSDNEEVVAGPAPAHAK	K	FBXW5
172	LYDTVPCVEVQTLR	R	FBXW5
173	TFFSWLASQR	R	FBXW5
174	DNILVSGNADSTVK	K	FBXW7
175	ITSVQPPTGLQEWLK	K	FBXW7
176	NFVITSSDDGTVK	K	FBXW7
177	IVSGGEEGLVSVWDYR	R	FBXW8
178	LCQQEGHLPDSSISDYSCWK	K	FBXW8
179	SGNIALSLSAHQLR	R	FBXW8
180	HIISGSEDHTLVVVDR	R	FBXW9
181	NFDWPAACIALEQHLSR	R	FBXW9
182	NVNLWDLR	R	FBXW9
183	LPFAAAQIGNSFR	R	GARS
184	NNIIQTWR	R	GARS
185	TVNVVQFEPSK	K	GARS
186	AHYEAEIK	K	GLMN
187	CIEEGHTDQLLEIIQNEK	K	GLMN
188	IMASLNLLR	R	GLMN
189	LFVSGACDASAK	K	GNB1
190	LLLAGYDDFNCNVWDALK	K	GNB1
191	LLLAGYDDFNCNIWDAMK	K	GNB2
192	TFVSGACDASIK	K	GNB2
193	LIVWDSYTTNK	K	GNB3
194	LLVSASQDGK	K	GNB3
195	VGILSGHDNR	R	GNB3
196	LLLAGYDDFNCNVWDTLK	K	GNB4
197	TFVSGACDASSK	K	GNB4
198	LHDVELHQVAER	R	GNB5
199	SGQCVQAFETHESDINSVR	R	GNB5
200	VSILFGHENR	R	GNB5
201	GQVEVFALR	R	GRWD1
202	LLQVVEEPQALAAFLR	R	GRWD1
203	VSWLGEEPVAGVWSEK	K	GRWD1
204	FCPSGAWELPGTPR	R	GTF3C2
205	FSSITAHPER	R	GTF3C2
206	LGLLALACSDGK	K	GTF3C2
207	IINEPTAAAIAYGLDR	R	HSPA6
208	EVLAWLEHNQLAEK	K	HSPA6
209	ELEQICRPIFSR	R	HSPA6
210	AEIQNAEDYNEIFQPK	K	KATNB1
211	IPQQAELVDEDAMSQIR	R	KATNB1
212	LNTPEELIVAGSQSGSIR	R	KATNB1
213	EGIPPQQQR	R	NEDD8
214	EIEIDIEPTDK	K	NEDD8
215	ILGGSVLHLVLALR	R	NEDD8
216	FWDLSTETPHFTCK	K	NLE1
217	TLESQAVETEK	K	NLE1
218	YLASGSGDTTVR	R	NLE1
219	IEITSLLPSR	R	NUP43
220	TPEILTVNSIGQLK	K	NUP43
221	VPLHCVDR	R	NUP43
222	GHTDSVQDISFDHSGK	K	PAFAH1B1
223	TAPYVVTGSVDQTVK	K	PAFAH1B1
224	VWDYETGDFER	R	PAFAH1B1
225	FFDCDSLVCLCEFK	K	PAK1IP1
226	GQVTFLSIHPSGK	K	PAK1IP1
227	LALSVGTDK	K	PAK1IP1
228	GEQLVVSGSWDQTVK	K	PEX7

229	HGYAAEFSPYLPGR	R	PEX7
230	IVIPAHQAEILSCDWCK	K	PEX7
231	AQSYDIQAWK	K	PHIP
232	NNALVPGTIQVNGHGGQPSK	K	PHIP
233	VVVDPVVTEQPSTSSAAK	K	PHIP
234	LLYTLHGHQGPATTVAFSR	R	POC1A
235	SNFDIVDHGEVTK	K	POC1A
236	TGEYFASGGSDEQVMVWK	K	POC1A
237	AAITSLDLSPNGK	K	POC1B
238	DVVTSVQFSPHGNLLASASR	R	POC1B
239	LHFDSPPHLLDIYPR	R	POC1B
240	FIASTGMDR	R	PRPF19
241	IWSVPNASCVQVVR	R	PRPF19
242	QELSHALYQHDAACR	R	PRPF19
243	AQEALDFYGEVR	R	PTEN
244	EYLVLTLTK	K	PTEN
245	YVYYYSYLLK	K	PTEN
246	GCLVTASADK	K	PWP1
247	NSSISGPFGSR	R	PWP1
248	SVALYDCR	R	PWP1
249	CWEVQDSGQTIPK	K	RAE1
250	GHEFYNPQK	K	RAE1
251	GLIVYQLENQPSEFR	R	RAE1
252	GEFGGFGSVSGK	K	RBBP4
253	LHSFESHK	K	RBBP4
254	YMPQNPCIIATK	K	RBBP4
255	HVVLPVDDDSDLNVVASFDR	R	RBBP5
256	TDSQDLVASFR	R	RBBP5
257	VTTGTSNTTAIK	K	RBBP5
258	LHTFESHK	K	RBBP7
259	VHIPNDDAQFDASHCDSDK	K	RBBP7
260	YMPQNPHIIATK	K	RBBP7
261	QVCPLDNR	R	RBX1
262	WNAVALWAWDIVVDNCAICR	R	RBX1
263	LTAHFEDLEQCYFSTR	R	RFWD2
264	LWSTNLDNSVASIEAK	K	RFWD2
265	TASQLDEFQECLSK	K	RFWD2
266	VQVMDACLR	R	RNF7
267	CPLCQQDWVVQR	R	RNF7
268	WNAVAMWSWDVECDTCAICR	R	RNF7
269	IPEEHDLESQIR	R	RPTOR
270	QDLLVASLFR	R	RPTOR
271	SYNCTPVSSPR	R	RPTOR
272	LPENQTSPGESPER	R	SCAP
273	LPLPGTGPVEFTTPVK	K	SCAP
274	YISLLPVIPVTLR	R	SCAP
275	NPEHFVVCNR	R	SMU1
276	SLGSTAGTDITVNSVILLPK	K	SMU1
277	YIHLENLLAR	R	SMU1
278	GHTSFVNSCYPAR	R	SNRNP40
279	GPQLVCTGSDDGTVK	K	SNRNP40
280	IFQGNVHNFEK	K	SNRNP40
281	VLAQASGNGVIHLLDLK	K	SPAG16
282	VLEEALGMGLTAAGDAR	R	SPAG16
283	VVGQISGLQETLK	K	SPAG16
284	ALIASAGADALAK	K	STRN4
285	APPGPAGLSGGESLLVK	K	STRN4
286	NAALDVEPIHAFR	R	STRN4

287	EELFGEASAGK	K	STXBP5L
288	SLSGSTNTVASEGVTK	K	STXBP5L
289	TAGMMTSAEAFSK	K	STXBP5L
290	LQEDSYNYLIR	R	TAF5L
291	LWSAQQGNSVR	R	TAF5L
292	YLASAGEDQR	R	TAF5L
293	EGGSHFINTSSPR	R	TBL1X
294	GNYILSAGVDK	K	TBL1X
295	GVCTHTLTK	K	TBL1X
296	TFQGHTNEVNAIK	K	TBL1XR1
297	HQEPVYSVAFSPDGR	R	TBL1XR1
298	AATMTPAAISQQNPPK	K	TBL1Y
299	GLQYVEAEISINK	K	TBL1Y
300	IWTENGNLASTLGQHK	K	TBL1Y
301	LPVPAAAPTPWETHK	K	TBL3
302	NTAPDNGPILLQAQTTQR	R	TBL3
303	VNILEVASGAVLR	R	TBL3
304	DDVVTFIDAK	K	THOC3
305	EFLAHSAK	K	THOC3
306	TLSFSHDGK	K	THOC3
307	GHTDYIHCLALR	R	THOC6
308	HLLSAGDGEVK	K	THOC6
309	SPEVLSGGEDGAVR	R	THOC6
310	DASSSPASTASSASSTSLK	K	TLE1
311	EPGTSNSLLVPDSLR	R	TLE1
312	FTIPESLDR	R	TLE1
313	ELILNDLPASTPASK	K	TLE2
314	LWTGGLDNTVR	R	TLE2
315	SPVMAFESHPHLR	R	TLE2
316	ESSSVLSCDISADDK	K	TLE3
317	NDAPTPGTSTTPGLR	R	TLE3
318	QFQGHTDGASCIDISHDGTK	K	TLE3
319	ADAHLGSSSVALPK	K	TOR1AIP2
320	DHQEVETEGPESADTGDK	K	TOR1AIP2
321	FTNSDTPTSFNHMDSDK	K	TOR1AIP2
322	ETVSILLNPDR	R	TRPC4AP
323	GTTSYADQMFLLK	K	TRPC4AP
324	WSGIPQLLLK	K	TRPC4AP
325	EAAEVLQNNR	R	UBE2M
326	LFEQNVQR	R	UBE2M
327	TCDISFSDPDDLLNFK	K	UBE2M
328	ILVLQNELER	R	UVRAG
329	TILLQVDQNCVR	R	UVRAG
330	YQHGLGTPDLR	R	UVRAG
331	HSFTEDHYVEFSK	K	VPRBP
332	LLTLFNPDLANNYK	K	VPRBP
333	VLLSLLSIK	K	VPRBP
334	APLYDLAAHEDK	K	WDR12
335	GHAGSVDSIAVDGSGTK	K	WDR12
336	VFNCISYSPLCK	K	WDR12
337	LSQSDEDVIR	R	WDR26
338	MSQSHEDSLTSVAWNPDGK	K	WDR26
339	TVLASDTHQR	R	WDR26
340	DPSHQLLILR	R	WDR27
341	GEQVEVTFPVLR	R	WDR27
342	SGLCSQPEESQLPSTSALGK	K	WDR27
343	DAITQALFLR	R	WDR3
344	SFDLIHSPHGELK	K	WDR3

345	YVASAVFGVIGSQK	K	WDR3
346	DNTLLLWDVVTGQSVER	R	WDR31
347	GLQVAHMFPAK	K	WDR31
348	YGRPDEIIEER	R	WDR31
349	EFENLYIENLELR	R	WDR37
350	IIALPHDNR	R	WDR37
351	LAAEGQAIDGAELSK	K	WDR37
352	GVLDVAHTCAFTPDGK	K	WDR38
353	ILVSGAADQTR	R	WDR38
354	SIAFSPDELWLASAGYSR	R	WDR38
355	ATFDNVTSYLK	K	WDR4
356	CTALTFIASEEK	K	WDR4
357	SGDVYSFSVLEPHGCGR	R	WDR4
358	AAYADLLTPLISK	K	WDR47
359	LTHDASNIHTSTPR	R	WDR47
360	MVQSYHPHSSDVR	R	WDR47
361	DAGFSSPDGSDPK	K	WDR48
362	DTNNNVAYWDVLK	K	WDR48
363	SADPPPAIWVATTK	K	WDR48
364	FTLAGHTK	K	WDR5
365	IWDTASGQCLK	K	WDR5
366	TLPAHSDPVSAVHFNR	R	WDR5
367	FQGADDVTSVLFSPSCPTK	K	WDR53
368	ITLWDANSEVEK	K	WDR53
369	LYASHGETISVLDVR	R	WDR53
370	DGSGEVGTTLQGHTR	R	WDR59
371	NANCLATSHDGDVR	R	WDR59
372	VIIQDIACLLPVHK	K	WDR59
373	AQLALSSSANQSK	K	WDR5B
374	FSPNGEWLASSSADR	R	WDR5B
375	TLVDDDNPPVSFVK	K	WDR5B
376	ENSETVVTGSLDDLVK	K	WDR61
377	LWDLENGK	K	WDR61
378	VNIFGVESGK	K	WDR61
379	DTLAHSAPLLTEK	K	WDR66
380	SFEVLGYTNSK	K	WDR66
381	YLATISDAEVQK	K	WDR66
382	IPDSHEITLK	K	WDR70
383	LVTGGYDYDVK	K	WDR70
384	VGTHGGTLSSYIVK	K	WDR70
385	AESTLQNSSSAVHTESNK	K	WDR76
386	DTHIYDAR	R	WDR76
387	SIASAYFSPLTGNR	R	WDR76
388	ETPPPLVPPAAR	R	WDR77
389	EWNLPPNAPACMER	R	WDR77
390	VWDLAQQVVLSSYR	R	WDR77
391	DTNIYLAGTEEGHIHK	K	WDR78
392	SSYIFAAANENR	R	WDR78
393	TNPDLLAVGYGHFGFK	K	WDR78
394	HTGPITCLQFNPK	K	WDR82
395	IHVWNGESGIK	K	WDR82
396	YTHAANTVVYSSNK	K	WDR82
397	DGQCTLVSSLDSTLR	R	WDR83
398	LDCCLSER	R	WDR83
399	TLDCGQGAVR	R	WDR83
400	AWDILSGEQLR	R	WDR86
401	GGINWLSLSPDGQR	R	WDR86
402	ILVANNQLFSSSYDR	R	WDR86

403	ATDLQILSTQVEQR	R	WDR87
404	DIFPSAHASVEK	K	WDR87
405	DVTYSVLTDGANR	R	WDR87
406	ELFLTAGGAGGLHLWK	K	WDR92
407	GFNYTVFDCK	K	WDR92
408	GTGVIQLYEIQHGDLK	K	WDR92
409	ILITGAADSK	K	WDTC1
410	VHVHDLTVK	K	WDTC1
411	YHVTDPFIR	R	WDTC1
412	FGQDQLLLATGLNNGR	R	WSB1
413	SVSFSHDGLHVASLADDK	K	WSB1
414	TIGELLAPAAPFDK	K	WSB1
415	DLSFTPSGSLILVSASR	R	WSB2
416	LIPWPLEEQFIPK	K	WSB2
417	SFLTTYQVLALPIPK	K	WSB2

Supplemental Table 3.2

CRL4 SpikeMix Mass Table – 116 targets, 58 peptides, 37 proteins						
Compound	Formul	Adduct	m/z	z	t start (min)	t stop (min)
LEQSEAQLGR			565.7937	2	17.25	22.25
LEQSEAQLGR			570.79783	2	17.25	22.25
IIHVGPNQVK			552.82933	2	18.41	23.41
IIHVGPNQVK			556.83643	2	18.41	23.41
LTHYIEEANVGR			701.359455	2	22.95	27.95
LTHYIEEANVGR			706.36359	2	22.95	27.95
FTNSDTPTSFNHMDSDK			972.40641	2	25.77	30.77
FTNSDTPTSFNHMDSDK			976.41351	2	25.77	30.77
DQEQVELEGESSAPPR			885.910175	2	28.5	33.5
DQEQVELEGESSAPPR			890.91431	2	28.5	33.5
TAVSCLSQNDWK			704.82951	2	30.36	35.36
TAVSCLSQNDWK			708.83661	2	30.36	35.36
VVVDPVVTEQPSTSSAAK			907.48045	2	32.83	37.83
VVVDPVVTEQPSTSSAAK			911.48755	2	32.83	37.83
AQSYDIQAWK			605.29814	2	33.18	38.18
AQSYDIQAWK			609.30524	2	33.18	38.18
NATLHSEVQFPCSASSNNFA			1169.03664	2	35.06	40.06
NATLHSEVQFPCSASSNNFA			1174.04077	2	35.06	40.06
ASFLYSLPHR			595.818985	2	35.51	40.51
ASFLYSLPHR			600.82312	2	35.51	40.51
TASQLDEFQECLSK			828.3823	2	39.4	44.4
TASQLDEFQECLSK			832.3894	2	39.4	44.4
LLDPSTPVHILR			680.900465	2	40.53	45.53
LLDPSTPVHILR			685.9046	2	40.53	45.53
GGSYPHLLWDVR			700.35954	2	43.01	48.01
GGSYPHLLWDVR			705.36367	2	43.01	48.01
FNLILADTNSDR			689.851515	2	44.52	49.52
FNLILADTNSDR			694.85565	2	44.52	49.52
YGIINLQSLK			574.83671	2	46.54	51.54
YGIINLQSLK			578.84381	2	46.54	51.54
TLSHNLLVSEVYNQLK			620.007147	3	47.56	52.56
TLSHNLLVSEVYNQLK			622.678547	3	47.56	52.56
YLSWDTPQEVIAVK			824.93333	2	51.55	56.55
YLSWDTPQEVIAVK			828.94043	2	51.55	56.55
WSGIPQLLLK			577.84989	2	55.08	60.08
WSGIPQLLLK			581.85699	2	55.08	60.08
SIFLFLDR			505.786485	2	57.68	62.68
SIFLFLDR			510.79062	2	57.68	62.68
VHVHDLTVK			349.869702	3	13.25	18.25
VHVHDLTVK			352.541102	3	13.25	18.25
HGLGAGLGGPGAR			373.872106	3	17.05	22.05
HGLGAGLGGPGAR			377.208196	3	17.05	22.05
SVALYDCR			492.234295	2	22.62	27.62
SVALYDCR			497.23843	2	22.62	27.62
ILITGAADSK			494.78712	2	23.85	28.85
ILITGAADSK			498.79422	2	23.85	28.85
NSSISGPFGSR			554.772175	2	25.26	30.26
NSSISGPFGSR			559.77631	2	25.26	30.26
DSPPASEAPASEPGYVNYTK			1040.47862	2	32.11	37.11
DSPPASEAPASEPGYVNYTK			1044.48572	2	32.11	37.11
LPDNYTQDTWR			704.828015	2	32.65	37.65
LPDNYTQDTWR			709.83215	2	32.65	37.65
TVGVAFNQETGHWER			577.61302	3	31.72	36.72
TVGVAFNQETGHWER			580.94911	3	31.72	36.72

GTWLASGSDDLK			625.30619	2	34.52	39.52
GTWLASGSDDLK			629.31329	2	34.52	39.52
LINEGDVPHLPVNR			524.954606	3	36.75	41.75
LINEGDVPHLPVNR			528.290696	3	36.75	41.75
YDYILATASADSR			723.348705	2	38.28	43.28
YDYILATASADSR			728.35284	2	38.28	43.28
TQVELATGQLGLR			693.390645	2	40.27	45.27
TQVELATGQLGLR			698.39478	2	40.27	45.27
TLLATGGDNPNSLAIYR			888.468155	2	44.31	49.31
TLLATGGDNPNSLAIYR			893.47229	2	44.31	49.31
ALTLIAGSPLK			542.34208	2	43.7	48.7
ALTLIAGSPLK			546.34918	2	43.7	48.7
IMASLNLLR			515.80756	2	45.68	50.68
IMASLNLLR			520.8117	2	45.68	50.68
LAFLDPISGK			530.80516	2	48.1	53.1
LAFLDPISGK			534.81226	2	48.1	53.1
NWLLAMAAK			509.28074	2	48.18	53.18
NWLLAMAAK			513.28784	2	48.18	53.18
LLTLFNPDLANNYK			818.44059	2	54.98	59.98
LLTLFNPDLANNYK			822.44769	2	54.98	59.98
SNPELAALFESIQK			773.90867	2	57.5	62.5
SNPELAALFESIQK			777.91577	2	57.5	62.5

Supplemental Table 3.3

CRL4 QconCAT protein standard sequence:

MAGRSSYVGDEASSKEAVEAIQNSTSIKYNLEELYQAVENLCSYKAVQSSTSIRYNLEELYQAVEN
LCSHKQLLGEHLTAILQKETVEEQVSTTERQVCPLDNRETVEEQASTTERSIFLFLDRAHTDFFEAF
KTASQLDEFQECLSKLEELHVIDVKALTLIAGSPLKDGETSLVTGEADEGRADVFHAYLSLLKNAA
QVLVGIPLETGQKLYLEDDDPVQAEAYINRIHIPFISKEIEIDIEPTDKILGGSVLHLVLALRGLPVYN
KYLHQQWDKTFHLLHTVPALDQCRASFLYSLPHRVISHFLPNDLGFTDSYSQKYLAIAPPIIKYNPP
VDATPDTRVLLSLLSIKLTHYIEEANVGRSLEVGSYPILRLYNTESQSFRLVTAAGDQTAKEEQDFG
IEIVKDDSLPSNPIDFSYRSALLPTIPDTEDEISPDKYDYILATASADSRIHGGGINTLDIEPVEGRIWA
PTAEASTELTGLKILITGAADSKLNFTDEWSSIASSSRQSPSAGVHTFCDRSCGVPEESASSEKTLLA
STHVNHNIYITEVKFVTDLLLHFIKEWEFQKLAFLDPISGKLINEGDVPHLPVNRISLPFVVTDLRST
FLLAFSPDRWSGIPQLLLKETVSILLNPDRVVVDPVVTEQPSTSSAAKDSPPASEAPASEPGYVNYT
KSVALYDCRLQHGLEGHTGCVNTLHFNQRNSSISGPFGSRLLDPSTPVHILRYTSEDVVTLRTEPIN
TTYSYTDFQKNATLHSEVQFPCSASSNNFARLWSTNLDNSVASIEAKSLETICANHNNGRDGSMGL
WEVTDDVLTKVFASQWLNHRFNLILADTNSDRGGDIMLWNFGIKYGIINLQSLKAAAPEPETETET
SSKLAAALEHHHHHH

67 concatenated peptides, representing 32 proteins

Peptide ID	Peptide Sequence
DET	NATLHSEVQFPCSASSNNFAR
DCAF8	LQHGLEGHTGCVNTLHFNQR
DCAF11	VISHFLPNDLGFTDSYSQK
DCAF15	DSPPASEAPASEPGYVNYTK
CUL4B	YNLEELYQAVENLCSYK
AMBRA1	TLLASTHVNHNIYITEVK
CUL4A	YNLEELYQAVENLCSHK
COPS4	LYLEDDDPVQAEAYINR
CRBN	SALLPTIPDTEDEISPDK
PHIP	VVVDPVVTEQPSTSSAAK
DCAF16	TEPINTTYSYTDFQK
ERCC8	IHGGGINTLDIEPVEGR
DCAF13	DGSMGLWEVTDDVLTK
VPRBP	TFHLLHTVPALDQCR
RFWD2	LWSTNLDNSVASIEAK
DCAF6	LNFTDEWSSIASSSR
DCAF8	IWAPTAEASTELTGLK
COPS4	NAAQVLVGIPLETGQK
CRBN	DDSLPSNPIDFSYR
RFWD2	TASQLDEFQECLSK
BRWD3	LINEGDVPHLPVNR
none	AAAPEPETETETSSK
DCAF15	DGETSLVTGEADEGR
CUL4AB	QLLGEHLTAILQK
NEDD8	ILGGSVLHLVLALR
ERCC8	YDYILATASADSR
DCAF5	SLETICANHNNGR
none	LAAALEHHHHHH
CUL4A	ETVEEQVSTTER

WDTC1	QSPSAGVHTFCDR
DCAF10	LTHYIEEANVGR
CUL4B	EAVEAIQNSTSIK
CUL4B	ETVEEQASTTER
DCAF4	FNLILADTNSDR
CAND1	ADVFHAYLSLLK
DCAF16	LLDPSTPVHILR
DDB2	GGDIMLWNFGIK
PHIP	FVTDLLLHFIK
DCAF11	YNPPVDATPDTR
DCAF6	SCGVPEESASSEK
CRBN	EEQDFGIEIVK
NEDD8	EIEIDIEPTDK
DCAF15	ISLPFVVTDLR
DCAF12	VFASQWLNHR
TRPC4AP	ETVSILLNPDR
AMBRA1	STFLLAFSPDR
DTL	LYNTESQSFR
DCAF10	SLEVGSYPILR
COPS2	AHTDFFEAFK
DDB1	LEELHVIDVK
DDB2	ASFLYSLPHR
DET1	YTSEDVVTLR
TRPC4AP	WSGIPQLLLK
DCAF4	YGIINLQSLK
none	SSYVGDEASSK
DDA1	YLHQQWDK
PWP1	NSSISGPFGSR
DDB1	YLAIAPPIIK
CAND1	ALTLIAGSPLK
DTL	LVTAAGDQTAK
BRWD3	LAFLDPISGK
CUL4AB	SIFLFLDR
WDTC1	ILITGAADSK
VPRBP	VLLSLLSIK
COPS2	IHIPFISK
CUL4A	AVQSSTSIR
RBX1	QVCPLDNR
PWP1	SVALYDCR
RBX1	EWEFQK
DDA1	GLPVYNK

Supplemental Table 3.4

CRL4 QconCAT Mass Table – 122 targets, 61 peptides, 31 proteins							
Pepide ID	Compound	Formu	Adduct	m/z	z	t start (min)	t stop (min)
AMBRA1	STFLLAFSPDR			627.32987	2	50.88	58.88
AMBRA1	STFLLAFSPDR			632.33400	2	50.88	58.88
AMBRA1	TLLASTHVNHNIYITEVK			685.04073	3	32.65	40.65
AMBRA1	TLLASTHVNHNIYITEVK			687.71213	3	32.65	40.65
BRWD3	LINEGDVPHLPVNR			524.95460	3	35.12	43.12
BRWD3	LINEGDVPHLPVNR			528.29069	3	35.12	43.12
BRWD3	LAFLDPISGK			530.80549	2	46.48	54.48
BRWD3	LAFLDPISGK			534.81259	2	46.48	54.48
CAND1	ADVFHAYLSLLK			688.88227	2	57.06	65.06
CAND1	ADVFHAYLSLLK			692.88936	2	57.06	65.06
CAND1	ALTLIAGSPLK			542.34224	2	42.07	50.07
CAND1	ALTLIAGSPLK			546.34934	2	42.07	50.07
COPS2	AHTDFFEAFK			606.78783	2	38.08	46.08
COPS2	AHTDFFEAFK			610.79493	2	38.08	46.08
COPS2	IHIPFISK			477.79219	2	41.9	49.9
COPS2	IHIPFISK			481.79929	2	41.9	49.9
COPS4	NAAQVLVGIPLETGQK			819.46468	2	47.19	55.19
COPS4	NAAQVLVGIPLETGQK			823.47178	2	47.19	55.19
COPS4	LYLEDDDPVQAEAYINR			1012.484	2	47.36	55.36
COPS4	LYLEDDDPVQAEAYINR			1017.4881	2	47.36	55.36
CRBN	EEQDFGIEIVK			653.8299	2	41.66	49.66
CRBN	EEQDFGIEIVK			657.83699	2	41.66	49.66
CRBN	DDSLPSNPIDFSYR			813.37573	2	48	56
CRBN	DDSLPSNPIDFSYR			818.37986	2	48	56
CRBN	SALLPTIPDTEDEISPDK			970.98858	2	49.5	57.5
CRBN	SALLPTIPDTEDEISPDK			974.99568	2	49.5	57.5
CUL4A	ETVEEQVSTTER			704.33353	2	19.51	27.51
CUL4A	ETVEEQVSTTER			709.33766	2	19.51	27.51
CUL4B	EAVEAIQNSTSIK			695.36463	2	25.9	33.9
CUL4B	EAVEAIQNSTSIK			699.37173	2	25.9	33.9
CUL4AB	SIFLFLDR			505.78711	2	56.09	64.09
CUL4AB	SIFLFLDR			510.79124	2	56.09	64.09
CUL4AB	QLLGEHLTAILQK			488.62419	3	41.54	49.54
CUL4AB	QLLGEHLTAILQK			491.29559	3	41.54	49.54
CUL4B	ETVEEQASTTER			690.31788	2	13.34	21.34
CUL4B	ETVEEQASTTER			695.32201	2	13.34	21.34
VPRBP	VLLSLLSIK			493.33643	2	54.41	62.41
VPRBP	VLLSLLSIK			497.34353	2	54.41	62.41
VPRBP	TFHLLHTVPALDQCR			603.31391	3	35.64	43.64
VPRBP	TFHLLHTVPALDQCR			606.65000	3	35.64	43.64
DCAF10	SLEVGSYPILR			617.34552	2	43.15	51.15
DCAF10	SLEVGSYPILR			622.34965	2	43.15	51.15
DCAF10	LTHYIEEANVGR			701.35969	2	21.31	29.31
DCAF10	LTHYIEEANVGR			706.36382	2	21.31	29.31
DCAF11	YNPPVDATPDTR			673.32277	2	23.18	31.18
DCAF11	YNPPVDATPDTR			678.32690	2	23.18	31.18
DCAF11	VISHFLPNDLGFTDSYSQ			723.36013	3	47.15	55.15
DCAF11	VISHFLPNDLGFTDSYSQ			726.03153	3	47.15	55.15
DCAF12	VFASQWLNHR			419.88775	3	31.28	39.28
DCAF12	VFASQWLNHR			423.22384	3	31.28	39.28
DCAF13	DGSMGLWEVTDDVLTK			883.41928	2	60.23	68.23
DCAF13	DGSMGLWEVTDDVLTK			887.42638	2	60.23	68.23
DCAF15	DSPPASEAPASEPGYVNY			1040.4789	2	30.56	38.56
DCAF15	DSPPASEAPASEPGYVNY			1044.4860	2	30.56	38.56

DCAF15	ISLPFVVTDLR			630.37153	2	58.27	66.27
DCAF15	ISLPFVVTDLR			635.37567	2	58.27	66.27
DCAF16	LLDPSTPVHILR			680.90099	2	38.9	46.9
DCAF16	LLDPSTPVHILR			685.90512	2	38.9	46.9
DCAF16	TEPINTTYSYTDFQK			904.42288	2	36.55	44.55
DCAF16	TEPINTTYSYTDFQK			908.42998	2	36.55	44.55
DCAF4	FNLILADTNSDR			689.85169	2	43.02	51.02
DCAF4	FNLILADTNSDR			694.85583	2	43.02	51.02
DCAF4	YGIINLQSLK			574.83733	2	44.96	52.96
DCAF4	YGIINLQSLK			578.84443	2	44.96	52.96
DCAF15	DGETSLVTGEADEGR			768.34463	2	27.34	35.34
DCAF15	DGETSLVTGEADEGR			773.34876	2	27.34	35.34
DCAF5	SLETICANHNNGR			495.90028	3	12.95	20.95
DCAF5	SLETICANHNNGR			499.23637	3	12.95	20.95
DCAF6	LNFTDEWSSIASSSR			850.39974	2	49.91	57.91
DCAF6	LNFTDEWSSIASSSR			855.40387	2	49.91	57.91
DCAF8	LQHGLEGHTGCVNTLHF			773.37842	3	22.07	30.07
DCAF8	LQHGLEGHTGCVNTLHF			776.71450	3	22.07	30.07
DCAF8	IWAPTAEASTELTGLK			844.44870	2	46.98	54.98
DCAF8	IWAPTAEASTELTGLK			848.45580	2	46.98	54.98
DDA1	GLPVYNK			395.72652	2	18.58	26.58
DDA1	GLPVYNK			399.73362	2	18.58	26.58
DDA1	YLHQQWDK			373.18569	3	13.22	21.22
DDA1	YLHQQWDK			375.85709	3	13.22	21.22
DDB1	LEELHVIDVK			398.89580	3	32.87	40.87
DDB1	LEELHVIDVK			401.56720	3	32.87	40.87
DDB1	YLAIAPPIIK			549.84971	2	47.05	55.05
DDB1	YLAIAPPIIK			553.85680	2	47.05	55.05
DDB2	GGDIMLWNFGIK			675.84737	2	58.18	66.18
DDB2	GGDIMLWNFGIK			679.85447	2	58.18	66.18
DDB2	ASFLYSLPHR			397.54874	3	33.84	41.84
DDB2	ASFLYSLPHR			400.88483	3	33.84	41.84
DET1	YTSEDVVTLR			591.80368	2	29.28	37.28
DET1	YTSEDVVTLR			596.80781	2	29.28	37.28
DET	NATLHSEVQFPCSASSNN			1169.0374	2	33.48	41.48
DET	NATLHSEVQFPCSASSNN			1174.0416	2	33.48	41.48
DTL	LYNTESQSFR			622.79893	2	20.86	28.86
DTL	LYNTESQSFR			627.80306	2	20.86	28.86
ERCC8	IHGGGINTLDIEPVEGR			888.96558	2	35.23	43.23
ERCC8	IHGGGINTLDIEPVEGR			893.96971	2	35.23	43.23
ERCC8	YDYILATASADSR			723.34898	2	43.42	51.42
ERCC8	YDYILATASADSR			728.35312	2	43.42	51.42
NEDD8	EIEIDIEPTDK			651.32719	2	37.88	45.88
NEDD8	EIEIDIEPTDK			655.33428	2	37.88	45.88
NEDD8	ILGGSVLHLVLALR			487.64856	3	60.14	68.14
NEDD8	ILGGSVLHLVLALR			490.98465	3	60.14	68.14
PHIP	FVTDLLLHFIK			449.26746	3	63.23	71.23
PHIP	FVTDLLLHFIK			451.93886	3	63.23	71.23
PHIP	VVVDPVVTEQPSTSSAA			907.48073	2	31.27	39.27
PHIP	VVVDPVVTEQPSTSSAA			911.48783	2	31.27	39.27
PWP1	SVALYDCR			492.23438	2	20.97	28.97
PWP1	SVALYDCR			497.23851	2	20.97	28.97
PWP1	NSSISGPFGSR			554.77271	2	23.56	31.56
PWP1	NSSISGPFGSR			559.77685	2	23.56	31.56
RBX1	QVCPLDNR			501.24528	2	15.13	23.13
RBX1	QVCPLDNR			506.24941	2	15.13	23.13
RFWD2	TASQLDEFQECLSK			828.38270	2	37.88	45.88
RFWD2	TASQLDEFQECLSK			832.38980	2	37.88	45.88

RFWD2	LWSTNLDNSVASIEAK			874.44669	2	45.75	53.75
RFWD2	LWSTNLDNSVASIEAK			878.45379	2	45.75	53.75
TRPC4AP	WSGIPQLLLK			577.85024	2	53.46	61.46
TRPC4AP	WSGIPQLLLK			581.85734	2	53.46	61.46

BIBLIOGRAPHY

Ahn, J., Novince, Z., Concel, J., Byeon, C.H., Makhov, A.M., Byeon, I.J.L., Zhang, P., and Gronenborn, A.M. (2011). The cullin-RING E3 ubiquitin ligase CRL4-DCAF1 complex dimerizes via a short helical region in DCAF1. Biochemistry.

Alexandru, G., Graumann, J., Smith, G.T., Kolawa, N.J., Fang, R., and Deshaies, R.J. (2008). UBXD7 Binds Multiple Ubiquitin Ligases and Implicates p97 in HIF1 a Turnover. 804–816.

Ambroggio, X.I., Rees, D.C., and Deshaies, R.J. (2004). JAMM: A metalloprotease-like zinc site in the proteasome and signalosome. PLoS Biol.

An, S., and Fu, L. (2018). Small-molecule PROTACs: An emerging and promising approach for the development of targeted therapy drugs. EBioMedicine.

Angers, S., Li, T., Yi, X., MacCoss, M.J., Moon, R.T., and Zheng, N. (2006). Molecular architecture and assembly of the DDB1-CUL4A ubiquitin ligase machinery. Nature.

Aufderheide, A., Unverdorben, P., Baumeister, W., and F??rster, F. (2015). Structural disorder and its role in proteasomal degradation. FEBS Lett. *589*, 2552–2560.

Bakalarski, C.E., Elias, J.E., Villen, J., Haas, W., Gerber, S.A., Everley, P.A., and Gygi, S.P. (2008). The impact of peptide abundance and dynamic range on stable-lsotope-based quantitative proteomic analyses. J. Proteome Res.

Bennett, E.J., Rush, J., Gygi, S.P., and Harper, J.W. (2010). Dynamics of cullin-RING ubiquitin ligase network revealed by systematic quantitative proteomics. Cell.

Berger, I., Fitzgerald, D.J., and Richmond, T.J. (2004). Baculovirus expression system for heterologous multiprotein complexes. Nat. Biotechnol.

Besten, W. Den, Verma, R., Kleiger, G., Oania, R.S., and Deshaies, R.J. (2012). NEDD8 links cullin-RING ubiquitin ligase function to the p97 pathway. Nat. Struct. Mol. Biol.

Birol, M., Enchev, R.I., Padilla, A., Stengel, F., Aebersold, R., Betzi, S., Yang, Y., Hoh, F., Peter, M., Dumas, C., et al. (2014). Structural and biochemical characterization of the Cop9 signalosome CSN5/CSN6 heterodimer. PLoS One.

Boh, B.K., Smith, P.G., and Hagen, T. (2011). Neddylation-induced conformational control regulates cullin RING ligase activity in vivo. J. Mol. Biol.

Bondeson, D.P., Mares, A., Smith, I.E.D., Ko, E., Campos, S., Miah, A.H., Mulholland, K.E., Routly, N., Buckley, D.L., Gustafson, J.L., et al. (2015). Catalytic in vivo protein knockdown by small-molecule PROTACs. Nat. Chem. Biol.

Bosu, D.R., Feng, H., Min, K., Kim, Y., Wallenfang, M.R., and Kipreos, E.T. (2010). C. elegans CAND-1 regulates cullin neddylation, cell proliferation and morphogenesis in specific tissues. Dev. Biol.

Briggs, G.E., and Haldane, J.B.S. (1925). A Note on the Kinetics of Enzyme Action. Biochem. J. *19*, 338–339.

Brownell, J.E., Sintchak, M.D., Gavin, J.M., Liao, H., Bruzzese, F.J., Bump, N.J., Soucy, T.A., Milhollen, M.A., Yang, X., Burkhardt, A.L., et al. (2010). Substrate-Assisted Inhibition of Ubiquitin-like Protein-

Activating Enzymes: The NEDD8 E1 Inhibitor MLN4924 Forms a NEDD8-AMP Mimetic In Situ. Mol. Cell.

Bulatov, E., and Ciulli, A. (2015). Targeting Cullin–RING E3 ubiquitin ligases for drug discovery: structure, assembly and small-molecule modulation. Biochem. J.

Cavadini, S., Fischer, E.S., Bunker, R.D., Potenza, A., Lingaraju, G.M., Goldie, K.N., Mohamed, W.I., Faty, M., Petzold, G., Beckwith, R.E.J., et al. (2016). Cullin-RING ubiquitin E3 ligase regulation by the COP9 signalosome. Nature *531*, 598–603.

Chen, C.-Y., Tsai, M.-S., Lin, C.-Y., Yu, I.-S., Chen, Y.-T., Lin, S.-R., Juan, L.-W., Chen, Y.-T., Hsu, H.-M., Lee, L.-J., et al. (2012). Rescue of the genetically engineered Cul4b mutant mouse as a potential model for human X-linked mental retardation. Hum. Mol. Genet. *21*, 4270–4285.

Choi, H., Larsen, B., Lin, Z.Y., Breitkreutz, A., Mellacheruvu, D., Fermin, D., Qin, Z.S., Tyers, M., Gingras, A.C., and Nesvizhskii, A.I. (2011). SAINT: Probabilistic scoring of affinity purificationg-mass spectrometry data. Nat. Methods.

Chu, G., and Chang, E. (1988). Xeroderma pigmentosum group E cells lack a nuclear factor that binds to damaged DNA. Science (80-.).

Chuang, H.W., Zhang, W., and Gray, W.M. (2004). Arabidopsis ETA2, an apparent ortholog of the human cullin-interacting protein CAND1, is required for auxin responses mediated by the SCF TIR1 ubiquitin ligase. Plant Cell.

Cope, G.A., and Deshaies, R.J. (2003). COP9 signalosome: A multifunctional regulator of SCF and other cullin-based ubiquitin ligases. Cell.

Cope, G.A., and Deshaies, R.J. (2006). Targeted silencing of Jab1 / Csn5 in human cells downregulates SCF activity through reduction of F-box protein levels. *10*, 1–10.

Cope, G.A., Suh, G.S.B., Aravind, L., Schwarz, S.E., Zipursky, S.L., Koonin, E. V, and Deshaies, R.J. (2002). Role of Predicted Metalloprotease Motif of Jab1 / Csn5 in Cleavage of Nedd8 from Cul1. *298*, 608–611.

Cox, J., and Mann, M. (2008). MaxQuant enables high peptide identification rates, individualized p.p.b.-range mass accuracies and proteome-wide protein quantification. Nat. Biotechnol.

Cox, J., Neuhauser, N., Michalski, A., Scheltema, R.A., Olsen, J. V., and Mann, M. (2011). Andromeda: A peptide search engine integrated into the MaxQuant environment. J. Proteome Res.

Das, I., Krzyzosiak, A., Schneider, K., Wrabetz, L., D'Antonio, M., Barry, N., Sigurdardottir, A., and Bertolotti, A. (2015). Preventing proteostasis diseases by selective inhibition of a phosphatase regulatory subunit. Science (80-.).

Deshaies, R.J. (1995). The self-destructive personality of a cell cycle in transition. Curr. Opin. Cell Biol.

Deshaies, R.J. (2015). prime time for PROTACS. ACS Chem. Biol. *10*, 1831–1837.

Deshaies, R.J., and Joazeiro, C. a P. (2009a). RING domain E3 ubiquitin ligases. Annu. Rev. Biochem. *78*, 399–434.

Deshaies, R.J., and Joazeiro, C.A.P. (2009b). RING Domain E3 Ubiquitin Ligases. Annu. Rev. Biochem.

Dimova, N. V., Hathaway, N.A., Lee, B.H., Kirkpatrick, D.S., Berkowitz, M.L., Gygi, S.P., Finley, D., and King, R.W. (2012). APC/C-mediated multiple monoubiquitylation provides an alternative degradation signal for cyclin B1. Nat. Cell Biol.

Dougherty, W.G., Cary, S.M., and Dawn Parks, T. (1989). Molecular genetic analysis of a plant virus polyprotein cleavage site: A model. Virology.

Duda, D.M., Borg, L.A., Scott, D.C., Hunt, H.W., Hammel, M., and Schulman, B.A. (2008). Structural Insights into NEDD8 Activation of Cullin-RING Ligases: Conformational Control of Conjugation. Cell.

Duda, D.M., Olszewski, J.L., Tron, A.E., Hammel, M., Lambert, L.J., Waddell, M.B., Mittag, T., DeCaprio, J.A., and Schulman, B.A. (2012). Structure of a Glomulin-RBX1-CUL1 Complex: Inhibition of a RING E3 Ligase through Masking of Its E2-Binding Surface. Mol. Cell.

Echalier, A., Pan, Y., Birol, M., Tavernier, N., Pintard, L., Hoh, F., Ebel, C., Galophe, N., Claret, F.X., and Dumas, C. (2013). Insights into the regulation of the human COP9 signalosome catalytic subunit, CSN5/Jab1. Proc. Natl. Acad. Sci. U. S. A.

Emberley, E.D., Mosadeghi, R., and Deshaies, R.J. (2012). Deconjugation of Nedd8 from Cul1 is directly regulated by Skp1-F-box and substrate, and the COP9 signalosome inhibits deneddylated SCF by a noncatalytic mechanism. J. Biol. Chem.

Enchev, R.I., Schreiber, A., Beuron, F., and Morris, E.P. (2010). Structural Insights into the COP9 Signalosome and Its Common Architecture with the 26S Proteasome Lid and eIF3. Structure.

Enchev, R.I., Scott, D.C., da Fonseca, P.C.A., Schreiber, A., Monda, J.K., Schulman, B.A., Peter, M., and Morris, E.P. (2012). Structural Basis for a Reciprocal Regulation between SCF and CSN. Cell Rep.

Enchev, R.I., Schulman, B.A., and Peter, M. (2015). Protein neddylation: Beyond cullin-RING ligases. Nat. Rev. Mol. Cell Biol.

Eng, J.K., Jahan, T.A., and Hoopmann, M.R. (2013). Comet: an open-source MS/MS sequence database search tool. Proteomics.

Feldman, R.M.R., Correll, C.C., Kaplan, K.B., and Deshaies, R.J. (1997). A complex of Cdc4p, Skp1p, and Cdc53p/cullin catalyzes ubiquitination of the phosphorylated CDK inhibitor Sic1p. Cell.

Feng, S., Shen, Y., Sullivan, J.A., Rubio, V., Xiong, Y., Sun, T.P., and Deng, X.W. (2004). Arabidopsis CAND1, an unmodified CUL1-interacting protein, is involved in multiple developmental pathways controlled by ubiquitin/proteasome-mediated protein. Plant Cell.

Fischer, E.S., Scrima, A., Böhm, K., Matsumoto, S., Lingaraju, G.M., Faty, M., Yasuda, T., Cavadini, S., Wakasugi, M., Hanaoka, F., et al. (2011a). The molecular basis of CRL4 DDB2/CSA ubiquitin ligase architecture, targeting, and activation. Cell.

Fischer, E.S., Scrima, A., B??hm, K., Matsumoto, S., Lingaraju, G.M., Faty, M., Yasuda, T., Cavadini, S., Wakasugi, M., Hanaoka, F., et al. (2011b). The molecular basis of CRL4 DDB2/CSA ubiquitin ligase architecture, targeting, and activation. Cell *147*, 1024–1039.

Förster, F., Unverdorben, P., Śledź, P., and Baumeister, W. (2013). Unveiling the long-held secrets of the 26S proteasome. Structure *21*, 1551–1562.

Gandhi, A.K., Kang, J., Havens, C.G., Conklin, T., Ning, Y., Wu, L., Ito, T., Ando, H., Waldman, M.F., Thakurta, A., et al. (2014). Immunomodulatory agents lenalidomide and pomalidomide co-stimulate T cells

by inducing degradation of T cell repressors Ikaros and Aiolos via modulation of the E3 ubiquitin ligase complex CRL4 CRBN. Br. J. Haematol.

Garbett, D., and Bretscher, A. (2014). The surprising dynamics of scaffolding proteins. Mol. Biol. Cell.

Goldberg, A.L. (2007). Functions of the proteasome: From protein degradation and immune surveillance to cancer therapy. In Biochemical Society Transactions, p.

Goldenberg, S.J., Cascio, T.C., Shumway, S.D., Garbutt, K.C., Liu, J., Xiong, Y., and Zheng, N. (2004). Structure of the Cand1-Cul1-Roc1 complex reveals regulatory mechanisms for the assembly of the multisubunit cullin-dependent ubiquitin ligases. Cell.

Han, T., Goralski, M., Gaskill, N., Capota, E., Kim, J., Ting, T.C., Xie, Y., Williams, N.S., and Nijhawan, D. (2017). Anticancer sulfonamides target splicing by inducing RBM39 degradation via recruitment to DCAF15. Science (80-.).

Hannah, J., and Zhou, P. (2015). Distinct and overlapping functions of the cullin E3 ligase scaffolding proteins CUL4A and CUL4B. Gene *573*, 33–45.

He, Y.J., McCall, C.M., Hu, J., Zeng, Y., and Xiong, Y. (2006a). DDB1 functions as a linker to recruit receptor WD40 proteins to CUL4-ROC1 ubiquitin ligases. Genes Dev.

He, Y.J., McCall, C.M., Hu, J., Zeng, Y., and Xiong, Y. (2006b). DDB1 functions as a linker to recruit receptor WD40 proteins to CUL4-ROC1 ubiquitin ligases. Genes Dev. *20*, 2949–2954.

Hershko, A., and Ciechanover, A. (1998). The Ubiquitin System. Annu. Rev. Biochem. *67*, 425–479.

Hershko, A., and Ciechanover, A. (2003). The Ubiquitin System for Protein Degradation. Annu. Rev. Biochem.

Higa, L.A., Wu, M., Ye, T., Kobayashi, R., Sun, H., and Zhang, H. (2006). CUL4-DDB1 ubiquitin ligase interacts with multiple WD40-repeat proteins and regulates histone methylation. Nat. Cell Biol. *8*, 1277–1283.

Hyer, M.L., Milhollen, M.A., Ciavarri, J., Fleming, P., Traore, T., Sappal, D., Huck, J., Shi, J., Gavin, J., Brownell, J., et al. (2018). A small-molecule inhibitor of the ubiquitin activating enzyme for cancer treatment. Nat. Med.

Ito, T., Ando, H., Suzuki, T., Ogura, T., Hotta, K., Imamura, Y., Yamaguchi, Y., and Handa, H. (2010). Identification of a primary target of thalidomide teratogenicity. Science *327*, 1345–1350.

Jackson, S., and Xiong, Y. (2009). CRL4s: the CUL4-RING E3 ubiquitin ligases. Trends Biochem. Sci. *34*, 562–570.

Jiang, T., Tang, H., Wu, Z., Chen, J., Lu, S., Zhou, C., Yan, D., and Peng, Z. (2013). Cullin 4B is a novel prognostic marker that correlates with colon cancer progression and pathogenesis. Med. Oncol. *30*, 534.

Jin, J., Cardozo, T., Lovering, R.C., Elledge, S.J., Pagano, M., and Harper, J.W. (2004). Systematic analysis and nomenclature of mammalian F-box proteins. Genes Dev.

Jin, J., Arias, E.E., Chen, J., Harper, J.W., and Walter, J.C. (2006). A Family of Diverse Cul4-Ddb1-Interacting Proteins Includes Cdt2, which Is Required for S Phase Destruction of the Replication Factor Cdt1. Mol. Cell.

Kaur, M., Khan, M.M., Kar, A., Sharma, A., and Saxena, S. (2012). CRL4-DDB1-VPRBP ubiquitin ligase mediates the stress triggered proteolysis of Mcm10. Nucleic Acids Res.

Kelley, L.A., Mezulis, S., Yates, C.M., Wass, M.N., and Sternberg, M.J.E. (2015). The Phyre2 web portal for protein modeling, prediction and analysis. Nat. Protoc.

King, R.W., Deshaies, R.J., Peters, J.M., and Kirschner, M.W. (1996). How proteolysis drives the cell cycle. Science (80-.).

Komander, D., and Rape, M. (2012). The Ubiquitin Code. Annu. Rev. Biochem.

Kortüm, K.M., Zhu, Y.X., Shi, C.X., Jedlowski, P., and Stewart, A.K. (2015). Cereblon binding molecules in multiple myeloma. Blood Rev.

Krönke, J., Udeshi, N.D., Narla, A., Grauman, P., Hurst, S.N., McConkey, M., Svinkina, T., Heckl, D., Comer, E., Li, X., et al. (2014). Lenalidomide causes selective degradation of IKZF1 and IKZF3 in multiple myeloma cells. Science *343*, 301–305.

Krzyzosiak, A., Sigurdardottir, A., Luh, L., Carrara, M., Das, I., Schneider, K., and Bertolotti, A. (2018). Target-Based Discovery of an Inhibitor of the Regulatory Phosphatase PPP1R15B. Cell.

Kurz, T., Özlü, N., Rudolf, F., O'Rourke, S.M., Luke, B., Hofmann, K., Hyman, A.A., Bowerman, B., and Peter, M. (2005). The conserved protein DCN-1/Dcn1p is required for cullin neddylation in C. elegans and S. cerevisiae. Nature.

Kusebauch, U., Campbell, D.S., Deutsch, E.W., Chu, C.S., Spicer, D.A., Brusniak, M.Y., Slagel, J., Sun, Z., Stevens, J., Grimes, B., et al. (2016). Human SRMAtlas: A Resource of Targeted Assays to Quantify the Complete Human Proteome. Cell.

Lee, J., and Zhou, P. (2007). DCAFs, the Missing Link of the CUL4-DDB1 Ubiquitin Ligase. Mol. Cell *26*, 775–780.

Leitner, A., Walzthoeni, T., and Aebersold, R. (2014). Lysine-specific chemical cross-linking of protein complexes and identification of cross-linking sites using LC-MS/MS and the xQuest/xProphet software pipeline. Nat. Protoc.

Li, T., Robert, E.I., van Breugel, P.C., Strubin, M., and Zheng, N. (2010). A promiscuous α-helical motif anchors viral hijackers and substrate receptors to the CUL4–DDB1 ubiquitin ligase machinery. Nat. Struct. Mol. Biol.

Liakopoulos, D., Doenges, G., Matuschewski, K., and Jentsch, S. (1998). A novel protein modification pathway related to the ubiquitin system. EMBO J.

Lin, Y.C., Boone, M., Meuris, L., Lemmens, I., Van Roy, N., Soete, A., Reumers, J., Moisse, M., Plaisance, S., Drmanac, R., et al. (2014). Genome dynamics of the human embryonic kidney 293 lineage in response to cell biology manipulations. Nat. Commun.

Lingaraju, G.M., Bunker, R.D., Cavadini, S., Hess, D., Hassiepen, U., Renatus, M., Fischer, E.S., and Thomä, N.H. (2014). Crystal structure of the human COP9 signalosome. Nature.

Linghu, B., Callis, J., and Goebl, M.G. (2002). Rub1p processing by Yuh1p is required for wild-type levels of Rub1p conjugation to Cdc53p. Eukaryot. Cell.

Liu, J., Furukawa, M., Matsumoto, T., and Xiong, Y. (2002). NEDD8 modification of CUL1 dissociates p120CAND1, an inhibitor of CUL1-SKP1 binding and SCF ligases. Mol. Cell.

Liu, J., Song, T., Zhou, W., Xing, L., Wang, S., Ho, M., Peng, Z., Tai, Y.T., Hideshima, T., Anderson, K.C., et al. (2019a). A genome-scale CRISPR-Cas9 screening in myeloma cells identifies regulators of immunomodulatory drug sensitivity. Leukemia.

Liu, L., Lee, S., Zhang, J., Peters, S.B., Hannah, J., Zhang, Y., Yin, Y., Koff, A., Ma, L., and Zhou, P. (2009). CUL4A Abrogation Augments DNA Damage Response and Protection against Skin Carcinogenesis. Mol. Cell.

Liu, X., Reitsma, J.M., Mamrosh, J.L., Zhang, Y., Straube, R., and Deshaies, R.J. (2018). Cand1-Mediated Adaptive Exchange Mechanism Enables Variation in F-Box Protein Expression. Mol. Cell.

Liu, Y., Mi, Y., Mueller, T., Kreibich, S., Williams, E.G., Van Drogen, A., Borel, C., Frank, M., Germain, P.L., Bludau, I., et al. (2019b). Multi-omic measurements of heterogeneity in HeLa cells across laboratories. Nat. Biotechnol.

Lo, S.-C., and Hannink, M. (2006). CAND1-Mediated Substrate Adaptor Recycling Is Required for Efficient Repression of Nrf2 by Keap1. Mol. Cell. Biol.

Lu, G., Middleton, R.E., Sun, H., Naniong, M., Ott, C.J., Mitsiades, C.S., Wong, K.-K., Bradner, J.E., and Kaelin, W.G. (2014). The myeloma drug lenalidomide promotes the cereblon-dependent destruction of Ikaros proteins. Science *343*, 305–309.

Lu, J., Qian, Y., Altieri, M., Dong, H., Wang, J., Raina, K., Hines, J., Winkler, J.D., Crew, A.P., Coleman, K., et al. (2015a). Hijacking the E3 Ubiquitin Ligase Cereblon to Efficiently Target BRD4. Chem. Biol.

Lu, Y., Wang, W., and Kirschner, M.W. (2015b). Specificity of the anaphase-promoting complex: A single-molecule study. Science (80-.).

Lyapina, S., Cope, G., Shevchenko, A., Serino, G., Tsuge, T., Zhou, C., Wolf, D.A., Wei, N., Shevchenko, A., and Deshaies, R.J. (2001). Promotion of NEDD8-CUL1 conjugate cleavage by COP9 signalosome. Science (80-.).

Lydeard, J.R., Schulman, B.A., and Harper, J.W. (2013). Building and remodelling Cullin-RING E3 ubiquitin ligases. EMBO Rep.

MacLean, B., Tomazela, D.M., Shulman, N., Chambers, M., Finney, G.L., Frewen, B., Kern, R., Tabb, D.L., Liebler, D.C., and MacCoss, M.J. (2010). Skyline: An open source document editor for creating and analyzing targeted proteomics experiments. Bioinformatics.

Matyskiela, M.E., and Martin, A. (2013). Design principles of a universal protein degradation machine. J. Mol. Biol. *425*, 199–213.

Mayor-Ruiz, C., Jaeger, M.G., Bauer, S., Brand, M., Sin, C., Hanzl, A., Mueller, A.C., Menche, J., and Winter, G.E. (2019). Plasticity of the Cullin-RING Ligase Repertoire Shapes Sensitivity to Ligand-Induced Protein Degradation. Mol. Cell.

Meyer, H.J., and Rape, M. (2014). Enhanced protein degradation by branched ubiquitin chains. Cell.

Mindell, J.A., and Grigorieff, N. (2003). Accurate determination of local defocus and specimen tilt in electron microscopy. J. Struct. Biol.

Mosadeghi, R., Reichermeier, K.M., Winkler, M., Schreiber, A., Reitsma, J.M., Zhang, Y., Stengel, F., Cao, J., Kim, M., Sweredoski, M.J., et al. (2016). Structural and kinetic analysis of the COP9-Signalosome activation and the cullin-RING ubiquitin ligase deneddylation cycle. Elife *5*.

Nabet, B., Roberts, J.M., Buckley, D.L., Paulk, J., Dastjerdi, S., Yang, A., Leggett, A.L., Erb, M.A., Lawlor, M.A., Souza, A., et al. (2018). The dTAG system for immediate and target-specific protein degradation. Nat. Chem. Biol.

Neklesa, T.K., Winkler, J.D., and Crews, C.M. (2017). Targeted protein degradation by PROTACs. Pharmacol. Ther.

Nguyen, T. Van, Li, J., Lu, C.-C. (Jean), Mamrosh, J.L., Lu, G., Cathers, B.E., and Deshaies, R.J. (2017). p97/VCP promotes degradation of CRBN substrate glutamine synthetase and neosubstrates. Proc. Natl. Acad. Sci.

Olma, M.H., Roy, M., Le Bihan, T., Sumara, I., Maerki, S., Larsen, B., Quadroni, M., Peter, M., Tyers, M., and Pintard, L. (2009). An interaction network of the mammalian COP9 signalosome identifies Dda1 as a core subunit of multiple Cul4-based E3 ligases. J. Cell Sci.

Orthwein, A., Noordermeer, S.M., Wilson, M.D., Landry, S., Enchev, R.I., Sherker, A., Munro, M., Pinder, J., Salsman, J., Dellaire, G., et al. (2015). A mechanism for the suppression of homologous recombination in G1 cells. Nature.

Ottis, P., Toure, M., Cromm, P.M., Ko, E., Gustafson, J.L., and Crews, C.M. (2017). Assessing Different E3 Ligases for Small Molecule Induced Protein Ubiquitination and Degradation. ACS Chem. Biol.

Paiva, S.L., and Crews, C.M. (2019). Targeted protein degradation: elements of PROTAC design. Curr. Opin. Chem. Biol.

Pappin, D.J.C., Creasy, D.M., Perkins, D.N., and S., C.J. (1999). Probability-based protein identification by searching sequence databases using mass spectrometry data. Electrophoresis.

Patil, A., Manzano, M., and Gottwein, E. (2019). Genome-wide CRISPR Screens Reveal Genetic Mediators of Cereblon Modulator Toxicity in Primary Effusion Lymphoma. BioRxiv.

Patton, E.E., Willems, A.R., Sa, D., Kuras, L., Thomas, D., Craig, K.L., and Tyers, M. (1998). Cdc53 is a scaffold protein for multiple Cdc34/Skp1/F-box protein complexes that regulate cell division and methionine biosynthesis in yeast. Genes Dev.

Peterson, A.C., Russell, J.D., Bailey, D.J., Westphall, M.S., and Coon, J.J. (2012). Parallel Reaction Monitoring for High Resolution and High Mass Accuracy Quantitative, Targeted Proteomics. Mol. Cell. Proteomics.

Pettersen, E.F., Goddard, T.D., Huang, C.C., Couch, G.S., Greenblatt, D.M., Meng, E.C., and Ferrin, T.E. (2004). UCSF Chimera - A visualization system for exploratory research and analysis. J. Comput. Chem.

Pfaffl, M.W. (2001). A new mathematical model for relative quantification in real-time RT-PCR. Nucleic Acids Res.

Pickart, C.M. (2004). Back to the Future with Ubiquitin Review. *116*, 181–190.

Picotti, P., and Aebersold, R. (2012). Selected reaction monitoring–based proteomics: workflows, potential, pitfalls and future directions. Nat. Methods *9*, 555–566.

Picotti, P., Rinner, O., Stallmach, R., Dautel, F., Farrah, T., Domon, B., Wenschuh, H., and Aebersold, R. (2010). High-throughput generation of selected reaction-monitoring assays for proteins and proteomes. Nat. Methods.

Pierce, N.W., Kleiger, G., Shan, S.O., and Deshaies, R.J. (2009). Detection of sequential polyubiquitylation on a millisecond timescale. Nature.

Pierce, N.W., Lee, J.E., Liu, X., Sweredoski, M.J., Graham, R.L.J., Larimore, E. a., Rome, M., Zheng, N., Clurman, B.E., Hess, S., et al. (2013). Cand1 promotes assembly of new SCF complexes through dynamic exchange of F box proteins. Cell *153*, 206–215.

Politis, A., Stengel, F., Hall, Z., Hernández, H., Leitner, A., Walzthoeni, T., Robinson, C. V., and Aebersold, R. (2014). A mass spectrometry-based hybrid method for structural modeling of protein complexes. Nat. Methods.

Pontén, F., Jirström, K., and Uhlen, M. (2008). The Human Protein Atlas - A tool for pathology. J. Pathol.

Del Pozo, J.C., and Estelle, M. (1999). The Arabidopsis cullin AtCUL1 is modified by the ubiquitin-related protein RUB1. Proc. Natl. Acad. Sci. U. S. A.

Pratt, J.M., Simpson, D.M., Doherty, M.K., Rivers, J., Gaskell, S.J., and Beynon, R.J. (2006). Multiplexed absolute quantification for proteomics using concatenated signature peptides encoded by QconCAT genes. Nat. Protoc.

Ravid, T., and Hochstrasser, M. (2008). Diversity of degradation signals in the ubiquitin-proteasome system. Nat. Rev. Mol. Cell Biol. *9*, 679–690.

Reitsma, J.M., Liu, X., Reichermeier, K.M., Moradian, A., Sweredoski, M.J., Hess, S., and Deshaies, R.J. (2017). Composition and Regulation of the Cellular Repertoire of SCF Ubiquitin Ligases. Cell.

Ritchie, M.E., Phipson, B., Wu, D., Hu, Y., Law, C.W., Shi, W., and Smyth, G.K. (2015). Limma powers differential expression analyses for RNA-sequencing and microarray studies. Nucleic Acids Res.

Rock, K.L., Gramm, C., Rothstein, L., Clark, K., Stein, R., Dick, L., Hwang, D., and Goldberg, A.L. (1994). Inhibitors of the proteasome block the degradation of most cell proteins and the generation of peptides presented on MHC class I molecules. Cell.

Rosenthal, P.B., and Henderson, R. (2003). Optimal determination of particle orientation, absolute hand, and contrast loss in single-particle electron cryomicroscopy. J. Mol. Biol.

Roy, M.J., Winkler, S., Hughes, S.J., Whitworth, C., Galant, M., Farnaby, W., Rumpel, K., and Ciulli, A. (2019). SPR-Measured Dissociation Kinetics of PROTAC Ternary Complexes Influence Target Degradation Rate. ACS Chem. Biol.

Saha, A., and Deshaies, R.J. (2008). Multimodal Activation of the Ubiquitin Ligase SCF by Nedd8 Conjugation. Mol. Cell *32*, 21–31.

Sakamoto, K.M., Kim, K.B., Kumagai, a, Mercurio, F., Crews, C.M., and Deshaies, R.J. (2001). Protacs: chimeric molecules that target proteins to the Skp1-Cullin-F box complex for ubiquitination and degradation. Proc. Natl. Acad. Sci. U. S. A. *98*, 8554–8559.

Sakamoto, K.M., Kim, K.B., Verma, R., Ransick, A., Stein, B., Crews, C.M., and Deshaies, R.J. (2003). Development of Protacs to target cancer-promoting proteins for ubiquitination and degradation. Mol. Cell. Proteomics *2*, 1350–1358.

Sarikas, A., Hartmann, T., and Pan, Z.Q. (2011). The cullin protein family. Genome Biol.

Sato, Y., Yoshikawa, A., Yamagata, A., Mimura, H., Yamashita, M., Ookata, K., Nureki, O., Iwai, K., Komada, M., and Fukai, S. (2008). Structural basis for specific cleavage of Lys 63-linked polyubiquitin chains. Nature.

Scheres, S.H.W. (2012). RELION: Implementation of a Bayesian approach to cryo-EM structure determination. J. Struct. Biol.

Scheres, S.H.W., and Chen, S. (2012). Prevention of overfitting in cryo-EM structure determination. Nat. Methods.

Schlierf, A., Altmann, E., Quancard, J., Jefferson, A.B., Assenberg, R., Renatus, M., Jones, M., Hassiepen, U., Schaefer, M., Kiffe, M., et al. (2016). Targeted inhibition of the COP9 signalosome for treatment of cancer. Nat. Commun.

Schmidt, M.W., McQuary, P.R., Wee, S., Hofmann, K., and Wolf, D.A. (2009). F-Box-Directed CRL Complex Assembly and Regulation by the CSN and CAND1. Mol. Cell.

Scott, K.B., Turko, I. V., and Phinney, K.W. (2016). QconCAT: Internal Standard for Protein Quantification. In Methods in Enzymology, p.

Scrima, A., Koníčková, R., Czyzewski, B.K., Kawasaki, Y., Jeffrey, P.D., Groisman, R., Nakatani, Y., Iwai, S., Pavletich, N.P., and Thomä, N.H. (2008). Structural Basis of UV DNA-Damage Recognition by the DDB1-DDB2 Complex. Cell *135*, 1213–1223.

Scudellari, M. (2019). Protein-slaying drugs could be the next blockbuster therapies. Nature.

Shabek, N., Ruble, J., Waston, C.J., Garbutt, K.C., Hinds, T.R., Li, T., and Zheng, N. (2018). Structural insights into DDA1 function as a core component of the CRL4-DDB1 ubiquitin ligase. Cell Discov.

Shalem, O., Sanjana, N.E., Hartenian, E., Shi, X., Scott, D.A., Mikkelsen, T.S., Heckl, D., Ebert, B.L., Root, D.E., Doench, J.G., et al. (2014). Genome-scale CRISPR-Cas9 knockout screening in human cells. Science (80-.).

Shi, Y. (2009). Serine/Threonine Phosphatases: Mechanism through Structure. Cell.

Sievers, Q.L., Gasser, J.A., Cowley, G.S., Fischer, E.S., and Ebert, B.L. (2018). Genome-wide screen identifies cullin-RING ligase machinery required for lenalidomide-dependent CRL4CRBN activity. Blood.

Skaar, J.R., Pagan, J.K., and Pagano, M. (2013). Mechanisms and function of substrate recruitment by F-box proteins. Nat. Rev. Mol. Cell Biol.

Skowyra, D., Craig, K.L., Tyers, M., Elledge, S.J., and Harper, J.W. (1997). F-box proteins are receptors that recruit phosphorylated substrates to the SCF ubiquitin-ligase complex. Cell.

Smyth, G.K. limma: Linear Models for Microarray Data. In Bioinformatics and Computational Biology Solutions Using R and Bioconductor, p.

Smyth, G.K., Ritchie, M., and Thorne, N. (2011). Linear Models for Microarray Data User ' s Guide. Bioinformatics.

Soucy, T. a, Smith, P.G., Milhollen, M. a, Berger, A.J., Gavin, J.M., Adhikari, S., Brownell, J.E., Burke, K.E., Cardin, D.P., Critchley, S., et al. (2009). An inhibitor of NEDD8-activating enzyme as a new approach to treat cancer. Nature *458*, 732–736.

Sperling, A.S., Burgess, M., Keshishian, H., Gasser, J.A., Bhatt, S., Jan, M., Słabicki, M., Sellar, R.S., Fink, E.C., Miller, P.G., et al. (2019). Patterns of substrate affinity, competition and degradation kinetics underlie biological activity of thalidomide analogs. Blood.

Straube, R., Shah, M., Flockerzi, D., and Wolf, D.A. (2017). Trade-off and flexibility in the dynamic regulation of the cullin-RING ubiquitin ligase repertoire. PLoS Comput. Biol.

Suh, G.S.B., Poeck, B., Chouard, T., Oron, E., Segal, D., Chamovitz, D.A., and Zipursky, S.L. (2002). Drosophila JAB1/CSN5 acts in photoreceptor cells to induce glial cells. Neuron.

Sun, X., Wang, J., Yao, X., Zheng, W., Mao, Y., Lan, T., Wang, L., Sun, Y., Zhang, X., Zhao, Q., et al. (2019). A chemical approach for global protein knockdown from mice to non-human primates. Cell Discov.

Theile, C.S., Witte, M.D., Blom, A.E.M., Kundrat, L., Ploegh, H.L., and Guimaraes, C.P. (2013). Site-specific N-terminal labeling of proteins using sortase-mediated reactions. Nat. Protoc.

Thibaudeau, T.A., and Smith, D.M. (2019). A practical review of proteasome pharmacology. Pharmacol. Rev.

Tran, H.J.T.T., Allen, M.D., Löwe, J., and Bycroft, M. (2003). Structure of the Jab1/MPN domain and its implications for proteasome function. Biochemistry.

Tron, A.E., Arai, T., Duda, D.M., Kuwabara, H., Olszewski, J.L., Fujiwara, Y., Bahamon, B.N., Signoretti, S., Schulman, B.A., and DeCaprio, J.A. (2012). The Glomuvenous Malformation Protein Glomulin Binds Rbx1 and Regulates Cullin RING Ligase-Mediated Turnover of Fbw7. Mol. Cell.

Uehara, T., Minoshima, Y., Sagane, K., Sugi, N.H., Mitsuhashi, K.O., Yamamoto, N., Kamiyama, H., Takahashi, K., Kotake, Y., Uesugi, M., et al. (2017). Selective degradation of splicing factor CAPERα by anticancer sulfonamides. Nat. Chem. Biol.

Varshavsky, A. (1997). The ubiquitin system. Trends Biochem. Sci. *22*, 383–387.

Vulto-van Silfhout, A.T., Nakagawa, T., Bahi-Buisson, N., Haas, S.A., Hu, H., Bienek, M., Vissers, L.E.L.M., Gilissen, C., Tzschach, A., Busche, A., et al. (2015). Variants in CUL4B are associated with cerebral malformations. Hum. Mutat. *36*, 106–117.

Wang, D., Eraslan, B., Wieland, T., Hallström, B., Hopf, T., Zolg, D.P., Zecha, J., Asplund, A., Li, L., Meng, C., et al. (2019). A deep proteome and transcriptome abundance atlas of 29 healthy human tissues. Mol. Syst. Biol.

Wang, Y., Zhang, P., Liu, Z., Wang, Q., Wen, M., Wang, Y., Yuan, H., Mao, J.-H., and Wei, G. (2014). CUL4A overexpression enhances lung tumor growth and sensitizes lung cancer cells to Erlotinib via transcriptional regulation of EGFR. Mol. Cancer *13*, 252.

Wee, S., Geyer, R.K., Toda, T., and Wolf, D.A. (2005). CSN facilitates Cullin-RING ubiquitin ligase function by counteracting autocatalytic adapter instability. Nat. Cell Biol.

Wei, N., and Deng, X.W. (2003). The COP9 Signalosome. Annu. Rev. Cell Dev. Biol.

Wenzel, D.M., Lissounov, A., Brzovic, P.S., and Klevit, R.E. (2011). UBCH7 reactivity profile reveals parkin and HHARI to be RING/HECT hybrids. Nature.

Winter, G.E., Buckley, D.L., Paulk, J., Roberts, J.M., Souza, A., Dhe-Paganon, S., and Bradner, J.E. (2015). Phthalimide conjugation as a strategy for in vivo target protein degradation. Science (80-.).

Wolfenden, R., and Snider, M.J. (2001). The Depth of Chemical Time and the Power of Enzymes as Catalysts. *34*, 938–945.

Wu, S., Zhu, W., Nhan, T., Toth, J.I., Petroski, M.D., and Wolf, D.A. (2013). CAND1 controls in vivo dynamics of the cullin 1-RING ubiquitin ligase repertoire. Nat. Commun.

Yamoah, K., Oashi, T., Sarikas, A., Gazdoiu, S., Osman, R., and Pan, Z.Q. (2008). Autoinhibitory regulation of SCF-mediated ubiquitination by human cullin 1's C-terminal tail. Proc. Natl. Acad. Sci. U. S. A.

Yau, R., and Rape, M. (2016). The increasing complexity of the ubiquitin code. Nat. Cell Biol.

Zemla, A., Thomas, Y., Kedziora, S., Knebel, A., Wood, N.T., Rabut, G., and Kurz, T. (2013). CSN-and CAND1-dependent remodelling of the budding yeast SCF complex. Nat. Commun.

Zengerle, M., Chan, K.H., and Ciulli, A. (2015). Selective Small Molecule Induced Degradation of the BET Bromodomain Protein BRD4. ACS Chem. Biol.

Zhang, W., Ito, H., Quint, M., Huang, H., Noël, L.D., and Gray, W.M. (2008). Genetic analysis of CAND1-CUL1 interactions in Arabidopsis supports a role for CAND1-mediated cycling of the SCFTIR1 complex. Proc. Natl. Acad. Sci. U. S. A.

Zhang, X., Crowley, V.M., Wucherpfennig, T.G., Dix, M.M., and Cravatt, B.F. (2018). [Cravatt]Electrophilic PROTACs that degrade nuclear proteins by engaging DCAF16. BioRxiv.

Zheng, N., and Shabek, N. (2017). Ubiquitin Ligases: Structure, Function, and Regulation. Annu. Rev. Biochem.

Zheng, J., Yang, X., Harrell, J.M., Ryzhikov, S., Shim, E.H., Lykke-Andersen, K., Wei, N., Sun, H., Kobayashi, R., and Zhang, H. (2002a). CAND1 binds to unneddylated CUL1 and regulates the formation of SCF ubiquitin E3 ligase complex. Mol. Cell.

Zheng, N., Schulman, B.A., Song, L., Miller, J.J., Jeffrey, P.D., Wang, P., Chu, C., Koepp, D.M., Elledge, S.J., Pagano, M., et al. (2002b). Structure of the Cul1-Rbx1-Skp1-F boxSkp2 SCF ubiquitin ligase complex. Nature.

Zimmerman, E.S., Schulman, B. a, and Zheng, N. (2010). Structural assembly of cullin-RING ubiquitin ligase complexes. Curr. Opin. Struct. Biol. *20*, 714–721.

Zou, Y., Liu, Q., Chen, B., Zhang, X., Guo, C., Zhou, H., Li, J., Gao, G., Guo, Y., Yan, C., et al. (2007). Mutation in CUL4B, which encodes a member of cullin-RING ubiquitin ligase complex, causes X-linked mental retardation. Am. J. Hum. Genet. *80*, 561–566.

Zou, Y., Mi, J., Cui, J., Lu, D., Zhang, X., Guo, C., Gao, G., Liu, Q., Chen, B., Shao, C., et al. (2009). Characterization of nuclear localization signal in the N terminus of CUL4B and its essential role in cyclin E degradation and cell cycle progression. J. Biol. Chem.